Dissecting Synaptogenesis and Axonal Branching Mechanisms in *Drosophila Melanogaster*

Dissertation

zur

Erlangung des Doktorgrades (Dr. rer. nat.)

der

Mathematisch-Naturwissenschaftlichen Fakultät

der

Rheinischen Friedrich-Wilhelms-Universität Bonn

vorgelegt von

Nicole Barbara Kucharowski

aus Hilden

Bonn 2024

Angefertigt mit Genehmigung der Mathematisch-Naturwissenschaftlichen Fakultät

der Rheinischen Friedrich-Wilhelms-Universität Bonn

Gutachter/Betreuer: Prof. Dietmar Schmucker

Gutachterin: Priv.-Doz. Dr. Margret Bülow

Tag der Promotion: 14.11.24

Erscheinungsjahr: 2024

„Nothing in life is to be feared, it is only to be understood."

- Marie Skłodowska-Curie

Für meine Mama, die stärkste Frau die ich kenne

Table of content

Acknowledgements

When I first considered pursuing a PhD in molecular biomedicine, I was scared and filled with self-doubt, questioning whether I possessed the intelligence to succeed. I asked the great women in the lab during my master thesis, if they think I am smart enough to get the PhD. My former mentor and now dear friend, Dr. Julia Sellin, offered words that resonate deeply with me: “You don’t need to be exceptionally intelligent to achieve this goal. Earning your Master of Science degree has already proven you capable. What matters more than intelligence is frustration tolerance, for this journey will be full of challenges and frustrations.” At the time, I didn’t fully grasp her wisdom. Reflecting on the past four years, the most demanding period of my life, I now understand what she meant, and I am very grateful for having chosen this path.

This journey would not have been possible without the support of many individuals, whom I wish to acknowledge in this chapter.

First and foremost, I want to thank my promoter, Prof. Dr. Dietmar Schmucker, for granting me the opportunity to pursue my PhD in his laboratory and for his invaluable advice and stimulating discussions regarding my project. We faced challenges, particularly with the onset of the COVID-19 pandemic shortly after my project began, making lab work even more daunting. Nevertheless, we persevered through these tough times, and I am deeply thankful for the scientific perspective you imparted to me. Your constant challenge to strive for my best and your guidance in scientific research have been essential.

I am also immensely grateful to my co-promoter, Priv.-Doz. Dr. Margret Bülow, for her unwavering advice and support. Margret, your efficiency is unparalleled, and I have learned so much from you about conducting experiments, presenting research, and writing publications. Your guidance, advice, and the appreciation you showed me have been beyond valuable. The scientific community needs more people like you!

I wish to thank Priv.-Doz. Dr. Gerhild van Echten-Deckert and Prof. Dr. Carmen Ruiz de Almodóvar for agreeing to serve on my doctoral committee, taking the time to read my thesis, and being present for my defense. A special thank you to Priv.-Doz. Dr. Gerhild van Echten-Deckert, who has morally supported me since our meeting at the Women in Science seminar. Your encouragement and listening ear have been a blessing for me.

This work would not have been possible without the members and former members of the Schmucker lab. My deepest thanks to my colleague and friend, Dr. Pilar Carrera, with whom I have closely worked over the years. Your positivity and endless patience have been priceless. Without you, this would not have been possible. I am also grateful to Dr. Gabriela Edwards-Faret for her constant support and for helping me see the bigger picture. It has been a privilege to work with and learn from you. A heartfelt thank you to Arabo Apresyan for his assistance with the bioinformatics of RNA-sequencing and for always taking the time to explain everything in detail. I also extend my gratitude to the other members and former members of the lab: Torsten, Kathrin, Lennart, Melanie, Sina, Azadeh, Leonie, Faiba, Kimberley, Sofie, Anke, Tine and Zenjing. I feel honored to have been surrounded by such wonderful and supportive individuals. Your help with my experiments and your advice over the years have been invaluable, and I would not have gained the expertise and knowledge I have without you.

The most beautiful outcome is when colleagues become friends. Thank you, Barbara, Bernhard, and Lea, for your friendship. You were my rock during difficult times, lifting me up when I was down. I am so grateful for all the experiences we shared, the lunches, and coffee dates. I feel incredibly lucky to have met all of you.

I owe a deep debt of gratitude to my friend and mentor, Dr. Julia Sellin. You inspire me every day! Your advice and support over the years have been a gift, and I am honored to be considered your friend. Your willingness to listen, answer my questions, and treat me as an equal has meant the world to me.

Finally, I am mostly grateful for the love and support of my family and friends. There is nothing more beautiful in life than being surrounded by people who love you unconditionally, and I am fortunate to have such people in my life. I feel your love every day, and without you, I wouldn’t be who I am today.

Kochana rodzina jesteście moim sercem! Dziękuję wam za bezwarunkowa miłość i wsparcie w tych ostatnich latach. Kocham was z całego serca!

1. Abstract

Axonal branching and synaptogenesis are critical mechanisms in neuronal development, enabling the formation of complex neural communication networks. Despite their importance, the specific regulatory factors and signaling pathways involved in these processes remain poorly understood. This dissertation aims to identify and elucidate these regulatory mechanisms.

In a targeted genetic screening approach, I focused on Yorkie (Yki) downstream genes and identified Brain tumor (Brat) as one novel regulator of axonal branching and synapse modulation. Loss-of-function Brat MARCM analyses revealed a dosage-dependent effect of Brat on synaptogenesis, leading to either enhanced synapse formation or synapse depletion. These findings were corroborated by RNAi-mediated knock-down (K.D.) assays and null allele studies.

In order to better study the molecular specialization of Yki in postmitotic neurons in the future, I adapted a *Drosophila Melanogaster* (*D.m.*) neuronal cell culture system (Bg3c2 cells) to investigate the effects of Yki overexpression in the central nervous system (CNS). My research uncovered that Yki localizes primarily within the nucleus, particularly enriched at the lamina, but is absent from the nucleolus. RNA-sequencing analysis of the effects of overexpressing a specific Yki isoform on gene expression revealed several novel potential target genes specifically regulated in postmitotic neurons, providing new insights into Yki signaling in CNS cells.

This dissertation also explores the role of Cysteine-rich with EGF-like domain (Creld), a newly identified regulatory factor in axonal branching and synaptogenesis, that we previously found to play a role in mitochondria-ER contact sites (Paradis *et al.*, 2022). Through a series of genetic molecular analyses, I demonstrate how Creld and Yki independently influence neuronal differentiation and metabolism.

In conclusion, this dissertation advances our understanding of the complex regulatory networks governing neuronal development and function, highlighting the pivotal roles of Yki and Creld in these processes.

2. Zusammenfassung

Axonale Verzweigung und Synaptogenese sind entscheidende Mechanismen in der neuronalen Entwicklung und ermöglichen die Bildung komplexer neuronaler Kommunikationsnetzwerke. Trotz ihrer Bedeutung sind die spezifischen regulatorischen Faktoren und Signalwege, die an diesen Prozessen beteiligt sind, noch wenig verstanden. Diese Dissertation zielt darauf ab, diese regulatorischen Mechanismen zu identifizieren und zu erläutern.

In einem gezielten genetischen Screening-Ansatz konzentrierte ich mich auf die nachgeschalteten Gene von Yorkie (Yki) und identifizierte Brain tumor (Brat) als neuen Regulator der axonalen Verzweigung und Synapsen Modulation. Verlustfunktionsanalysen (Loss-of-function, LOF) von Brat mittels MARCM zeigten einen dosisabhängigen Effekt von Brat auf die Synaptogenese, der entweder zu einer verstärkten Synapsenbildung oder zu einem Synapsen Schwund führte. Diese Ergebnisse wurden durch RNAi Knock-Down (K.D.) -Assays und Null-Allel-Studien bestätigt.

Um die molekulare Spezialisierung von Yki in postmitotischen Neuronen zukünftig besser zu untersuchen, passte ich ein neuronales Zellkultursystem von *Drosophila Melanogaster* (*D.m.*) (Bg3c2-Zellen) an, um die Effekte der Yki-Überexpression im zentralen Nervensystem (ZNS) zu untersuchen. Meine Forschung ergab, dass Yki hauptsächlich im Zellkern lokalisiert ist, besonders angereichert in der Lamina, aber im Nucleolus nicht vorhanden ist. Die RNA-Sequenzierungsanalyse der Auswirkungen der Überexpression einer spezifischen Yki-Isoform auf die Genexpression offenbarte mehrere neuartige potenzielle Zielgene, die speziell in postmitotischen Neuronen reguliert werden, und lieferte neue Einblicke in die Yki-Signalgebung in ZNS-Zellen.

Diese Dissertation untersucht auch die Rolle von Cysteine-rich with EGF-like domain (Creld), einem neu identifizierten regulatorischen Faktor in der axonalen Verzweigung und Synaptogenese, welches zuvor von uns als relevant für die Kontaktstellen zwischen Mitochondrien und ER identifiziert wurde (Paradis *et al.*, 2022). Durch eine Reihe genetischer und molekularer Analysen zeige ich, wie Creld und Yki unabhängig voneinander die neuronale Differenzierung und den Stoffwechsel beeinflussen.

Abschließend trägt diese Dissertation zum Verständnis der komplexen regulatorischen Netzwerke bei, welche die neuronale Entwicklung und Funktion steuern, und hebt die entscheidenden Rollen von Yki und Creld in diesen Prozessen hervor.

3. List of Abbreviations

20E	20-hydroxyecdysone, Ecdysone
Abl	Abelson
aDC	Anterior Dorsocentral
Alrm	Astrocytic Leucine-rich Repeat Molecule
APF	After Puparium Formation
App	Approximated
AJ	Adherens Junctions
BLJ	Basolateral Junctions
Bon	Bonus
Brp	Bruchpilot
BSA	Bovine Serum Albumin
CNS	Central Nervous System
Crb	Crumbs
Crm	Cramped
$CuSO_4$	Copper Sulfate
CycE	Cyclin E
DAPI	4’,6-Diamidino-2-Phenylindole, Dihydrochloride
DC	Dorsal Central
Dco	Disc Overgrown
DGRC	Drosophila Genomics Resource Center
Diap1	Diapherous 1
DIP	Dpr Interacting Proteins
Dlg	Disc Large
D.m.	*Drosophila Melanogaster*
Dpr	Defective Proboscis Extension Response
Ds	Dachsous
DSHB	Developmental Studies Hybridoma Bank
E(spl)m6-BFM	Enhancer of Split m6, Bearded Family Member
ECM	Extracellular Matrix
EcR	Ecdysone Receptor
EGFR	Epidermal Growth Factor Receptor
ER	Endoplasmic Reticulum
Ex	Expanded
FACS	Fluorescent Activated Cell Sorting
Fj	Four-jointed
FLP	Flippase
FRT	Flippase Recognition Target
Ft	Fat
Gat	GABA Transporter
GMC	Ganglion Mother Cell
GOF	Gain-of-function
Hey	Hairy/E(spl)-related with YRPW Motif
Hpo	Hippo
Hth	Homothorax
IgSF	Immunoglobulin Superfamily

iINP	Immature Intermediate Neural Progenitor
Insb	Insensible
Insc	Inscuetable
Jub	Drosophila Ajuba
Lft	Lowfat
Lgl	Lethal Giant Larvae
LncRNA:noe	Long Non-coding RNA:noe
LOF	Loss-of-function
MAPK	Mitogen Activated Protein Kinase
MARCM	Mosaic Analysis with a Repressible Cell Marker
Mats	Mob as a Tumor Suppressor
Mct1	Monocarboxylate Transporter 1
Mer	Merlin
mINP	Mature Intermediate Neural Progenitor
Mira	Miranda
Ms	Mechanosensory
MTZ	Maternal-to-zygotic
Mus301	Mutagen-sensitive 301
Myo	Myoglianon
NaAc	Sodium Acetate
NB	Neuroblast
NHL	NCL-1, HT2A, Lin41
NMJ	Neuro-muscular Junction
Nos	Nanos
NPC	Neuronal Progenitor Cell
NSyb	Neuronal Synaptobrevin
O.E.	Overexpression
Para	Paralytic
PBS	Phosphate Buffered Saline
PBS-TX 100	Phosphate Buffered Saline containing 0.1 or 0.3 % (v/v) Triton X-100
PBT	Phosphate Buffered Saline with Tween-20
PCA	Principal Composition Analysis
PFA	Paraformaldehyde
Plzf	Promyelocytic Leukemia Zinc Finger
PNR	Pannier
Pum	Pumilio
Pus7	Pseudouridine Synthase 7
Ptk	Protein Tyrosine Kinase
Ptp	Protein Tyrosine Phosphatase
Rassf	Ras-associated Factor
Repo	Reversed Polarity
RPM	Rounds Per Minute
RT	Room Temperature
Sav	Salvador
Scrib	Scribble
Sd	Scalloped
SOP	Sensory Organ Progenitor

Sty	Sprouty
TF	Transcription Factor
tNB	Tumor Neuroblast
Tor	Target of Rapamycin
TRIM	Tripartite Motif
Tsh	Teashirt
UAS	Upstream Activator Sequence
UPR	Untranslated Protein Response
VNC	Ventral Nerve Chord
Wnk	With No Lysine (K) kinase
Wts	Warts
Yki	Yorkie

4. List of Figures and Tables

5. Introduction

5.1. Neurogenesis

Asymmetric Division: Insights into Notch/Delta Signaling and Cellular Patterning

Neuronal development, epitomized as the intricate process of neurogenesis, represents a cornerstone of biological exploration within the realms of neuroscience. Embodied within the dynamic developmental process of the fruit fly (*Drosophila Melanogaster*), it unfolds across diverse ontogenetic stages, encompassing embryonic, larval, and adult neurogenesis. At its inception, the genesis of mature neurons is orchestrated by the concerted activity of neuronal progenitor cells (NPCs) or stem cells.

Central to this developmental process are the neuroblasts (NBs) and sensory organ progenitor (SOP) cells, whose proliferation and differentiation lead to the genesis of neurons. Originating from proneuronal clusters, these cellular protagonists provide the foundation for an elaborate orchestration of neuronal maturation (Campos-Ortega, 1999). In the genesis of the nervous system, the inaugural wave of neurogenesis begins with the delamination of NBs from the neuroectoderm, marking the commencement of asymmetrical division. This division culminates in the emergence of either neurons or glial cells, a process orchestrated by the complex process of lateral inhibition. Here the Notch/Delta signaling network emerges as a principal orchestrator, dictating the trajectory of neuronal fate. Within this dynamic milieu, asymmetric division emerges as a pivotal mechanism, equipping each progenitor cell with divergent destinies. One progeny retains a reservoir of self-renewal capacity, while the other embarks upon a trajectory of differentiation, thus ensuring cellular diversity and developmental progression (Bray, 2016).

This interplay between Notch/Delta signaling and cellular fate determination assumes paramount significance in embryonic nervous system development, steering the pivotal epidermal/neural lineage decision. Through the nuanced regulation of gene expression, cellular patterning is achieved, coordinating a rich array of diverse cell fates. In detail, the heightened expression of Delta (acting as the “Sender”) within a cell exerts a suppressive influence on Delta expression in adjacent cells. Consequently, this cascade engenders a milieu characterized by diminished Delta levels but augmented Notch expression (serving

as the “Receiver”) within these cellular entities. This interplay culminates in the attainment of cellular patterning, whereby these cells become pivotal agents, orchestrating a spectrum of target gene expressions, and thus precipitating divergent cellular destinies (Figure 1) (Bocci, Onuchic and Jolly, 2020).

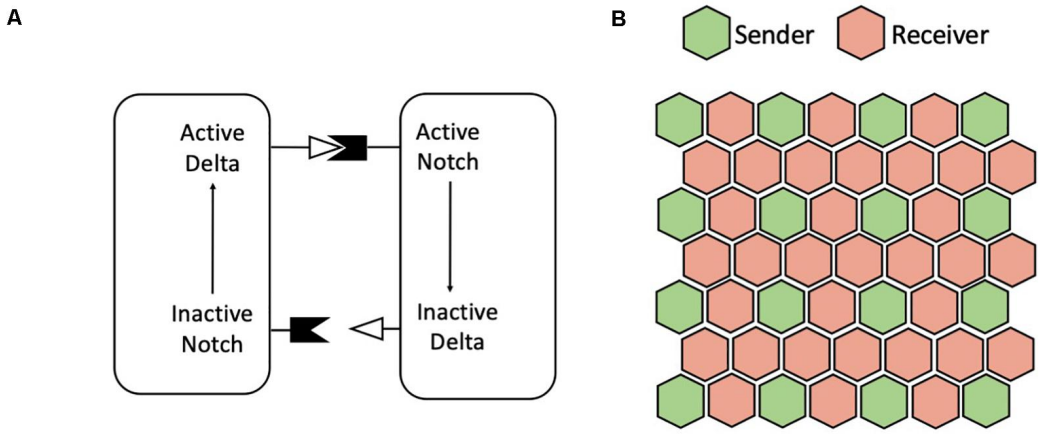

Figure 1. Notch/Delta Signaling leads to Patterning.

(A) Graphic illustrates Notch/Delta signaling model in neighboring cells adapted from (Collier *et al.*, 1996).

(B) Display of cell patterning with Sender cells depicted in green and Receiver cells depicted in red. Illustration adapted from (Bocci, Onuchic and Jolly, 2020).

As the development unfolds, a dichotomy emerges, delineating two distinct waves of neurogenesis. The embryonic genesis, while instrumental in larval central nervous system (CNS) development, accounts for a modest fraction (approx. 10%) of adult nervous system cells. In contrast, the subsequent wave of neurogenesis, dominated by NB division, substantiates the lion’s share (approx. 90%) of adult CNS cellular composition, a phenomenon underscored by the vanishing act of NBs during pupal stages of development (Figure 2) (Homem and Knoblich, 2012).

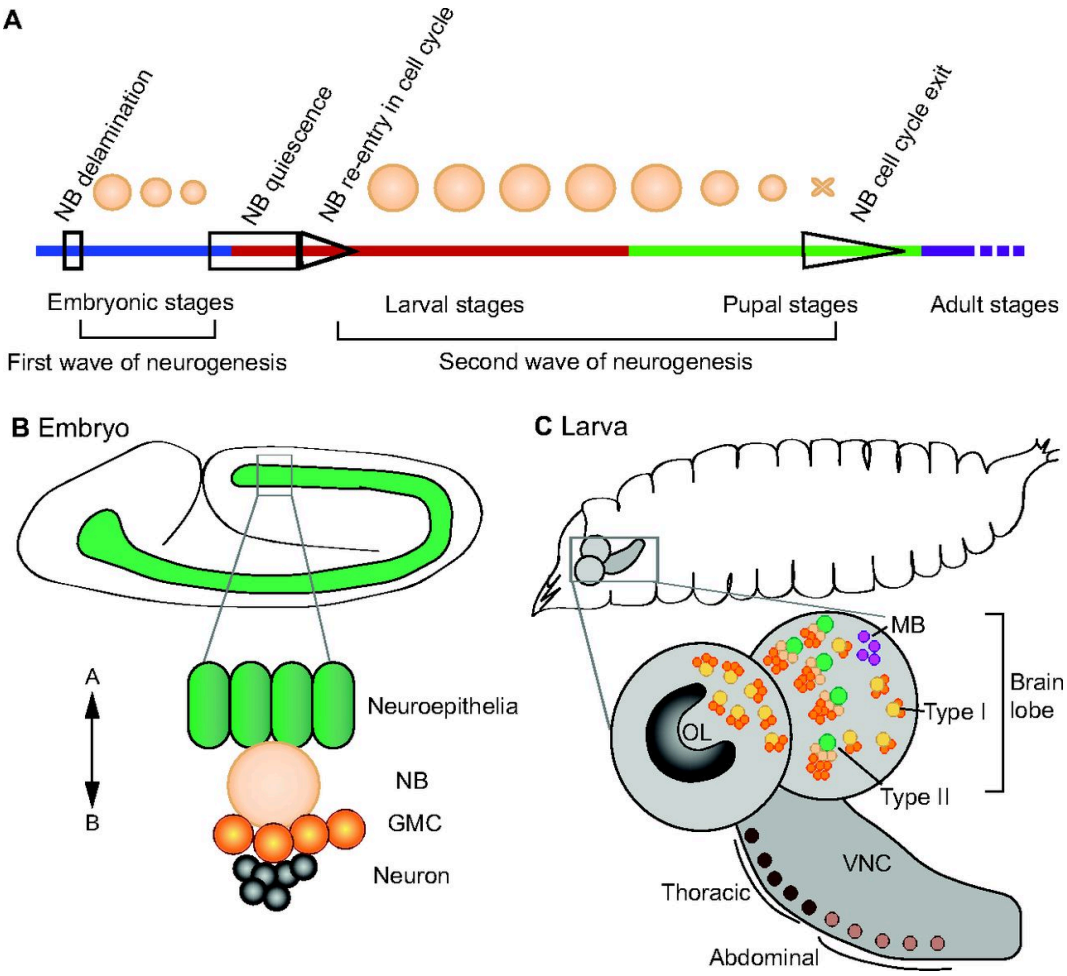

Figure 2. Schematic Depiction of Neurogenesis in *Drosophila Melanogaster* Embryo and Larvae.

(A) Graphic illustration of the two waves of neurogenesis. Neuroblasts (NBs) are depicted in beige during diverse stages of the neurogenesis timeline. Generation of NBs starts during embryonic stages through delamination from the neuro-ectoderm. The NBs of the embryonic stage lack re-growth after each division, while becoming quiescent during late embryogenesis and re-entering growth to start the second wave of neurogenesis in the larval stage. In comparison, NBs of larval stage are re-growing after each division, hence, divide regularly. Furthermore, NBs of pupal stages disappear, which marks the end of the second wave neurogenesis.

(B) Graphic illustration of neurogenesis in *D.m.* embryo. Delamination of neuro-ectodermal cells (green). Further division of NBs lead to ganglion mother cells (GMCs; orange), which after further division generate two neurons (gray). A: for apical, and B: for basal.

(C) Graphic illustration of a 3rd instar larva and a close-up of the larval CNS. Larval brain is shown with the main brain regions, with optic lobes (OL); mushroom body NBs (magenta); type I (yellow), and type II NBs (green). VNC is depicted with thoracic (dark brown) and abdominal NBs (light brown).

Image adapted from (Homem and Knoblich, 2012).

Transitioning to the peripheral nervous system, sensory organ precursor cells (SOPs) undergo a series of asymmetric divisions, driven by Notch/Delta signaling, leading to the formation of external sensory organs. These divisions, characterized by their apical-basal or anterior-posterior orientation, underscore the remarkable plasticity inherent within SOP dynamics (Roegiers *et al.*, 2001). The first asymmetric division within SOPs unfolds along an anterior-posterior axis (Figure 3B), setting the stage for subsequent cellular events (Schweisguth, 2015). Subsequently, the resultant daughter cell proceeds to undergo further division in an apical-basal orientation.

Amidst this complexity, the role of Notch/Delta signaling emerges as a guiding system, essential for a deeper understanding of neurogenesis (Schweisguth, 2004).

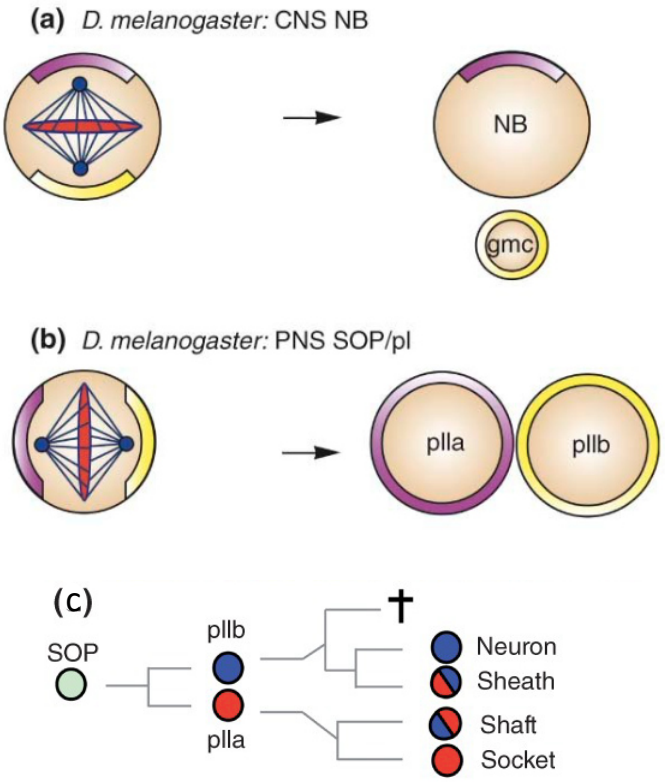

Figure 3. Graphic of Asymmetric Division of Neuronal Progenitors in *Drosophila Melanogaster*.

(A) Asymmetrical division in *D.m.* central nervous system (CNS) neuroblasts (NBs) showing apical proteins in purple and basal proteins in yellow, together with the spindle apparatus showing apical-basal orientation. After division apical cell forms self-renewing NB and basal cell forms ganglion mother cell (gmc).

(B) Asymmetrical division in *D.m.* peripheral nervous system (PNS) sensory organ precursors (SOPs) showing anterior proteins in purple and posterior proteins in yellow, together with the spindle apparatus showing anterior-posterior orientation. After cell division anterior cell forms plla and posterior cell forms pllb SOP daughter cell.

(C) SOP divides asymmetrically into pllb shown in blue and plla shown in red. The daughter cells further divide and generate the neuron and sheath cell, in the pllb lineage, and the socket and shaft cells, in the plla lineage.
Image adapted: (A) & (B) from (Keder and Carmena, 2013); (C) from (Schweisguth, 2015).

Axonal Development and Synaptogenesis

In the complex orchestration of nervous system development, neuronal precursor cells undergo asymmetric division, a pivotal process generating both neurons and glia cells. Subsequent maturation and differentiation of postmitotic neurons is marked by the extension of axons, facilitating the establishment of crucial synaptic connections with diverse cellular targets, including neurons, muscles, and glia cells. These synaptic connections form the backbone of cellular communication within neural networks, dictating the precise functioning of the nervous system. Guided by complex genetic mechanisms, the developmental journey of axon growth, pathfinding, and synaptogenesis unfolds with remarkable precision, ensuring the formation of an exact circuitry essential for neuronal connectivity. This interplay of genetic regulation in axon guidance and synapse formation has been extensively studied, shedding light on the fundamental principles underlying the development of the nervous system (Tessier-Lavigne and Goodman, 1996).

Axon Outgrowth and Pathfinding

In the pioneering work of Ramón y Cajal, the complex process of axon outgrowth was first demonstrated through the observation of dynamic growth cone structures (Dahl *et al.*, 1920). The dynamics guide the axon along predetermined trajectories, extending far from the neuronal soma to establish synaptic connections with other cellular counterparts. Integral to this process are the dynamics of the cytoskeleton, driven by the interplay of actin and microtubule dynamics. While actin arranges the guidance of growth cones, by a steady myosin-driven retrograde motion of filopodia and lamellipodia, microtubules facilitate their advancement, delineating a finely tuned dance of cellular navigation (Figure 4) (Dent and Gertler, 2003).

Amidst the journey of neuronal development, growth cones navigate through a maze of environmental cues, forging precise pathways to their intended destinations. Each step

along this journey is influenced by discrete guidance cues present in the cellular milieu (Dickson, 2002). Notably, the orchestration of axonal growth and pathfinding hinges upon the interplay of attractive and repulsive cues, spanning both short and long-range distances. Key among these cues are four families: the Semaphorins, Ephrins, Slits, and Netrins (Kolodkin and Tessier-Lavigne, 2011).

Moreover, beyond these canonical cues, cell-adhesion molecules (CAMs), residing in the membrane of neurons and glia cells, wield significant influence over axonal pathfinding. Among these, members of cadherin and immunoglobulin (Ig) superfamily, including Dscam and N-cadherin, play pivotal roles. Of particular intrigue is Down-syndrome-cell-adhesion-molecule (Dscam), renowned for its staggering array of alternatively spliced isoforms, endowing neurons with a vast repertoire of attraction and repulsion (Schmucker *et al.*, 2000).

Collectively, the complex interplay of guidance cues and molecules orchestrates not only axonal growth and pathfinding but also underpins processes crucial for target recognition, axonal branching, and synaptogenesis.

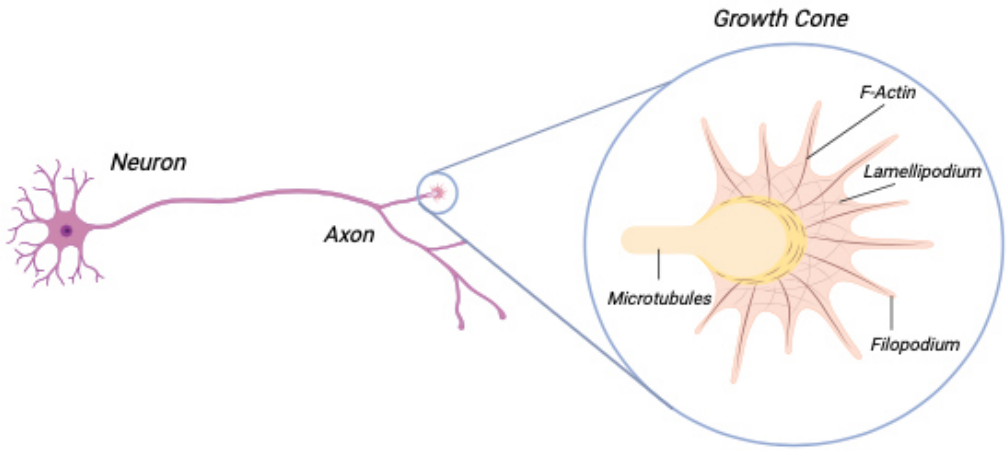

Figure 4. Molecular Architecture of Neuronal Growth Cone Dynamics.

Schematic representation of a neuron illustrating the dynamic process of axonal outgrowth. The growth cone, depicted at the distal tip of the axon, exhibits complex molecular structures crucial for axonal navigation and extension. Microtubules provide structural support throughout the axon, while the spike-like protrusions represent filopodia composed of F-actin filaments. The flat like region depict lamellipodia, contributing to axonal exploration and guidance.
Graphic designed using BioRender.

Synaptogenesis and Circuit Formation

Neuronal circuit development, the construction of functional connections extends beyond mere axonal growth to encompass the delicate orchestration of synaptogenesis. This process hinges upon the establishment of asymmetric junctions linking presynaptic neurons with an array of postsynaptic targets, including neurons, glia cells, and muscle cells (Chou, Johnson and Van Vactor, 2020).

Synaptogenesis unfolds through a series of meticulously coordinated stages. Initially, the axon must navigate to its designated target, a crucial step preceding the initiation of synapse formation. Subsequently, a cascade of adhesive interactions, orchestrated by CAMs and other guidance cues, culminates in the formation of presynaptic terminals. As the synapse matures, the complex assembly of neurotransmitter release machinery, including the recruitment and clustering of synaptic vesicles, occurs in tandem with the establishment of active zones housing Ca^{2+} ion-gated channels and postsynaptic densities (Sudhof, 2004).

In the realm of *D.m.* neuroscience, the neuro-muscular junction (NMJ) stands as a beacon of study, offering unparalleled accessibility and cellular resolution. Here, the assembly of the NMJ is facilitated by a presynaptic motoneuron, interacting with a singular postsynaptic target: the muscle (Menon, Carrillo and Zinn, 2013). Yet, the study of CNS synaptogenesis lags behind, constrained by the complex nature and limited accessibility of CNS synapse formation.

However, as technological advancements and genetic techniques evolve, focused studies on CNS synapse formation within specific brain and VNC regions of *D.m.* have emerged. Investigations into the development of neurons within the Mushroom Body (MB), Antennal Lobe (AL), and Mechanosensory Neurons (Ms-Neurons) have yielded significant insights (Mosca and Luo, 2014; Urwyler *et al.*, 2015; Elkahlah *et al.*, 2020).

Functional synaptogenesis heralds the successful assembly of neuronal circuits within the CNS. Circuit formation is contingent upon robust neurogenesis, as neurons project their axons along precise pathways to establish connections with their targets. The culmination of this process manifests in specific organismal behaviors, as sensory and motor inputs and outputs are woven into the fabric of circuitry.

Furthermore, a hallmark of correct neuronal circuit formation is the phenomenon of neuronal plasticity. While neurogenesis and axon development proceed independently of activity, synaptogenesis is profoundly influenced by neural activity, exhibiting dynamic changes throughout the organism's lifespan (Figure 5) (Südhof, 2018). This phenomenon of neuronal plasticity embodies the adaptive nature of neuronal circuits, facilitating their modulation in response to varying environmental stimuli. Thus, neuronal plasticity serves as a cornerstone of neural flexibility, perpetuating the ever-changing dynamics of neuronal circuits.

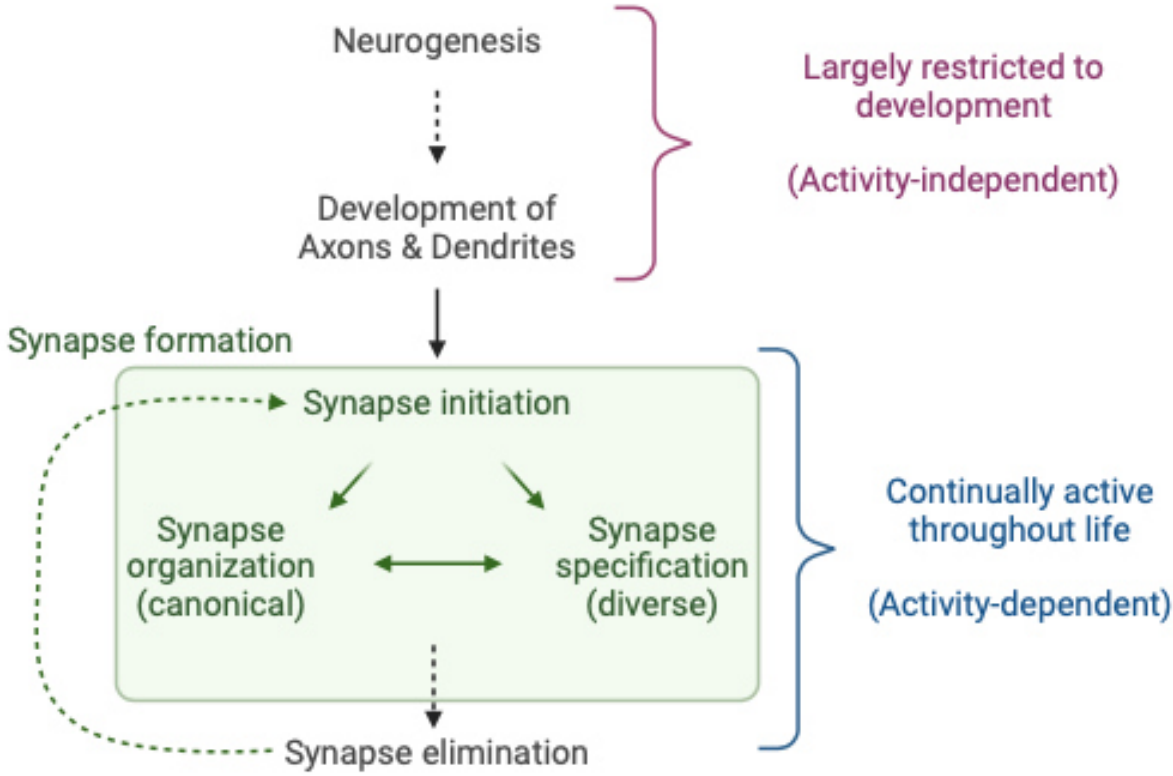

Figure 5. Dynamics of Neurogenesis and Synaptogenesis in Neuronal Development.

Illustration depicting the temporal dynamics of neurogenesis, axonal, and dendritic development, which occur during specific developmental windows. Additionally, the process of activity-dependent synapse formation is depicted, involving initiation, organization, and specification of synapses, and can also lead to synapse elimination in certain contexts. Unlike neurogenesis, synaptogenesis is not temporally restricted and continues throughout life.
Graphic adapted from (Südhof, 2018) designed using BioRender.

Axon Branching

In the developmental journey of a single neuron, the appearance of axonal branching represents a pivotal phase, facilitating the establishment of connections with multiple cellular partners. This branching phenomenon engenders a sophisticated network of diverse neuronal circuits, amplifying the complexity of wiring and broadening the input and output fields of neurons.

In-depth investigations into *D.m.* axonal branching have unveiled a multitude of molecular mechanisms orchestrating this complex process. Essential growth-promoting proteins, such as Epidermal Growth Factor Receptor (EGFR), play indispensable roles in fostering sufficient axonal branching (Zschätzsch *et al.*, 2014). Additionally, proteins involved in cytoskeletal dynamics and growth cone structure, exemplified by Abelson (Abl), have been implicated in modulating axonal branching (Clarke *et al.*, 2020).

Among the multitude of molecular players, the Dscam1 protein emerges as a particularly captivating protagonist. As a member of the immunoglobulin (Ig) superfamily of transmembrane receptors, Dscam1 showcases a remarkable capacity for alternative splicing, giving rise to an extensive repertoire of isoforms, each capable of highly selective homophilic interactions (Schmucker *et al.*, 2000). Manipulation of Dscam1 has been shown to exert a disruptive effect on postmitotic axonal branching, underscoring its pivotal role in collateral formation (Figure 6) (Hattori *et al.*, 2008). Notably, changes in Dscam1 isoform abundance have been linked to dominant dosage-sensitive inhibition of branching, illuminating the complex interplay between cell-intrinsic diversity and normal axonal branching during neuronal circuit formation (He *et al.*, 2014).

Thus, axonal branching emerges as an evolutionary strategy aimed at extending synaptic network complexity, displaying the multifaceted orchestration of molecular mechanisms underlying neuronal circuit development.

Through the continued exploration, novel therapeutic avenues can be developed aimed at addressing neurological diseases defined by aberrant axonal branching and connectivity.

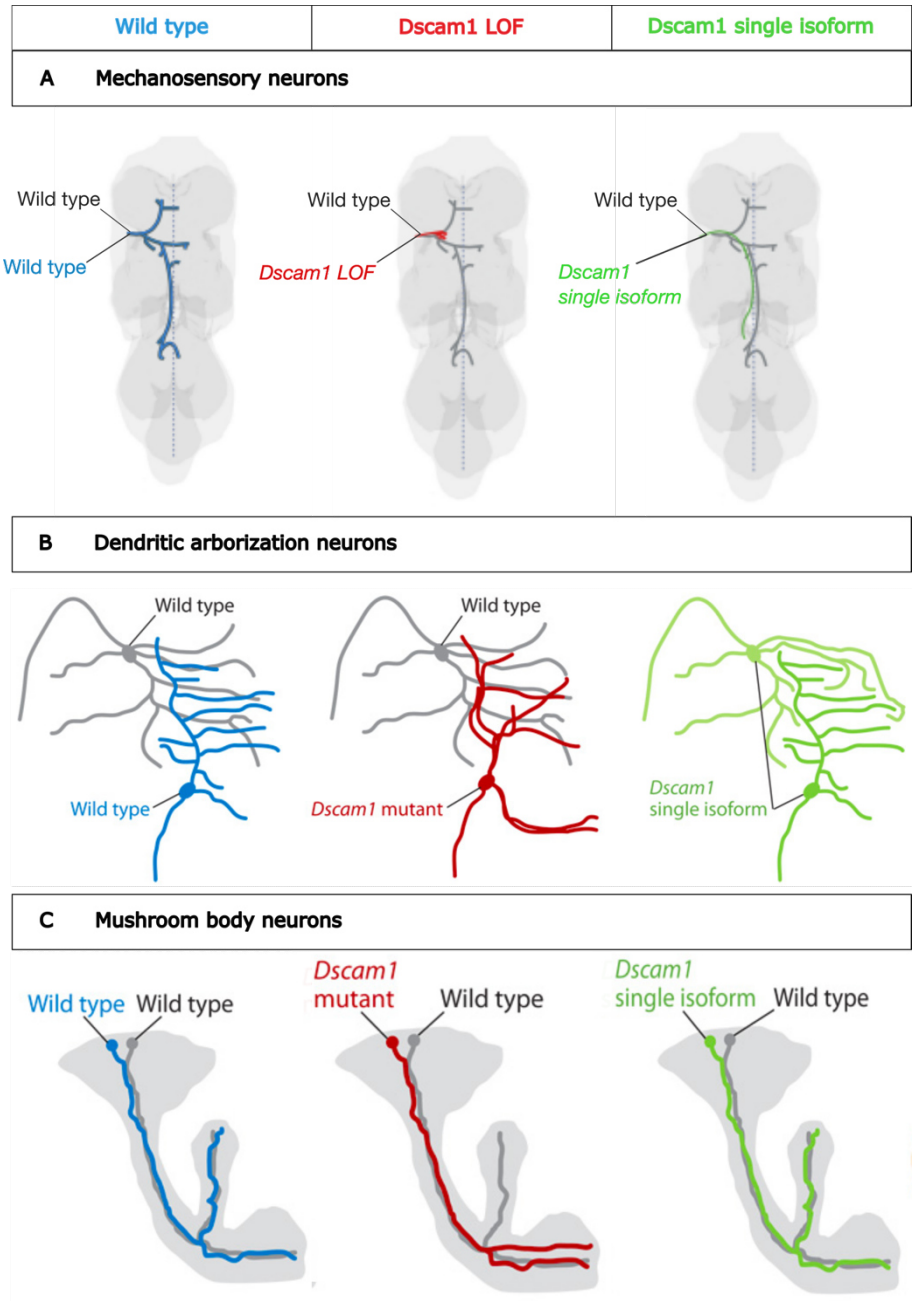

Figure 6. Influence of Dscam1 on Neurite Organization and Branching Patterns.

Illustration depicting the impact of Dscam1 loss-of-function (LOF) and single isoform gain-of-function (GOF) phenotypes in different neuronal types.

(A) Graphical representation of Ms-neurons showing Dscam1 LOF resulting in neurite clumping due to intertwined branches (depicted in red), while single isoform GOF leads to axon development without collaterals (depicted in green).

(B) Illustration of DA neurons exhibiting disrupted self-avoidance of sister neurites with Dscam1 LOF (depicted in red), whereas single isoform Dscam1 GOF induces ectopic repulsion of dendrites (depicted in green).

(C) Graphical depiction of MB neurons displaying segregation defects of axons with Dscam1 LOF (depicted in red). Conversely, GOF of Dscam1 single isoform shows no effect in branching and resembles wild-type (WT) structure (depicted in green).

Adapted from (Hattori *et al.*, 2008) and (Dascenco, 2015).

Axon Pruning and Synapse Pruning

The process of neuronal circuit formation and plasticity relies upon cellular dynamics characterized by the continual formation and elimination of axons and synapses (Figure 5). Central to this process is axon and synapse pruning, a finely orchestrated developmental program that selectively removes branches and synapses without inducing cell death. Within the realm of *D.m.*, the phenomenon of axon pruning during metamorphosis serves as a captivating paradigm, offering profound insights into the mechanisms underlying neural remodeling (Truman, 1990).

Among the neurons undergoing metamorphic remodeling, the MB-γ neurons stand as prominent subjects of such studies. During this transformative, phase, the dendrites of MB-γ neurons undergo elimination, while the axons experience pruning followed by regrowth. Precisely, 18h after puparium formation (APF) axons of these neurons are entirely eradicated and initiate axonal regrowth (Figure 7) (Watts, Hoopfer and Luo, 2003). Crucial cellular mechanisms underpinning this process have been elucidated, with the Ubiquitin-Proteasome System (UPS) and signaling pathways such as TGF-β and MAPK cascade emerging as pivotal players (Yu and Schuldiner, 2014; Borgen *et al.*, 2017).

Moreover, glial cells emerge as indispensable contributors to axon and synapse pruning, initiating the process through the secretion of myoglianon (Myo) and facilitating the removal of cell debris during neuronal recycling (Awasaki and Ito, 2004; Awasaki *et al.*, 2011). This complex interplay between neurons and glia cells underscores the multifaceted nature of developmental pruning.

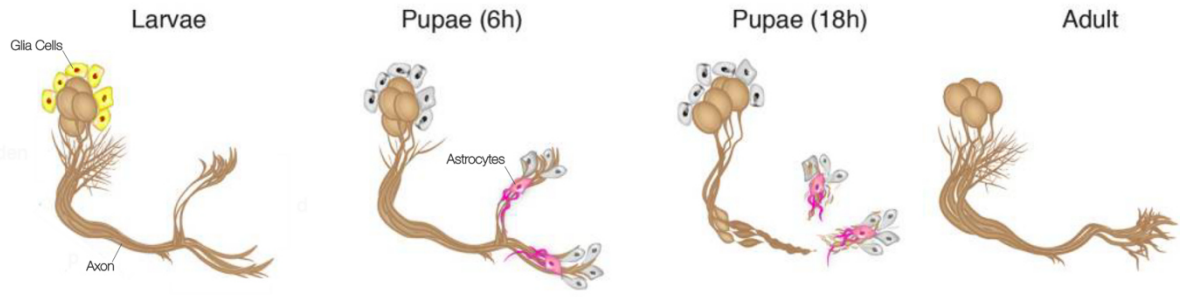

Figure 7. Glia Cell-Mediated Axon Pruning in MB-γ Neurons During *Drosophila Melanogaster* Metamorphosis.

Schematic representation illustrating the process of MB-γ neuron remodeling during *D.m.* metamorphosis. Glia cells (depicted in yellow) in the larval stage initiate axon pruning through the segregation of the TGF-β ligand myoglianon (Myo). By 6 hours after puparium formation (APF), astrocytes (depicted in magenta) invade the neuron position. By 18 hours APF, astrocytes engulf neuronal fragments following their disassembly. Eventually, MB-γ axons regrow and form new synapses in the adult central nervous system (CNS).
Illustration adapted from (Yu and Schuldiner, 2014).

Other studies have shown that throughout metamorphosis, the local degeneration of axons unfolds in a precisely regulated temporal and spatial manner, arranged by a complex coaction of cell-autonomous signaling and communication between neuronal and glial cells. Notably, the With No Lysine (K) (Wnk) kinase emerges as a key regulator of axon maintenance, with its dysregulation leading to branch loss and degeneration during metamorphosis of Ms-neurons (Izadifar *et al.*, 2021).

In conclusion, the process of neuronal circuit formation and plasticity during *D.m.* metamorphosis is marked by dynamic remodeling and precise elimination of axons, dendrites, and synapses. This arranged transition from larval to adult central nervous system is defined by a well-structured developmental program, highlighting the intricacy and precision of molecular mechanisms governing axonal remodeling. Thus, current studies provide profound insights into the complexity of neuronal development and plasticity, offering a glimpse into the remarkable adaptability of the nervous system.

Role of Transcription Factors

The complexities of the nervous system arise from a multitude of factors, chief among them being its genetic composition – a mosaic of diverse genes dynamically expressed in specific developmental windows and distinct tissue locales. In this complex task of gene expression, transcription factors (TFs) emerge as pivotal creators.

TFs are the architects of neuronal specification, differentiation, and maintenance, sculpting the molecular, morphological, and physiological landscapes of diverse neuronal cell types. Previous investigations have unveiled the nuanced expression patterns of TFs within postembryonic neuronal lineages, offering invaluable insights into the complex tapestry of neural development. Indeed, the construction of gene expression map based on TF expression has illuminated the distinct identities of postembryonic lineages (Figure 8) (Lacin *et al.*, 2014).

The profound influence of TFs on neuronal differentiation and complexity beckons us to delve deeper into the networks governing growth and proliferation. Factors such as Yorkie (Yki), part of the Hippo (Hpo) signaling network, come into view as promising subjects for further exploration, offering to unveil the molecular mechanisms of neuronal development.

Figure 8. Transcription Factor Expression Map of Postembryonic Neuronal Lineages.

Illustration depicting the gene expression patterns of transcription factors (TFs) in postembryonic neuronal lineages within a thoracic neuromere. The left half of circles represents the Notch^{ON} hemilineage, while the right half indicated the Notch^{OFF} hemilineage.
Illustration adapted from (Lacin *et al.*, 2014).

5.2. Introduction into Hippo Signaling Network

As elucidated earlier, neuronal development unfolds as a multifaceted journey encompassing growth, pathfinding, remodeling, and plasticity, elaborately orchestrated by distinct molecular pathways operating within precise temporal and spatial contexts. Among these pathways, the Hippo signaling network emerges as a pivotal regulator, long approved in the branch of cancer research and further recognized as a key regulator of organ size control during development, thus demonstrating its evolutionary conservation (Harvey, Pfleger and Hariharan, 2003).

Comprising proteins, kinases, and phosphatases, the Hippo (Hpo) network can be stratified into three principal classes: the core kinase cassette, upstream regulators, and downstream effectors (Staley and Irvine, 2012). Central to this network are the core proteins – Hpo, Warts (Wts), Salvador (Sav), and Mob-as-tumor-suppressor (Mats) – identified as tumor suppressors, as loss-of-function mutations in any of these components' result in overgrowth and hinder apoptosis (Figure 9).

Activation of Hpo core kinase cassette initiates a cascade of phosphorylation events, with Hpo and Wts phosphorylating Sav and Mats, respectively, culminating in the phosphorylation of the downstream effector Yorkie (Yki) (Wu *et al.*, 2008). Phosphorylated Yki undergoes cytoplasmic sequestration and subsequent degradation mediated by the protein 14-3-3, thereby regulating its activity (Oh and Irvine, 2008; Ren, Zhang and Jiang, 2010). Thus, the core kinase cassette exerts its influence through the spatial regulation of Yki, determining its functional status within the nucleus or cytoplasm.

Moreover, upstream regulators within the Hpo network offer insights into cellular architecture and the microenvironment, predominantly influencing aspects of cell polarity and cellular junctions (Staley and Irvine, 2012). As we unravel the complexity of this signaling cascade, we glean invaluable insights into the fundamental mechanisms governing neuronal development and plasticity, paving the way for transformative discoveries in neurobiology.

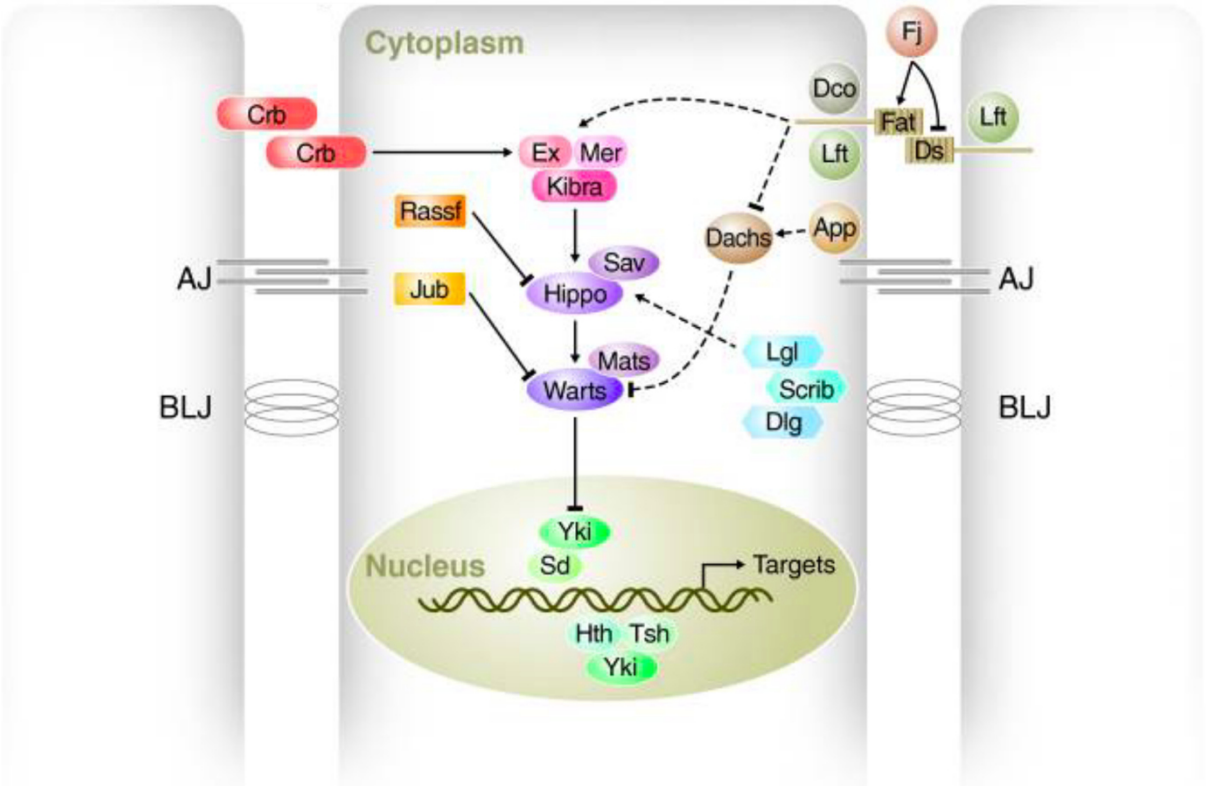

Figure 9. The Hippo Signaling Network: Core Components and Regulatory Factors.

Graphic representation of the Hippo (Hpo) signaling network in *Drosophila Melanogaster.* Neuronal cells are depicted as grey rectangles with adherens junctions (AJ) and basolateral junctions (BLJ) connecting them. Components of the Hpo network are color-coded, illustrating their various interactions through arrowheads indicating inhibitory (blunted arrow) or activating (pointed arrow) interactions. Direct interactions are depicted with continuous lines, while dotted lines represent unknown molecular mechanisms. Core kinase cassette proteins (Hpo, Sav, Wts, and Mats) are shown in purple. Upstream regulators include the tumor suppressor complex Ex-Mer-Kibra (depicted in magenta), the apical-basal polarity organizer Crb (depicted in red), the cell-polarity complex Fat (depicted in beige), and the neoplastic tumor suppressor complex (LGL). Downstream regulators feature Yki and its DNA binding partner Sd, Hth, or Tsh.

Abbreviations: App, Approximated; Crb, Crumbs; Dco, Disc overgrown; Dlg, Discs large; Ds, Dachsous; Ex, Expanded; Fj, Four-jointed; Hth, Homothorax; Jub, Drosophila Ajuba; Lft, Lowfat; Lgl, Lethal giant larvae; Mer, Merlin; Mats, Mob as a tumor suppressor; Rassf, Ras-associated factor; Sav, Salvador; Scrib, Scribble; Sd, Scalloped; Tsh, Teashirt; Yki, Yorkie.

Graphic adapted from (Halder and Johnson, 2011).

Yki Structure and Function

The main role of the Hpo network revolves around the twisted function of its key effector, Yki. Activation of the Hpo network triggers phosphorylation of its core proteins, culminating in the phosphorylation of Yki and subsequent degradation. Conversely, inactivation of the Hpo network leads to Yki translocating from the cytoplasm to the nucleus, where it orchestrates the transcription of specific growth and proliferation genes – a testament to the dynamic connection between molecular pathways dictating cellular fate.

Delving into the multifaceted functions of Yki shows its diverse roles across biological contexts. Structurally, Yki harbors an N-terminal region implicated in non-transcriptional functions at the cell cortex (J. Xu *et al.*, 2018). Moreover, Yki features several Serine (Ser) residues (Ser^{97}, Ser^{111}, Ser^{168}, Ser^{250}) targeted for phosphorylation by the Hpo core cassette kinases, modulating its activity and downstream signaling (Oh and Irvine, 2010). Additionally, Yki's WW-domains facilitate protein-protein interactions with key partners of the network, such as Expanded (Ex) and Merlin (Mer), underscoring its role as a nexus in the complex web of signaling pathways (Figure 9) (Snigdha *et al.*, 2019).

Furthermore, Yki undergoes alternative splicing, leading to the presence of various isoforms within the organism. Specifically, the Exon 3 produces the Yki1 variant with a single WW-domain, while the absence of splicing in Exon 3 results in the Yki2 variant, which contains two WW-domains (Srivastava *et al.*, 2021). According to FlyBase, three distinct isoforms of Yki have been identified, differing in their N-terminal regions, total amino acid lengths, and the number of WW-domains (Figure 10) (*JBrowse 2R:24065912..24068147*, no date).

Functionally, Yki operates as a transcriptional co-activator, collaborating with DNA-binding partners, such as Scalloped (Sd) or Homothorax (Hth), to drive the expression of genes critical for cell proliferation, survival, and cytoskeletal dynamics (Goulev *et al.*, 2008). Canonical target genes include Diapherous 1 (Diap1), Ex, Cyclin E (CycE), and Kibra, implicated in cell cycle progression and anti-apoptotic pathways (Wu *et al.*, 2008; Zhao, Moberg and Veraksa, 2023). Notably, some Yki target genes are interconnected with the Hpo network, engendering a negative feedback loop that perpetuates network dynamics (Figure 9).

Thus, the multifaceted functions of Yki within the Hpo network illuminate its central role in facilitating cellular fate and homeostasis, showing its significance as a hub in the complex landscape of molecular signaling pathways governing neuronal development and plasticity.

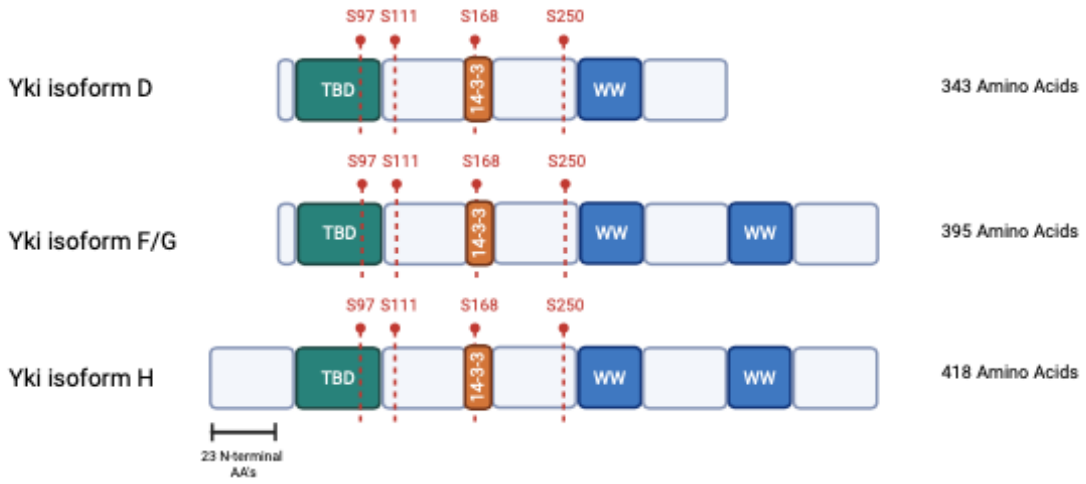

Figure 10. Structural Features of *Drosophila Melanogaster* Yorkie Protein Isoforms.

Graphic depiction of *D.m.* Yki protein structure isoforms. Key structural domains are highlighted, including the Scalloped (TBD) binding domain (depicted in green), essential for Ykis transcriptional activator function. WW-domains are illustrated (depicted in blue), crucial for Ykis various protein-protein interactions. Additionally, important Serine (Ser) phosphorylation sites (Ser^{97}, Ser^{111}, Ser^{168}, Ser^{250}) are highlighted (depicted in red). Yki isoform D possesses only one WW-domain and lacks the 23 N-terminal amino acids, which are present in Yki isoform H. Furthermore, Yki isoform F/G consist of two WW-domains, like Yki-H but lacks the N-terminal features, like Yki-D.
Graphic designed using BioRender.

Control of Yki Subcellular Localization

The activity of the Hpo network hinges upon the subcellular localization of Yki, serving as a hub in defining cellular fate. Yki collaborates with DNA-binding partner proteins to function as a transcription factor, instigating the transcription of genes vital for growth and survival – a process precisely regulated to maintain cellular homeostasis. Recent advancements in research have shed light on the dynamic nature of Yki subcellular localization. Manning *et al.*, (2018) employed live multiphoton microscopy to elucidate the dynamics of Yki in epithelial tissues, unveiling rapid shuttling between the cytoplasm and nucleus. Notably, their findings revealed distinct rates of Yki shuttling across different cell populations, showing the nuanced regulation of this essential signaling node.

In a developmental quest to unravel Yki target genes in neurons, Brat (Brain Tumor) emerged as a notable candidate (Kowalczyk *et al.*, 2022). Characterized as a tumor suppressor gene, Brat exerts multifaceted developmental functions, including involvement in early embryonic patterning. This comprehensive understanding illuminates the complexity of the Hpo-Yki signaling network and its profound implications for developmental biology. As I delved deeper into the complexities of this signaling cascade, I unraveled the complex mechanisms facilitating cellular fate and display the pivotal role of Yki in managing the delicate balance between growth and survival during neuronal development.

5.3. Introduction into Function of Brat

The *D.m.* gene Brain Tumor (Brat) encodes a member of the TRIM-NHL protein family, playing a pivotal role as a translational repressor that effectively curtails cell proliferation. Structurally, the Brat protein comprises 1037 amino acids, featuring and N-terminal Tripartite Motif (TRIM) domain and a C-terminal NHL (NCL-1, HT2A, and Lin41) domain. Notably, the C-terminal domain harbors a crucial β-Propeller structure essential for Brat's optimal functionality, facilitating its RNA-binding capacity. Conversely, the N-terminal domain houses two B-box zinc finger regions crucial for DNA binding, delineating Brat's multifaceted molecular architecture (Figure 11) (Arama *et al.*, 2000; Edwards *et al.*, 2003; Loedige *et al.*, 2014).

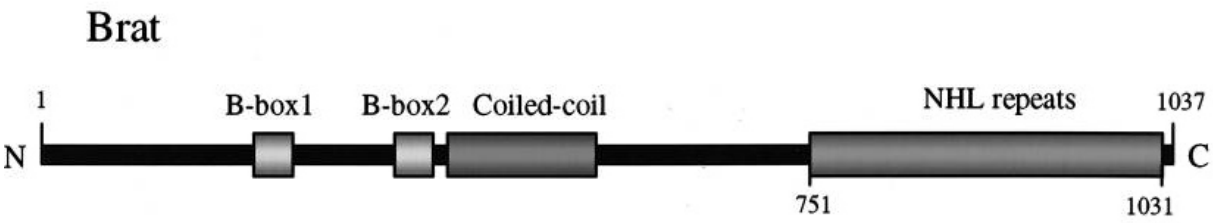

Figure 11. Structural Features of the *Drosophila Melanogaster* Brat Protein.

Graphic representation of the Brat Protein structure. The Brat amino acid sequence consist of an N-terminal domain containing two B-box regions and a Coiled-coil domain, essential for protein-protein interactions. Additionally, the C-terminal domain comprises an NHL region, including the β-Propeller domain, crucial for RNA-binding.
Graphic adapted from (Edwards *et al.*, 2003).

Functionally, Brat operates as a sequence-specific RNA-binding protein, capable of binding to specific mRNAs and stimulating their degradation. This mode of developmental control enables precise regulation of translation without altering transcript levels, particularly crucial during critical developmental time points such as early embryogenesis and the maternal-to-zygotic transition (MTZ) (Sonoda and Wharton, 2001; Cho *et al.*, 2006). Furthermore, studies in larval brain development underscore Brat's tumor suppressor function, as mutations in Brat lead to tumorous overgrowth, particularly evident during neuroblast asymmetric division, disrupting neuronal tissue homeostasis and fostering the emergence of additional neuroblasts (Figure 12) (Arama *et al.*, 2000; Reichardt *et al.*, 2018). Notably, Brat also plays a crucial role in postmitotic neuron development, where it collaborates with cofactors Pumilio (Pum) and Nanos (Nos) to modulate motor neuron excitability by repressing translation of voltage-gated sodium channel subunit Paralytic (Para). Importantly, this regulatory function of Brat exhibits cell type specificity for neurons, underscoring its multifaceted involvement across various developmental processes such as synaptic growth regulation, endocytosis, and neuronal differentiation (Muraro *et al.*, 2008). In summary, Brat emerges as a versatile regulator integral to numerous developmental processes, shedding light on its pivotal role in managing complex molecular mechanisms governing neuronal development in *D.m*.

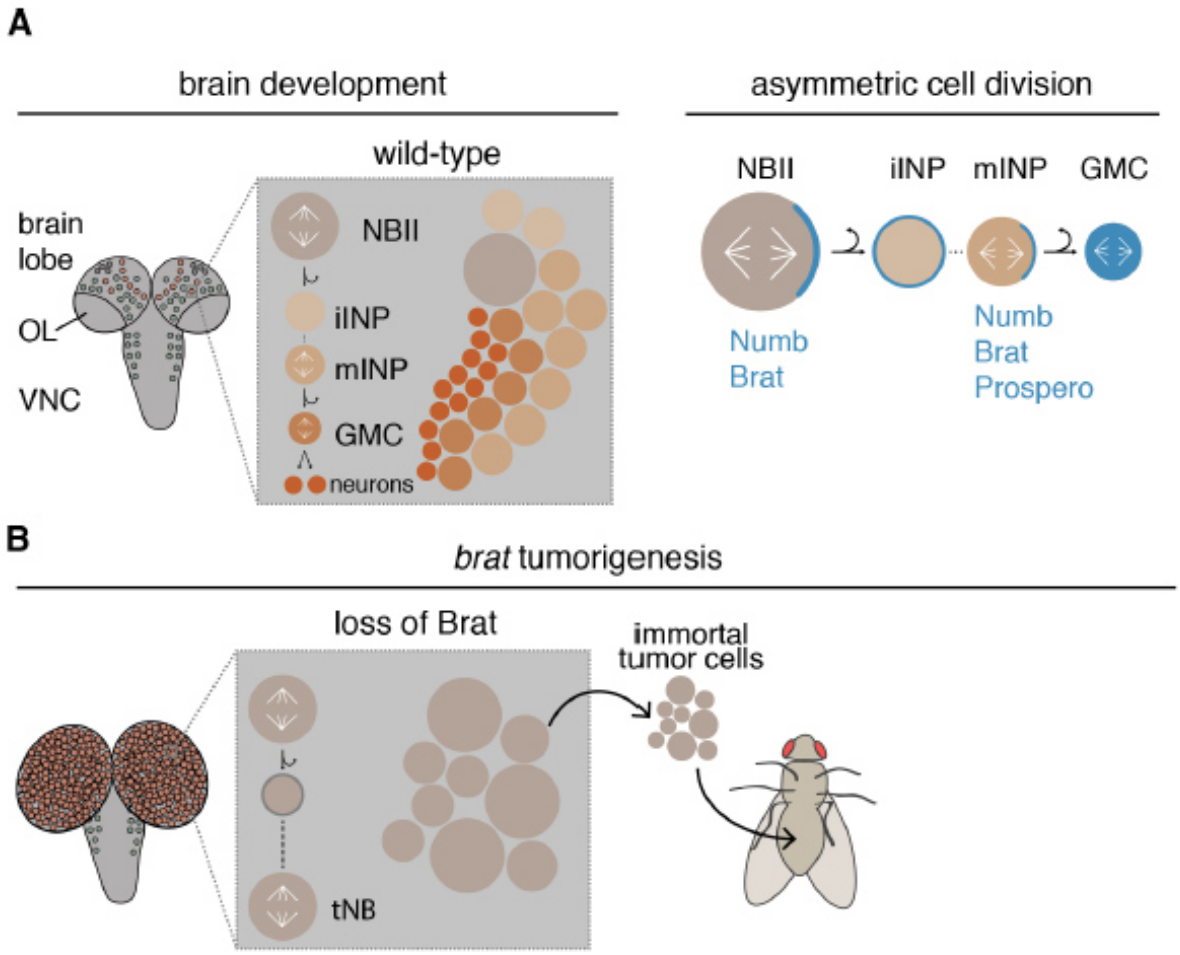

Figure 12. Impact of Brat Mutation on *Drosophila Melanogaster* Neuroblast Development.

Illustration depicting the consequences of Brat mutation on neuroblast (NB) development in *D.m.*

(A) Developmental stages of the larval brain, depicted with brain lopes (optic lobes (OP)) and ventral nerve chord (VNC) in wild-type NBII (depicted in grey), immature intermediate neural progenitor (iINP) (depicted in light beige), mature intermediate neural progenitor (mINP) (depicted in beige), ganglion mother cell (GMC) (depicted in light orange), and neurons (depicted in orange). The asymmetric cell division process is highlighted in wild-type NBII development, showcasing the localization of Brat, Prospero, and Numb proteins (depicted in blue) influencing lineage directionality.

(B) Brat tumorigenesis leads to failed differentiation of daughter cells, resulting in the formation of ectopic tumor neuroblasts (tNB). Additionally, Brat tumors exhibit continuous growth even after transplantation.

Graphic adapted from (Landskron *et al.*, 2018).

5.4. Aim of this Study

This dissertation aims to elucidate the intricate processes underlying neuronal development, with a particular focus on the formation of axon branching patterns and synaptogenesis. Recognizing the multifaceted nature of neuronal circuit formation, the study delves into both cell-autonomous mechanisms and the dynamic interplay with surrounding tissue. Building upon recent findings implicating the Hpo signaling network in axon branching, our investigation, informed by new insights form the Halder lab, seeks to unravel the role of Yki and its target genes in the fundamental processes.

Drawing from established knowledge of Brat as a translational repressor and Yki as a transcriptional co-activator, I hypothesize a regulatory balance between these molecules in modulating axon branching and synaptogenesis in Ms-neurons. To test this hypothesis, I undertook an RNAi screen targeting Ykis neuronal target genes during Ms-neuron development in *D.m*. Additionally, I explored the consequences of Brat LOF on axon branching and synapse number in Ms-neurons.

Moreover, I investigated Ykis function and subcellular localization in *D.m.* cell culture, examining the impact of Yki GOF on gene expression and neuronal cell proliferation. Finally, bulk RNA-sequencing analyses aim to uncover differential gene expression patterns upon Yki overexpression in neurons compared to non-neuronal cells.

By addressing these research objectives, the dissertation endeavors to provide insights into the role of Yki and its targets in postmitotic neurons, thereby advancing our understanding of the molecular mechanisms underlying neuronal development and circuit formation.

6. Material & Methods

6.1. Materials

Flystocks and Crossbreeds

Table 1. Genotypes of Flies Used in this Dissertation.

Figure	Genotype
1C	*w Lac-Z-RNAi; +/ DC1.4-Flp; UAS-FRT>STOP>FRT-CD8::GFP-2A-APEP-mCherry::Syt1 pnr-Gal4/+*
2A	*w Lac-Z-RNAi; +/ DC1.4-Flp; UAS-FRT>STOP>FRT-CD8::GFP-2A-APEP-mCherry::Syt1 pnr-Gal4/+*
2B	*w; +/ DC1.4-Flp; Dpr18-RNAi (BL-#29604)/ UAS-FRT>STOP>FRT-CD8::GFP-2A-APEP-mCherry::Syt1 pnr-Gal4*
2C	*w; Ptp61F-RNAi (BL-#56036)/ DC1.4-Flp; UAS-FRT>STOP>FRT-CD8::GFP-2A-APEP-mCherry::Syt1 pnr-Gal4/+*
2D	*w; Spen-RNAi (BL-#50529)/ DC1.4-Flp; UAS-FRT>STOP>FRT-CD8::GFP-2A-APEP-mCherry::Syt1 pnr-Gal4/+*
2E	*w; +/ DC1.4-Flp; Sty-RNAi (VDRC-#6948)/ UAS-FRT>STOP>FRT-CD8::GFP-2A-APEP-mCherry::Syt1 pnr-Gal4*
2F	*w; Scrib-RNAi (VDRC-#100363)/ DC1.4-Flp; UAS-FRT>STOP>FRT-CD8::GFP-2A-APEP-mCherry::Syt1 pnr-Gal4/+*
3A	*w Lac-Z-RNAi; +/ DC1.4-Flp; UAS-FRT>STOP>FRT-CD8::GFP-2A-APEP-mCherry::Syt1 pnr-Gal4/+*
3B	*w; +/ DC1.4-Flp; Brat-RNAi (BL-#28590)/ UAS-FRT>STOP>FRT-CD8::GFP-2A-APEP-mCherry::Syt1 pnr-Gal4*
3C	*w; +/ DC1.4-Flp; Brat-RNAi (BL-#34646)/ UAS-FRT>STOP>FRT-CD8::GFP-2A-APEP-mCherry::Syt1 pnr-Gal4*
3D	*w; Brat-RNAi (BL-#105054)/ DC1.4-Flp; UAS-FRT>STOP>FRT-CD8::GFP-2A-APEP-mCherry::Syt1 pnr-Gal4/+*
3E	*w; Brat-RNAi (BL-#105054)/ DC1.4-Flp; Brat-RNAi (BL-#28590)/ UAS-FRT>STOP>FRT-CD8::GFP-2A-APEP-mCherry::Syt1 pnr-Gal4*
3F	*w; UAS-Brat (BL-#22170)/ DC1.4-Flp; UAS-FRT>STOP>FRT-CD8::GFP-2A-APEP-mCherry::Syt1 pnr-Gal4/+*
4A	*w; tub-Gal80, FRT40A/ FRT40A; pnr-Gal4 UAS-CD8::mCherry UAS-Brp^{short}::GFP/ DC1.4-Flp*
4B	*w; tub-Gal80, FRT40A/FRT40A, Brat^{1}; pnr-Gal4 UAS-CD8::mCherry UAS-Brp^{short}::GFP/ DC1.4-Flp*
4C	*w; tub-Gal80, FRT40A/FRT40A, Brat$^{2L\text{-}150\text{-}11}$; pnr-Gal4 UAS-CD8::mCherry UAS-Brp^{short}::GFP/ DC1.4-Flp*
4D	*w; tub-Gal80, FRT40A /FRT40A, Brat^{11}; pnr-Gal4 UAS-CD8::mCherry UAS-Brp^{short}::GFP/ DC1.4-Flp*
4E	*w; tub-Gal80, FRT40A/FRT40A, Brat^{18}; pnr-Gal4 UAS-CD8::mCherry UAS-Brp^{short}::GFP/ DC1.4-Flp*
4F	*w; tub-Gal80, FRT40A/FRT40A, Brat^{K06028}; pnr-Gal4 UAS-CD8::mCherry UAS-Brp^{short}::GFP/ DC1.4-Flp*
6A	*w Lac-Z-RNAi; +/ DC1.4-Flp; UAS-FRT>STOP>FRT-CD8::GFP-2A-APEP-mCherry::Syt1 pnr-Gal4/+*
6B	*w; Creld-RNAi (BL-#67323)/ DC1.4-Flp; Creld-RNAi (BL-#51741)/ UAS-FRT>STOP>FRT-CD8::GFP-2A-APEP-mCherry::Syt1 pnr-Gal4*

Antibodies

Table 2. Primary Antibodies Used in this Dissertation.

Primary Antibody	Manufacturer	Dilution
Polyclonal α-GFP	Invitrogen	1:250
Polyclonal α-DsRed	Takara	1:350
Polyclonal α-Yki	Davids Biotechnologie	1:250
Monoclonal α-mNeonGreen	Chromotek	1:250
Monoclonal α-Lamin	DSHB	1:500
Monoclonal α-Repo	DSHB	1:250
Monoclonal α-Elav	DSHB	1:250
DAPI	Invitrogen	1:1000

Table 3. Secondary Antibodies Used in this Dissertation.

Secondary Antibody	Manufacturer	Dilution
α-mouse-488	Invitrogen	1:500
α-rabbit-555	Invitrogen	1:500
α-rat-633	Invitrogen	1:500
α-HRP-637	Invitrogen	1:500
α-guinea pig-555	Invitrogen	1:500
α-phalloidine-488	Invitrogen	1:500

6.2. Methods

Flywork & Crossing

Flies were maintained on standard medium (see 9.4) at room temperature (RT). For experimental crossings, flies were housed at either 25°C or 29°C in incubators with a consistent day and night cycle.

Drosophila Genetics

D.m. genotypes utilized in this dissertation are outlined in Table 1. UAS-RNAi knock-down lines were procured from the Vienna Drosophila Resource Center (VDRC) and the Bloomington Drosophila Stock Center (BDSC).

Genetic Labeling of Mechanosensory Neurons

To label single neurons in the VNC of *D.m.*, the *pannier* (pnr) Gal4 driver was employed. This driver is expressed broadly along the dorsal midline of the imaginal tissue (Heitzler *et al.*, 1996). Specificity was achieved through the use of the DC1.4 enhancer, active only in the precursor cells of DC neurons (García-García *et al.*, 1999). The proneural enhancer DC1.4 restricts pnr Gal4 activity via a FLP-recombinase (DC1.4-Flp), which excises an FRT-flanked transcriptional STOP cassette, enabling single-cell labeling (Figure 13). Consequently, transgenes for labeling and gene knock-down (e.g., UAS-Brat RNAi) can be selectively expressed in single DC neurons (Urwyler *et al.*, 2015).

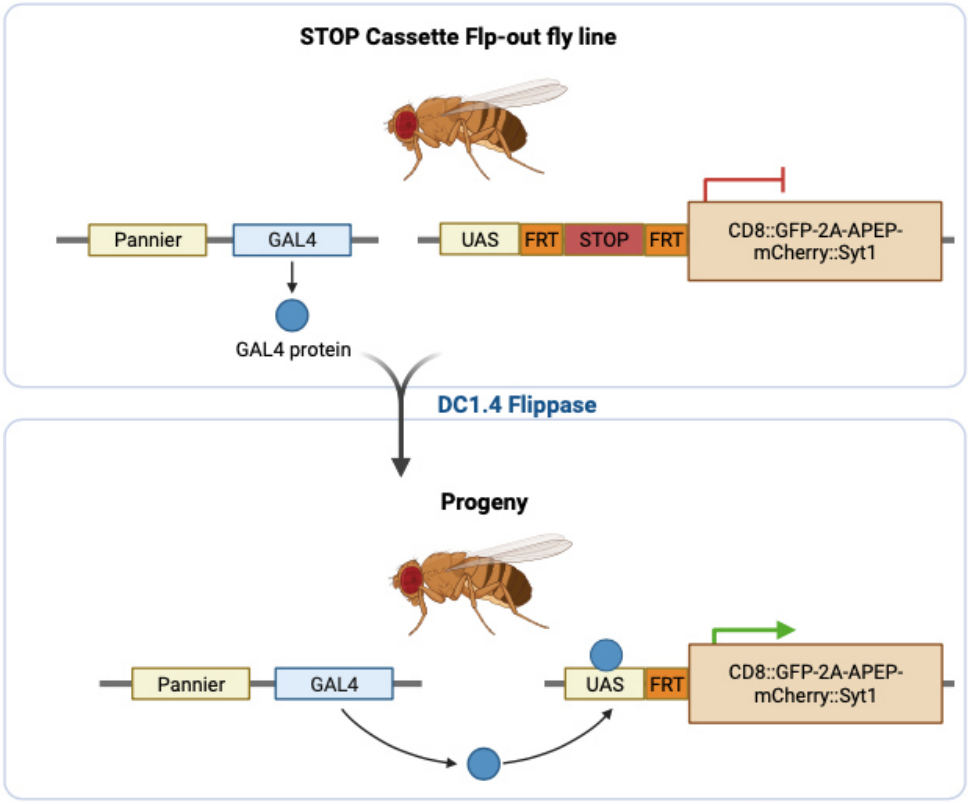

Figure 13. Illustration of Flp-out Fly Line.

The Flp-out fly line comprises the *pannier* promoter driving the Gal4 protein and a Flippase enzyme, specifically activated in DC neurons by the DC1.4 enhancer. This triggers the excision of the FRT-flanked STOP cassette, leading to the expression of fluorescent proteins in axonal membranes and synapses. The 2A virus sequence induces ribosome skipping during translation, while APEP serve as a consensus acceptor peptide for a biotin ligase (Beckett, Kovaleva and Schatz, 1999; Szymczak *et al.*, 2004; Urwyler *et al.*, 2015).

Mosaic Analysis with Repressible Cell Marker (MARCM) Fly Generation

For generating MARCM stocks, the proneural enhancer DC1.4 was utilized to confer specificity in Ms-neurons. Typically, MARCM stocks encompass an FLP recombinase, a tubulin1-promoter driving the Gal80 repressor, an FRT site, Gal4, and a UAS-marker (Wu and Luo, 2006). Flies employed in this dissertation harbored the FRT40A site. In conjunction with the DC1.4 Flippase, mutant clones were specific to DC neurons. The crossing schemes for MARCM fly generation are depicted in Figure 14.

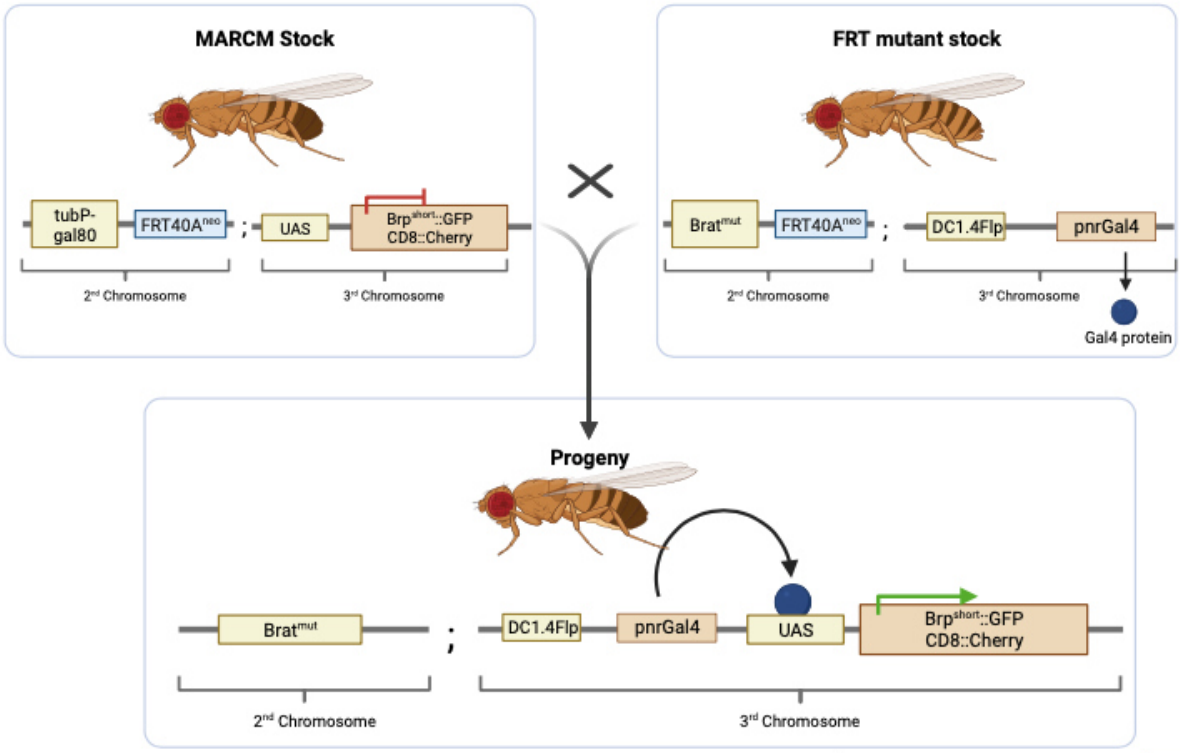

Figure 14. Cross Between Mosaic Analysis with Repressible Cell Marker (MARCM) Stock and a Brat Mutant Fly Stock.

Illustration of genetic maneuver combining the sophisticated Mosaic Analysis with Repressible Cell Marker (MARCM) technique with the genetic background of a Brat mutant fly strain. In the MARCM stock, strategically positioned genetic elements orchestrate the spatial and temporal expression patterns. Specifically, the tubP-gal80 repressor and FRT40A^{neo} site on the 2nd Chromosome, alongside the UAS-Brp^{short}::GFP synapse marker and CD8::Cherry axon membrane marker on 3rd Chromosome, delineate intricate cellular territories. On the other hand, the FRT mutant stock comprises the Brat mutation and FRT 40A^{neo} site on 2nd chromosome, complemented by the *pannier* promoter driving the expression of Gal4 protein and a Flippase enzyme, selectively activated in DC neurons via the DC1.4 enhancer on the 3rd Chromosome. The deliberate crossing of these stocks yields a fluorescently labeled DC neuron harboring a mutation in the Brat gene.

Immunohistochemistry

For immunostaining, adult *D.m.* VNCs were dissected in a glass dish in 1X PBS and subsequently transferred to 2% (v/v) paraformaldehyde in 0.1% (v/v) PBS-TX100 for 90 minutes at RT. After fixation, VNCs underwent 4x 15-minute washes in 0.1% PBS-TX100 and were then blocked overnight in 5% (m/v) milk in PBS-TX100 at 4°C. Following further washes, 4x 15 minutes in 0.1% PBS-TX100, VNCs were incubated with primary antibody (Table 2) in 5% milk/PBS-TX100 overnight at 4°C. The next day VNCs were washed again, 4x for 15 minutes with 0.1% PBS-TX100, and then incubated with secondary antibody (Table 3) for 2 hours at RT in the dark. Afterwards, the last washing steps were performed, 4x for 15 minutes with 0.1% PBS-TX100, and finally mounted in Vectashield prior to imaging. All steps were caried out on a rocking platform with gentle shaking.

Cell Culture

Cell culture experiments utilized larval CNS-derived ML-BG3-c2 (Bg3c2) (Ui *et al.*, 1994) and embryo-derived Schneider (S2) cells obtained from the DGRC. Cells were cultured at 25°C in Schneider's medium supplemented with 10% heat-inactivated FBS and 100 units/mL penicillin – 100 µg/mL streptomycin. Bg3c2 cells received additional supplementation with 10 µg/mL insulin. Culturing of Bg3c2 cells involved diverse coatings; poly-D-lysine, laminin, and fibronectin-coated cell culture dishes were incubated with 5 µg/cm^2 coating solutions for 45 minutes at RT. To maintain healthy culture conditions, cell density was kept within the exponential growth range (Cherbas and Gong, 2014). S2 cells have a faster grow rate than Bg3c2 cells and required more regular splitting.

Plasmid Cloning

The *D.m.* metallothionine-inducible pMT/V5-HisA plasmid (Figure S1) served as the vector for Yki overexpression in this study. To construct the Yki overexpression vector, the Yki-RD* gene transcript (Figure 15) was first amplified via PCR, utilizing the FMO01054 vector as template (Figure S2). Primers designed for Gibson cloning, as described by (Gibson *et al.*, 2009), were employed in this cloning process. Simultaneously, the gene encoding the fluorescent mNeonGreen protein (Shaner *et al.*, 2013) was amplified through PCR, utilizing the gBlock as template, with primers designed for Gibson cloning. Subsequently, the

pMT/V5-HisA vector was linearized and purified through gel electrophoresis. Following, the PCR amplified Yki-RD* and mNeonGreen transcripts were cloned into the linearized pMT/V5-HisA vector (Figure S3). As control solely the mNeonGreen transcript was cloned into the pMT/V5-HisA vector (Figure S4). The resulting colonies were verified through sequencing to ensure accuracy of cloning. Plasmid maps and sequences are depicted in the Appendix.

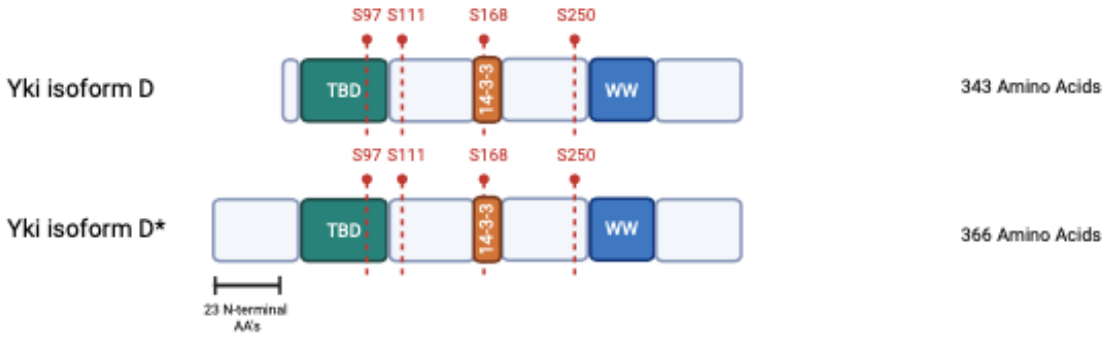

Figure 15. Structural Features of Yki Isoform used for Cloning.

Illustration of Yki isoform D and D* highlighting their structural features. The isoform D* used in this cloning includes 23 additional N-terminal amino acids, while maintaining overall structural similarity to the D isoform.
Graphic designed using BioRender.

Transfection

Transfection of cells was performed using the Effectene transfection reagent (QIAGEN, (*Effectene Transfection Reagent*). Cells were grown to a confluency of 60-80%, corresponding to approx. 1.0-3.0 x 10^5 cells/ml for Bg3c2 cells and 1.0-2.0 x 10^6 cell/ml for S2 cells. Transfection was carried out with 0.15 µg DNA, which was incubated with Buffer EC and Enhancer to achieve optimal salt conditions for DNA condensation. The DNA/Buffer/Enhancer mix was incubated with Effectene to form Effectene-DNA complexes, which were subsequently mixed into the cell medium according to the manufacturer's protocol (*Effectene Transfection Reagent*). Plasmids were induced with 750 µM copper sulfate 24 hours post-transfection due to the presence of a metallothionein-inducible promoter in the plasmids.

Staining

For immunostaining of Bg3c2 and S2 cells, cells were washed for 5 minutes in pre-warmed 1x PBS. Subsequently, fixation was performed with 3.7% (v/v) PFA in 1x PBS for 15 minutes at RT. After fixation, cells underwent washes with 1x PBS (2x 10 minutes) and 0.3% (v/v) PBST (1x 10 minutes), followed by blocking with 1% (m/v) BSA in 1x PBS for 30 minutes at RT. Cell were then incubated with primary antibodies (Table 2) diluted in 0.3% PBST overnight at 4°C. The next day, cells were washed with 1 x PBS at RT (3x 5 minutes) and incubated with secondary antibodies (Table 3) diluted in 0.3% PBST for 90 minutes at RT in the dark. Following additional washes with 1x PBS at RT (3x 5 minutes), cells were incubated with DAPI for 8 minutes at RT in the dark. After 3x washings with 1x PBS for 5 minutes, cells were mounted in ProLong™ Diamond mounting medium (Invitrogen) and stored at 4°C until imaging. All incubation and washing steps were caried out on a rocking platform with gentle shaking.

EdU Staining

Proliferating cells were stained using the Click-iT™ EdU assay (Daul, Komori and Lee, 2010), employing a protocol divided in several steps. Initially, following transfection and induction (Transfection), cells were exposed to a 10 µM EdU solution for 2-4 hours at 25°C. Subsequently, cells were fixed in 3.7% (v/v) PFA in 1x PBS, washed with 3% (m/v) BSA in 1x PBS, and then permeabilized with 0.5% (v/v) Triton® X-100 in 1x PBS, adhering strictly to the manufacturer's guide regarding incubation and washing times (Invitrogen, Molecular Probes). Hybridization was then performed to identify EdU in proliferating cells. This involved preparing a reaction cocktail with $CuSO_4$, reaction buffer, and an Alexa Flour-555 azide as per the manufacturer's instructions, which was then added to the cells for a 30-minute period, protected from light. Subsequent steps involved washing and staining with primary and secondary antibodies, as well as nuclear staining. All steps, including incubations and washes, were carried out on a rocking platform with gentle shaking.

RNA extraction & Quantitative Real Time PCR

Total RNA extraction was conducted using TRIzol® Reagent (*TRIzol™ Reagenz*). For cell suspension or 10 larval/adult brains, 600 µL of TRIzol® was utilized. Homogenization was performed using a Precellys 24 homogenizer for larval and adult brains, or with a fresh pestle for cell suspension. The homogenized TRIzol® suspension was incubated at RT for 5 minutes before adding chloroform ($CHCl_3$) in a ratio of 1:5. After mixing and incubation for 3 minutes at RT, the suspensions was centrifuged at 12,000 g for 10 minutes at 4°C. The aqueous phase was then collected and precipitated with isopropanol in a ratio of 1:1, followed by an overnight incubation at -20°C. The following day, the solution was centrifuged at 12,000 g for 30 minutes at 4°C, and the supernatant was removed. The resulting pellet was washed with 500 µL 80% ethanol (EtOH) and centrifuged again (12,000 g for 5 minutes at 4°C). After centrifugation ethanol was removed, and the pellet was dried and resuspended in 100 µL nuclease-free H_2O. After resuspension 10 µL of 3M NaAc was added together with 3 volumes of 100% EtOH, followed by incubation overnight at -20°C. The solution was then centrifuged at maximum speed for 30 minutes at 4°C, followed by removal of the supernatant and addition of 200 µL of 80% cold EtOH. Finally, the solution was centrifuged at maximum speed for 15 minutes at 4°C, followed by removal of the supernatant and drying of the pellet with subsequent resuspension in 20 µl nuclease-free H_2O. RNA concentration was determined using a NanoDrop 8000 Spectrophotometer.

For cDNA synthesis, RNA was processed according to manual for LunaScript RT SuperMix Kit (*LunaScript® RT SuperMix Kit | NEB*). Quantitative real-time PCR experiments were conducted using Luna Universal qPCR Master Mix (*Luna® Universal qPCR Master Mix | NEB*) and the Real-time PCR Detection System (*CFX Connect Real-Time PCR Detection System | Bio-Rad*), following the manufacturer's instructions. Data analysis utilized the comparative C_T method ($\Delta\Delta C_T$) with Actin5c as housekeeping gene. Primer sequences are detailed in Table S.

Fluorescence-Activated Cell Sorting and RNA-Sequencing

We conducted fluorescent activated cell sorting (FACS) using the AriaIII cell sorter (*BD FACSAria™ III | High Sensitivity Flow Cytometer*, no date). Initially, wells were scraped and centrifuged at 1000 rpm for 5 minutes. The resulting cell pellets were resuspended in 1x PBS containing 100 mM (v/v) EDTA. To prevent cell clumping, the cell suspension was passed through a 30 µM cell strainer and kept on ice until sorting. Sorting was performed using a 70 µM nozzle with a flow rate of 1.0 to optimize sorting conditions. If necessary, cell suspension was diluted with 1x PBS to achieve optimal sorting conditions ranging from 1000 to 3000 events/second. Following sorting, cells were resuspended in cold 1xPBS, centrifuged at 1000 rpm for 5 minutes, and then resuspended in TRIzol® for storage at -80°C until further processing. RNA extraction was carried out as described in section 0.
Subsequently, RNA sequencing library preparation was conducted using the QuantSeq 3' mRNA-Seq Library Prep Kit FWD (Lexogen, 2015). The resulting libraries were subjected to sequencing using the NovaSeq 6000 platform, facilitated by the NGS core facility ('Next Generation Sequencing').

Image Acquisition & Analysis

Image acquisition was performed utilizing a Zeiss LSM 710 confocal microscope. For graphical design purposes, ImageJ/FIJI, Gimp-2.10, Adobe-Photoshop and Inkscape software were employed. Confocal stacks underwent flattening and despeckling, with adjustments made to their levels. Additionally, images were rotated to position the axon entry point on the left side. Illustration of data and statistical analysis was carried out using GraphPad Prism and Excel 2018. Significance testing, with experiments involving $n \geq 5$, was conducted by calculating the Student's T-test for normally distributed data. For data not following normal distribution, the Mann-Whitney-U test was employed. Significance levels were denoted as follows: * = $p < 0.05$; ** = $p < 0.01$; *** = $p < 0.001$ and **** = $p < 0.0001$.

7. Results

7.1. A Comprehensive Reverse Genetic Screen for Identifying Key Genes in Axonal Development and Synaptogenesis

Reverse genetic screens, ubiquitous in life sciences, serve as a foundational method to elucidate gene functions during specific developmental periods and within targeted tissues. Numerous screens within the nervous system have employed distinct cellular systems, with a primary focus on the central nervous system (CNS) development, emphasizing genes associated with neuronal growth regulation and synaptogenesis. Despite the wealth of publications concentrating on various cellular systems, such as the CNS of developing embryos, neuronal morphogenesis in the mushroom body, wiring specificity in the olfactory system, and regulation of target specificity in photoreceptor neurons, several studies face limitations (Hong and Luo, 2014; Yogev and Shen, 2014; Boulanger and Dura, 2015; Accogli, Addour-Boudrahem and Srour, 2020). The challenges arise from the complex structure and morphology of neurons and the simultaneous labeling of multiple axons or dendrites, making the precise characterization of specific gene phenotypes a formidable task.

In pursuit of a more nuanced understanding of axonal development and synaptogenesis, this dissertation adopts a unique approach by investigating the mechanosensory neurons (Ms-neurons) of adult *Drosophila Melanogaster*. These Ms-neurons, characterized by their stereotyped axonal branching pattern as illustrated in Figure 16 (Ghysen, 1980), present an ideal model system for *in vivo* exploration of synapse development and plasticity. Prior research projects have underscored the advantages of Ms-neurons, paving the way for the establishment of diverse genetic and imaging tools, including the *D.m.* fly lines introduced by Urwyler *et al.*, (2015). These resources enable the study of individual Ms-neurons within the heterogenous CNS, offering insights into axonal morphology and synapse number.

The dissertation narrows its focus to the morphology and synapse number of specific Ms-neurons innervating the thoracic anterior dorsocentral macrochaeta. These Ms-neurons project their axons into the ventral nerve cord (VNC) during pupal remodeling, providing a critical developmental context for the study (Ghysen, 1978).

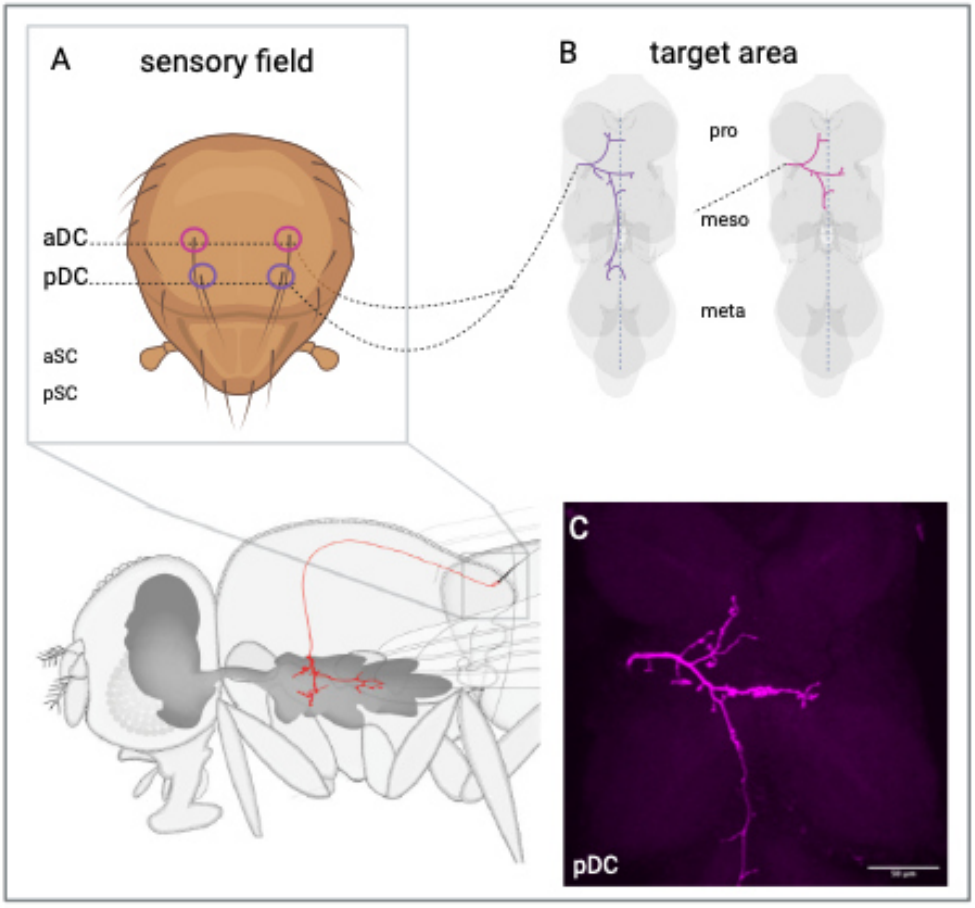

Figure 16. Stereotyped Axonal Branching Pattern of Mechanosensory Neurons.

(A) Overview *of Drosophila Melanogaster* thorax: Schematic representation of *D.m.* central nervous system (CNS) featuring Ms-neuron innervating a thoracic bristle and projecting into the ventral nerve cord (VNC) highlighted in red. Inset shows a detailed depiction of the *D.m.* thorax sensory field with four distinct types of Ms-neurons: aDC (anterior dorsocentral), pDC (posterior dorsocentral), aSC (anterior scutellar), and pSC (posterior scutellar).

(B) Ventral nerve cord target area: Schematic illustration of the VNC target area with innervating aDC Ms-neuron (depicted in pink) on the right and innervating pDC Ms-neuron (depicted in purple) on the left. Different thoracic neuromeres (pro, meso, meta) are indicated, and dotted lines represent the CNS midline.

(C) Single genetically labeled pDC neuron: Microscopic visualization of a single genetically labeled pDC neuron (genotype details in table 1).
Orientation: Anterior is at the top, and posterior is at the bottom. Scale bar: 50 µm.

To unravel the function of specific genes during the development of sensory Ms-neurons, an RNA interference (RNAi) based gene knock-down (K.D.) of several Yki target genes was executed. As detailed in Section 6.2, this involved genetic labeling of single Ms-neurons concomitant with the knock-down of genes using UAS-RNAi fly lines (Table 1). This manipulation of gene abundance during Ms-neuron development yielded distinctive morphological phenotypes, as illustrated in Figure 17.

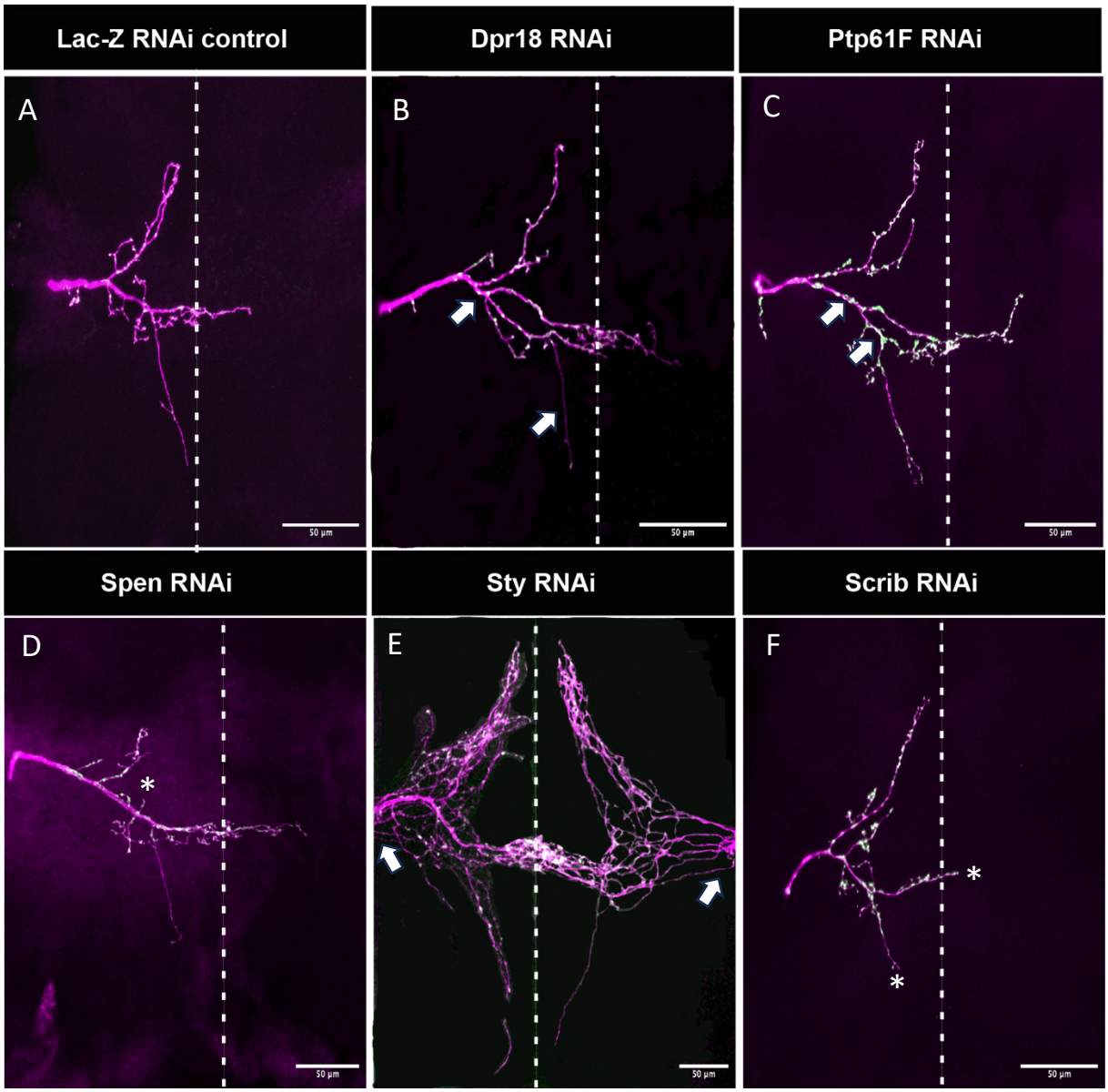

Figure 17. Molecular Players in the Axonal Growth and Synaptogenesis of Ms-neurons.

(A-F) Representative confocal images from a reverse genetic screen highlighting diverse phenotypes.

(A) Control Lac-Z RNAi Ms-neuron: Confocal image showcasing a control Ms-neuron subjected to Lac-Z RNA interference.

(B) Dpr18 gene knock-down: Mistargeting of ipsilateral collateral observed (indicated by arrows).

(C) Ptp61F gene knock-down: Increased synapse numbers evident (indicated by arrows).

(D) Spen gene knock-down: Missing anterior collateral highlighted (indicated by asterisk).

(E) Sty gene knock-down: Axon overgrowth observed (indicated by arrows.

(F) Scrib gene knock-down: Shortened collaterals and missing secondary/tertiary branches illustrated (indicated by asterisk).

Dotted lines indicate the CNS midline. Orientation: Anterior is at the top, and posterior is at the bottom. Scale bar: 50 µm.

Noteworthy among the investigated genes is Dpr-18, where K.D. resulted in mistargeting of axons and the formation of ectopic synapses (Figure 17 B). Dprs, membrane-linked cell adhesion molecules within the immunoglobulin superfamily, serve as neuronal recognition proteins, binding specifically to DIPs and forming a network of heterophilic interactions crucial for defined neuronal patterning (Sergeeva *et al.*, 2020). With 21 members in the Dpr protein family and 11 members in the DIP protein family, each expressed in specific subsets of neurons, the unique combinations provide a broad range of specificity in synaptogenesis (Morey, 2017; Cosmanescu *et al.*, 2018). Dpr18, specifically binding to DIP-ε and DIP-ζ (Sergeeva *et al.*, 2020), establishes a precise synaptic network, emphasizing its vital role in Ms-neuron development.

The exploration extends to the Ptp61F gene, encoding a tyrosine phosphatase primarily involved in tyrosine-phosphorylation dependent signaling. Known for its role in retinal axon guidance and negative regulation of JAK/STAT signaling in the *D.m.* CNS (Willoughby *et al.*, 2017), Ptp61F K.D. in Ms-neurons resulted in the observed ectopic formation of synapses (Figure 17 C), indicating its integral function in synaptogenesis for sensory neurons.

Further investigation into the Spen gene, encoding an RNA-binding protein with roles in neuron differentiation, axon elongation and the Notch and Wingless signaling pathway (Kuang *et al.*, 2000; Jin *et al.*, 2009; Gu *et al.*, 2017), revealed a phenotype characterized by the loss of the anterior branch in Ms-neurons (Figure 17 D). This observation hints at an axonal subcompartment-specific function, similar to the axonal collateral synaptogenesis function of the Prl-1 protein described by Urwyler et al. in a 2019 science paper (Urwyler *et al.*, 2019). Multiple Spen RNAi fly lines consistently produced the same anterior collateral missing phenotype (Appendix, Figure), underscoring the critical role of protein abundance during axonal branching in the CNS of Ms-neurons.

The Sty gene, encoding a member of the Sty family associated with negative feedback-loop modulation of growth-mediated factors (Strutt and Strutt, 2003; Sieglitz *et al.*, 2013), displayed a massive overgrowth phenotype upon K.D. in Ms-neurons (Figure 17 E). Investigation into whether these branches form upon the neuron entering the CNS or at the soma necessitates further exploration. Given Sty's involvement in general growth processes, the observed overgrowth will need more careful studies addressing the temporal progression of branching during development and interactions with other branching factors.

The final gene under scrutiny is Scrib, encoding a protein forming a complex with Disc large (Dlg) and Lethal giant (Lgl). This complex, initially described as a neoplastic tumor suppressor, plays a pivotal role in processes linked to cell polarity (Su *et al.*, 2012). Scrib's involvement in the Hpo network, downstream of the Fat (Ft) receptor, interacting with Expanded (Ex) and Dachs (D), suggest a role in controlling Warts (Wts) levels in epithelial cells (Verghese *et al.*, 2012). Knock-down of Scrib in Ms-neurons results in a shortage of collaterals and missing secondary and tertiary branches (Figure 17 F), indicating a function in postmitotic neuronal branching. The potential collaboration of Scrib with Dlg and Lgl in these neurons awaits further investigation.

While each of the examined genes exhibited diverse phenotypes upon K.D. in Ms-neurons, only those with a phenotype penetrance of 50% or more were selected for further experiments. Among these, one gene stood out with a particularly complex and severe phenotype, warranting special attention. Thus, the dissertation's focus lies on unraveling the intricacies of this specific gene, promising a deeper understanding of its profound impact on Ms-neuron development.

7.2. Elucidating the Role of Brat in the Development Dynamics of Postmitotic Axons

Brat, identified as an RNA-binding protein, has well established functions in early embryonic patterning during oogenesis and has emerged as a significant tumor suppressor in subsequent studies (Sonoda and Wharton, 2001; Reichardt *et al.*, 2018; Connacher and Goldstrohm, 2021). While Brat's roles in neuronal development have been extensively characterized, its specific function in postmitotic neurons remains elusive. This chapter explores Brat's potential involvement in axonal branching and synaptic connectivity of Ms-neurons through a reverse genetic screen.

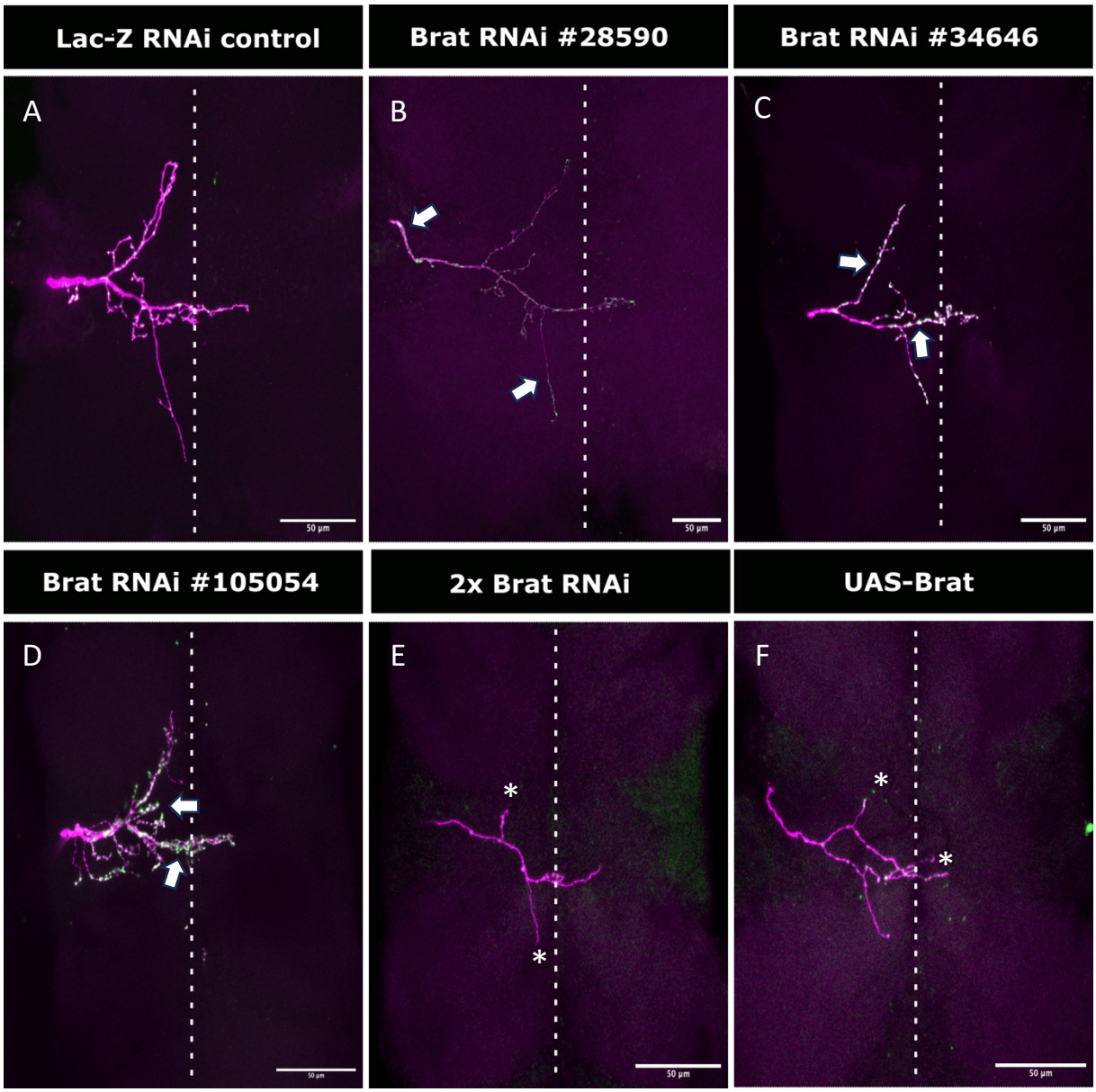

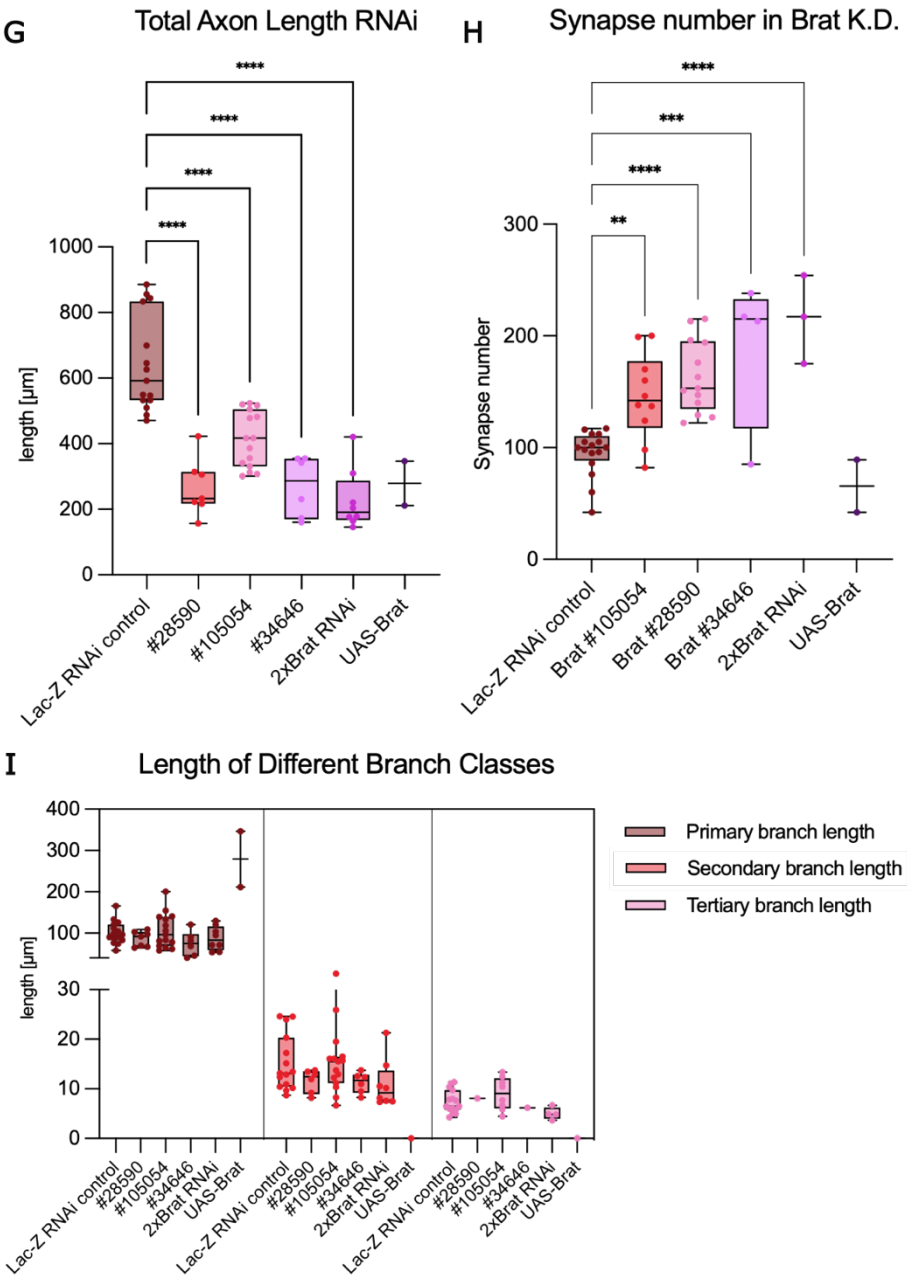

Figure 18. Impact of Brat Knock-down on Axon Length and Synaptogenesis in Ms-neurons.

(A-F) Confocal images depicting the consequences of Brat gene knock-down in Ms-neurons.

(A) Control Lac-Z RNAi Ms-neuron.

(B) RNAi #28590 knock-down of Brat displays a reduction in axonal diameter (indicated by arrows).

(C) RNAi #34646 knock-down exhibits ectopic synapses (indicated by arrows).

(D) RNAi #105054 knock-down results in axonal branching defects and extensive synaptogenesis (indicated by arrows).

(E) Simultaneous knock-down of RNAi #105054 and #28590 leads to branch and synapse loss (indicated by asterisks)

(F) Overexpression of Brat in Ms-neurons induced axonal branching defects (indicated by asterisks.

(G-I) Quantitative analysis of axon length and synapse number following Brat knock-down.

(G) All Brat RNAi lines demonstrate a significantly smaller total axon length compared to Lac-Z RNAi control.
(H) Quantification reveals an increased number of synapses for all Brat RNAi lines compared to Lac-Z RNAi control.
(I) Measurement of axonal length divided into primary, secondary, and tertiary branches. Branch size vary between different RNAi lines.
Significance was determined using One-way ANOVA. Dotted lines indicate CNS midline. Anterior is top and posterior is bottom. Scale bar: 50 µm.

Knock-down (K.D.) of Brat in Ms-neurons resulted in a notable effect, including a reduction in total axon length compared to Lac-Z RNAi controls (Figure 18 G), highlighting a potential role in axonal growth dynamics. Intriguingly, despite defects and axonal length shortages upon entry into the CNS, the axon still reached its destination, suggesting a specific function for Brat in branching and establishing synaptic connections within the CNS.

Further analysis of branching classes revealed that Brat K.D. primarily led to shortened primary branches, with secondary and tertiary branches showing significant reduction only in the 2xBrat RNAi condition (Figure 18 I). Notably, overexpression of Brat did not result in increased total axon length but rather exhibited a reduction (Figure 18 G). However, a closer examination of branching classes indicated an increase in primary branches without concurrent development of secondary or tertiary branches (Figure 18 I).

Synaptogenesis, quantified as a higher number of synapses in all Brat K.D. RNAi lines (Figure 18 H), adds additional functions of Brat in synaptic connectivity.

In contrast, primary data for UAS-Brat overexpression hinted at a reduction in synapses (Figure 18 H). These findings, while intriguing, warrant further validation with increased sample sizes or *in vitro* cell culture experiments to ascertain their significance.

These results shed light on the multifaceted role of Brat in postmitotic axonal development. The observed reduction in total axon length upon Brat K.D. suggests its involvement in axonal growth regulation, with a particular impact on primary branches. The intriguing discrepancy between Brat K.D. and overexpression outcomes emphasizes the complexity of Brat's function, highlighting the need for additional investigations to unravel the underlying mechanism. The complex synaptogenesis phenotypes upon Brat K.D. hints at a potentially independent role in synaptic connectivity, warranting further exploration.

7.3. Exploring Diverse Phenotypic Outcomes in Mechanosensory Neurons Due to Varied Loss-of-function Mutations in the Brat Allele

To substantiate the RNAi-induced phenotypes, I delved into the consequences of Brat gene loss-of-function (LOF) by scrutinizing mutant Brat MARCM clones. Employing mosaic analysis facilitated the generation of homozygous Brat LOF within individual cells of mosaic flies. My observations revealed that homozygous Brat LOF exerted a notable influence on axonal length compared to FRT40A control neurons, manifesting as a measurable reduction in branching complexity and fewer branches.

The range of Brat alleles utilized in that MARCM analysis exhibited mutations in diverse gene regions. The Brat alleles subjected to MARCM analysis included EMS- induced mutations (e.g. $Brat^{1}$, $-^{18}$, and $-^{11}$) or P-element inserted mutations ($Brat^{K06028}$) (Figure 19). The wildtype Brat protein comprises two B-Box domains recognized as zinc finger domains, a Coiled-coil domain crucial for protein-protein interactions, and a β-propeller domain, the vertebrate homolog to an NHL-domain associated with RNA-binding (Figure 11) (Connacher and Goldstrohm, 2021).

Diverse mutations were identified among the available Brat alleles. $Brat^{11}$, induced by EMS, resulted in an earlier stop due to an amino acid exchange, rendering the β-propeller domain untranslated. Despite this, the residual protein was deemed non-functional, thereby classified as a null protein. Similar mutations were identified for $Brat^{18}$ and $Brat^{1.1}$, both lacking a functional RNA-binding domain. Unfortunately, limited information is available regarding the molecular characteristics of the gene changes in $Brat^{1}$. In contrast, $Brat^{K06028}$, a well-documented P-element inserted mutation, underwent directed mutation analysis, confirming an integration of a P-LacW element into the 4^{th} exon, rendering the Brat protein non-functional (*FlyBase Insertion Report: Dmel\P{lacW}brat[k06028]*) (Figure 19). Considering these EMS-induced mutations it was hypothesized that these would corroborate the RNAi-induced phenotypes.

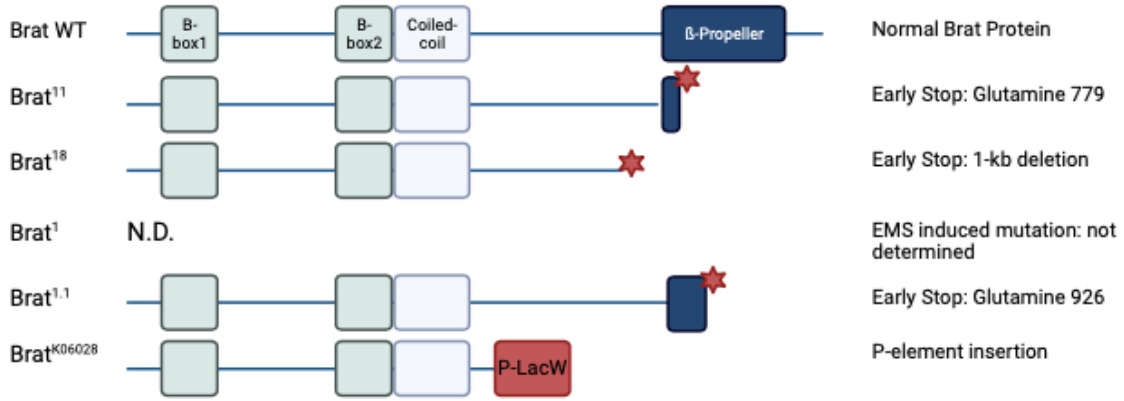

Figure 19. Diverse Brat Alleles: Unravelling Genetic Variations in Brat.

The wild-type (WT) Brat allele showcases the structural integrity with two B-Box domains, a Coiled-coil domain, and a β-propeller domain near the 3' end of the gene. Contrarily, mutant alleles exhibit variations at distinct base pairs. $Brat^{11}$, $Brat^{18}$, and $Brat^{1.1}$ illustrate amino acid exchanges leading to premature translational stops. $Brat^{K06028}$ displays a P-element inserted mutation, where P-LacW integrates into the 4th exon of the Brat WT gene. The $Brat^{1}$ allele, induced by EMS, bears an undefined molecular mutation.
Illustration created using BioRender, depicting the genetic landscape of Brat alleles in diverse mutant forms.

Quantitative analysis uncovered the most significant difference in total axon length between the P-element inserted mutation $Brat^{K06028}$ and the FRT40A control (Figure 20 G), emphasizing that Brat LOF contributes to axonal branch loss and disruptions in synaptic connectivity within Ms-neurons. Further quantitative analyses demonstrated a significant reduction in secondary and tertiary branches with Brat LOF (Figure 20 I), raising questions about Brat's role in the initiation or consolidation of these neurites (Luo and O'Leary, 2005). Intriguingly, none of the Brat mutations altered the axon guidance of Ms-neurons from the periphery to the CNS.

Synaptic development of Brat LOF displayed diverse outcomes depending on the mutation. Some mutations exhibited no Brp fluorescence, while others showed ectopic formation of active zones shown by the Brp marker (Figure 20 B-F). Dosage-dependent effects were evident, indicating that truncated residual parts of the Brat protein might interact indirectly with structural proteins, leading to opposing phenotypes (Henikoff, 1996).

Quantification of Brat mutant synapse number highlighted its role in active zone formation. Importantly, these findings underscored Brat's function in synaptic development and active zone formation at *D.m.* neuromuscular junctions (NMJs) (Shi *et al.*, 2013). However, using the active zone synapse marker Brp^{short}::GFP (Wagh *et al.*, 2006; Fouquet *et al.*, 2009) in

MARCM analysis revealed different functions for Brat synaptogenesis compared to the synaptic vesicle marker mCherry::Syt1 (Fernández-Chacón and Südhof, 1999) used in RNAi analysis (Figure 18). Additional MARCM analyses are required for Brat LOF utilizing a synaptic marker that depicts synaptic vesicles to replicate the ectopic synapse formation observed in RNAi-mediated conditions.

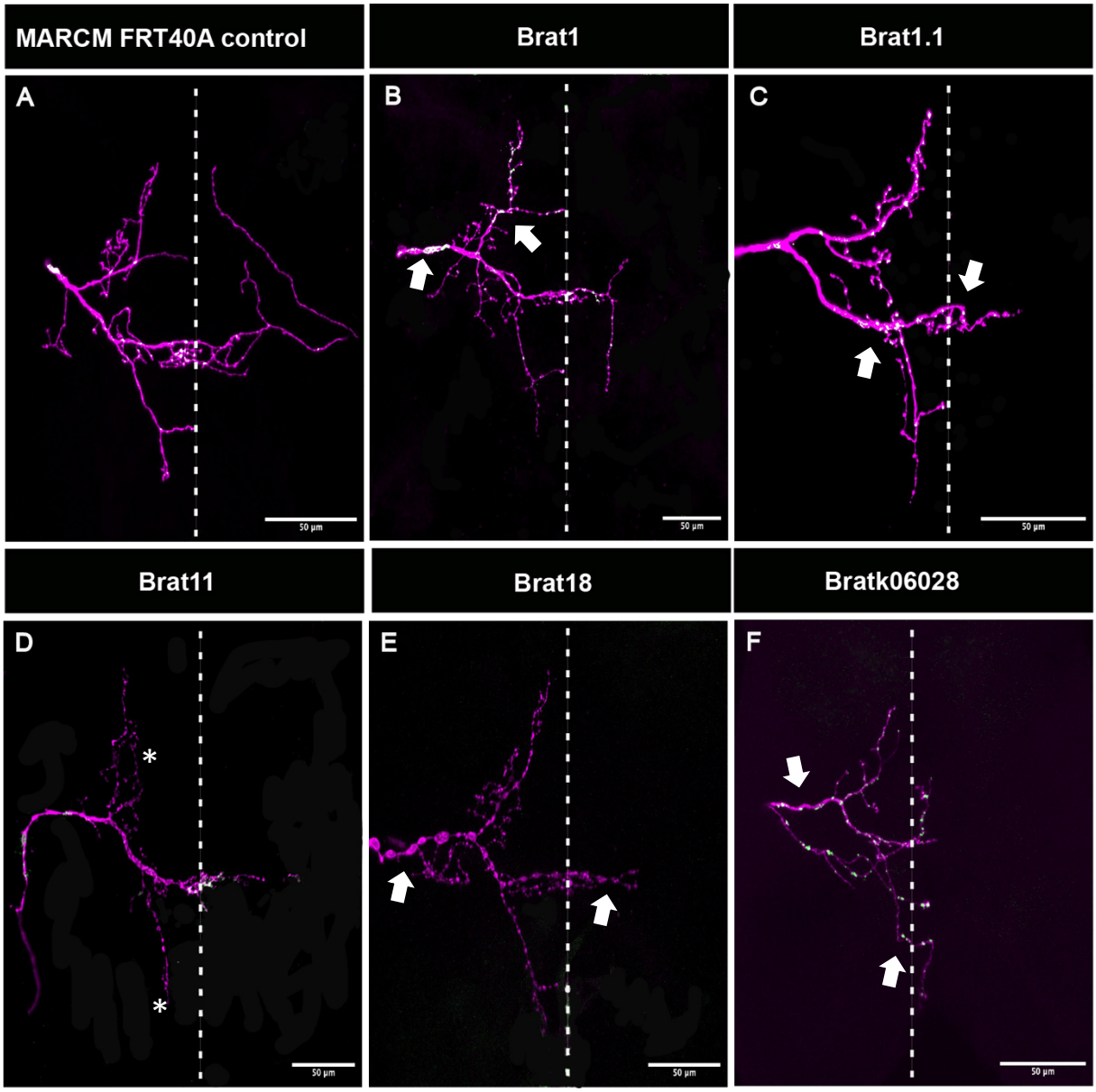

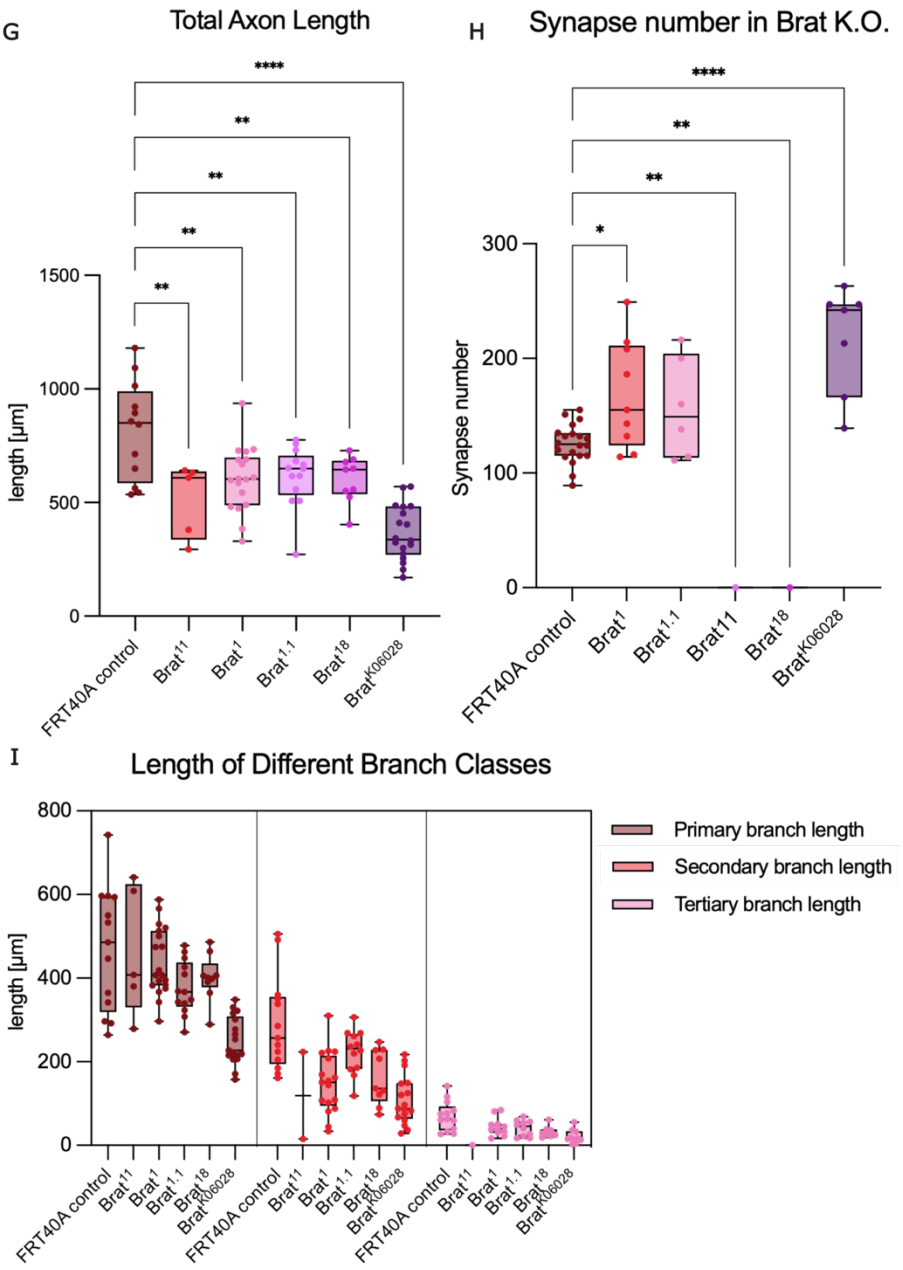

Figure 20. Unraveling the Role of RNA-binding protein Brat in Axon Development and Synaptogenesis.

(A-F) Representative confocal images of Ms-neurons through MARCM clone formation depict distinct phenotypes.

(A) FRT40A control neuron exhibits a stereotyped axonal branching pattern with secondary and tertiary branches, showcasing synapse distribution within the VNC.

(B) $Brat^{1}$ allele exhibits ectopic synapses (indicated by arrows) and reduced branch complexity.

(C) $Brat^{1.1}$ allele mirrors $Brat^{1}$, displaying altered branch complexity and synaptogenesis (indicated by arrows).

(D) $Brat^{11}$ allele lacks visible synapse markers and shows aberrations in primary and collateral structure (indicated by asterisk).

(E) $Brat^{18}$ allele displays no detectable synapse marker and a clump-like axon structure (indicated by arrows).

(F) $Brat^{K06028}$ allele presents ectopic synapse formation and axon arbor deformations (indicated by arrows).

(G) Quantitative analysis of Brat MARCM alleles show a significant decrease in total axon length compared to FRT40A control, with $Brat^{K06028}$ exhibiting highly significant values ($p<0.0001$) and other Brat alleles showing significant values ($p=0.0011$, $p=0.0012$, $p= 0.050$, $p=0.0075$).

(H) Synapse number quantification significant deviations for all Brat alleles expect $Brat^{1.1}$, with varied effects, including increased synapses for $Brat^{1}$ and $-^{K06028}$ and decreased synapses for $Brat^{18}$ and $-^{11}$.

(I) Quantitative analysis of axonal length categorized by primary, secondary and tertiary branches. Branch length variations among LOF alleles, with $Brat^{K06028}$ showing the most significant decreases in all categories. Highly significant effects on secondary branch length for $Brat^{1}$ ($p<0.0001$) and significant values for $Brat^{11}$ ($p=0.0211$) and $Brat^{18}$ ($p=0.0014$), but not for $Brat^{1.1}$. Tertiary branch length exhibits measurable significance for all alleles ($p=0.0306$, $p=0.0296$, $p=0.0045$, $p<0.0001$), except $Brat^{1}$.
Significance calculated with One-way ANOVA. Dotted lines indicate CNS midline. Anterior is top, and posterior is bottom. Scale bar: 50µm.

In conclusion, my data and experiments emphasize Brat's pivotal function in postmitotic axonal development of sensory neurons. Coupled with the insights into other Yki target genes, it becomes evident that Yki orchestrates a network of distinct protein functions crucial for the development of Ms-neurons and their stereotyped neuronal circuit.

One of the distinct cellular targets of Yki has been its role in mitochondrial biology (Nagaraj *et al.*, 2012).

Therefore, exploration into other protein networks associated with mitochondrial function, in particular in axons, holds promise in understanding the broader influences of Yki and related regulatory networks on axon branching during development, and likely with relevance to neurodegenerative diseases (Islam, 2017). In the subsequent sections, I describe my efforts of characterizing Creld, a protein regulating mitochondrial-ER interactions and associated with Parkinson's disease (Paradis *et al.*, 2022), exploring also a potential impact on synaptogenesis in Ms-neurons.

7.4. Exploring the Impact of Creld Knock-down on Synaptogenesis in Mechanosensory Neurons: A Developmental Perspective

We have previously identified *D.m.* Cysteine-rich with EGF like domain (Creld) as a novel regulator of ER-mitochondria contact sites with an essential role in locomotion and neuromotor function. Creld protein is ubiquitously expressed within the *D.m.* organism, including the brain. In a recent publication I researched the role of Creld in the dopaminergic neurons of the *D.m.* brain, establishing a connection between its LOF and a Parkinson's disease-like phenotype (Paradis *et al.*, 2022) (Appendix 9.1).

The observed neuromotor function of Creld in dopaminergic neurons prompted a comprehensive analysis of Creld function in synaptogenesis. Its vertebrate homolog CRELD2 plays a role in ER stress response and unfolded protein response (UPR) (Kern *et al.*, 2021), and the murine CRELD1 was identified as a risk gene for heart failure (Beckert *et al.*, 2021). In work on mature *C. elegans* synapses, D'Alessandro *et al.*, (eLife 2018) uncovered Creld's influence on the assembly of acetylcholine receptors. Synaptogenesis, a critical aspect of neuronal development, has not been a focal point of previous research involving Creld.

Indeed, the analysis of Creld K.D. in Ms-neurons revealed a remarkable finding – massive synaptogenesis, as evidenced by the synaptic vesicle marker Syt1::GFP (Figure 21), suggesting a previously undiscovered role of Creld in synaptogenesis. This finding fits together with published data from single-cell analysis showing that there is a subset of dopaminergic neurons in the VNC (Allen *et al.*, 2020).

Intriguingly, the previously observed locomotion impairment in Creld$^{-/-}$ flies (Paradis *et al.*, 2022) could be connected to the newly discovered function of Creld in synaptogenesis, which should be addressed in future studies.

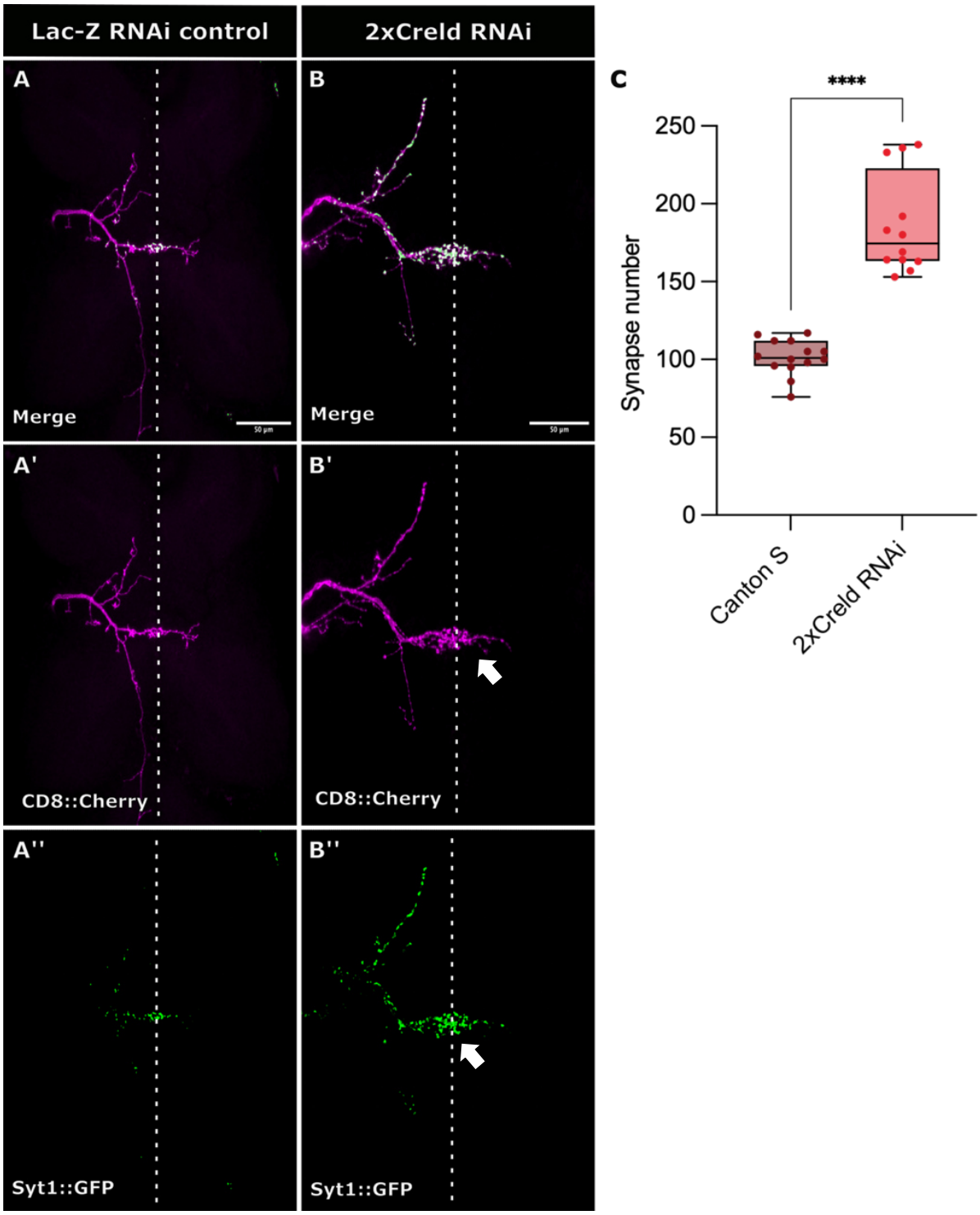

Figure 21. Enhanced Synaptogenesis in 2xCreld RNAi in Ms-neurons.

(A-B) Confocal images of Ms-neurons showcasing individual channels for (A') the axonal marker CD8::Cherry and (A'') the synaptic vesicle marker Syt1::GFP in control flies. Additional single-channel images for (B') and (B'') highlight the specificity of the axonal and synaptic markers, respectively, in Creld mutated flies. The 2xCreld RNAi confocal image (indicated by arrows) reveals a substantial increase in synapse number while maintaining a normal axonal structure.

(C) Qualitative quantification of synaptic vesicles demonstrates a highly significant elevation in Creld knock-down Ms-neurons.
Statistical significance was determined using Mann-Whitney-U test ($p<0.0001$). Dotted lines indicate the CNS midline. The orientation is anterior at the top and posterior at the bottom. Scale bar: 50 µm.

7.5. *In Vitro* Modeling of Neuronal Development Using *Drosophila Melanogaster* Bg3c2 Cells

Cell culture systems often constitutive an indispensable tool in molecular studies, offering a versatile platform for investigating cellular signaling. The *D.m.* model organism, widely employed for *in vivo* studies, also boasts a rich array of *D.m.* cell culture lines, contributing significantly to research endeavors (*Drosophila Cells in Culture - 2nd Edition*).

The Bg3c2 cell line, originating from the larval CNS of *D.m.*, specifically derived from the VNC of third-instar larvae (L3), promised to serve as a valuable resource for our neuron-specific interests. The establishment of the Bg3c2 cell line involved the extraction and culture of larval VNC tissue, followed by successive dilution transfers, culminating in the development of the parental cell line ML-DmBG (Ui *et al.*, 1994). These cell lines exhibit a dependency on insulin in their growth medium for optimal proliferation (Luhur *et al.*, 2019), as illustrated in the schematic overview of ML-DmBG cell generation and culture handling (Figure 22).

In the exploration of Yki's influence on neuronal development, Bg3c2 cells were cultivated to attain a functional mature neuron culture. Various culture conditions, including the presence and absence of insulin, were tested. Staining against nuclear proteins, microtubule-specific proteins, and glial cell markers (DAPI, Phalloidin, and Repo, respectively) provided insights. Experimental findings revealed an intact nuclear structure and the formation of cell clusters (Figure 22 C and C'), aligning with existing literature on ML-DmBG cells (Ui *et al.*, 1994). Notably, the abundance of cells was higher in insulin-treated cultures than in those without insulin (Figure 22 B and C), corroborating the established role of insulin in promoting proliferation. Crucially, insulin not only led to proliferation but also resulted in a reduction in $Repo^{+}$ detected cells, supporting the hypothesis that insulin also promotes the differentiation of neuronal progenitors into mature neurons (Nieto-Estévez *et al.*, 2016).

In conclusion the examined data shed light on Bg3c2 cell behavior, underlining the important role of insulin in proliferation and differentiation. Further investigations into molecular mechanisms of neuronal development can be performed due to the establishment of this cell line as a functional mature neuron culture. Furthermore, the importance of coating for cultured cells to efficiently proliferate and differentiate is underscored by several published papers (Lin *et al.*, 2009; TANG and SAITO, 2017; Tudureanu *et al.*, 2022). The following chapter provides a comprehensive exploration of the Bg3c2 cell line, shedding light on its behavior under different conditions and laying the groundwork for understanding its role in neuronal development.

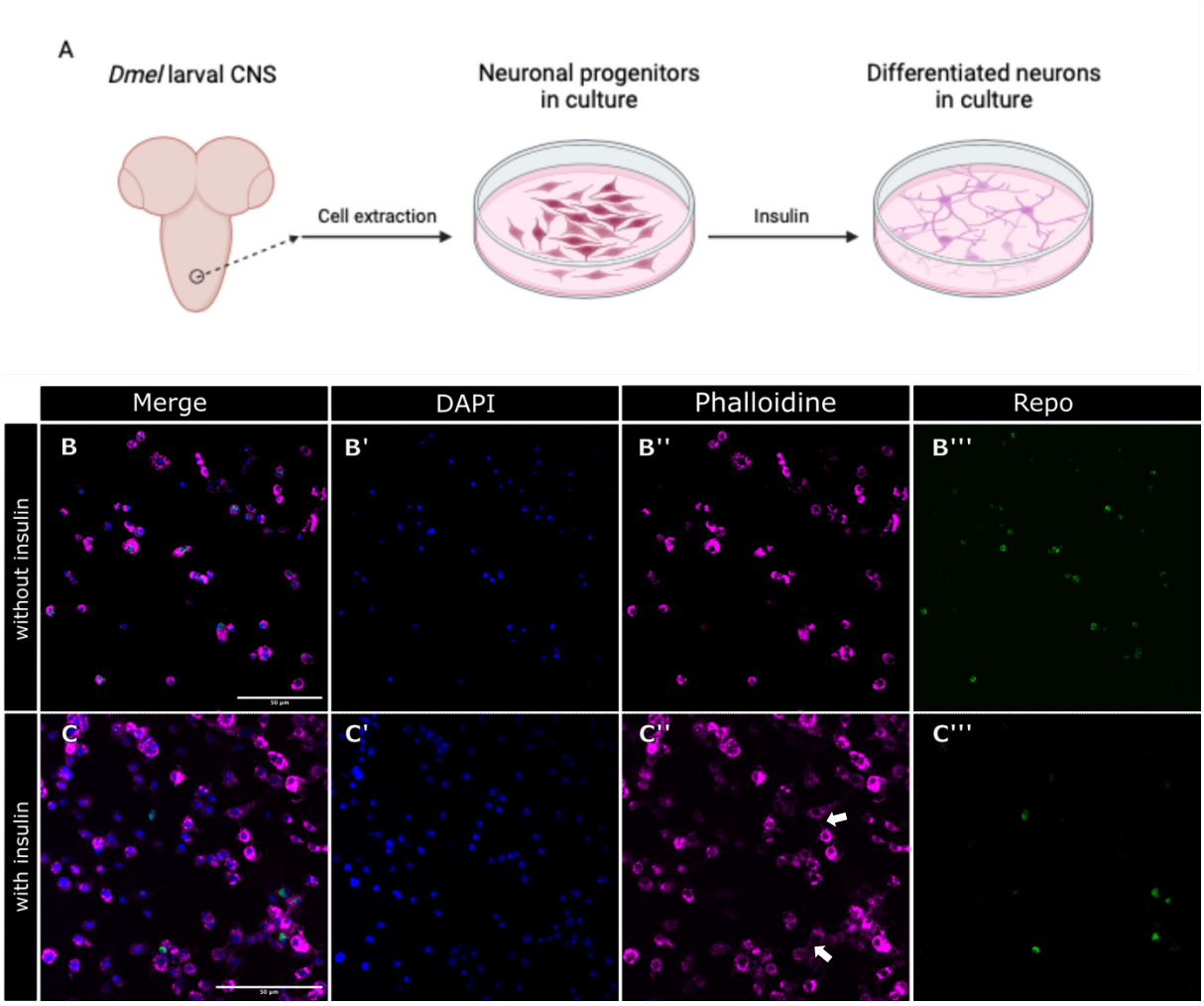

Figure 22. Neurite Formation in *Drosophila Melanogaster* Bg3c2 Cells Induced by Insulin Treatment.

(A) Schematic representation of *D.m.* L3 larval VNC derived Bg3c2 cells in a progenitor cell state. Upon the addition of insulin to the culture medium, these cells undergo differentiation, marked by the observable neurite formation.

(B) Merged channels depicting cultured Bg3c2 cells without insulin. (B') DAPI staining revealing intact nuclei, and (B'') phalloidine staining illustrating the microtubule structure of progenitor cells. (B''') Repo staining present in approx. half of the nuclei.
(C) Merged channel displaying cultured Bg3c2 cells with insulin. (C'') Phalloidine staining highlights neurites formed by differentiated neurons (indicated by arrows). (C''') Repo staining is less abundant compared to cells without insulin.
Scale bar: 50µm.

7.6. Effect of Various Coating Media on the Differentiation Patterns of *Drosophila Melanogaster* Bg3c2 Cells

Cell culture vessels, commonly constructed from polystyrene, offer superior cell adhesion surfaces compared to glass, providing a favorable environment for cellular growth. Coating these plastic dishes allows for the replication of the biological extracellular matrix (ECM), enhancing cell adherence and more closely resembling the natural state of cultured tissues. Coating, a crucial step in working with cultures, supplies proteins and peptides that enhance cell adherence, particularly important for rare cell types, as untreated polystyrene surfaces are inherently hydrophobic. ECM proteins, including Laminin and Fibronectin, are commonly employed as coating materials. While Laminin and Fibronectin are expensive purified proteins isolated from animal tissue, Poly-L/D-Lysine, are cheaper amino acids, frequently used for surface coating, especially in neuronal cultures (Kleinman *et al.*, 1987; Stil *et al.*, 2023).

Culturing neurons presents challenges due to the limited division and maturity of postmitotic neurons. Immortal neuronal cultures derived from tumors, such as SH-SY5Y cells, offer an alternative but lack the ability to faithfully mimic *in vivo* neuronal properties. Consequently, many research groups work with neuronal progenitors in culture (NPCs), which are proliferative and capable of self-renewal (Gordon, Amini and White, 2013).

While *D.m.* primary neuron cultures have historically been employed to complement *in vivo* findings, our experiments focused on *D.m.* neuronal progenitor cells, Bg3c2, extracted from larval L3 VNC. Insulin addition was used to enhance neuron proliferation and investigations were conducted to determine whether coating influenced the ratio of glia to neuron cells, as indicated by $Repo^+$ and HRP^+ markers, respectively.

Coating on various surfaces, including control without coating, Laminin, Fibronectin, and Poly-L-Lysine, at different time points of cultures yielded diverse results. Quantification of $Repo^+$ versus HRP^+ cells consistently showed a prevalence of neurons over glia cells,

irrespective of culturing time or surface coating. Poly-L-Lysine coating after 24 hours displayed the highest number of glia cells, albeit with a marginal ratio compared to neurons (Figure 23 J). Importantly, cell density increased with longer culturing time, although a slight decrease was observed after 7 days for all surface coatings. In general, Fibronectin coating after 4 days emerged as the most favorable surface coating regarding cell number and HRP^+ marker (Figure 23 K). Neurite length analysis displayed an increase for all coatings form 24 hours to 4 days, followed by a decrease, mirroring the observed trend in cell density after 7 days. Quantification indicates that the most beneficial coating surface and culturing time for Bg3c2 cells, in term of cell density and neurite length, is a Fibronectin coating with a minimum of 4 days in culture (Figure 23 J-L).

In conclusion, these findings provide valuable insights into the nuanced interplay between coating strategies, culturing duration, and the behavior of *D.m.* Bg3c2 neuronal progenitor cells. Fibronectin coating, coupled with a minimum 4-day culturing period, emerged as the most favorable condition, prompting optimal cell density and neurite length. These findings lay the groundwork for establishing ideal culture conditions for Bg3c2 cells, offering a foundation for further investigations into molecular characterizations of mature neurons in subsequent chapters.

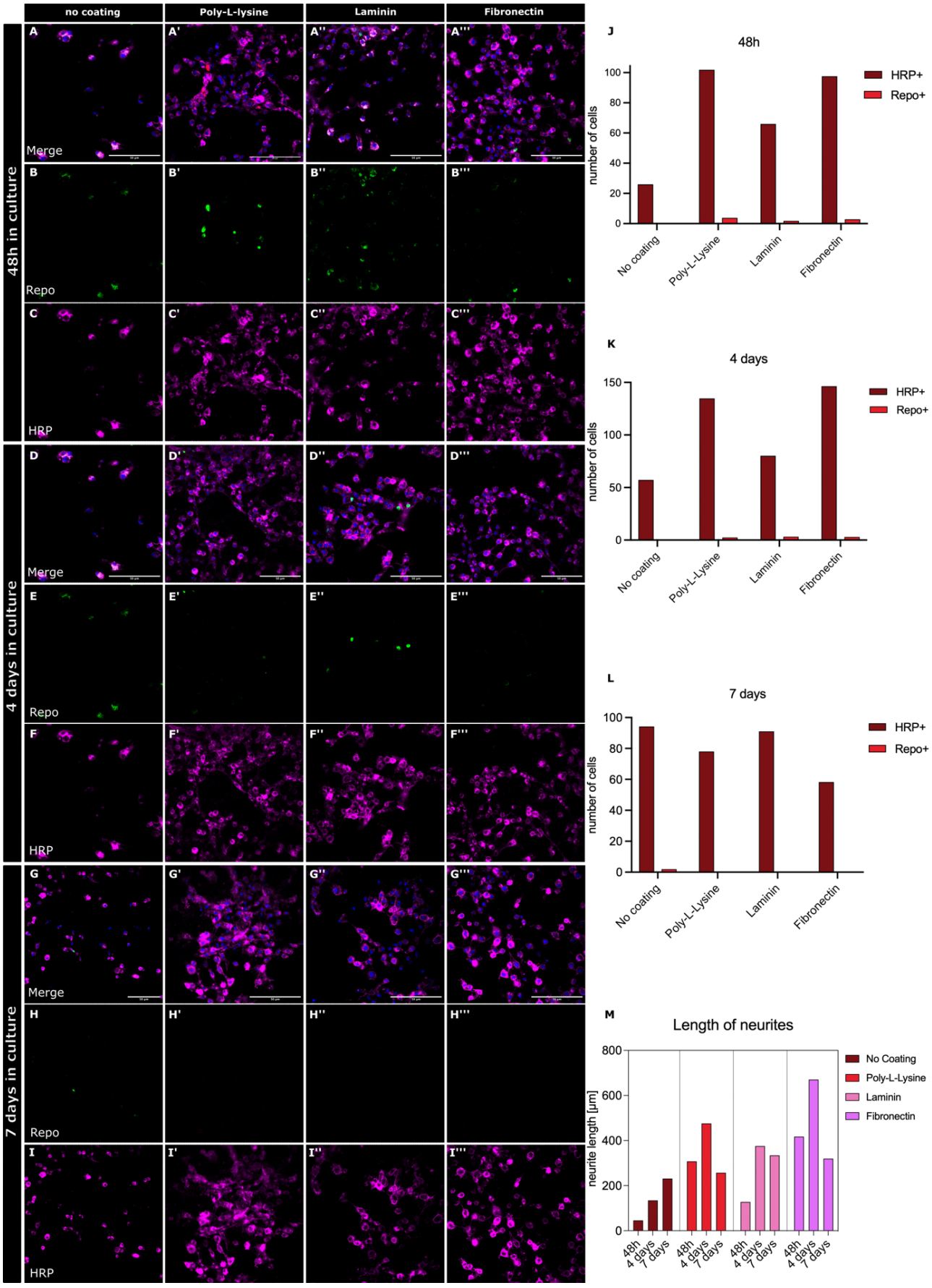

Figure 23. *Drosophila Melanogaster* Bg3c2 Cell Growth Dynamics Modulated by Coating Variations.

(A-C) Morphological differences in Bg3c2 cells cultivated on diverse coating media after 48 hours, with Repo (B) as glia cell marker, observed in nucleus, and HRP (C), a neuron cell marker, visible in the cell membrane. The strongest Repo signaling is evident in cells on Poly-L-Lysine coating (B').

(D-F) Bg3c2 cells on different coatings after 4 days in culture, displaying Repo (E) and HRP (F) markers. The most robust Repo signal is observed in cells growing on Laminin (E'').

(G-I) Bg3c2 cells on varied coating media after 7 days in culture, showcasing Repo (H) and HRP (I) signals. Repo signal is significantly low on all coatings (H-H''').

(J-L) Quantification of cell numbers, comparing HRP^+ and $Repo^+$ cells on different coatings at (J) 48 h, (K) 4 days, and (L) 7 days in culture. Cell numbers increase from 48 hours to 4 days, with Poly-L-Lysine and Fibronectin coatings displaying the highest cell counts. After 7 days, cell numbers decrease on all coatings except for the no coating condition, where cell numbers continue to rise. Repo signal is detected in a significantly low number of cells.

(M) Neurite length quantification on different coatings and culturing times, revealing the longest neurites on Fibronectin culture medium after 4 days.
Scale bar: 50 µm.

7.7. Developmental Heterogeneity in Bg3c2 Cells: Insights from Molecular Characterization and 20-hydroxyecdysone Treatment

Postmitotic neurons arise from neuroblasts through asymmetric division, giving rise to a neuroblast and a ganglion mother cell (gmc). Gmcs further differentiate into postmitotic cells, leading to the formation of neurons or glia cells (Egger, Chell and Brand, 2008). Each stage of neuronal development is associated with distinct target gene expressions. Progenitor cells and intermediate neural progenitors (INPs) are marked by an increase in CycE and Mira, while gmcs express Insb and Insc. Immature neurons express Hey and (Espl)m6-BFM, and mature neurons express nSyb and lncRNA:noe. Glia cells are identified by Repo and Gcm expression, while astrocytes express Gat and Alrm (Michki *et al.*, 2021).

To comprehend the developmental state of Bg3c2 cells, qPCR analysis was conducted, revealing a heterogenous mixture of developing neurons. Progenitor cell genes were least expressed, suggesting that the majority of neurons had already undergone asymmetric division into gmcs. Interestingly, qPCR results demonstrated both downregulation and upregulation of gmc markers. Immature and mature neuron genes showed the highest expression, with varying regulation patterns for individual genes (Figure 24 A). Additionally, genes associated with glia cells and astrocytes were upregulated, confirming the heterogenous composition of Bg3c2 cell culture (Figure 24 A).

To steer the expression of these heterogenous cells towards mature neurons, the cells were treated with 20-hydroxyecdysone (20E), a steroid hormone known for its role in *D.m.*

metamorphosis and neurite growth (Stoiber *et al.*, 2016). Previous research data indicated that 20E indeed enhances neurite growth, fostering a significant increase in total neurite length in mushroom body intrinsic neurons after 2-4 days of exposure (Kraft, Levine and Restifo, 1998). Further, neurite elongation unfolded in neural Bg2-c6 cell culture through the addition of 10 µg/ml 20E (Tominaga *et al.*, 2010).

For the Bg3c2 cell culture, 20E treatment resulted in a heterogenous gene expression pattern, with significant upregulation observed after 7 days of exposure to 10 µg/ml 20E (Figure 24 B). This upregulation included genes associated with mature neurons, immature neurons, gmcs, glia cells and astrocytes. Notably, astrocyte gene expression increased even after 4 days of 20E treatment, remaining constant after 7 days (Figure 24 B). These findings indicate that 20E influences CNS cells at various developmental stages, promoting not only neurite growth but also the expression of diverse neuronal lineage genes.

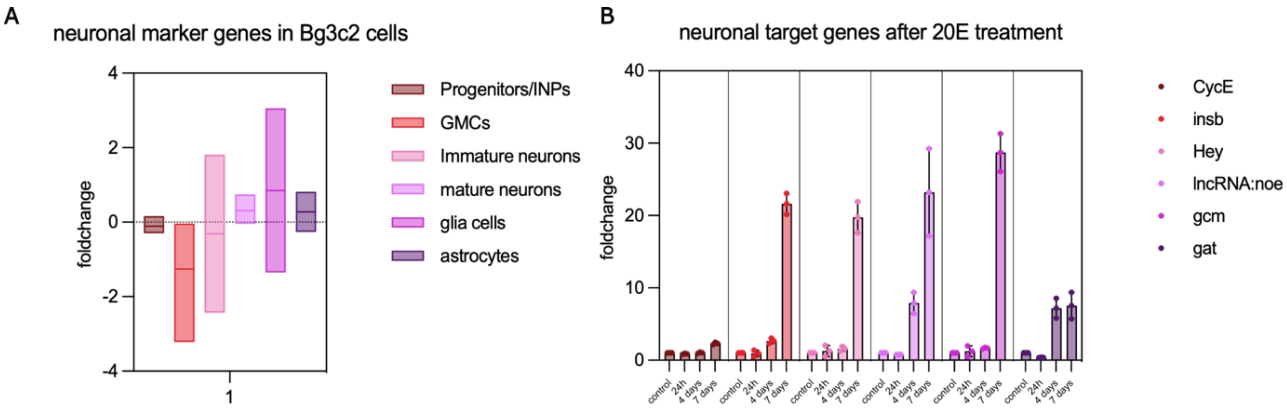

Figure 24. Intricacies of Neuronal Target Marker Expression in Bg3c2 Cells Post 20-hydroxyecdysone Treatment.

(A) Untreated Bg3c2 cells revealed, through qPCR analyses, a nuanced transcriptional landscape of neuronal marker genes. The markers associated with immature and mature neurons displayed an increase, albeit with substantial variability.

(B) The orchestration of neuronal target genes unfolded after 20E induction (10 µg/ml) at different time intervals – control, 24 hours, 4 days, and 7 days post-induction. Intriguingly, all genes exhibited an upswing after 7 days of 20E treatment. While the marker for neuronal progenitor cells (CycE) exhibited the smallest increase, those for gmcs (Insb), immature neurons (Hey), mature neurons (lncRNA:noe), glia cells (gcm), and astrocytes (Gat) all demonstrated an elevation following 20E induction and with prolonged culturing time.

Significance, evaluated through One-way ANOVA, revealed no statistical significance in both (A) and (B), emphasizing the dynamic and complex nature of gene expression patterns in Bg3c2 cells in response to 20E treatment.

To explore the concentration-dependent effect of 20E on gene expression, different concentrations were tested. The highest concentration exhibited a significant increase in astrocyte gene (Gat) and glia gene (Gcm) expression after 24 hours (Figure 25 A). Lower concentrations demonstrated significant effects on glia cells, immature neurons and gmc neuron genes after a more extended treatment period (Figure 25 B). After 7 days, all concentrations influenced Gat expression significantly, along with increased expression of glia cell, immature neuron, and gmc neuron genes, while mature neuron gene markers showed no increase regardless of concentration or treatment duration (Figure 25 C). Notably, the active zone gene Brp (Wichmann and Sigrist, 2010) exhibited increased expression after 20E treatment, emphasizing the hormone's tole in neuronal plasticity and post-metamorphosis. Furthermore, the results indicated a slight increase in Yki expression after 20E treatment, suggesting an influence on cell differentiation (Figure 25 D).

In summary, the study demonstrated that 20E has an increasing effect on neuronal lineage genes, with a preference for astrocyte and glia cell development. While neuronal plasticity is positively influenced, the hormone does not significantly impact the development of mature neurons. These findings lay the groundwork for subsequent investigations into the influence on Yki on CNS cells in Bg3c2 experiments.

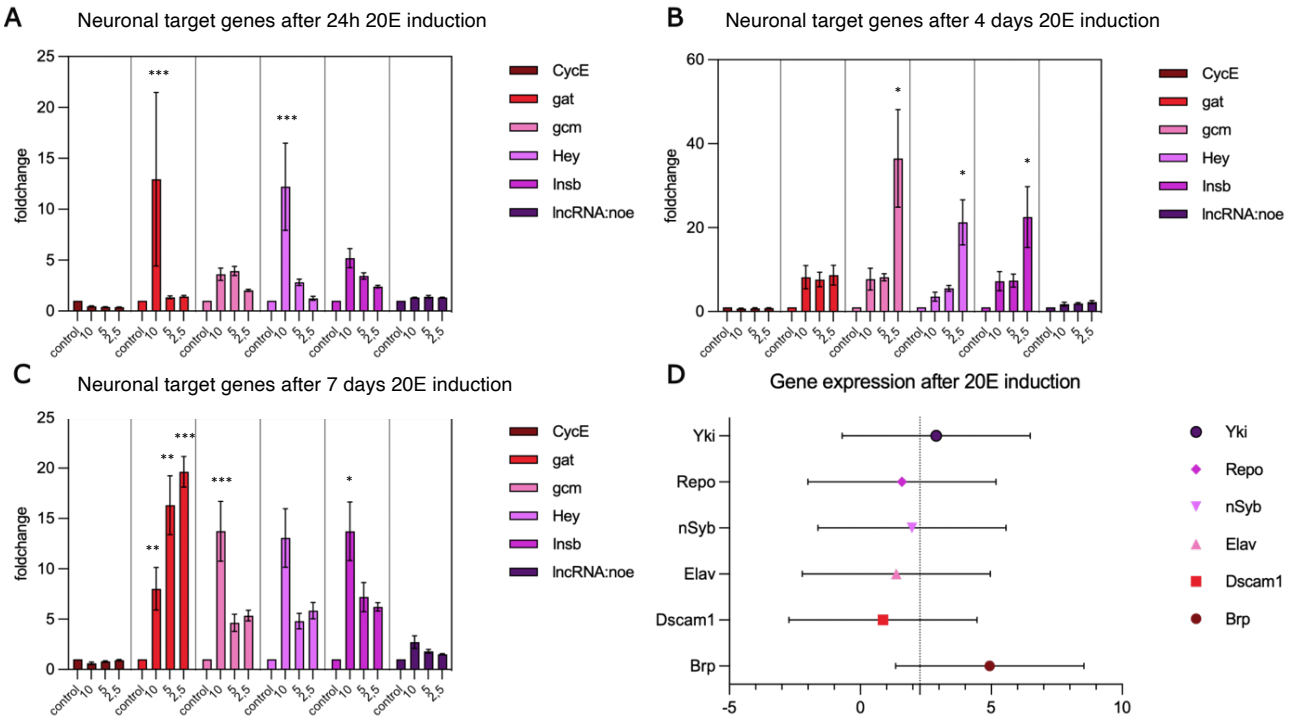

Figure 25. Impact of Varied 20-hydroxyecdysone Concentrations on Neuronal Marker Gene Expression in Bg3c2 Cells.

(A) Quantitative PCR analysis of neuronal target genes following a 24-hour induction with three different concentrations of 20E (2, 5, and 10 µg) unveils a significant transcriptional upswing in the Gat and Hey genes specifically at a 20E concentration of 10 µg. Significance, determined through Chi-square test, yielded a p-value <0.0010.

(B) The 4-day induction of Bg3c2 cells with three distinct 20E concentrations exhibits a noteworthy increase in the transcription of Gcm, Hey and Insb genes after 2.5 µg 20E induction. Statistical significance, calculated using Student's T-test, shows p-values <0.04 (Gcm, Insb) and <0.02 (Hey).

(C) The 7-day induction with three different 20 E concentrations results in a substantial increase in Gat expression across all concentrations. Additionally, significant transcriptional upregulation is observed for Gcm and Insb genes at 10 µg 20E. Significance, assessed through Student's T-test, reflects p-values <0.0027, <0.0027, <0.0001, <0.0004, and <0.04.

(D) Examination of gene expression post-20E induction reveals a transcriptional increase in the active zone marker Brp and a slight elevation of Yki. Conversely, the neuronal surface receptor Dscam1 and neuronal marker Elav show a decrease. For the glia cell gene Repo and the synapse gene nSyb, expression remains largely unchanged following 20E induction. No statistical significance could be derived from this analysis.

7.8. Yorkie Nuclear Localization in Developing Bg3c2 Cells

Preliminary data from our laboratory indicate that distinct mutations in the Hpo signaling network lead to varied branching phenotypes in postmitotic neurons, with Yki LOF causing axonal overbranching and Yki GOF resulting in the loss of axon collateral (Izadifar A., unpublished data).

Understanding the intracellular localization of Yki is pivotal for unraveling its role in the growth of axonal branches in developing Ms-neurons. In this investigation on insulin treated Bg3c2 cells, Yki demonstrated a predominant presence in the nucleus (Figure 26). The translocation of Yki from the cytoplasm to the nucleus is a crucial step in its function, where it binds to a cofactor with a DNA-binding site, activating target genes associated with proliferation and growth across various tissues (Huang *et al.*, 2005).

Upon meticulous staining of insulin treated Bg3c2 cells, the evident nuclear localization of Yki was further substantiated through quantitative analysis, revealing a highly significant increase in Yki intensity within the nucleus compared to the cytoplasm (Figure 26 C). Notably, the co-staining of Yki with Lamin, a marker for the nuclear envelope (Nikolakaki, Mylonis and Giannakouros, 2017), disclosed a co-localization pattern, suggesting the localization of Yki in the nuclear envelope (Figure 26 B). Additionally, DAPI staining, which delineates the nucleolus, did not entirely overlap with Yki, affirming the absence of Yki in this cellular compartment.

While the role of Yki as a transcription factor in growth and proliferation is well-established in literature, its function in postmitotic neurons, where proliferation ceases, remains unknown. To substantiate the transcriptional function of Yki in Bg3c2 cells, I cloned and transfected a Yki overexpression construct, the findings of which are expounded in the subsequent chapter.

In conclusion, this investigation provides compelling evidence of Yki's specific subcellular localization within the nuclear envelope of developing Bg3c2 cells, opening avenues for understanding its potential transcriptional functions in postmitotic neurons. The subsequent exploration of Yki overexpression will shed light on its role in driving transcriptional processes in this context.

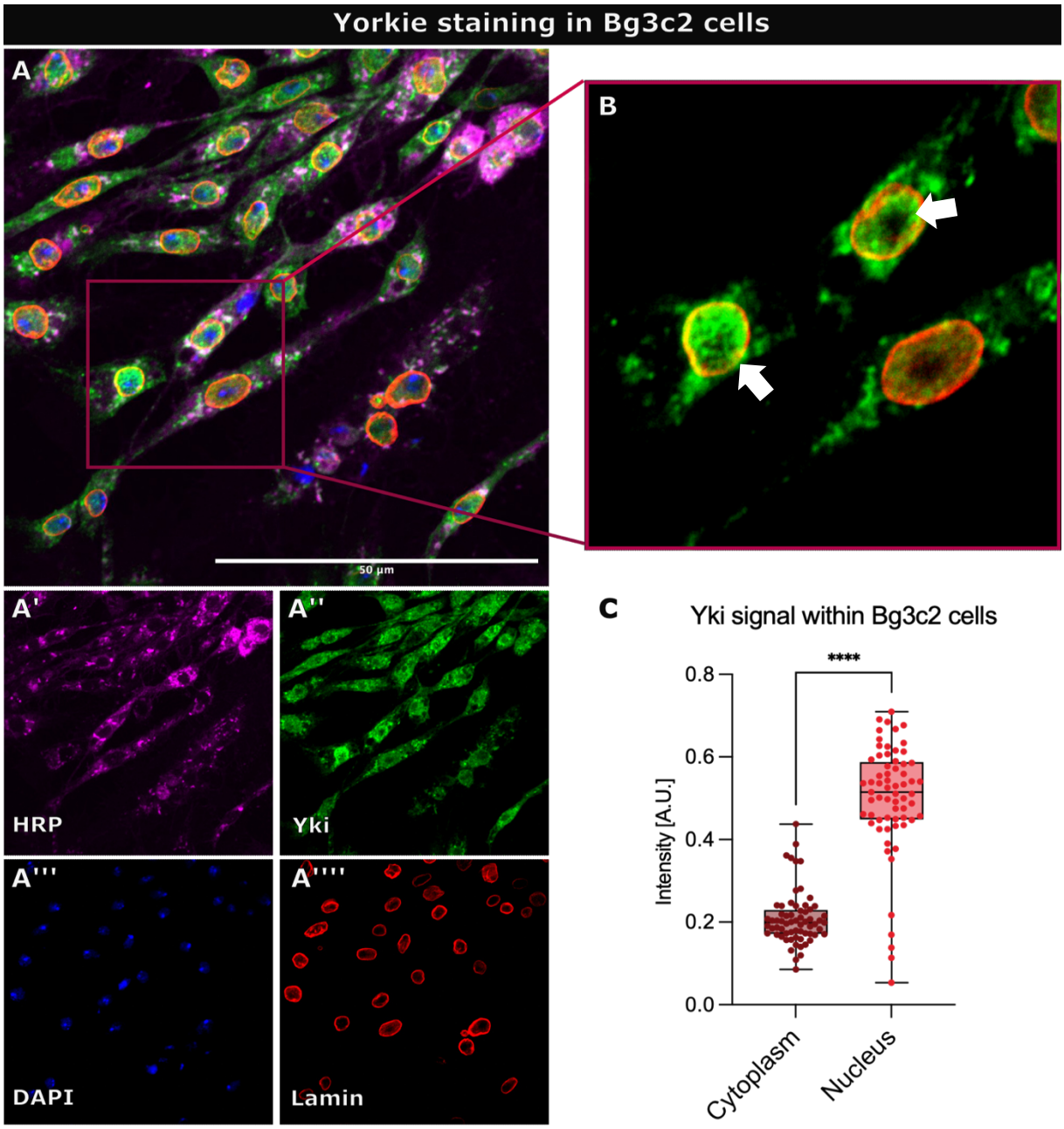

Figure 26. Yorkie Localization in Developing Bg3c2 Cells Indicate Nuclear Envelope Residency.

(A-B) Immunofluorescence staining of Bg3c2 cells with diverse markers.

(A) Merged channels with HRP (A'), Yki (A''), DAPI (A'''), and Lamin (A'''') staining, showing heightened Yki intensity within the nucleus.

(B) Zoomed view of merged Lamin and Yki channels highlighting Yki localization predominantly at the nuclear envelope (indicated by arrows).

(C) Quantitative analysis of Yki intensified, indicating a significantly increased intensity in the nucleus compared to cytoplasm.

Significance assessed wit Student's T-test ($p<0.0001$). Scale bar: 50 µm.

7.9. Variations in Canonical Target Gene Expression upon Yki Overexpression

The preceding section illuminated the predominate nuclear localization of endogenous Yki in developing CNS cells, prompting the exploration of the genes it regulates in this context. To decipher the transcriptional impact of Yki, an inducible Yki plasmid was designed for transfecting Bg3c2 cells (0), inducing a specific Yki-isoform expression under the metallothionein promoter. Post-transfection, GFP-positive cell sorting yielded an adequate cell population for RNA extraction and subsequent qPCR analysis (Figure 27 A-B).

Yki overexpression exhibited an approx. 30-fold increase in expression compared to control Bg3c2 cells (Figure 27 C). Canonical Yki upstream regulators displayed no consistent increase or decrease, and Dscam1 exhibited only a slight reduction (Figure 27 C). Furthermore, Yki overexpression demonstrated no elevating influence on neuronal target genes. Instead, a marginal decrease in progenitor, gcms, and immature neuron genes (Figure 27 D) supported a function independent of proliferation and fate specification in Bg3c2 cells.

Crucially, a notable decrease in canonical Yki target genes was observed (Figure 27 E). While the Hpo signaling network conventionally regulates organ size and growth, including brain size through neuroblast cells (Poon *et al.*, 2016), these results suggested a diverse gene expression pattern influenced by Yki in postmitotic neurons. This implied a potential independence of Yki's function from the canonical network studied in the context of tissue growth.

To validate the cell culture findings, I induced a Yki K.D. construct along with a constitutively active form of Yki in developing neurons of L3 larvae. Despite an observable increase in Yki transcripts *in vivo* following Yki overexpression, no significant effects on canonical genes were noted, aligning with the cell culture results (Figure 27 & Figure 28). Additionally, *in vivo* Yki overexpression failed to induce upregulation of the immature neuron target Hey, indicating an absence of proliferative effects (Figure 28).

Subsequent chapters delve into the proliferative state of Yki overexpression Bg3c2 and S2 cells, aiming to corroborate the molecular results presented here.

In conclusion, this exploration unravels the nuanced role of Yki in regulating gene expression in developing CNS cells, offering insights into potential pathways independent of canonical Hpo signaling.

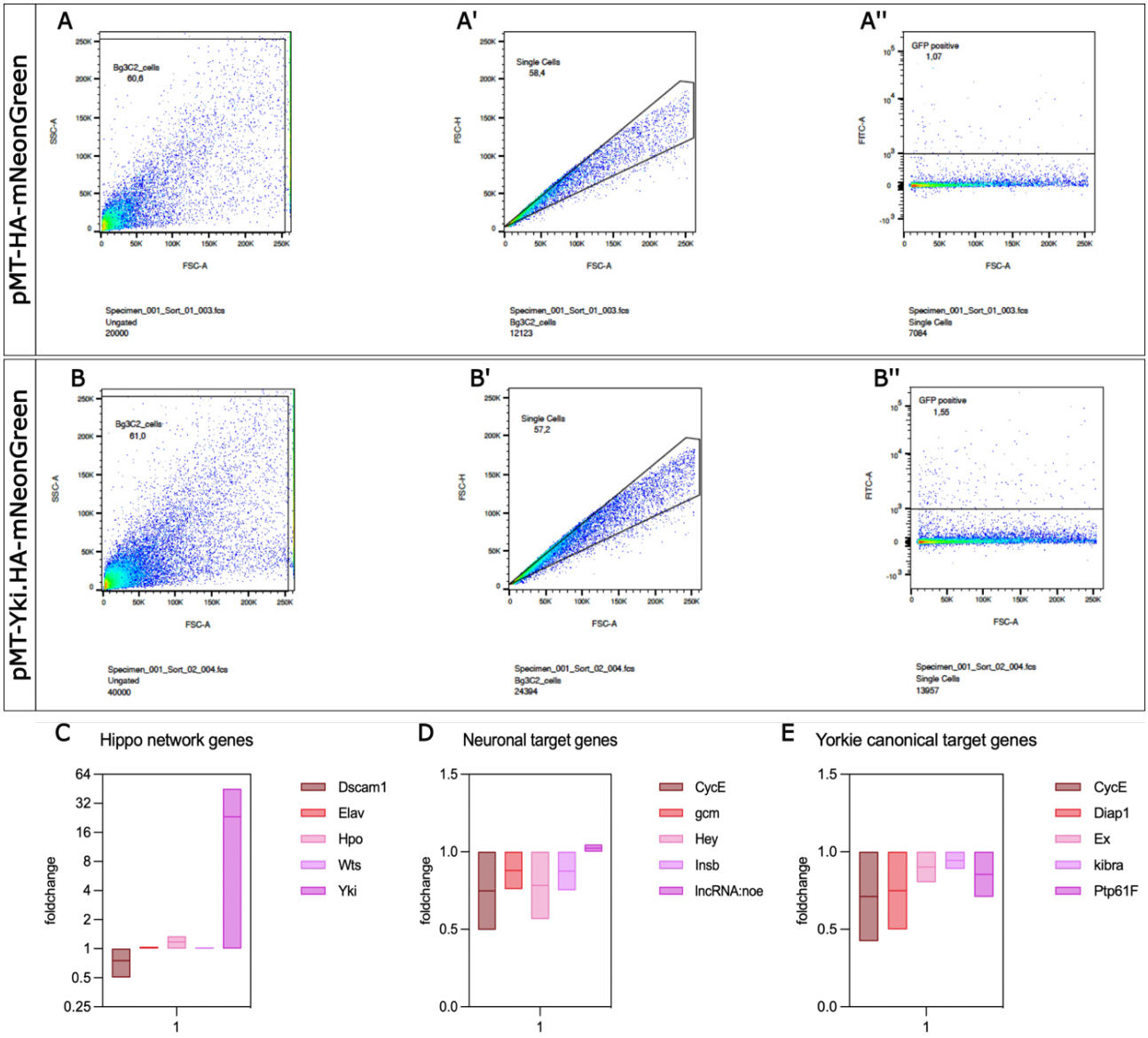

Figure 27. Yki Overexpression in Bg3c2 Cells Diminished Canonical Target Gene Expression.

(A-B) FACS sorting of transfected pMT-HA-mNG control cells (A-A'') and pMT-Yki-HA-mNG Bg3c2 cells (B-B''). Sorting resulted in approx. 1% sorted control cells and 1.5% sorted Yki overexpression Bg3c2 cells.

(C) qPCR confirmed upregulated transcripts of Yki gene but showed no upregulation of Hpo network genes.

(D) Neuronal target genes were predominantly downregulated in Yki overexpression cells.

(E) Canonical Yki target genes exhibited downregulation upon Yki overexpression in Bg3c2 cells. Significance calculated using One-way ANOVA showed no significance for (C), (D) and (E).

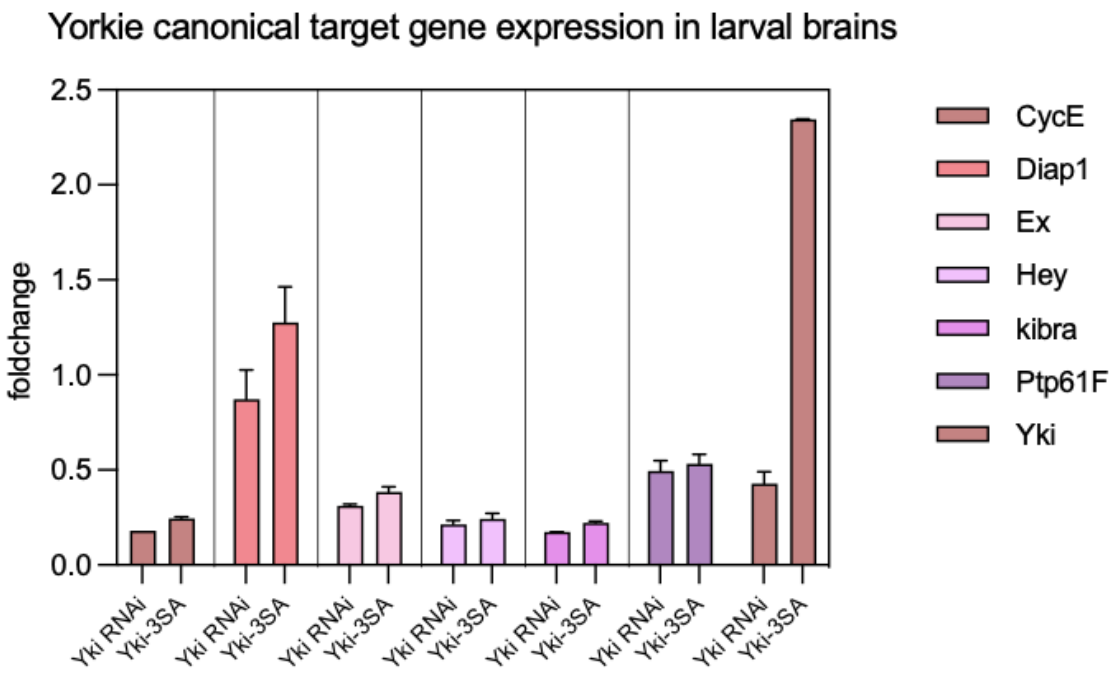

Figure 28. Neurons Expressing a Constitutively Active Form of Yki Fail to Induce Proliferation Genes.

Yki RNAi and Yki-3SA (constitutively active) were expressed in developing neurons using the UAS-Gal4 system through the nSyb-Gal4 construct. Results indicated upregulated Yki transcripts in L3 larval brains for Yki-3SA, with no significant upregulation or decrease in Yki RNAi constructs. Canonical Yki target genes and the mature neuron gene Hey exhibited no significant upregulation in Yki overexpression larval brains. Significance calculated using Student's T-test showed no significance in all measurements.

7.10. Lack of Proliferative Induction by specific Yki-isoform Overexpression in Bg3c2 Cells

The distinctive nuclear presence of endogenous Yki in heterogenous CNS cells suggests a potential role for the Yki network in developing neurons (Figure 26 C). However, whether Yki induces proliferative and growth genes in these cells remains uncertain. To address this, I scrutinized the proliferative state of Bg3c2 cells following transfection with an inducible Yki plasmid. The construction of the metallothionein-inducible plasmid facilitated a specific Yki-isoform overexpression post copper sulfate exposure. Immunostaining of cells revealed a conspicuous increase in mNeonGreen fluorescence in control plasmid transfected cells, while Yki intensity remained unchanged, confirming the control's lack of influence on Yki expression (Figure 29 B' and B"). In contrast, the Yki overexpression plasmid showed overlapping high fluorescence signals for both Yki and mNeonGreen, indicating successful

Yki overexpression (Figure 29 C' and C"). Intriguingly, Yki overexpression distribution spanned the entire cell, with no specific localization to the nucleus or cytoplasm.

In vivo, Yki overexpression in neurons failed to increase canonical gene expression associated with proliferation and growth, aligning with previous findings (Huang *et al.*, 2005; Poon *et al.*, 2016). Subsequently, I evaluated the proliferative status of Bg3c2 and S2 cells, serving as a non-neuronal control, using EdU staining. Salic and Mitchison (2008) enabled the detection of DNA synthesis in growing cells through EdU incorporation and subsequent fluorescent dye detection.

Upon specific Yki-isoform overexpression construct transfection, no colocalization was observed between EdU-positive and Yki overexpression-positive cells in either Bg3c2 or S2 cells (Figure 30 C-D), suggesting Yki's lack of involvement in the proliferation of CNS cells. Notably, Yki overexpression and EdU showed no colocalization, indicating no role in proliferation induction in either tissue.

In summary, both *in vivo* and *in vitro* experiments demonstrated that specific Yki-isoform overexpression neither induced proliferation nor contributed to the growth of neurons. The absence of an increase in canonical Yki gene expression and the lack of colocalization in EdU staining underscored this conclusion. This necessitates further exploration of alternative pathways through which Yki influences neuron function and synapse formation. Our subsequent investigation into Yki gene expression through bulk RNA sequencing in Bg3c2 and S2 cells is detailed in the following chapter.

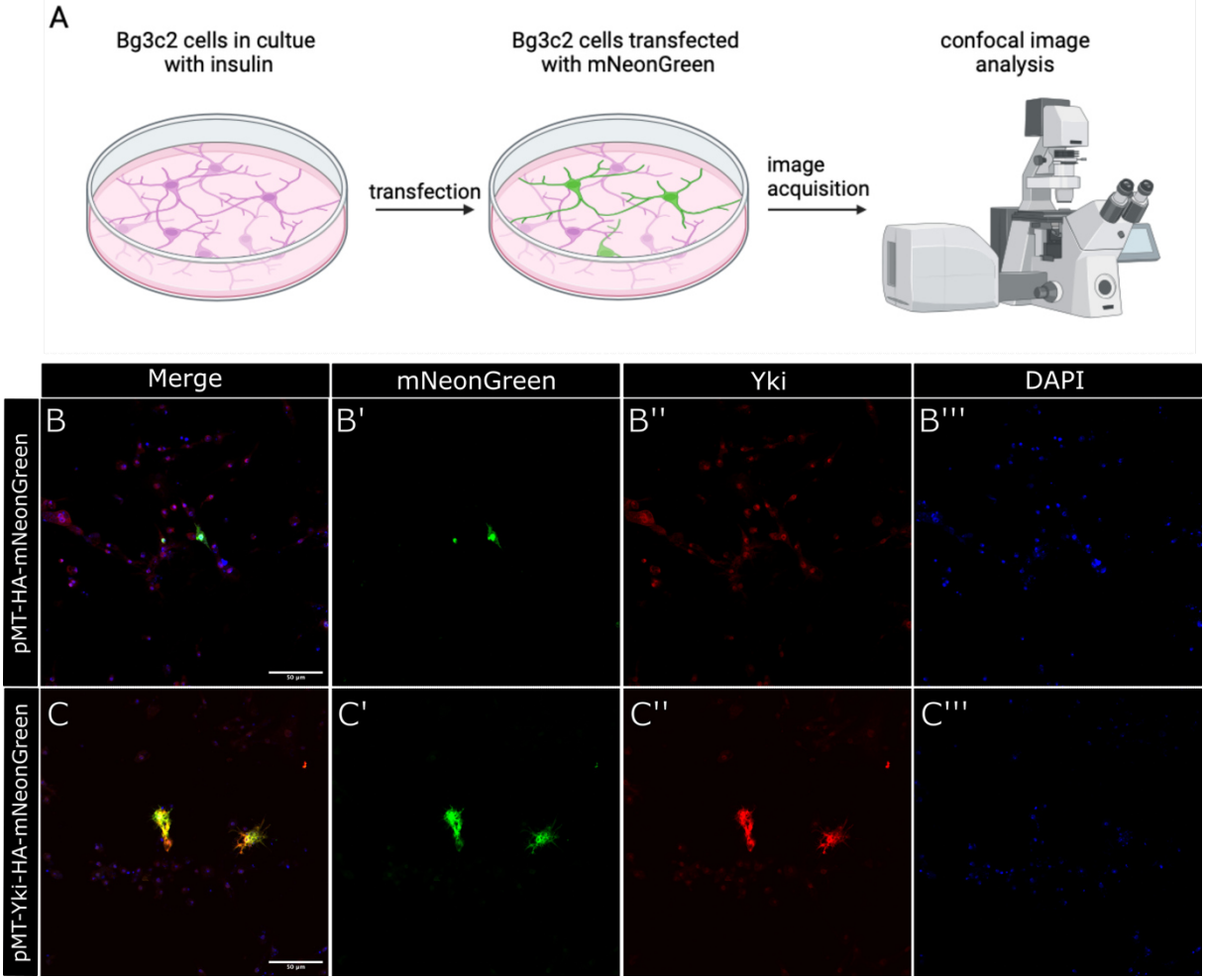

Figure 29. Inducible Yki Plasmid Confirms Yki Overexpression in Bg3c2 Cells.

(A) Schematic representation of cultured Bg3c2 cells before and after transfection with pMT-Yki-HA-mNeonGreen plasmid, followed by image analysis confocal microscopy.

(B) pMT-HA-mNeonGreen control plasmid expressed in Bg3c2 cells reveals mNeonGreen fluorescent protein expression in (B'). Immunostaining visualizes endogenous Yki expression in (B'') and nuclear staining in (B'''').

(C) pMT-Yki-HA-mNeonGreen plasmid expressed in Bg3c2 cells exhibits mNeonGreen fluorescent protein expression in (C') and Yki expression in (C''). Nuclear staining with DAPI is visualized in (C'''). Scale bar: 50µm.

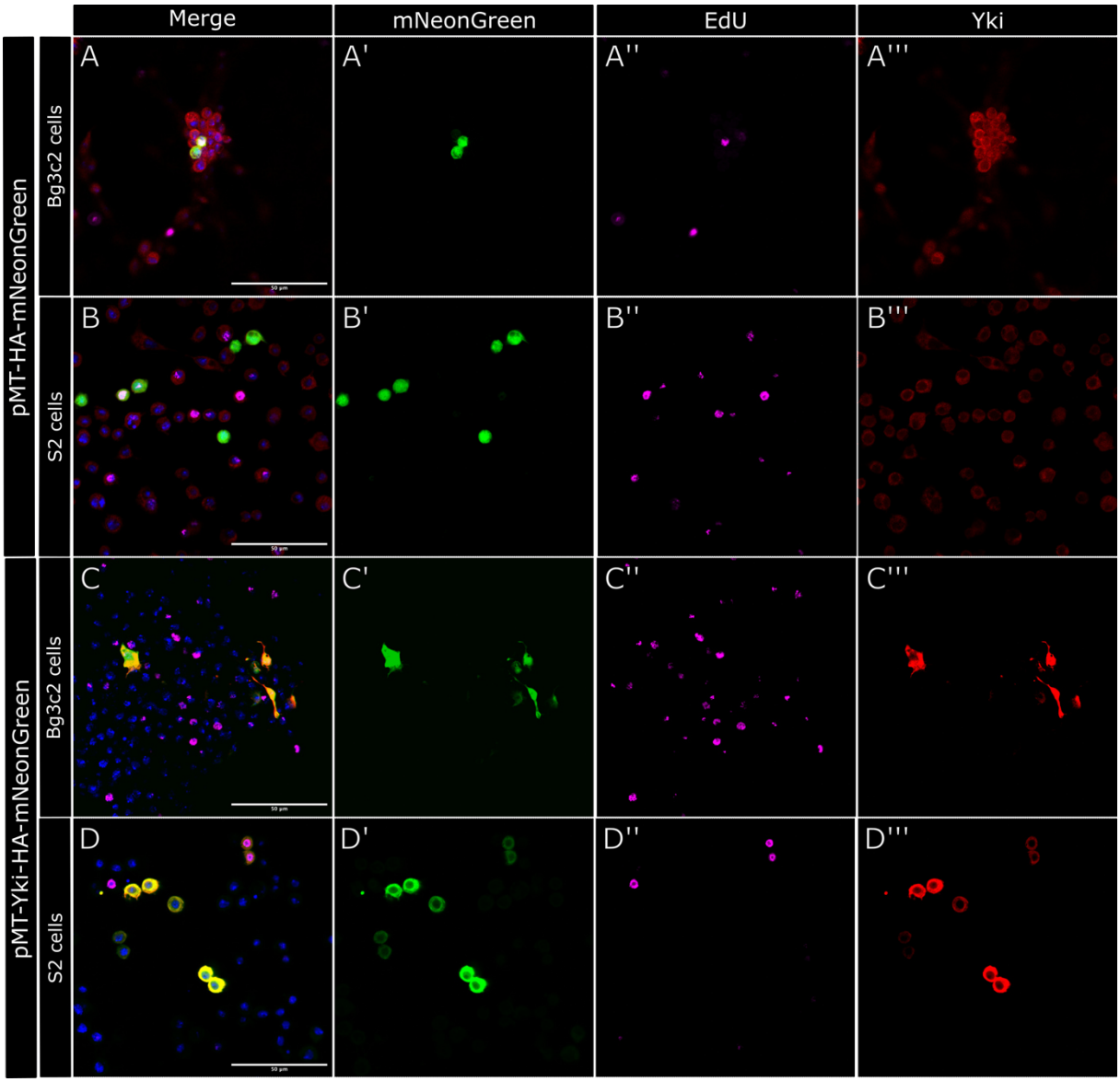

Figure 30. Lack of EdU Staining Colocalization with Yki Overexpression in Bg3c2 cells.

(A) pMT-HA-mNeonGreen plasmid expression in Bg3c2 cells with mNeonGreen expression displayed in (A'). EdU staining of proliferating cells shown in (A'') and endogenous Yki staining in (A'''). Transfected cells colocalize with EdU staining (indicated by arrows).

(B) pMT-HA-mNeonGreen plasmid expression in S2 cells with mNeonGreen expression displayed in (B'). EdU staining of proliferating cells is shown in (B'') and endogenous Yki staining in (B'''). Several transfected cells show colocalization with EdU staining (indicated by arrows).

(C) pMT-Yki-HA-mNeonGreen plasmid expression in Bg3c2 cells with mNeonGreen expression displayed in (C'). EdU staining of proliferating cells is shown in (C'') and Yki expression in (C'''). All transfected cells overexpressing a specific Yki-isoform lack positive EdU staining.

(D) pMT-Yki-HA-mNeonGreen plasmid expression in S2 cells with mNeonGreen expression displayed in (D'). EdU staining of proliferating cells is shown in (D'') and Yki expression in (D'''). None of the Yki overexpression transfected cells are positive for EdU staining. Scale bar: 50µm.

7.11. Bulk Sequencing Reveals Altered Gene Expression in Yki Overexpressed Bg3c2 Cells

Yki overexpression, both *in vitro* and *in vivo*, demonstrated a distinctive impact on canonical Yki target genes, suggesting an unconventional role in CNS cells. This observation aligns with *in vivo* Ms-neuron mutation data (Izadifar A., unpublished data) emphasizing Yki's importance in postmitotic neuronal development. Complementing earlier *in vitro* findings, Yki induces a unique set of target genes unrelated to canonical endothelial proliferative genes. To scrutinize transcriptomic alterations following a specific Yki-isoform overexpression in CNS cells, I conducted bulk RNA sequencing analysis on Bg3c2 cells in comparison to S2 cells, characterized as hemocytes (Schneider, 1972).

RNA-seq. data illustrated visible transcriptome distinctions between S2 and Bg3c2 cells (Figure 31). In the absence of Yki overexpression, Bg3c2 cells expressed genes crucial for neurogenesis and gliogenesis (Figure 31 F). Differential gene expression analysis underscored a clear disparity in expression between these tissues, highlighting their diverse tissue progenitor origins, CNS, and hemocyte for Bg3c2 and S2 cells, respectively.

Yki overexpression was achieved through transfection of an inducible Yki plasmid, followed by FACS sorting and bulk RNA-seq analysis. Comparative analysis between control CNS cells and Yki-induced cells revealed an upregulation in several neuronal genes. Particularly, Monocarboxylate transporter 1 (Mct1), implicated in synaptogenesis (Böhme *et al.*, 2021), and Defective Proboscis Extension Response 10 (Dpr10), associated with neuronal tissue development and communication (S. Xu *et al.*, 2018), exhibited increased expression upon specific Yki-isoform overexpression (Figure 31 B). Notably, a noteworthy upregulation in mTor levels was observed in Yki overexpression Bg3c2 cells. The mTor gene encodes for mechanistic Target of Rapamycin (mTor) protein, which exists in two different complexes (mTOR1 and mTOR2). mTOR1 functions as a key player in nutrient homeostasis, orchestrating growth responses in reaction to changes in nutritional conditions or periods of starvation (Oldham *et al.*, 2000). Additionally, in S2 cells, there was an elevation in Merlin (Mer) expression following specific Yki-isoform overexpression. Mer is recognized as a constituent of the Hpo network, contributing to its tumor suppressor function within a complex involving Ex and Kibra, thereby governing Hpo signaling (Yu *et al.*, 2010). This suggests a feedback loop involving Hpo network genes in S2 cells in response to increased

Yki levels, while in CNS cells, Yki overexpression modulates growth through the nutrient-sensing mTor pathway.

Bulk sequencing data comparisons emphasized Bg3c2 cells as CNS cells, showcasing both distinct and shared gene expression patterns with S2 cells. Hierarchical clustering and correlation analysis reinforced the specificity of Yki overexpression samples in both Bg3c2 and S2 cells (Figure 31 A-A'''). Moreover, gene ontology (GO) enrichment analysis highlighted neurogenesis and gliogenesis as the most expressed categories in both control and Yki overexpression samples (Figure 32 D-E).

Venn diagrams of differentially expressed genes revealed minimal overlap between Bg3c2 and S2 cells (Figure 33 A), indicating divergent functions of Yki in these cell types. Comparison with published Yki overexpression data in wing discs (Oh *et al.*, 2013) demonstrated specific gene regulation patterns in CNS cells. Upregulated and downregulated genes post-Yki overexpression exhibited marginal overlap between Bg3c2 and S2 cells (Figure 33 B). The comparison further substantiated the unique influence of Yki on the gene expression in distinct cellular contexts.

In conclusion, overexpression of a specific Yki-isoform in Bg3c2 cells induces significant alterations in gene expression, particularly in nutrient homeostasis genes associated with neurogenesis and gliogenesis. The distinctive gene expression patterns underscore the context dependent nature of Yki's function in CNS cells, emphasizing its multifaceted role in neuronal development. These findings contribute valuable insights into the intricate regulatory mechanisms orchestrated by Yki in postmitotic neurons, opening avenues for further exploration into the underlying molecular pathways.

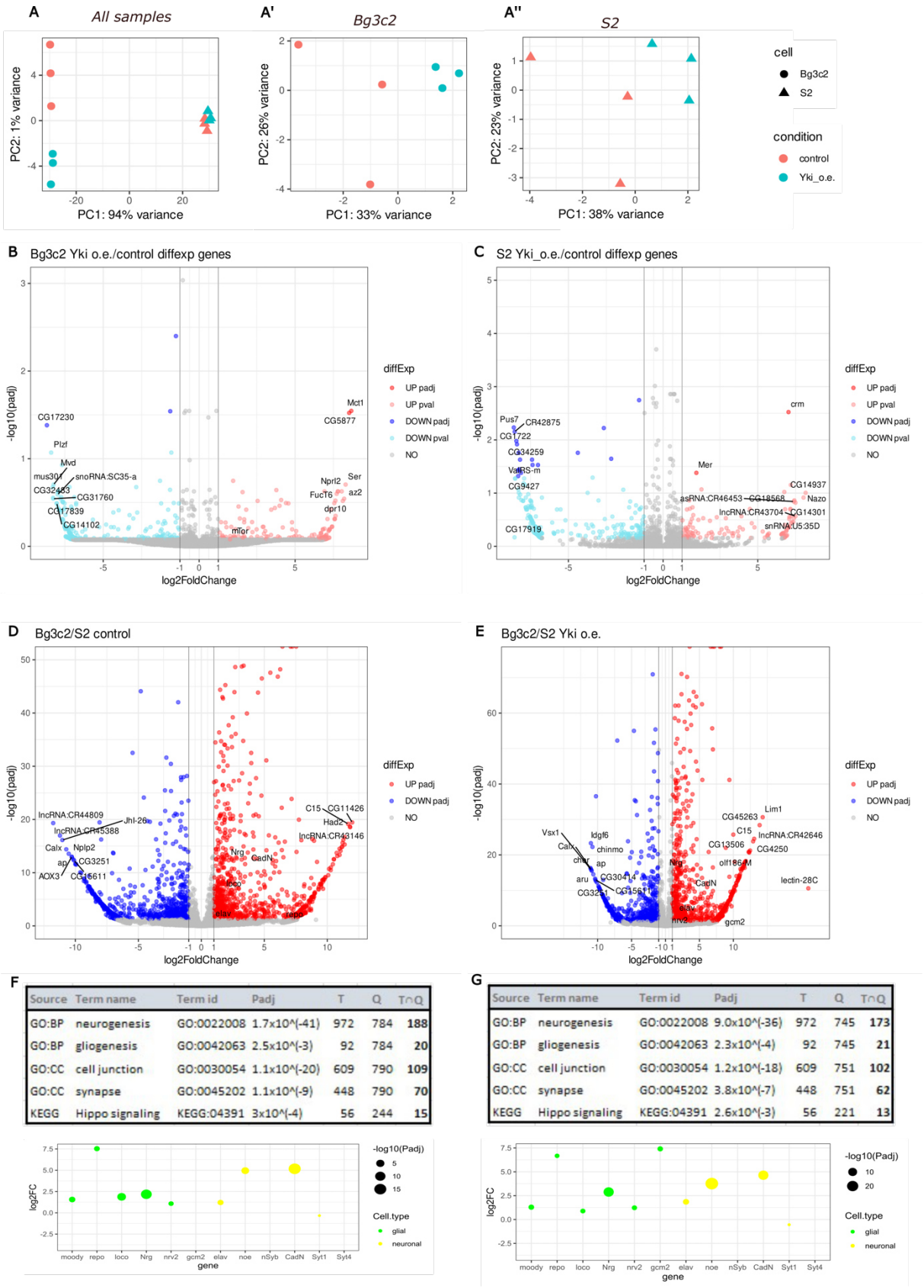

Figure 31. Yki Overexpression Elicits Divergent Gene Expression Patterns in Bg3c2 and S2 Cells.

(A) Principal component analysis (PCA) of Bg3c2 versus S2 samples reveals substantial variation between tissues and limited variability between control and specific Yki-isoform overexpression conditions. Triangles represent S2 samples, while circles represent Bg3c2 samples, with control samples in red and Yki overexpression samples in blue, respectively. (A') Subsequent PCA of Bg3c2 control and Yki overexpression samples demonstrate a clustering of Yki overexpression samples, contrasting with greater expression differences observed in control samples. The overall variance is at approx. 59%. (A'') PCA of S2 control and Yki overexpression samples result in the formation of clusters for Yki overexpression samples and increased expression difference in control samples. The overall variance is at approx. 61%.

(B) Log2foldchange analysis of differentially expressed genes in Yki overexpression Bg3c2 cells, compared to controls, shows upregulation of various genes such as Mct1, mTor and Dpr10, along with downregulation of genes including Plzf, mus301 and CG17230.

(C) Log2foldchange analysis of differentially expressed genes in Yki overexpression S2 cells, compared to controls, shows upregulation of various genes such as Mer and Crm, and downregulation of genes, including Pus7 and CG34259.

(D) Examination of differentially expressed genes between control Bg3c2 and S2 samples indicates an increase in genes associated with neurogenesis and gliogenesis, indicative of a heterogenous mixture of CNS cells.

(E) Evaluation of differentially expressed genes in Yki overexpression Bg3c2 compared to S2 samples demonstrates an increase in genes associated with neurogenesis and gliogenesis.

(F) Detailed presentation of distinct glial and neuronal gene expressions, including Repo, Nrg and nSyb, in control Bg3c2 versus S2 cells.

(G) Detailed representation of glial and neuronal gene expression, including Repo, Nrg and nSyb, in Yki overexpression Bg3c2 versus S2 cells.

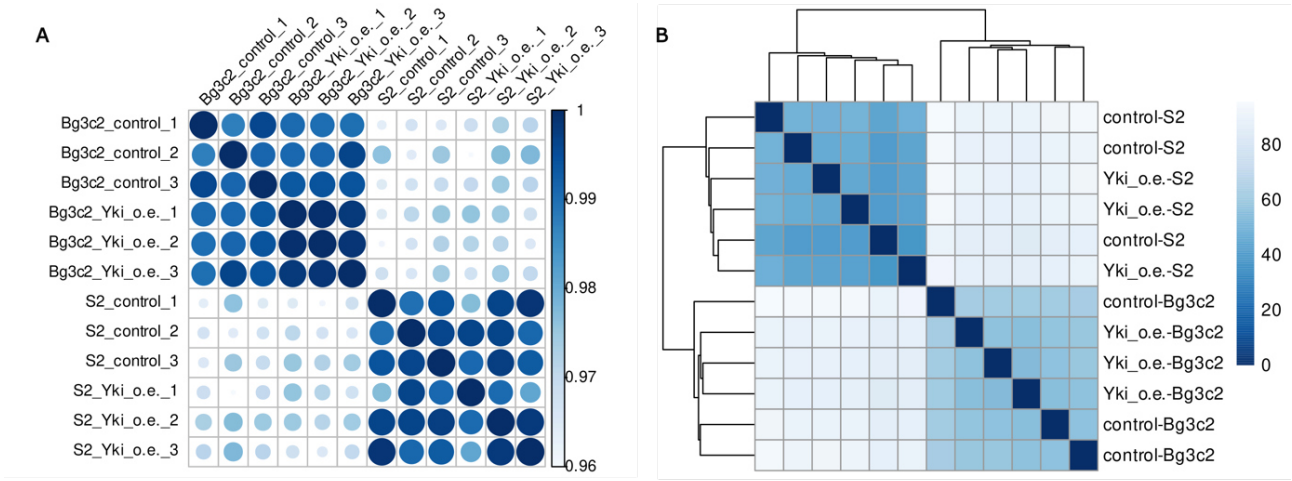

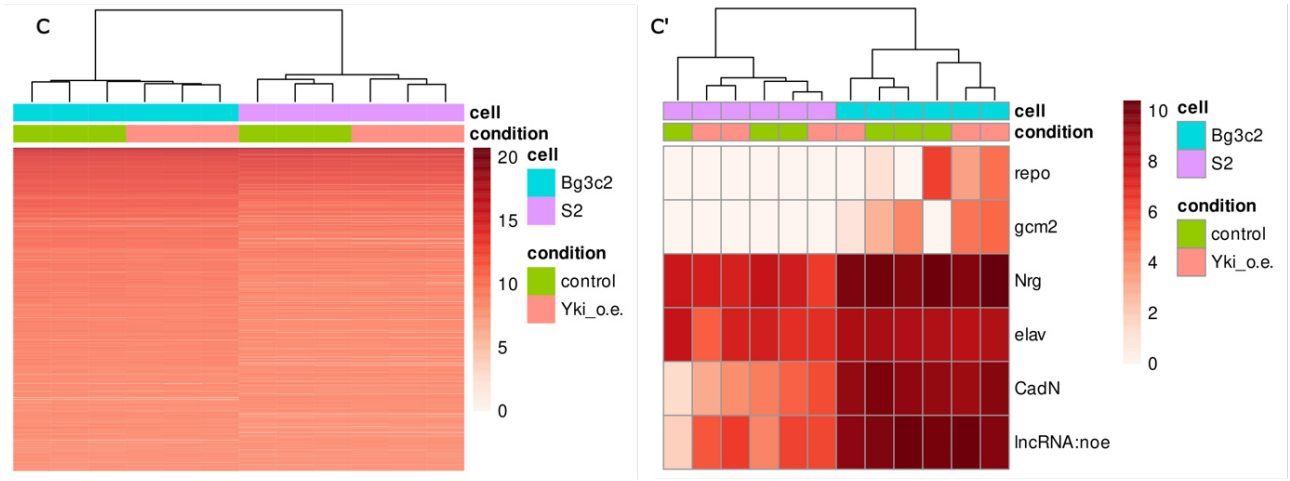

D **Control**

Source	Term Name	Term id	Padj	T	Q	T∩Q
GO:BP	neurogenesis	GO:0022008	1.7x10^(-41)	972	784	**188**
GO:BP	gliogenesis	GO:0042063	2.5x10^(-3)	92	784	**20**
GO:CC	cell juction	GO:0030054	1.1x10^(-20)	609	790	**109**
GO:CC	synapse	GO:0045202	1.1x10^(-9)	448	790	**70**
GO:CC	cytoskeleton	GO:0005856	1.2x10^(-7)	656	790	**85**
GO:CC	mitochondrion	GO:0005739	1	981	790	**43**
KEGG	Hippo signaling	KEGG:04391	3x10^(-4)	56	244	**15**

E **Yki o.e.**

Source	Term Name	Term id	Padj	T	Q	T∩Q
GO:BP	neurogenesis	GO:0022008	9.0x10^(-36)	972	745	**173**
GO:BP	gliogenesis	GO:0042063	2.3x10^(-4)	92	745	**21**
GO:CC	cell juction	GO:0030054	1.2x10^(-18)	609	751	**102**
GO:CC	synapse	GO:0045202	3.8x10^(-7)	448	751	**62**
GO:CC	cytoskeleton	GO:0005856	1.4x10^(-2)	656	751	**66**
GO:CC	mitochondrion	GO:0005739	1	981	751	**47**
KEGG	Hippo signaling	KEGG:04391	2.6x10^(-3)	56	221	**13**

Figure 32. Comparative Analysis of RNA Sequencing Data Highlight Bg3c2 Cells as CNS Cells.

(A) The correlation between gene expressions in Bg3c2 and S2 samples is depicted, with more correlated samples represented in dark blue with larger circle sizes, while less correlated samples are shown in light blue with smaller circle sizes. Higher correlation is observed between control and specific Yki-isoform overexpression samples within the same tissue.

(B) Hierarchical clustering of gene expression is presented, with trees displaying similar gene expression at smaller distances and opposing gene expression at larger distances. Yki overexpression Bg3c2 samples cluster together, contrasting with variable gene expression similarity observed in control samples. Two samples of S2 cells cluster together, while one sample exhibits higher variability in control and Yki overexpression conditions.

(C) Heatmap visualizing transcriptome comparisons between Bg3c2 and S2 cells under control and specific Yki-isoform overexpression conditions. (C') Heatmap focusing on neuronal and glial genes, highlighting the differential gene expression between Bg3c2 and S2 cells, with increased expression of neuronal genes in Bg3c2 cells compared to S2 cells.
(D) Gene ontology enrichment analysis of control samples.
(E) Yki overexpression samples categorize highly expressed genes as associated with neurogenesis and gliogenesis.

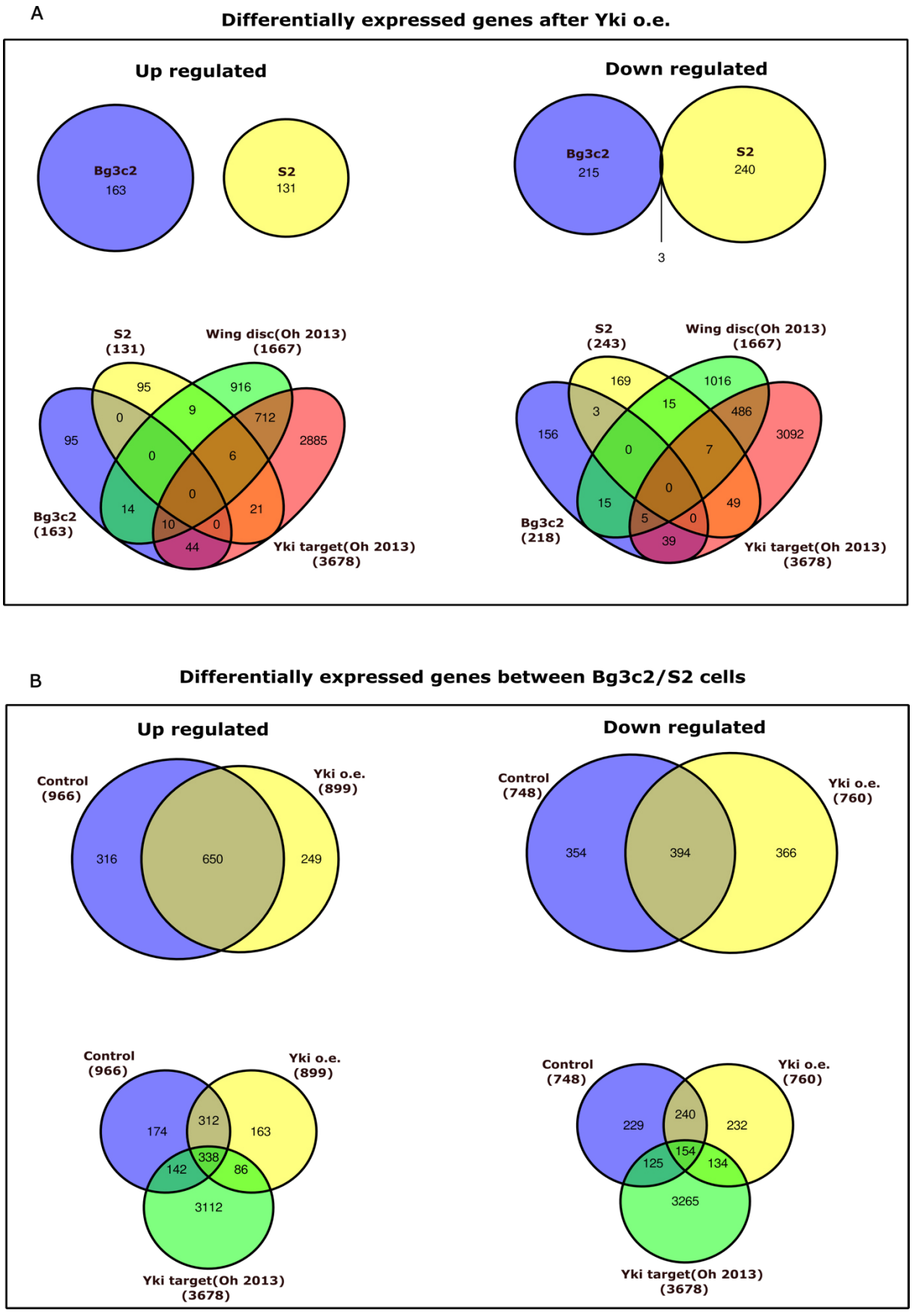

Figure 33. Comparative Analysis of Differentially Expressed Genes Highlights Divergent Roles of Yki in Bg3c2 and S2 Cells.

(A) The Venn diagram illustrates the limited overlap in upregulating and downregulated genes following specific Yki-isoform overexpression between Bg3c2 and S2 cells. A comparison with published Yki overexpression data in wing discs reveals 24 upregulated genes overlapping in Bg3c2 and 15 in S2 cells, along with 20 downregulated genes in Bg3c2 and 22 in S2 cells, demonstrating differential responses in distinct cellular contexts. Additionally, the comparison of identified Yki target genes in published wing disc data shows a more substantial overlap of 54 upregulated genes in Bg3c2 compared to 27 in S2 cells, while downregulated Yki target genes exhibit an overlap of 44 genes in Bg3c2 and 56 genes in S2 cells.

(B) The differential gene expression comparison between Bg3c2 and S2 cells displays a larger overlap in upregulated genes (650 genes) than downregulated genes (394 genes) between control and specific Yki-isoform overexpression samples. A comparison with published Yki overexpression wing disc data indicates an approx. 5% overlap in upregulated control and Yki overexpression genes, while downregulated genes show a total overlap of approx. 8% with published wing disc data, emphasizing the specificity of Yki's regulatory influence in diverse cellular environments.

8. Discussion

The complex process of neuronal development in *Drosophila Melanogaster* is a fascinating area of research, and fundamental mechanisms like axon branching, synaptogenesis and formation of neuronal circuits can be elucidated at single neuron resolution. The mechanosensory neurons (Ms-neurons) of *D.m.* represent a unique model to study the axonal branching and synapse formation in developing neurons during the second neurogenesis wave in the process of metamorphosis. Experiments performed in our lab using the Ms-neurons as developmental model, showed a significant impact of Hippo (Hpo) signaling network components on branching (Izadifar A., unpublished data). Based on this knowledge this dissertation elucidates the function of Yki target genes, specifically Brat, on Ms-neuron development *in vivo*.

Yorkie Downstream Function is Involved in Functional Axonal Branching and Synaptogenesis of Mechanosensory Neurons

Using the genetic tools available for *D.m.* I could show an impact of distinct Yki target genes on the axonal branch structure and synapse number in Ms-neurons (Figure 17 (A-F)). The RNAi studies suggest a role of specific Yki target genes in Ms-neuron development, such as knock-down (K.D.) of Dpr-18 and Ptp61F led to ectopic synapses, while Spen K.D. induced loss of the anterior axonal branch. Interestingly, Dpr-18 and Ptp61F show the same phenotypical outcome in Ms-neurons underlying the link between Protein Tyrosine Phosphatases (Ptps) and adaptor proteins in synaptogenesis. Previous research already identified the influence of the SH3/SH2 adaptor protein Dock on variants of Ptp61F and therefore stressed the relationship of these proteins in regulating Protein Tyrosine Kinase (Ptk) signaling (Willoughby *et al.*, 2017). Furthermore, also the structure of Dscam is characterized by a SH2/SH3 binding motif, which intriguingly interacts with Dock to initiate axon guidance in *D.m.* (Schmucker *et al.*, 2000; Apitanyasai *et al.*, 2019).

The captivating phenotype of Spen suggested a sub compartmentalized function in axonal branching (Figure 17 D & Figure). Spens function is known to be important in neuronal cell fate and axon guidance as well as cell cycle regulation and fat storage (Mace and Tugores, 2004; Jin *et al.*, 2009; Gillette *et al.*, 2020). Research stated that overexpression of Spen lead to disrupted axon outgrowth during metamorphosis in CCAP/bursicon neuron

development (Gu *et al.*, 2017). Together with the findings of this dissertation I propose a functional role in axon branching of Ms-neurons, specific for the anterior branch (Appendix 9). To strengthen this hypothesis, however, more studies will be necessary.

Conversely, our findings demonstrated that K.D. of Sty resulted in massive outgrowth in Ms-neurons (Figure 17 E), highlighting its crucial function in promoting general growth processes. This observation aligns with published studies on the negative feedback-loop modulation of growth factors and Stys function as an inhibitor of tracheal branching, suggesting its involvement in growth-mediated functions. I therefore conclude that it may not be specific to axonal branching mechanisms (Hacohen *et al.*, 1998; Sieglitz *et al.*, 2013). Furthermore, our results highlighted the K.D. of Scrib, which led to a shortage of collaterals and missing secondary and tertiary branches, suggesting a role in postmitotic neuronal branching. The protein is known to have distinct functions in regulating cell proliferation, epithelial polarity, integrity, and tumor suppression in the context of Hpo signaling network (Humbert, Russell and Richardson, 2003; Dow *et al.*, 2007; Bonello and Peifer, 2019; Nakajima, 2021). Intriguingly, as Scrib functions within the Hpo signaling pathway in a complex with Dlg and Lgl, I propose further studies of Dlg and Lgl K.D. in Ms-neurons to investigate if the complex is active during Ms-neuronal development.

Of particular fascination are the findings in Ms-neuron development concerning the Yki target gene Brat, which was found in a screen for Yki target genes by the George Halder laboratory. Brat being known as tumor suppressor and embryonic patterning gene shows variation in function depending on the proteins it interacts with as well as the tissue and time point. Our findings verified a dramatic effect on axonal branch length and synapse number in Ms-neurons (Figure 18 & Figure 20). The LOF phenotypes varied based on the mutation of the gene indicating a gradient specific function for Brat in neuronal development (Figure 20). Intriguingly, preliminary data of Brat overexpression indicate the opposite phenotype, with increased branch length but specific to the primary branch. Learning from established research of Brat as a translational repressor and Yki as a transcriptional co-activator, I hypothesize a regulatory balance between these molecules in modulating axon branching and synaptogenesis in Ms-neurons. Furthermore, our laboratory experiments demonstrated Yki LOF and GOF exert distinct influences on Ms-neuron axonal structure. Specifically, Yki LOF resulted in axonal overbranching, whereas Yki GOF led to loss of collaterals (Izadifar A., unpublished data). These observations give rise

to the intriguing hypothesis of a regulatory interplay between Yki and Brat in neuronal development. Notably, our preliminary data on Brat LOF and GOF suggest antagonistic effects compared to Yki, further supporting the notion of a regulatory balance between these key molecules. Importantly, Yki was shown to have a crucial function in the cell fate decision during nervous system development of the *D.m.* eye by interacting with the transcriptional regulator Bonus (Bon), which like Brat belongs to the TRIM family proteins (Zhao, Moberg and Veraksa, 2023). Brat and Bon being both TRIM family protein members contain therefore similar protein structures and may indicate a similar protein interaction activity between Yki and Brat. I propose therefore to investigate a physical interaction between Yki and Brat with experiments such as Co-immunoprecipitation and further recommend epistasis *in vivo* experiments in Ms-neurons, by checking for a phenotype rescue of either simultaneous LOF or GOF of these proteins.

Drosophila Melanogaster Bg3c2-Cells are Characterized by Cellular Heterogeneity of Central Nervous System

The utilization of cell culture systems constitutes a crucial cornerstone in scientific research, providing an invaluable platform for the study of diverse tissues through *in vitro* experiments. The intricate mosaic of nervous system cells engenders a mesh of developmental pathways requiring careful investigation. The Bg3c2-cell line, deriving from larval CNS of *D.m.*, has emerged as a protagonist in numerous scientific studies investigating genomic organization, gene regulation, and cellular dynamics (Boldyreva *et al.*, 2017; Yao *et al.*, 2018; Ulianov *et al.*, 2021).

Notably, the journey into establishing cell cultures has uncovered a fascinating interplay wherein insulin emerges as a catalyst, driving both proliferation and differentiation of neuronal progenitors into mature neurons within the Bg3c2 milieu (Ui *et al.*, 1994; Luhur, Klueg and Zelhof, 2019). The empirical data corroborate the profound influence of insulin on neurite growth and the maturation cascade into neurons, as depicted in Figure 22. Moreover, the investigations into cell culture substrate coatings, such as Poly-L-Lysine, Laminin, and Fibronectin, have illuminated their pivotal role in enhancing cell adherence and contributing to a more natural environment for growth (Figure 23). Strikingly, Fibronectin coating, after a 4-day incubation period, emerged as the optimal substrate, promising the attainment of optimal cell density and neurite length. These findings

resonate with the guidelines provided by manufacturers, emphasizing the indispensability of extracellular matrix proteins for the efficacious handling of cell cultures (*Extracellular Matrix Proteins and Tools for Cell Culture Optimization*).

However, amidst the increase of neurites and HRP^+ cells induced by Fibronectin coating and insulin supplementation, the gene expression analyses of Bg3c2 cells unveiled a mosaic of heterogeneity spreading through the developmental landscape of CNS cells. The experiments delineated the diverse expression patterns of genes associated with progenitors, differentiating and mature neurons, as depicted in Figure 24. Furthermore, our experiments to steer developmental trajectories towards mature neurons through 20-hydroxyecdysone (20E) treatment unveiled a nuanced effect, characterized by augmented neurite growth and gene expression signatures associated with distinct neuronal lineages, but without any specificity towards distinct postmitotic neurons. Intriguingly, concentration-dependent effect of 20E underscored a preference towards astrocyte and glia cell development, with negligible impact on mature neuron genes (Figure 25).

A retrospective review of previous studies unravels the pivotal role accorded to the steroid hormone 20E in orchestrating key developmental transitions within the CNS of *D.m.* Notably, 20E is involved in initiating metamorphosis by orchestrating the transcription of genes implicated in metabolism, immunity, and stress (Beckstead, Lam and Thummel, 2005). This modulatory function is primarily mediated through the ecdysone receptor (EcR), which finds ubiquitous residence within neurons, glia cells, and various other tissues (Hakim, Yaniv and Schuldiner, 2014; Boulanger and Dura, 2015). The concentration-dependent effects of 20E, as revealed by the investigations, resoundingly underscore its significant influence over glia cells and astrocytes, thereby corroborating the tissue-specific expression patterns of EcR isoforms, which undergo metamorphic flux during *D.m.* ontogenesis (Talbot, Swyryd and Hogness, 1993; *Ecdysone Receptor - an overview | ScienceDirect Topics*).

Considering these findings, I stress the necessity to define the isoformic landscape of EcR within Bg3c2 cells. Ideally, a single-cell analysis holds promise for providing an initial preview into the distribution of EcR isoforms and, by extension, the nuanced impact of 20E on developmental trajectories. Nonetheless, considering the marginal impact on mature neuron development, I decided to avoid 20E treatment in the subsequent investigations into the influence of Yki on neuronal dynamics.

Furthermore, our analysis of the Bg3c2 culture as heterogenous combination of *D.m.* CNS cells underscores the interplay between complexity and maintenance inherent in such systems. Despite the attendant challenges posed by heterogeneity, including complexities in standardization and potential experimental interference, I choose to emphasize the natural advantages of such a diverse cellular landscape. Indeed, the presence of distinct cell types within the culture milieu serves as a reminder of the complexities characterizing inherent cellular systems, thereby affording invaluable insights into the network of biological interactions and responses (Luhur, Klueg and Zelhof, 2019). Moreover, heterogeneity provides researchers with a multifaceted platform upon which to characterize the diverse nuances underlying cellular behaviors and responses to experimental challenges (Cherbas and Gong, 2014).

Ultimately, our experiments in establishing a neuronal cell culture line yielded a well-characterized heterogenous mixture of CNS cells, laying the foundation for subsequent investigations into the impact of Yki on these cellular dynamics.

Yorkie Subcellular Localization: Nuclear Lamina Residence and Nucleolar Exclusion

The activation state of the Hpo signaling network depends upon the subcellular localization of Yki, marking a pivotal determinant of cellular fate. Either the signaling network remains quiescent, designating Ykis phosphorylation by Wts, leading to its sequestration in the cytoplasm and subsequent degradation, or the pathway is activated, marking Ykis translocation to the nucleus and subsequent expression of genes governing proliferation and differentiation (Harvey, Pfleger and Hariharan, 2003). My investigations showed the prevalent nuclear localization of Yki in insulin treated Bg3c2 cells (Figure 26), manifesting its essential function in promoting proliferation and differentiation, as verified by our laboratories' *in vivo* LOF/GOF experiments (Izadifar A., unpublished data).

Intriguingly, the experiments shed light on a precise characterization of Ykis subcellular localization. Notably, I observe a co-localization of Yki with Lamin, suggesting its preferential localization at the nuclear envelope rather than within the nucleolus (Figure 26 B). The nucleolus, as depicted in literature, orchestrates crucial functions including ribosome generation, protein synthesis, and regulation of cellular mechanisms during oogenesis (Dapples and King, 1970; Baserga, DiMario and Duncan, 2020; Talbot *et al.*,

2023). Conversely, the nuclear lamina assumes a pivotal role in maintaining nuclear architecture, chromatin organization, and developmental processes (Pickersgill *et al.*, 2006; Barton *et al.*, 2013; Bronshtein *et al.*, 2015). The localization of Yki at the nuclear lamina thus hints at its involvement in chromatin dynamics.

Previous research claims Ykis association with chromatin remodeling complexes, such as the Switch/sucrose nonfermentable (SWI/SNF) complex, facilitating the transcriptional activation of target genes within imaginal eye discs of *D.m.* (Oh *et al.*, 2013). Additionally, Ykis interaction with histone methyltransferase complexes underscore its role in orchestrating modifications influencing chromatin structure (Hillmer and Link, 2019). Notably, Yki interacts directly with chromatin modifiers including Ncoa6, Brahma and the GAGA factor, thus influencing chromatin structure and modification in *D.m.* cells to promote differentiation and growth (Bayarmagnai *et al.*, 2012; Qing *et al.*, 2014; Zhu *et al.*, 2015).

Considering these findings, I propose a comprehensive exploration of direct Yki interaction partners within the cellular context of CNS cells, with particular focus on chromatin modifiers such as Ncoa6, through e.g. Co-immunoprecipitation. Moreover, elucidating the epistatic relationship through K.D. of chromatin modifiers in developing Ms-neurons *in vivo* promises to reveal the downstream functions of Yki during this intricate developmental mechanism.

Yorkie Drives mTor Transcription Over Canonical Genes in *Drosophila Melanogaster* Central Nervous System Cells

Numerous studies have underscored the pivotal role of the Hpo pathway and Yki transcriptional activation in regulating cell proliferation and growth across various transcriptional genes targeted by Yki, including CycE, Diap1, Ex, and Kibra, have been well-documented for their involvement in promoting growth, proliferation, and differentiation in different cellular contexts (Harvey, Pfleger and Hariharan, 2003; Wu *et al.*, 2008; Zhao, Moberg and Veraksa, 2023). Surprisingly, the experiments revealed a lack of increase in canonical gene expression upon overexpression of a specific Yki-isoform in the CNS cells, coupled with the absence of colocalization with EdU (Figure 27Figure 30), suggesting minimal involvement in proliferation. As postmitotic neurons cease differentiation, the expression of canonical growth and proliferation genes becomes obsolete.

Through bulk RNA sequencing analysis, I observed upregulation of neuronal genes and the mTor network (Figure 31), with neurogenesis and gliogenesis emerging as the most prominently affected categories by Yki in CNS cells. The novel function of mTor expression in CNS neurons is particularly intriguing, shedding light on a new signaling network that plays an important role in regulating growth by integrating signals from nutrients and cellular energy levels (Bar-Peled and Sabatini, 2014; Saxton and Sabatini, 2017).

Furthermore, these findings might suggest a connection between Yki-mediated mTor activation and autophagy regulation, which is known to impact neuron development and synaptogenesis in *D.m.* (Shen and Ganetzky, 2009). Recent studies have highlighted the interplay between autophagy regulation and neuronal circuit formation, reinforcing our results of Yki function through mTor activation in CNS cell development (Rabanal-Ruiz, Otten and Korolchuk, 2017; Schmeisser and Parker, 2019; Dutta *et al.*, 2023).

Moreover, previous studies have demonstrated a relationship between mTor and Yki in regulating wing size, emphasizing the integration of local patterning inputs by Yki with humoral inputs by mTor (Parker and Struhl, 2015).

In conclusion, these findings propose a novel mechanism in CNS cells wherein Yki plays a crucial role in axonal branching and synaptogenesis through the activation of the nutrient sensor mTor (Figure 34). However, these results merely scratch the surface of understanding Ykis influence on axonal branching and synaptogenesis. Further validation of bulk RNA sequencing results with single cell sequencing and *in vivo* experiments investigating Ykis influence on mTor are imperative to unravel the complex molecular mechanisms underlying CNS development and function.

This comprehensive approach will not only deepen our understanding of Ykis role in neuronal development but also pave the way for potential therapeutic interventions targeting these pathways in neurological disorders.

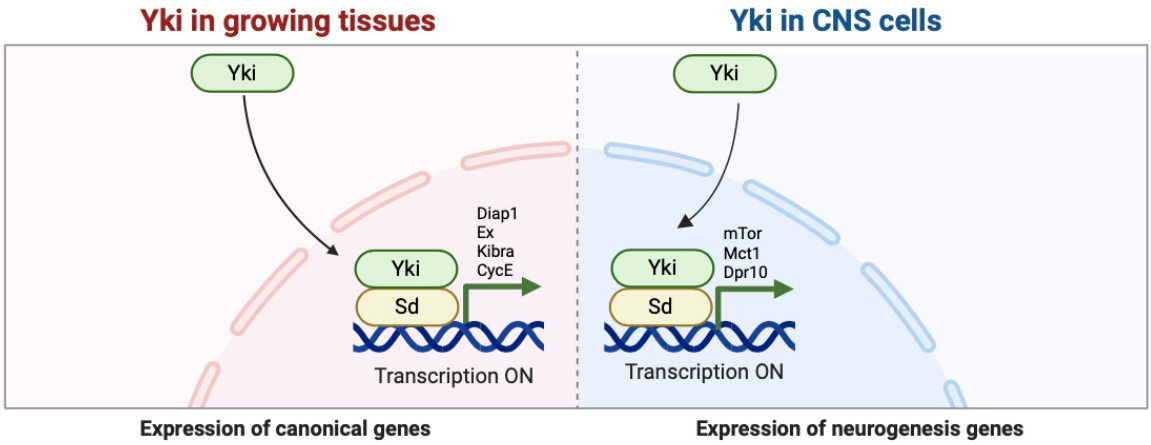

Figure 34. Hypothesis: Yorkie Induces mTor Expression in Bg3c2 Cells.

Yorkies established role in proliferating tissues involves the transcriptional activation of proliferation genes like Diap1, Ex and CycE. In the context of developing central nervous system cells, it is hypothesized that Ykis function entails the transcriptional activation of genes associated with neurogenesis and nutrient homeostasis genes, such as mTor, Mct1 and Dpr10.
Graphic designed using BioRender.

9. Appendix

9.1. The ER Protein Creld Regulates ER-mitochondria Contact Dynamics and Respiratory Complex 1 Activity

Marie Paradis*[1], Nicole Kucharowski*[1], Gabriela Edwards Faret[1, 2], Santiago José Maya Palacios[1], Christian Meyer[3], Birgit Stümpges[1], Isabell Jamitzky[1], Julia Kalinowski[1], Christoph Thiele[1], Reinhard Bauer[1], Achim Paululat[3], Julia Sellin[#1, 4], Margret H. Bülow[#1]
[#]correspondence to mbuelow@uni-bonn.de; jsellin@ukaachen.de
* equal contribution

[1]University of Bonn, Life and Medical Sciences (LIMES) Institute, Carl-Troll-Straße 31, 53115 Bonn, Germany
[2]VIB-KU Leuven Center for Brain and Disease Research, Leuven, Belgium
[3]University of Osnabrück, Department of Zoology and Developmental Biology, Barbarastr. 11, 49076 Osnabrück, Germany
[4]University Hospital Aachen, Institute for Digitalization and General Medicine, Pauwelsstr. 30, 52074 Aachen

Abstract
Dynamic contacts are formed between endoplasmic reticulum (ER) and mitochondria that enable the exchange of calcium and phospholipids. Disturbed contacts between ER and mitochondria impair mitochondrial dynamics and are a molecular hallmark of Parkinson's disease, which is also characterized by impaired complex I activity and dopaminergic neuron degeneration. Here we analyzed the role of Cysteine-rich with EGF-like domain (Creld), a poorly characterized risk gene for Parkinson's disease, in the regulation of mitochondrial dynamics and function. We found that loss of Creld leads to mitochondrial hyperfusion and reduced ROS signaling in Drosophila melanogaster, Xenopus tropicalis, and human cells. Creld fly mutants show differences in ER-mitochondria contacts as well as reduced respiratory complex I activity. The resulting low hydrogen peroxide levels are linked to disturbed neuronal activity and lead to impaired locomotion, but not neurodegeneration, in Creld mutants. We conclude that Creld regulates ER-mitochondria communication and thereby hydrogen peroxide formation, which is required for normal neuron function.

Introduction
The role of cellular reactive oxygen species (ROS) is ambiguous: according to the free radical theory of aging, oxidative stress caused by excessive ROS seems to be the major driver of aging and occurs due to a decline in mitochondrial function. This theory was challenged by findings that long-lived species have normal or elevated ROS levels, and increasing ROS genetically does not shorten the lifespan (Lapointe and Hekimi, 2010). Moreover, ROS are now acknowledged as important signaling molecules; for example, hydrogen peroxide (H_2O_2) is required for the excitability of neurons (Ohashi *et al.*, 2016), and certain types of ROS have been implicated in increasing longevity (Scialò *et al.*, 2016). Mitochondrial

oxidative phosphorylation is the major cellular source of ROS. Superoxide anions ($O_2^{\cdot -}$) are produced from small electron leaks mainly by the respiratory complexes I and III. They are cleared by superoxide dismutases, which convert them into H_2O_2. H_2O_2 can freely diffuse into the intermembrane space and into the cytosol, but is mostly converted to H_2O and oxygen by mitochondrial catalase. If the equilibrium between ROS production and scavenging is disturbed, $O_2^{\cdot -}$ and H_2O_2 accumulate (Morán *et al.*, 2012). Accumulation of ROS in the dopaminergic neurons of the substantia nigra as a result of dysfunctional mitochondria is considered as one of the main insults leading to degeneration of dopaminergic neurons in Parkinson's disease (PD) (Wei *et al.*, 2018; Trist, Hare and Double, 2019).

Mitochondria are highly dynamic and can form elongated tubes and networks or small, fragmented structures by undergoing cycles of fusion and fission. A key protein that coordinates mitochondrial quality control is PTEN Induced Putative Kinase 1 (PINK1), which is implicated in Parkinson's disease etiology (Haelterman *et al.*, 2014). PINK1 directly interacts with proteins that determine mitochondrial dynamics (Yang *et al.*, 2008; Han *et al.*, 2020), among them the key player in mitochondrial fission, the large GTPase Dynamin-related-protein 1 (Drp1). PINK1 phosphorylates Drp1 at Ser616, which promotes its pro-fission activity. PINK1 further influences mitochondrial dynamics by inhibiting the pro-fusion factor Mitofusin 2 (Yang *et al.*, 2008).

Mitochondrial fragmentation takes place at ER-mitochondria contact sites. Drp1 binds at these contact sites, and the ER structurally contributes to mitochondrial fission by wrapping itself around the fission site (Kraus *et al.*, 2021). ER-mitochondria contacts are altered in PD patients and animal models, although reports on whether the contacts increase or decrease are sometimes contradictory (Basso *et al.*, 2018; Gómez-Suaga *et al.*, 2018; Valadas *et al.*, 2018; Wilson and Metzakopian, 2021). Besides a role in mitochondrial fission, ER-mitochondria contacts also influence mitochondrial activity by allowing the exchange of calcium and phospholipids between both compartments, which also plays a role in Parkinson's disease pathology (Valadas *et al.*, 2018).

Mitochondria produce energy by means of their electron transport chain: it contains four protein complexes that pump protons into the intermembrane space, thereby producing a proton gradient that drives an ATPase, which is sometimes referred to as complex V. The first and largest of the complexes is NADH:ubiquinone oxidoreductase or complex I, which oxidizes NADH and reduces ubiquinone and transports protons from the inner mitochondrial membrane (IMM) to the intermembrane space (Babot *et al.*, 2014). Together with complex III, it is the main source of ROS production in eukaryotic cells. In neurons of PD patients, complex I is functionally impaired and misassembled (Keeney, 2006; Haelterman *et al.*, 2014), which is consistent with a role of ROS in PD pathology. Moreover, the complex I inhibitor rotenone, which has been used as a pesticide in agriculture, can induce PD in animal models, and PD is significantly more prevalent in people who were exposed to it (Pouchieu *et al.*, 2018). PINK1 is involved in the regulation of complex I: it mediates the phosphorylation of the complex I subunit NDUFA10 and thereby regulates its activity (Morais *et al.*, 2014). The phospholipids cardiolipin, phosphatidylethanolamine (PE) and phosphatidylcholine (PC), which are exchanged at ER-mitochondria contacts, support complex I function (Sharpley *et al.*, 2006); thus, ER-mitochondria communication might directly influence complex I activity. Strikingly, the functional relationship between ER-mitochondria contacts and complex I activity might be

bidirectional: inhibition of complex I with rotenone increases the expression of tether proteins in neuroblastoma cells (Ramalingam, Huh and Lee, 2019).
Genetically, PD is heterogeneous: risk genes for familial forms of PD comprise *leucine rich repeat kinase 2* (LRRK), *PINK1* and *Parkin*. PD is characterized by aggregates in neurons, the Lewy bodies, which contain α-synuclein folded into amyloid fibrils (Mahul-Mellier *et al.*, 2020). A recent study shows that Lewy bodies mostly contain organelles and membrane fragments, highlighting the importance of organelle quality control and neuronal organelle trafficking in PD insurgence (Shahmoradian *et al.*, 2019).
Proteins of the Creld family (cysteine-rich with EGF-like domains) are ER proteins that have been reported to regulate ER stress response and untranslated protein response (Oh-hashi *et al.*, 2009; Kern, Balzer, Blank, Cygon, Wunderling, Bender, Frolov, J. Sowa, *et al.*, 2021). CRELD1 is a risk gene for atrioventricular septal defects (AVSD) and murine CRELD1 is required during heart development (Beckert, Rassmann, Kayvanjoo, Klausen, Bonaguro, Botermann, Krause, Moreth, Spielmann, da Silva-Buttkus, Fuchs, Gailus-Durner, de Angelis, Händler, Ulas, Anna C. Aschenbrenner, *et al.*, 2021). A recent study links human CRELD1 to T-cell survival (Bonaguro *et al.*, 2020). Mechanistic studies in *C. elegans* show that Creld1 is required for the maturation and assembly of acetylcholine receptors in the ER (D'Alessandro *et al.*, 2018). Interestingly, CRELD1 is one of 10 genes that was identified as differentially regulated on both protein and mRNA level in PD, in a combined proteomics and RNA-Sequencing approach in samples from the prefrontal cortex (Dumitriu *et al.*, 2015a), suggesting a so far unknown connection to PD pathology.
Here we show that Drosophila Creld is indeed required for ER-mitochondria communication, mitochondrial dynamics and ROS signaling, all of which are known to play a role in PD pathology. Loss of Creld leads to failure of mitochondrial dynamics regulation and blocks mitochondrial fission. This results in increased mitochondrial abundance but decreased activity of the respiratory complex I. The subsequent lack of mitochondrial ROS inactivates dopaminergic neurons. We show that Creld is required for the transfer of phospholipids at ER-mitochondria contact sites and acts in parallel to the Pink1/Parkin pathway. In this study bridging from insect to vertebrate animal models to human cells, we describe the function of a novel player in PD pathology whose mutation results in severe locomotion deficits due to decreased rather than increased ROS levels.

Results

Creld is conserved between fly, frog and human

Cystein-rich with EGF-like domains (Creld) proteins belong to a family that is evolutionary conserved across species. Mammalian Creld proteins contain a signaling peptide at the N-terminus, a characteristic tryptophan and glutamic acid-rich (WE) domain, two epithelial-growth factor (EGF)-like and two calcium-binding domains (Fig. 1A, (Rupp *et al.*, 2002)).
Drosophila Creld shows high conservation to both the human CRELD1 and CRELD2: protein sequence identity is 44,1% and 43%, respectively, and 89% and 78% identity in the WE domain (Fig. S1A). The Drosophila Creld protein contains a transmembrane domain like its human counterpart CRELD1, which according to protein domain prediction anchors it in the ER membrane, with the N-terminus facing the lumen. The Drosophila genome contains only one gene for Creld, which results in two peptides, Creld-PA and Creld-PB, by alternative splicing. We raised an antibody against the conserved WE-domain of Creld and found that it co-localized primarily with the ER-marker KDEL (Fig. S1B). We generated a Creld mutant (Creld$^{\Delta 51}$) by homologous recombination that resulted in

complete deletion of the gene locus (Fig. S2A) and that it is a transcript null for both Creld transcripts (Fig. S2B). In the following text this strain is referred to as the Creld mutant, unless specifically stated otherwise. Creld mutants are homozygous viable, but show slightly lower survival rates on a control diet, which is further reduced on a sugar-depleted diet (Fig. S2C). The median lifespan of adult Creld mutants is shortened by ~ 30 % (Fig. S2D).

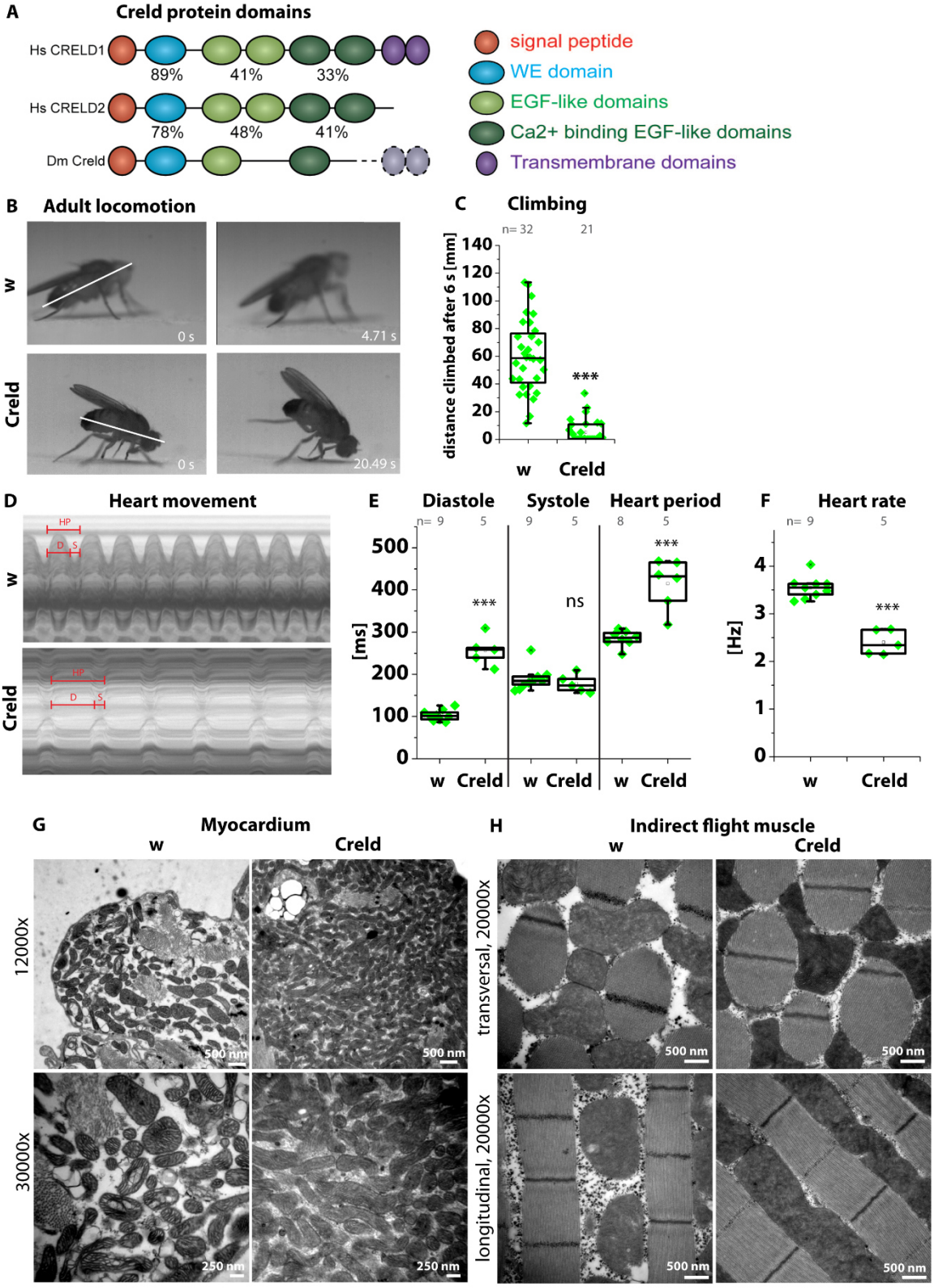

Figure 1: Impaired locomotion, increased diastole and mitochondrial accumulation in Creld mutants. *A) Domain structure of human CRELD1 and 2 and Drosophila Creld indicating protein identity of domains. B) Single images from videos of w^{1118} and Creld mutants, showing their walking behavior. C) Startle-induced negative geotaxis (SING) assay of 2 days old w^{1118} and Creld mutants. D) M-mode tracing of pixel movement of the adult heart. E) Quantification of diastole, systole (ns: p=0.43) and heart period. F) Heart rate of w^{1118} and Creld mutant flies. G) Transmission electron micrographs of abdominal tissue of w^{1118} and Creld mutant adults. Sections show myocardial cells. H) Transmission electron micrographs of thorax tissue of w^{1118} and Creld mutant adults. Sections show indirect flight muscles. Boxes represent the interquartile range and median, whiskers represent minimum and maximum. Asterisks represent ***p<0.001, ns: not significant*

Loss of Creld leads to severe locomotion impairment

Adult Creld mutants show a strong locomotion deficit: they climb slowly, and are almost unable to fly. Creld mutants show a distinct walking behavior: while wildtypic flies show coordinated walking movements with an upright body position and a body axis of about 45° in relation to the surface, Creld mutants show uncoordinated walking movements and a horizontal body position, which causes them to fall on their heads frequently (Fig. 1B and video S1 and S2). We used the startle-induced negative geotaxis (SING) assay to measure adult locomotion and found that Creld mutants are hardly able to climb (Fig. 1C). Ubiquitous expression of RNAi directed against Creld also impairs the climbing performance (Fig. S2E). We generated an independent allele by Crispr/Cas9-mediated k.o. ($Creld^{12\text{-}2}$), which resulted in a point mutation after 90 bases and a frame shift after 30 amino acids (Fig. S2F). We found that the $Creld^{12\text{-}2}$ mutant and transheterozygous $Creld^{\Delta 51/12\text{-}2}$ have reduced transcript levels of both transcripts and strongly reduced antibody signal (Fig. S G-I). Climbing performance is equally reduced in both mutants and transheterozygotes (Fig. S2 J).

Prolonged heart resting phase shows energy deficit in Creld mutants

Mutations in human CRELD1 are associated with heart development defects (Asim *et al.*, 2018), and mouse Creld1 mutants show defects in the proliferation of endocardial cells (Mass *et al.*, 2014). The insect heart is morphologically different from the mammalian heart, but contains valves and cardiac cells. Flies do not have a closed, but an open circulatory system, and the heart pumps the hemolymph through the body to supply organs with nutrients and signaling molecules (Rotstein and Paululat, 2016). We asked whether Creld mutants had heart defects and analyzed heart morphology and function. We found that heart development is normal, as is shown in 3rd instar larvae which show no morphological differences in the valve-like ostial cells (Fig. S3A). Next, we analyzed heart function in adult flies. M-mode recordings from semi-intact *Drosophila* heart preparations and digital high-speed movie analysis show that the heart rate is regular, but with a longer total heart period in Creld mutants compared to control flies (Fig. 1D). Upon quantification of the heart rate, we found that the total heart period is ~ 300 ms in wildtype flies and ~ 400 ms in Creld mutants, and that this prolongation of the heart rate is due to a longer diastolic interval. The systole duration of the heart period is unaltered in Creld mutants, but the diastole duration increases from ~ 100 ms in wildtypes to ~ 250 ms in Creld mutants (Fig. 1E), and the heart rate is reduced from 3.5 to 2.5 Hz (Fig. 1F). We thus conclude that the contractility of the heart is not disturbed, but that the resting phase between the contraction is delayed. Prolonged heart rates and an increased diastolic interval are associated with a deficiency in energy supply (Kass, Bronzwaer and Paulus, 2004). We thus hypothesized that Creld mutants are not sufficiently supplied with ATP. Indeed, analysis of phosphorylated AMP-activated protein kinase (AMPK) confirmed that levels of phospho-

AMPK are highly increased in protein extracts from adult Creld mutants compared to wildtypes (Fig. S3B, C). We conclude that heart development in *Drosophila* Creld mutants is normal, but that heart rate and diastolic interval are prolonged due to an energy deficit, which might also be involved in the locomotion defect displayed by Creld mutants.

Mitochondria accumulate and elongate in Creld mutants

Mitochondria are the major source of energy in eukaryotic cells. To investigate the energy crisis that provokes impaired locomotion and heart rate prolongation in Creld mutants, we analyzed mitochondrial morphology by transmission electron microscopy (TEM) for ultrastructural analysis. Since the energy deficit seemed to affect heart function and locomotion, we analyzed both cardiac cells as well as musculature. We found that in myocardial cells, mitochondria are more abundant and elongated in Creld mutants compared to wildtype (Fig. 1G, Fig. S3D). We also used TEM for ultrastructural analysis of mitochondria in indirect flight muscles (IFM) and found that cristae structure is unchanged in mitochondria of Creld mutants, but that mitochondria are more abundant and enlarged (Fig. 1H). Both transversal and longitudinal sections of IFM show that in Creld mutants, mitochondria occupy all the space between the muscle fibers, whereas single mitochondria are well discernible in the wildtype. Our results indicate that in Creld mutants, there is a defect in mitochondrial network regulation and an imbalance towards mitochondrial fusion.

Mitochondrial hyperfusion upon Creld dysfunction is conserved

Members of the Creld protein family have not been associated with mitochondrial dynamics before. To assess whether mitochondrial fusion under Creld1 dysfunction can also be observed in vertebrates, we used the claw frog *Xenopus tropicalis* as a model. We injected *X. tropicalis* embryos with control or Creld1 morpholinos and a mito-eGFP construct in the 2-cell stage and analyzed the mitochondrial morphology in bodywall muscles at stage 40. We found that muscles of animals injected with the control morpholino showed a balance between fused and fragmented mitochondria, while in animals injected with the Creld1 morpholino, mitochondria are mostly present as elongated and fused (Fig. 2A, morpholino-mediated knock-down efficiency is shown in Fig. S4A, B). We calculated the mitochondrial fragmentation index and found that it is significantly reduced in muscle cells of animals injected with the Creld1 morpholino (Fig. 2B). To test if a similar phenotype can be observed in mammalian cells, we used a double-stranded RNA construct against CRELD1 in HeLa cells. We stained control and dsRNA-treated cells with an antibody against Tom20, a receptor in the outer mitochondrial membrane (De Miranda *et al.*, 2020), and found that also in HeLa cells, mitochondria are mostly fragmented in controls (Collins, 2002), but are fused, elongated and network-like in cells that knock down CRELD1 (Fig. 2C, Fig. S4C). Our results indicate that loss of Creld leads to defects in mitochondrial network regulation and an imbalance towards mitochondrial fusion in various tissues and species.

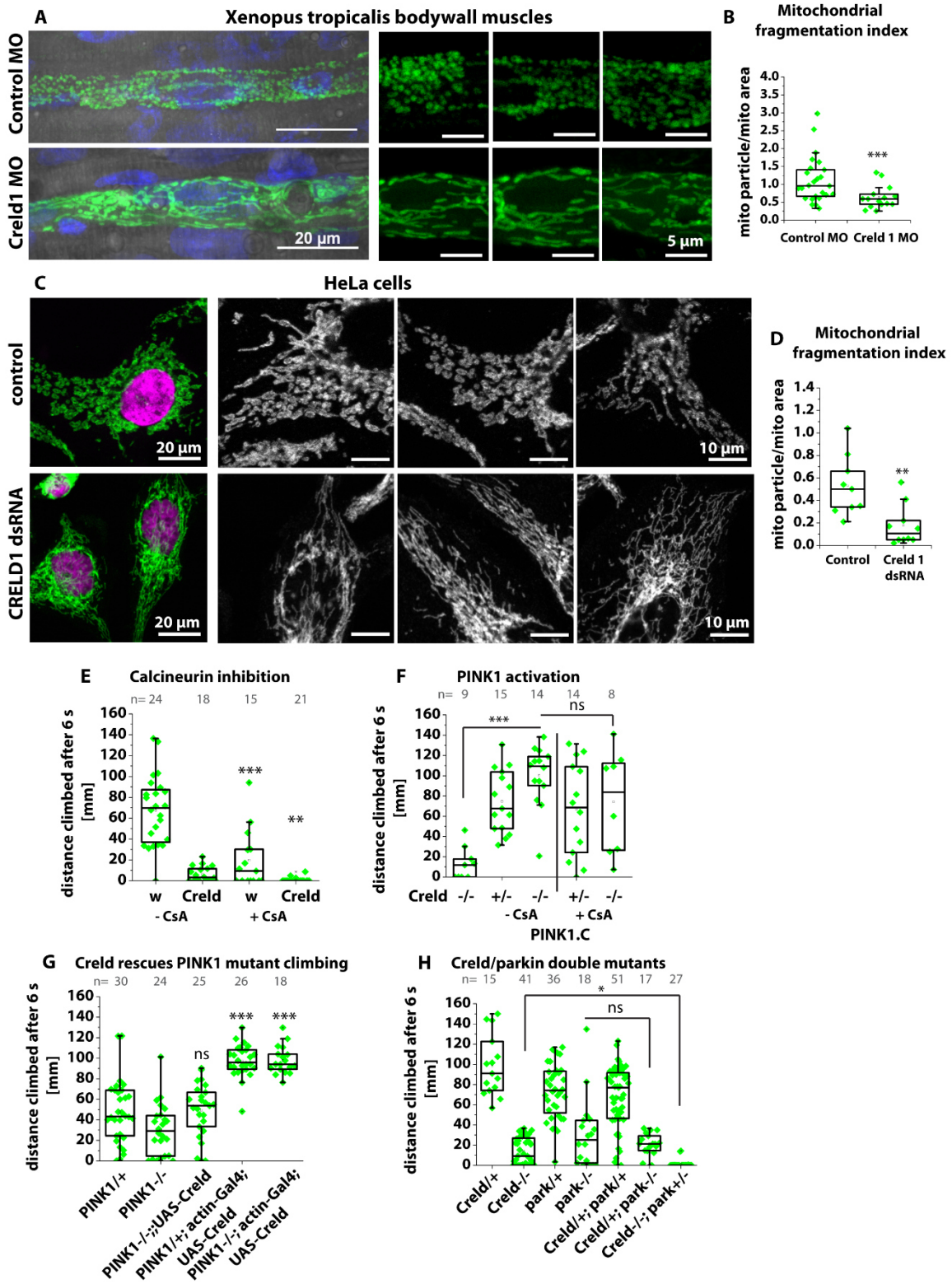

Figure 2: Creld interaction with Pink1 and Parkin. *A) Xenopus tropicalis stage 40 bodywall muscle cells labeled with mito-eGFP and close-ups. B) Quantification of the mitochondrial fragmentation index as the number of mitochondria divided by the total mitochondrial area of cells from animals injected with control and Creld1 morpholino (MO). C) Untreated (control) or transfected with dsRNA against CRELD1 HeLa cells and close-ups. Mitochondria are stained with anti-TOMM20. D) Quantification of the mitochondrial fragmentation index of based on Tom20 C). E) SING assay of w^{1118} and Creld mutants untreated or fed with 20 µM Cyclosporin A in 10% sucrose solution. ANOVA with F=34.662 and 77 degrees of freedom. F) SING assay of flies expressing a constitutively active form of Pink1. Genotypes are Creld-/-; tubulin Gal4/+, Creld/+ or -/-; tubulin Gal4/UAS Pink1.C. ANOVA with F=8.023 and 59 degrees of freedom. G) SING assay of Pink1*

*mutants expressing UAS-Creld-HA. Genotypes as indicated. ANOVA with F=39.562 and 122 degrees of freedom. ns: p=0.86. H) SING assay of Creld-Parkin double mutants, genotypes as indicated. ANOVA with F=56.584 and 204 degrees of freedom ns: p=0.29. Boxes represent the interquartile range and median, whiskers represent minimum and maximum. Asterisks represent **p<0.01, ***p<0.001, ns: not significant*

Reduced association of the pro-fission factor Drp1 with mitochondria in Creld mutants

Mitochondrial fission is regulated by Dynamin-related protein 1 (Drp1), which itself is regulated by several kinases and phosphatases. Drp1 localizes to mitochondria when activated to induce the fission process. To assess whether Drp1 locates to mitochondria in Creld mutants, we expressed a Drp1-HA fusion protein in Creld mutants and compared the presence of Drp1-HA in the cytoplasmic and the mitochondrial fraction. After normalization to the protein content of the fractions, we found that 80% of Drp1-HA is found in the mitochondrial fraction in heterozygous controls. In Creld mutants, the mitochondrial portion of Drp1 is reduced, and only ~60% associate with mitochondria, while ~40 % is found in the cytoplasmic fraction (Fig. S4 D-G). This shows that as a result of missing Creld function, Drp1 locates less to mitochondria, consistent with decreased fission activity.

Creld is required for the activation of the Drp1-activating phosphatase Calcineurin in mammals (Mass *et al.*, 2014; Yu *et al.*, 2019). To elucidate the Creld-Calcineurin interaction in flies, we fed adult control flies and Creld mutants with the Calcineurin inhibitor Cyclosporin (CsA). Treatment with CsA strongly reduces the climbing ability of wildtypes and thus mimics the phenotype of Creld mutants (Fig. 2I). However, CsA treatment further reduces the climbing performance of Creld mutants, suggesting that an additional function of Creld, apart from activating Calcineurin, is responsible for the locomotion phenotype. Drp1 can also be activated by phosphorylation by PTEN-induced kinase 1 (PINK1, (Han *et al.*, 2020)). We overexpressed a constitutively active form of Pink1 (Pink1.C) under the control of the ubiquitous *tubulin*-Gal4 driver and found that it rescues the climbing performance of homozygous Creld mutants (Fig. 2E). This Pink1-mediated rescue was maintained after treatment with CsA (Fig. 2E). This suggests that Creld interacts genetically with Pink1, in addition to Calcineurin, to regulate mitochondrial dynamics, and that both Pink1 and Calcineurin act downstream and/or in parallel with Creld in the activation of Drp1 and mitochondrial fission.

Creld rescues the locomotion deficit of PINK1 mutants

Human CRELD1 was identified as a Parkinson's disease (PD) pathology gene (Dumitriu *et al.*, 2015b), and the severe locomotion deficit we observe is reminiscent of the PD phenotype in fly models. Moreover, expression of constitutively active PINK1 rescues the climbing performance of Creld mutants. We asked if overexpression of Creld would rescue the locomotion deficit of PINK1 mutants. We generated a genetic rescue construct that allows for the expression of the full-length protein of Creld under the control of the binary Gal4/UAS system. We expressed the rescue construct under the control of the ubiquitous *actin*-Gal4 driver in Pink1 mutants and found that it significantly increases the climbing ability of Pink1 mutants (Fig. 2F). Pink1 recruits Parkin to mitochondria in the regulation of mitochondrial quality control. Heterozygous Creld and Parkin mutants show similar climbing performance. Heterozygous double mutants for Creld and Parkin show heterogenous, but not overall reduced climbing ability. Double mutants heterozygous for Creld and homozygous for Parkin show no further reduction of the climbing ability

compared to homozygous Parkin mutants. By contrast, double mutants homozygous for Creld and heterozygous for Parkin show significantly worsened climbing behavior compared to Creld mutants (Fig. 2G). We did not find flies homozygous for both mutations and assume that the combination is lethal. Our results suggest that Creld modulates the Pink1-Parkin pathway of mitochondrial quality control.

Creld is required in neurons for normal locomotion

To explore the connection between the defects in mitochondrial fission, locomotion and heart, we reintroduced Creld function genetically in specific tissues. We used the Creld rescue construct under the control of various tissue-specific Gal4 drivers. Homozygous Creld mutants that only carry the rescue construct, but no Gal4 driver, show impaired climbing similar to homozygous Creld mutants. Heterozygous Creld mutants show wildtype climbing performance. We found that expression in the heart with the *handC*-Gal4 driver (Sellin *et al.*, 2006) fails to rescue the climbing ability of Creld mutants. Expression in muscles with the *Mef2*-Gal4 driver partially rescues Creld mutants climbing. Similarly, ubiquitous expression of the genetic rescue construct with *tubulin*-Gal4 slightly but significantly rescues the climbing performance of homozygous Creld mutants (Fig. 3A). Intriguingly, expression of the genetic rescue construct in the nervous system by using the postmitotic neuron driver *elav*-Gal4 results in a strong rescue and markedly improves the climbing ability of homozygous Creld mutants (Fig. 3A). To further dissect the rescue in neurons, we used drivers specific for distinct neuron types. Expression of the rescue construct restricted to the insulin-producing cells (*dilp2,3*-Gal4), a group of median neurosecretory cells organized in two clusters in the *pars intercerebralis* of the adult brain that secrete the insulin-like peptides 2, 3 and 5 (Luo *et al.*, 2012), fails to rescue the climbing deficit of Creld mutants (Fig. 3B). By contrast, use of the *D42*-Gal4 driver, which directs the expression of the rescue constructs to motor neurons (Sanyal, 2009), resulted in a complete rescue of the climbing deficit. Dopaminergic neurons are expressed in distinct clusters in the larval and adult brain (Niens *et al.*, 2017) and integrate motor programs (Fuenzalida-Uribe and Campusano, 2018). In humans, dopaminergic neurons modulate locomotion by innervating the brain stem, and locomotion defects in Parkinson's disease (PD) are caused by degeneration of these neurons (Ryczko and Dubuc, 2017). This mechanism is strongly conserved, and also flies present impaired locomotion and other PD symptoms upon loss of dopaminergic neurons (Sun *et al.*, 2018). We used tyrosine hydroxylase (*TH*)-Gal4 to direct the expression of the rescue construct to dopaminergic neurons and found that it rescues the locomotion impairment of homozygous Creld mutants (Fig. 3B). Our findings indicate that loss of Creld affects locomotion because its function is required in motor neurons and dopaminergic neurons, not the heart, and only to a minor degree in muscles.

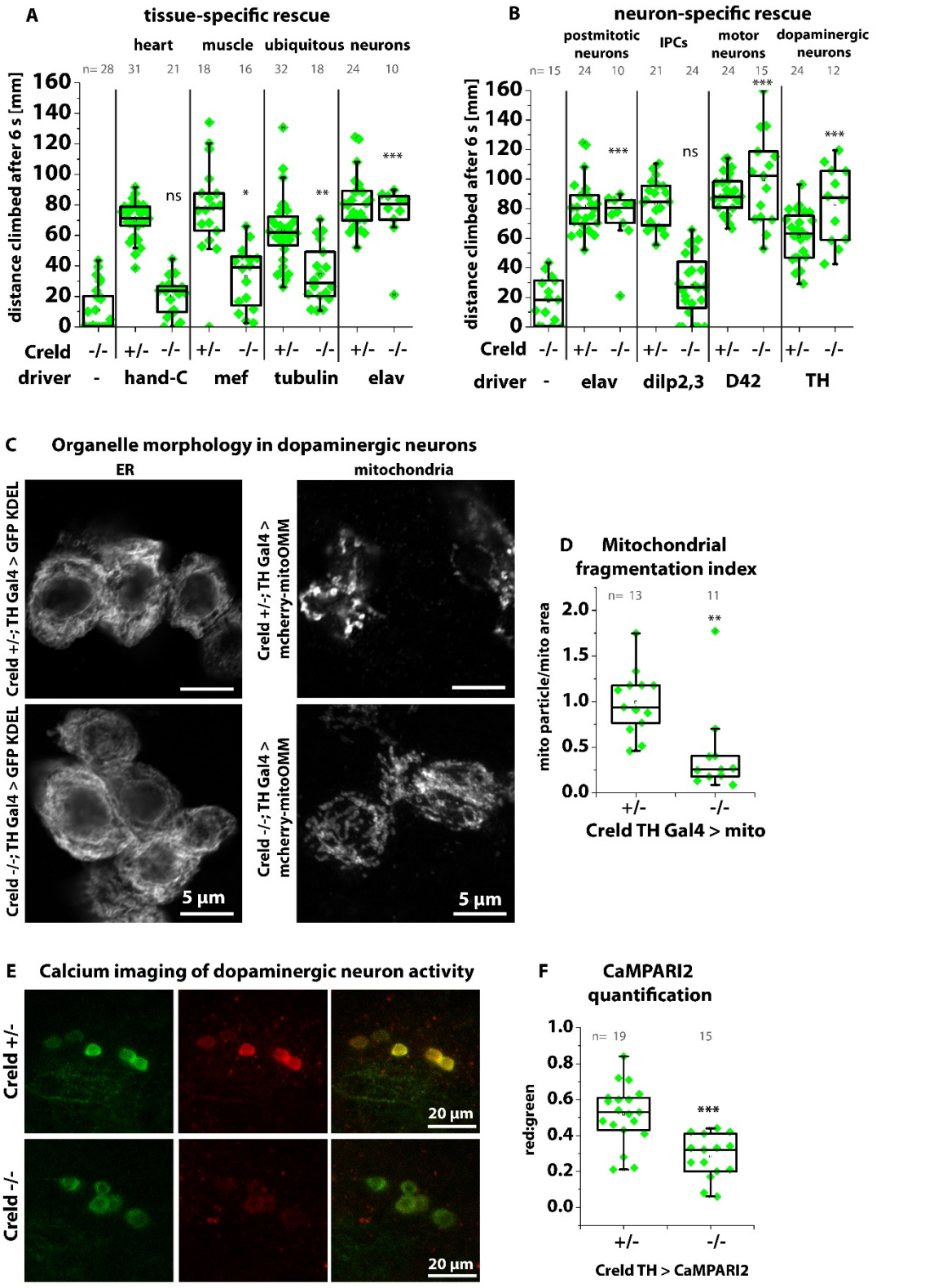

Figure 3: Creld is required in neurons for normal locomotion. *A) Startle-induced negative geotaxis (SING) assay of animals expressing UAS-Creld-HA in specific tissues. Climbed distance in mm was measured after 6 s. Genotypes are (from left to right) Creld-/-; UAS-Creld-HA/+, Creld/+ or -/- as indicated; tubulin-Gal4/UAS Creld-HA, Creld+/- or -/-; mef-Gal4; UAS-Creld-HA, Creld/+ or -/-; handC-Gal4; UAS-Creld-HA, Creld/+ or -/-; elav-Gal4; UAS-Creld-HA. ANOVA with F=46.1 and 195 degrees of freedom. B) SING assay of animals expressing UAS-Creld-HA in specific neurons. Climbed distance in mm was measured after 6 s. Genotypes are Creld-/-; UAS-Creld-HA/+, Creld/+ or -/- as indicated; elav-Gal4/UAS Creld-HA, Creld/+ or -/-; dilp2,3-Gal4; UAS-Creld-HA, Creld/+ or -/-; D42-Gal4; UAS-Creld-HA, Creld/+ or -/-; TH-Gal4; UAS-Creld-HA. ANOVA with*

*F=38.167 and 168 degrees of freedom. C) Airyscan confocal imaging of ER in PPL1 cluster of dopaminergic neurons labeled by GFP KDEL (left panel) and mitochondria labeled by mCherry-mitoOMM (left panel) under the control of TH-Gal4. Genotypes are Creld/+; TH Gal4/UAS GFP KDEL or mCherry-mitoOMM and Creld-/-; TH Gal4/UAS GFP KDEL or mCherry-mitoOMM. mCherry was detected with a DsRed antibody. D) Mitochondrial fragmentation index of mitochondria in somata of dopaminergic neurons. E, F) Calcium imaging in PPL2 clusters of dopaminergic neurons with UAS CaMPARI2. Images were taken after 30 s UV light induction and 4 min photoconversion. Genotypes are Creld/+ or -/-; TH Gal4/UAS CaMPARI2. Boxes represent the interquartile range and median, whiskers represent minimum and maximum. Asterisks represent *p<0.05, **p<0.01, ***p<0.001, ns: not significant*

Dopaminergic neurons are inactive in Creld mutants

Locomotion deficits in PD patients as well as PD fly models are elicited by degeneration of dopaminergic neurons. However, we found no loss of dopaminergic neurons in Creld mutants (Fig. S5A-C). We did not detect any enrichment of Creld protein in specific brain regions or neurons (Fig. S5D). Histological sections did not show any sign of neurodegeneration (Fig. S5E). The number of apoptotic cells in the brain is similar in wildtype flies and Creld mutants (Fig. S5E). We first evaluated ER morphology in dopaminergic neurons by expressing GFP with the ER retention signal KDEL under the control of the TH-Gal4 driver. We analyzed dopaminergic neurons in control and Creld mutants with super-resolution microscopy using Airyscan confocal imaging. We did not observe any differences in ER morphology (Fig. 3C). To evaluate mitochondrial morphology in dopaminergic neurons, we expressed a construct that carries the transmembrane domain of the mitochondrial protein Miro tagged with mCherry, and thus labels the outer mitochondrial membrane (mCherry-mitoOMM), under the control of *TH*-Gal4. We found that mitochondria are round and fragmented in heterozygous Creld mutants, but that the mCherry signal accumulates and shows mitochondria fused and elongated in homozygous Creld mutants (Airyscan confocal images in Fig. 3C, D, confocal images in Fig. S6A). Next, we asked if dopaminergic neurons are less active in Creld mutants. We used the Calcium-modulated photoactivatable ratiometric integrator CaMPARI2 (Moeyaert *et al.*, 2018) for calcium imaging of active dopaminergic neurons. We found that upon stimulation with UV light for 30 s and 4 min after stimulation, dopaminergic neuron somata show conversion of green to red in wildtypic controls, but less conversion in Creld mutants (Fig. 3E, F). This indicates that dopaminergic neurons are less active, rather than degenerated, in Creld mutants.

ROS homeostasis is impaired in Creld mutants

Dopaminergic neuron loss in PD fly models is induced by oxidative stress, elicited by old and dysfunctional mitochondria that accumulate as a result of defective mitochondrial quality control. However, it is important to note that ROS are also important signaling molecules and indispensable for cell differentiation and neuronal activity, including motor neurons (Oswald *et al.*, 2018). With these considerations in mind, we asked if reactive oxygen species (ROS) are altered in Creld mutants. We tested if the observed mitochondrial phenotype led to reduced ROS levels. We used the superoxide indicator DHE and the mitochondria-specific superoxide dye MitoSOX to assess superoxide levels in Creld mutants. We found that overall superoxide was reduced in both adult gut and brain (Fig. 4A, B and Fig. S6B). By contrast, mitochondrial superoxide levels as stained by MitoSOX were increased (Fig. 4A). Superoxide anions are relatively stable and remain in the mitochondrial matrix and intermembrane space, while hydrogen peroxide can diffuse freely into the cytoplasm (Morán *et al.*, 2012). Thus, we next measured hydrogen peroxide,

a product of superoxide dismutation by Sod 1 and 2, with AmplexRed, and found that hydrogen peroxide is drastically reduced in Creld mutants (Fig. 4C, Fig. S6C). We concluded that in mitochondria of Creld mutants, superoxide accumulates but is not degraded to hydrogen peroxide. Hydrogen peroxide is also reduced in extracts of X. tropicalis embryos that knock down Creld1 (Fig. S6D). We measured the transcript levels of ROS-scavenging enzymes in flies and found that catalase and nitric oxide synthase (NOS) are expressed at wildtype levels, while superoxide dismutase 1 and 2 are significantly downregulated (Fig. 4D), consistent with decreased hydrogen peroxide levels and therefore retention of ROS in mitochondria. To induce hydrogen peroxide formation in Creld mutants, we expressed Sod1 under the control of the ubiquitous *arm*-Gal4 driver and found that it rescues the climbing performance of Creld mutants (Fig. 4E), and ubiquitous expression of Pink1 and Sod1 as well as downregulation of the ROS scavenger catalase increase hydrogen peroxide to control levels in Creld mutants. By contrast, downregulation of Duox, which produces ROS by oxidation of cytoplasmic NADPH, does not restore hydrogen peroxide levels in Creld mutants (Fig. 4F). We tested if modulation of hydrogen peroxide in dopaminergic neurons was sufficient to restore the climbing of Creld mutants. Upon induction of hydrogen peroxide formation by expression Pink1, Sod1 or downregulation of catalase, the locomotion deficit was abolished. When hydrogen peroxide formation was repressed by downregulation of Duox, climbing was not restored (Fig. 4G). Our results show that aberrant ROS signaling underlies the locomotion deficit in Creld mutants, and suggest that reduced hydrogen peroxide export from mitochondria leads to inactivity of dopaminergic neurons.

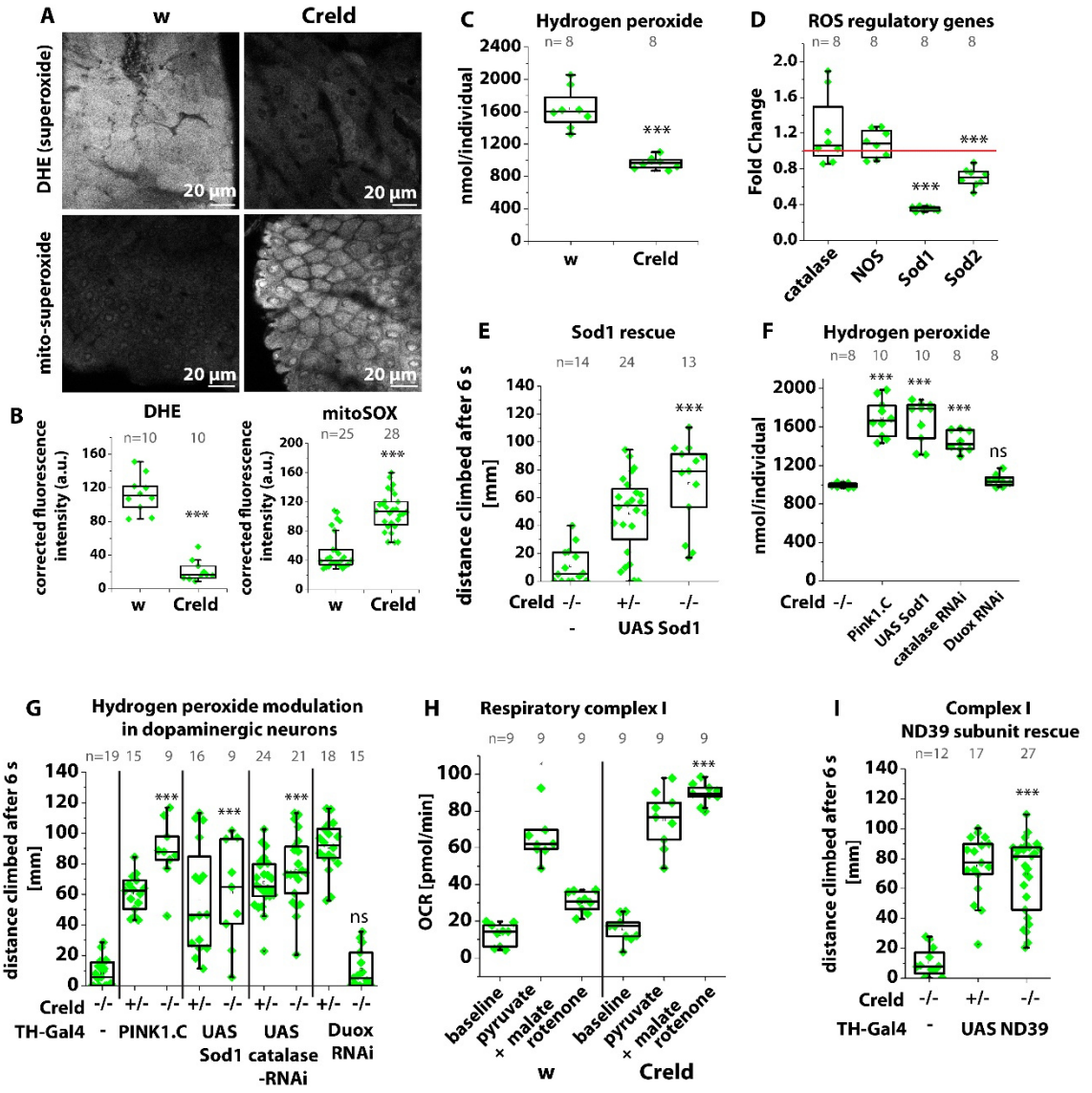

Figure 4: Low H_2O_2 impairs dopaminergic neuron function. *A, B) Adult gut tissue was stained with dihydroethidium (DHE) to label superoxide anions. Adult gut was stained with mitoSOX to label mitochondrial superoxide anions. C) Hydrogen peroxide was measured in extracts of whole adults with AmplexRed (n=8). D) Transcript levels of ROS-scavenging enzymes in Creld mutants, fold change normalized to w^{1118} (n=8). E) SING assay of Creld mutants ubiquitously expressing UAS Sod1. Genotypes are Creld-/-; armadillo Gal4/+, Creld/+ or -/-; armadillo Gal4/UAS Sod1. F) Hydrogen peroxide was measured in extracts of whole adults with AmplexRed. Genotypes are Creld-/-; armadillo Gal4/+, Creld/+ or -/-; armadillo Gal4/UAS Pink1.C, Creld/+ or -/-; armadillo Gal4/UAS Sod1, Creld/+ or -/-; armadillo Gal4/UAS catalase-RNAi, Creld/+ or -/-; armadillo Gal4/UAS Duox RNAi. G) SING assay of Creld mutants expressing PINK1, Sod1, catalase-RNAi or Duox-RNAi in dopaminergic neurons. Genotypes are Creld-/-; TH-Gal4;+; Creld/+ or -/-; TH-Gal4/UAS Pink1.C, Creld/+ or -/-; TH Gal4/UAS Sod1, Creld/+ or -/-; TH-Gal4/UAS catalase-RNAi, Creld/+ or -/-; TH-Gal4/UAS Duox-RNAi. ANOVA with F=33.627 and 145 degrees of freedom. H) Oxygen consumption of larval bodywall preparations of w^{1118} and Creld mutants treated with pyruvate and malate and rotenone. I) SING assay of Creld mutants expressing ND-39 in dopaminergic neurons. Genotypes are Creld-/-; TH-Gal4;+; Creld/+ or -/-; TH-Gal4/UAS ND-39. Boxes represent the interquartile range and median, whiskers represent minimum and maximum. Asterisks represent ***p<0.001, ns: not significant*

Mitochondrial activity is impaired at the level of respiratory complex I

A major source of superoxide and hydrogen peroxide in mitochondria is the respiratory complex I, which is regulated by Pink1 via phosphorylation of subunit ND-42 (Pogson *et al.*,

2014). We analyzed mitochondrial respiration in larval body wall muscles using a Seahorse analyzer (Agilent). We found that both wildtype and Creld mutant tissue react to injection of pyruvate and malate as substrates for complex I by increasing mitochondrial respiration, but that only oxygen consumption in wildtype tissue can be blocked with rotenone, a complex I inhibitor. Oxygen consumption in Creld mutant tissue remains at high levels upon rotenone treatment, which indicates that complex I is already inactive (Fig. 4H) and bypassed by other oxygen consuming processes. Feeding wildtype adults with sub-lethal levels of rotenone (100 µM) decreases their climbing performance, but not to the extent of Creld loss-of-function (Fig. S6E). By contrast, the poor climbing performance of Creld mutants is not further affected by rotenone, and even ameliorates slightly. Rotenone treatment lowers the levels of hydrogen peroxide in wildtype flies (although its mechanism of action leads to increased electron leakage, indicating a complex effect on ROS metabolism and transport), but not in Creld mutants, which already have low levels of hydrogen peroxide(Fig. S6F). This shows that the climbing deficit of Creld mutants can be attributed to low complex I activity and concomitant changes in ROS metabolism and transport. Knock-down of complex I subunit ND-39 has been shown to prevent ROS formation by decreasing complex I levels (Scialò *et al.*, 2016). Interestingly, expression of the complex I subunit ND-39 in dopaminergic neurons rescues the Creld mutant climbing deficit (Fig. 4I), and ubiquitous expression increases hydrogen peroxide levels (Fig. S6G). This suggests that complex I activity and its impact on ROS production and signaling is indispensable for dopaminergic neuron function and locomotion, specifically.

Creld expression is upregulated upon complex I inhibition

Complex 1 activity is altered in Creld mutants, and complex I defects are observed in PD. Creld was differentially expressed in PD prefrontal cortex samples (Dumitriu *et al.*, 2015b). We therefore asked if Creld reacts to conditions of low complex I activity and measured the transcript levels of Creld under different conditions in adult wildtype flies. We found that while normal under reduction of dietary sugar or upon starvation, Creld transcript levels indeed increase upon feeding with rotenone (Figure S7A). We expressed an UAS-Creld construct tagged with HA in dopaminergic neurons and co-stained with an antibody against endogenous Creld to observe Creld expression on the protein level. We found that upon rotenone feeding, the signal intensity of both the ectopically expressed Creld and endogenous Creld dramatically increase (Figure S7B). As this also affects the ectopically expressed UAS-Creld-HA, Creld accumulation upon complex I inhibition has to involve post-transcriptional mechanisms as well as transcriptional regulation. Our results show that Creld expression reacts to conditions of low complex I activity by upregulation.

Complex I inhibition enhances ER-mitochondria contacts

ER-mitochondria contacts regulate mitochondrial dynamics and are sites of material exchange (Flis and Daum, 2013). Drp1 binds at ER-mitochondria contacts to induce fission, and Pink1 and Parkin accumulate at contact sites in the regulation of mitophagy. Transfer of phospholipids and calcium ions (Ca^{2+}) between ER and mitochondria takes place at their contact sites and is required for mitochondrial function: for example, phospholipids support the function of respiratory complex I (Sharpley *et al.*, 2006). Human CRELD1 locates primarily in the ER (Bonaguro *et al.*, 2020), and *Drosophila* Creld also localizes mostly to the ER (Fig. S1B). We thus asked how Creld affects the function of respiratory complex I from its ER position by assessing ER-mitochondria contacts in dependence on complex I activity.

We expressed the mCherry-mitoOMM construct in dopaminergic neurons, co-stained with an antibody against the ER-marker KDEL and performed colocalization analysis on single confocal sections of single somata of dopaminergic neurons. In wildtypes, KDEL signal intensity is low and colocalization of ER and mitochondria markers is rare (Fig. 5A, B). To inhibit complex I activity, we treated the flies for 48 h with sublethal concentrations of rotenone. Upon rotenone treatment, KDEL signal intensity increases in the somata of dopaminergic neurons, resulting in enhanced colocalization of ER and mitochondria markers (Fig. 5C, D, Fig. S7D). Similarly, the ER marker GFP-KDEL enhances in signal upon rotenone treatment (Fig. S7C). We therefore suggest that complex I activity modulates ER-mitochondria contacts.

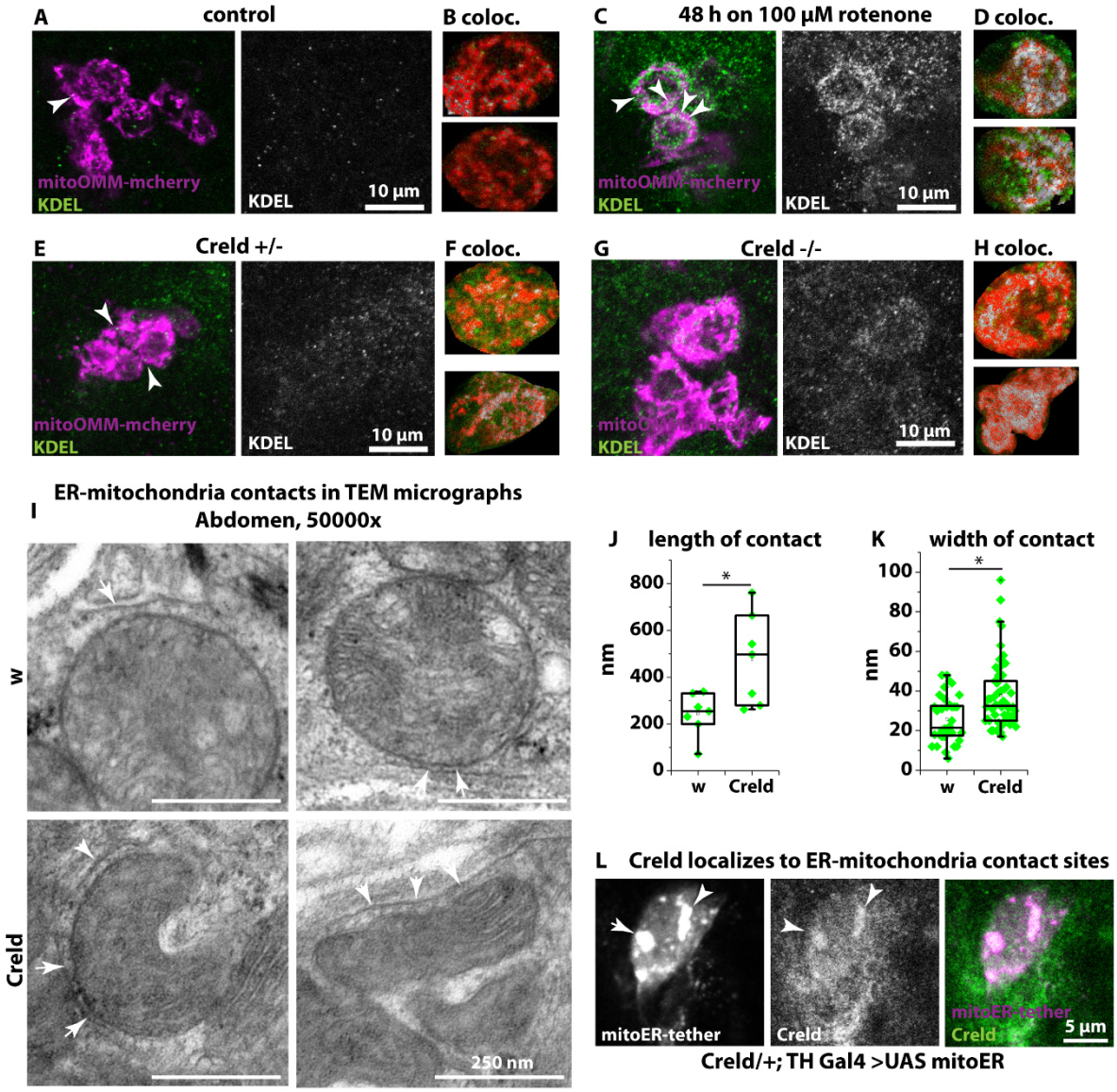

Figure 5: Creld and complex I activity modulate ER-mitochondria contact. *A) PPL1 cluster of dopaminergic neurons expressing mCherry-mitoOMM, stained with anti-DsRed and anti-KDEL in +/+; TH-Gal4/UAS mitoOMM. B, D, F, H) Regions of interest (ROI) of single somata of dopaminergic neurons after colocalization analysis with ImageJ colocalization threshold tool. C) PPL1 cluster of dopaminergic neurons expressing mCherry-mitoOMM, stained with anti-DsRed and anti-KDEL in +/+; TH-Gal4/UAS mitoOMM after treatment with rotenone. E, G) PPL1 cluster of dopaminergic neurons expressing mCherry-mitoOMM, stained with anti-DsRed and anti-KDEL in Creld/+; TH-Gal4/UAS mitoOMM (A) and Creld-/-; TH-Gal4/UAS mitoOMM. Arrowheads show colocalization of ER and mitochondria. I) TEM micrographs of adult abdomen showing ER-mitochondria contact sites. Scale bars as indicated. J) Quantification of ER-mitochondria contact*

*length. K) Quantification of ER-mitochondria contact width. K) PPL1 cluster of dopaminergic neurons expressing an artificial tether construct (mitoER-tether-RFP) stained with α-Creld. Boxes represent the interquartile range and median, whiskers represent minimum and maximum. Asterisks represent *p<0.05, ***p<0.001*

Creld localizes to ER-mitochondria contacts

Complex I and mitochondrial dynamics are inhibited in Creld mutants, and complex I inhibition enhances ER-mitochondria contacts and induces Creld expression. To investigate ER-mitochondria contacts in Creld mutants, we used again the mCherry-mitoOMM construct in dopaminergic neurons and co-stained with an antibody against the ER-marker KDEL. We found that in heterozygous controls, ER and mitochondrial markers show some few points of colocalization (Fig. 5 E, F, Fig. S7E). In homozygous Creld mutants, the KDEL signal is more intense in the somata of the dopaminergic neurons and colocalization between ER and mitochondrial markers is increased, similar to the situation in rotenone-treated wildtypes (Fig. 5G, H). Since ER-mitochondria contact sites are beyond the resolution of confocal microscopy, we analyzed them in TEM micrographs. We confirmed that ER-mitochondria contacts stretch over longer parts of mitochondria in Creld mutants, but that the gap between ER and mitochondrion is wider (Figure 5I-K), which poses the question of their functionality in terms of material exchange. To address if endogenous Creld is located at ER-mitochondria contact sites, we expressed a synthetic mito-ER tether (Basso *et al.*, 2018) in dopaminergic neurons. Tethering sites are marked with RFP in this line, and we found large spots of the RFP signal in the somata of dopaminergic neurons. The endogenous Creld signal colocalizes with these spots (Figure 5L). Our results show that contacts between ER and mitochondria increase upon loss of Creld and upon complex I inhibition, and that Creld localizes to ER-mitochondria contact sites that are induced by a synthetic mito-ER tether. Taking these observations together, it appears likely that Creld also localizes to endogenous ER-mitochondria contact sites in wildtypes.

Phospholipids accumulate at mitochondria-associated membranes (MAMs) in Creld mutants

ER-mitochondria contacts have been identified as so-called mitochondria-associated membranes (MAMs): crude mitochondrial fractions contain fragments of ER-membranes (54). These sites function as important signaling hubs in a number of physiological and pathological processes (Rodríguez-Arribas *et al.*, 2017). Phospholipids are transferred at ER-mitochondria contacts (Flis and Daum, 2013), and the phospholipids phosphatidylethanolamine (PE) and phosphatidylcholine (PC) are required for the function and stability of the respiratory complex I (Sharpley *et al.*, 2006). We thus asked if phospholipids can be transferred to mitochondria in Creld mutants. We isolated the cytoplasmic fraction, containing also plasma membrane, ER and lysosomes, the crude mitochondrial fraction comprising mitochondria and MAMs, and the MAM fraction by ultracentrifugation and subjected the fractions to lipidomics analysis. Importantly, we measured a technical sample containing only the buffers for each fraction and normalized the obtained data to the corresponding technical sample. We found that the total lipid content is by trend, albeit not quite significantly, in the cytoplasmic fraction in Creld mutants, while phospholipids are not significantly altered. Total lipids increase in the mitochondrial fraction, suggesting lipid allocation to mitochondria, but the phospholipid PE is reduced in Creld mutants. Total phospholipids accumulate in the MAM fraction, and when we looked at individual phospholipid species, we observed that PE and PC increase

in the MAM fraction of Creld mutants (Figure 6 A-C). Together, the data from our lipidomics analysis shows that phospholipid distribution between ER and mitochondrial compartments is disturbed. While we do not have direct evidence for altered phospholipid transport in Creld mutants, it appears likely that transfer of phospholipids from the ER to mitochondria is impaired, as this is a known function of MAMs impacting complex I function. PE and PC, which are required for complex I activity, seem to get stuck at ER-mitochondria contacts. This hypothesis is consistent with the observation of wider gaps at MAMS in electromicrographs of Creld mutant tissues, as distance is one important factor in the exchange of lipids at MAMs (Flis and Daum, 2013). ER-mitochondria contacts in Creld mutants could be increased as a compensatory measure (Fig. 6D-F), as this is also the case upon rotenone treatment and resulting complex I deficiency. We therefore propose that Creld normally functions under conditions of low complex I activity to facilitate phospholipid flux at ER-mitochondria contacts.

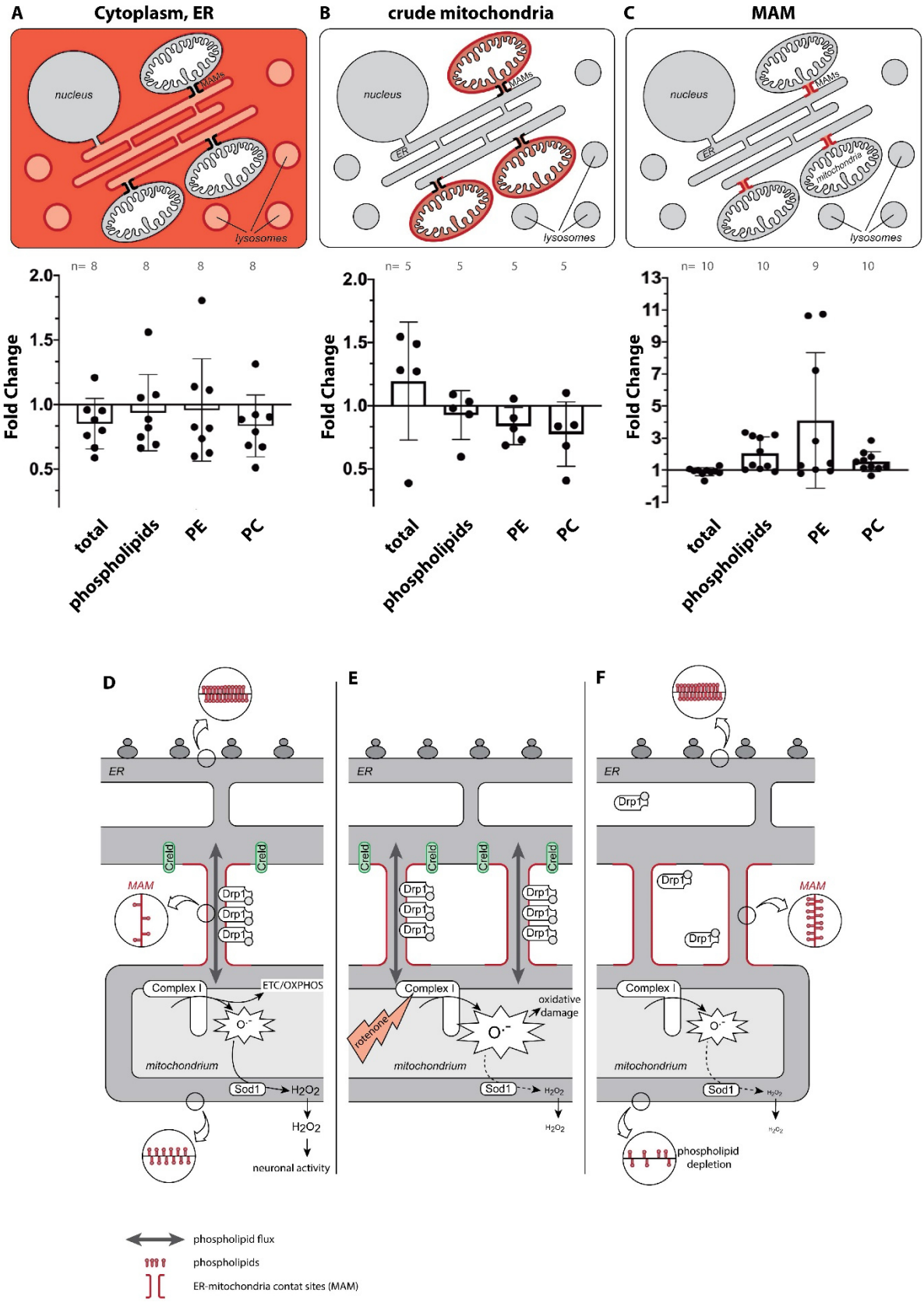

Figure 6: Phospholipid transfer at ER-mitochondria contacts is impaired in Creld mutants. *A) Total lipid, phospholipid, phosphatidylethanolamine (PE) and phosphatidylcholine (PC) content of fractions containing the cytoplasm, ER, plasma membrane and lysosomes. Fold change of extracts of Creld mutant flies normalized to w^{111}. B) Lipids as indicated in fractions containing mitochondria and MAM (crude mitochondria). C) Lipids as indicated in fractions containing MAM. D-E) Model of Creld action under D)*

wildtype, E) complex I-inhibited, F) Creld loss-of-function conditions. Bar charts show mean and SD, dots represent single data points. Asterisks represent p < 0.05, ns: not significant or p as indicated.

Discussion

Parkinson's disease (PD) is characterized by motor function defects as a result of dopaminergic neuron loss. It is believed that one of the main pathology-driving factors is oxidative stress induced by failure of mitochondrial quality control, leading to neuron loss. In accordance with this theory, PINK1, one of the commonest risk genes for PD, induces clearance of old mitochondria, but also directly regulates the machinery of mitochondrial fusion and fission. However, more recent data implicates PINK1 also in a role as a direct regulator of mitochondrial function via phosphorylation of the respiratory complex I subunit NDUFA10 (Morais *et al.*, 2014; Pogson *et al.*, 2014), although independent of the Pink1 mutant locomotion deficit (Pogson *et al.*, 2014). Moreover, complex I dysfunction has been observed in tissue of patients with PD (Keeney, 2006). Here we present data on an unexplored PD risk gene, Creld, and show that Creld mutants exhibit a strong, PD-like locomotion deficit and mitochondrial hyperfusion. We found that Creld interacts genetically with Pink1. In contrast to canonical PD models, dopaminergic neurons do not degenerate in Creld mutants, and oxidative stress in the form of hydrogen peroxide is absent. Consistently, mitochondrial ultrastructure appeared undamaged, while mitochondrial abundance and fusion increase. Of note, increasing hydrogen peroxide production in dopaminergic neurons rescues the Creld locomotion defect, implicating disturbed ROS signaling rather than oxidative stress as driving the locomotion defect of Creld mutants. Further studies are required to reveal Creld interacting proteins or Creld-dependent signaling that regulates mitophagy and mitochondrial biogenesis.

ROS, especially mitochondrial hydrogen peroxide, have been recognized as important signaling molecules in recent years: hydrogen peroxide is produced as a consequence of dopaminergic neuron activity, but is also required for their activity We argue that mitochondrial ROS signaling, especially hydrogen peroxide resulting from complex I activity, is required in dopaminergic neurons to support their function. This notion is supported by a study showing that ROS resulting from reverse electron transport (RET) at complex I is not detrimental, but instead delays aging (Scialò *et al.*, 2016),highlighting that ROS (as an umbrella term) can act differentially, depending on molecule, context and location in the cell. In the same line of evidence, the PD causing pesticide rotenone is a specific and well-studied complex I inhibitor which specifically blocks RET at complex I and reduces the formation of hydrogen peroxide (Scialò *et al.*, 2016), linking PD not only to complex I function in general, but specifically to complex I RET-dependent ROS production. Of note, we found that rotenone treatment provokes increased expression of Creld. It appears therefore likely that cells require Creld under conditions of low complex I activity and/or low levels of hydrogen peroxide signaling from mitochondria.

Creld is an ER protein that in *C. elegans* has been shown to act as a chaperone for the assembly of acetylcholine receptors (D'Alessandro *et al.*, 2018). Misassembly of acetylcholine receptors might account for a muscle-induced climbing deficit also in fly Creld mutants, but does not sufficiently explain mitochondrial hyperfusion and low complex I activity, nor the marked improvement of locomotion behavior upon expression of Sod1 or Creld in dopaminergic neurons. Instead, while the exact molecular mechanism of Creld in facilitating mitochondrial/ complex I function is still elusive, our data implicates ER-

mitochondria contacts as the site of Creld action. We could show that Creld accumulates at ER-mitochondria contacts that are artificially induced by expression of a synthetic tether. Both complex I inhibition by rotenone and Creld loss of function lead to increased regions of contact between ER and mitochondria. Interestingly, TEM imaging of Creld mutant tissue reveals broader gaps between the two compartments at the contact sites than in wildtype, suggesting that they are functionally impaired as a result of Creld loss of function, and implicating Creld in their function, maintenance, or regulation. Furthermore, the lipid composition of mitochondria-associated membranes (MAMs), ER, and mitochondria are altered, arguing for disturbed phospholipid exchange between the compartments in Creld mutants. This is an intriguing observation, since MAMs are known to play a role in phospholipid transport between ER and mitochondria (Flis and Daum, 2013) and phospholipids regulate complex I activity (Sharpley *et al.*, 2006). Our findings suggest that complex I dysfunction in Creld mutants could therefore be a direct consequence of impaired lipid exchange at ER-mitochondria contact sites, and in turn affect neuron function due to impaired ROS signaling from complex I. However, the resulting locomotion defect is not caused by dopaminergic neuron loss, nor do we observe other signs of neurodegeneration. Nevertheless, we cannot rule out that dopaminergic neurons might degenerate eventually as a result of their inactivity in old Creld mutants. Determination of direct interacting proteins of Creld might reveal how Creld participated in the regulation of ER-mitochondria contacts.

To date, it is not entirely clear if loose or tight contacts between ER and mitochondria better support the function of the cell: the formation of the contacts is important for mitochondrial dynamics quality control, but increased contacts have been associated with depletion of phospholipids from the ER (Valadas *et al.*, 2018). Furthermore, reduced contacts in flies as a result of knock-down of the tether protein Pdzd8 promotes mitochondrial turnover in neurons and decelerates age-related locomotion deficits (Hewitt *et al.*, 2020). Based on our data we hypothesize that Creld is required for the formation of functional contacts between ER and mitochondria to provide phospholipids for the support of complex I function and thus allowing the formation of hydrogen peroxide as a signaling molecule for the activity of dopaminergic neurons. Complex I turns to its inactive state when oxygen is limiting (Babot *et al.*, 2014), but phases of low complex I activity also occur during development and in dependence of nutrition (Perez-Gomez *et al.*, 2020). We suggest that Creld is required for dynamic ER-mitochondria contacts that enable the transfer of phospholipids to support or regulate complex I function and thus allows the formation of hydrogen peroxide as a signaling molecule for the activity of dopaminergic neurons. While direct interaction partners of Creld in the modulation of ER-mitochondrial contact dynamics are not yet known, it is conceivable that Creld might be required for the assembly of subunits of the respiratory complex I, a large protein complex comprising several subunits, or proteins that form the tether between ER and mitochondria. Further studies will reveal the molecular role of Creld and interaction in modulation of Pink1/Parkin pathway, ER-mitochondrial contact dynamics, and Complex I activity.

Acknowledgments

We thank Andreas Schoofs for sharing reagents and for his support with the CaMPARI experiments and Xabier Perez Garmendia for help with the subcellular fractionation. We thank Aurelio Teleman and Michael Pankratz for valuable comments on the manuscript. We thank Dietmar Schmucker for supporting the project and all Schmucker lab members

for helpful discussions. GEF received funding from the Belgium Fonds Wetenschappelijk Onderzoek (FWO, junior post-doctoral fellow grant 1214420N). AP received funding from the German Research Foundation (PA517/13-1, PA517/15-1, PA517/16-1, SFB 944-TP7, SFB 944 Z-Project). MHB received funding from the German Research Foundation (DFG, project number 417982926) and from the New Frontiers in Research Fund (NFRF, project number NFRFE-2019-00007).

Author contribution

Conceptualization: JS, MHB; Methodology: MHB, JS, MP, NK, CT, AP; Investigation: MHB, MP, NK, GEF, SJMP, BS, CM, JK, IJ; Writing – Original Draft: MHB; Resources – MHB, RB; Writing – Review & Editing: MHB, JS; Visualization: MHB, SJMP, JS; Funding Acquisition: MHB; Supervision: MHB, JS, AP, CT, RB.

Abbreviations

arm: armadillo; DHE: dihydroethidium; ER: endoplasmic reticulum; OMM: outer mitochondrial membrane; PD: Parkinson's disease; ROS: reactive oxygen species; TH: tyrosine hydroxylase; tub: tubulin

Material and Methods

Fly husbandry

Flies were reared on standard cornmeal food (130g yarn agar, 248g Baker's yeast, 1223g Cornmeal and 1.5 l sugar beet syrup in 20 l distilled water) and kept in a 25°C incubator with light-dark-cycle. Fly stocks were obtained from the Bloomington Drosophila Stock Center and the Vienna Drosophila Resource Center. For stainings and SING assays, 2-5 day old female flies were kept on control diet or on filter paper soaked with 10 % sucrose solution and 50 or 100 µM rotenone, or 20 µM Cyclosporin A. We obtained the UAS-CaMPARI2 and the TH-Gal4 line from Andreas Schoofs and the UAS mito-ER tether lines from Elena Ziviani. Other fly lines used in this study were w^{1118} (Bloomington Drosophila Stock center (BDSC) # 6326), elav-Gal4 (BDSC # 8760), tubulin-Gal4 (BDSC # 5138), mef-Gal4 (BDSC # 27390), handC-Gal4(Sellin *et al.*, 2006), actin-Gal4 (BDSC # 4414), armadillo-Gal4 (BDSC # 1561) UAS-Creld-HA (this study), UAS-mCherry-mitoOMM (BDSC # 66533), Drp1-HA (BDSC # 42208), UAS Pink1.C (BDSC # 51648), UAS catalase-RNAi (BDSC # 34020), UAS Duox-RNAi (BDSC # 33975), UAS-Sod1 (BDSC # 24750), UAS ND39 (BDSC # 15821) $PINK1^{5}$ (BDSC # 51649) and $park^{25,}$ (Greene *et al.*, 2003).

Creld mutant generation

The $Creld^{\Delta 51}$ mutant was generated by homologous recombination. 5' and 3' homology arms (HA) were cloned into the pGX-attP vector(Huang *et al.*, 2009) and injected into w^{1118} embryos. Primers were *5' HA fwd: GCGGCCGCCTTATTCGTATAGAACTTTGCCCG, 5' HA rev: GCGGCCGCTTTAACCGGCAAACTATCTGAG* (both including NotI restriction sites), *3' HA fwd: TTGGCGCGCCAAATGATACGGCAACTCTCC, 3' HA rev: TTGGCGCGCCAGTCCGCAGTGATTCAAACTC* (both including AscI restriction sites). Creld was deleted by homologous recombination and replaced by the mini-white ORF and an attP site. The white gene was removed by Cre-recombinase. The resulting mutants are transcript-null. Expression of the neighboring genes *zir* and *nhe1* was tested and found to be at wildtype levels. We generated a Crispr/Cas9-mediated mutant allele (Creld 12-2) by

non-homologous end-joining. Primers were *Creld_fwd: CTTCGCCTGTTCCGCCGCCCTGCA* and *Creld_rev: AAACTGCAGGGCGGCGGAACAGGC.* Annealed oligos were cloned into the *pU6-BbsI* vector and sent to BestGene Inc. (USA) for injection into vas-Cas9 (BDSC # 55821). Mutants were identified by high-resolution melting analysis and sequencing. For the rescue construct, we designed a gblock containing a UAS coding sequence, the open reading frame for the Creld gene and an HA tag (Integrated DNA Technologies, IDT). Cloning of the gblock construction was done by using EcoRI and NotI, followed by ligation into the pGE-attBGMR vector(Huang *et al.*, 2009). Clones where sequenced to confirm successful integration and the plasmid was send to BestGene Inc. (USA) for injection.

Determination of lifespan

For determination of the lifespan of w- and Creld mutants, isogenized (backcrossed for six generations) were separated by sex and transferred to Longevity (LG) food (37.5 g Baker's yeast, 10 g Agar Kobe I, 300 mL dH2O; 3ml of a 10 % Nipagin (in 70% EtOH) and 37.5 g glucose were added after autoclavation) with 20 flies per tube. Number of viable and dead flies was controlled every day and LG food was changed every two days.

Semi-intact *Drosophila* heart preparation and digital high-speed movie analysis

All dissection steps were done in artificial hemolymph (108 mM $NaCl_2$, 5 mM KCL_2, 2 mM $CaCl_2$ $2xH_20$, 8 mM $MgCl_2$ $6xH_20$, 1 mM NaH_2PO_4, 4 mM $NaHCO_3$, 15 mM HEPES, 1 mM sucrose, 0.5 mM Trehalose, pH 7.1). The flies were anesthetized with fly-nap, followed by transfer to a Petri dish coated with Vaseline for dissection. After dissection, the submerged hearts were kept in oxygenated hemolymph for 15 min at room temperature for equilibration. The heart movements were recorded with a digital high-speed camera (connected to a Leica DM-LB microscope with a 10x water immersion lens) and Fire capture Red 1.2 software. Movie analysis of the heart activity is then carried using the MATLAB R2010a software. Statistical analysis was done using Microsoft Excel. Images of morphology of semi-dissected fly hearts were taken by screenshots of the videos described above.

Startle-induced negative geotaxis (SING) assay

For the analysis of the adult climbing performance, we used the startle-induced negative geotaxis assay. Flies show an innate escape response after being tapped to the bottom of a cylinder (negative geotaxis), and by connecting several tubes that allow simultaneous recording of several genotypes or conditions, the climbing performance can be monitored reproducibly (Gargano *et al.*, 2005). 5-10 female flies were collected and allowed to recover from CO_2 anesthesia for 24 h. On the day of the experiment, flies were transferred into glass tubes for climbing. After 5 min of conditioning, flies were tapped to the bottom of the tubes and their climbing was recorded. The climbing apparatus was millimetrically marked to measure the climbing of the flies. Mp4 files were converted to JPEG using VideoProc – video converter or VirtualDub. The height climbed by each individual fly was measured after 3, 6 and 10 s with ImageJ.

Transmission electron microscopy (TEM)

Adult female flies were aged to 10 days on standard food. Heart tubes were dissected with the semi-dissection method described in section 2.2.9. For the imaging of indirect flight muscles, the thorax of the flies was cut open. Dissection was carried on in artificial

hemolymph on ice. The tissue was fixed in TEM fixation buffer (2.0 % paraformaldehyde and 2.5% glutaraldehyde (both electron miroscopy grade) in 0.1 M Na-Cacodylate buffer, pH 7.4) for 4h. Fixed specimens were further processed as previously described(Lehmacher, Abeln and Paululat, 2012; Dehnen *et al.*, 2020). In brief, samples were postfixed in 1% osmium tetroxide in PBS for 1h, dehydrated in a graded ethanol series up to 100% ethanol and transferred into mixture of 100% ethanol and propylenoxide (1:1) for 10 min. Afterwards samples were rinsed in mixture of propylenoxide and Epon 812 and finally embedded in Epon 812. Poylmerization was carried out at 60 °C for 72h. For transmission electron microscopy ultra-thin sections of 70 nm were prepared with a diamond knife on a Leica UC 6 microtome. Mounted sections were contrasted with 2% uranyl acetate and lead citrate and finally investigated with a Zeiss 902 transmission electron microscope. ER-mitochondria contact sites were analyzed as previously described (Dietrich, Liu and Horvath, 2013): a blinded investigator measured length and width of the entire contact region in high magnification images (50,000x).

Xenopus tropicalis husbandry, morpholino-mediated gene silencing and mitochondria labeling

2 cell stage embryos of *X. tropicalis* were obtained by natural mating using wild-type mature male and female frogs. Embryos were raised in 1/9x Modified Frog Ringers (1/9x MR) at 25°C. The stage of the embryos was defined according to Nieuwkoop and Faber (NF) (Gerhart and Kirschner, 2020). For knock-down of Creld1, a morpholino complementary to blocking the translation start of Creld1 in *X. tropicalis* was designed (5’ -3’ sequence: TGACATACCCATAGCTGAGTGACTC) and tagged with Lissamine by Gene Tools. A morpholino standard control (5’-3’ sequence: CCTCTTACCTCAGTTACAATTTATA) tagged with Lissamine was used as control. 5 ng of morpholino control or morpholino-Creld1 were injected in 1 or 2 cell stage embryos of *X. tropicalis* for hydrogen peroxide and mitochondria fragmentation analysis. For Western Blot analysis of knockdown efficiency, injection of morpholinos took place at the 1-cell stage, and protein extracts were taken from NF stage 9 embryos that are characterized by a homeostatic peak of Creld1 expression according to Xenbase (www.xenbase.org). To label mitochondria in the somatic muscle of *X. tropicalis*, 2 cell stage embryos (NF stage 2) were injected with 4 nl of 100 ng/µl mito-eGFP reporter construct were injected into 1 blastomere. The embryo was raised in 1/9x MR buffer, and keep at 25°C. Screening of eGFP+ injected embryos was performed under an epifluorescence microscope 24 h after the injection. Half body fluorescent animals were selected and keep in PTU buffer (0,03 g/L phenylthiourea in 1/9x MR buffer) at 25°C. Larvae at NF stage 40 were anesthetized and fixed in PFA 4% overnight at 4°C. After PBS washes, the nuclei were stained with DAPI (1:5000). Mitochondria fragmentation index (MFI) was calculated blind using ImageJ software. Briefly, images were first thresholded and converted to binary images, eGFP+ muscle cells were delimitated, and then the particle number was quantified. The MFI was calculated by dividing the number of particles by the total area of mitochondria.

Cell culture

HeLa cells were grown in T-75cm2 flasks using DMEM medium (Thermo Fisher Scientific), and Penicillin-Streptomycin 1x (Thermo Fisher Scientific), supplemented with 10% FBS, in an atmosphere of 37°C and 5% CO2. HeLa cells were subcultured 3 times a week at a ratio

of 1:3 and 1:5 depending on the confluence. Cell density was determined using a hemocytometer. Cells were detached using 2.5mL of Trypsin-EDTA solution (Thermo Fisher Scientific). Experiments were conducted between passages 5 to 20. DsiRNA were resuspended as described by the manufacturer. On the day of the experiment, 10nM of dsiRNA (combination of 1-hs-CRELD1 and 2-hs-CRELD1) were reverse transfected into 10.000 HeLa cells per well of an 8 well tissue culture chamber (SARSTEDT) using Lipofectamine RNAiMAX as transfection reagent. Cells used for transfection were grown in media without antibiotics and imaged after 48 hours. Validated Dicer-substrate for HPRT-S1 DsiRNA was used as positive control and a nontargeting DsiRNA was used as negative control and further used as imaging control. DsiRNA sequences are as follows: 1-hs-CRELD1 5'-AAAAGGCAUCAGUCUUACACAGGUAGUAAGACUGAU-3', 2-hs-CRELD1 1 5'-GCUGACCAAUUCUGCGUGCAGUGUUCACGCAGAAUU -3'.

Oxygen consumption assay

We used an Agilent Seahorse XFe96 to measure the oxygen consumption rate (OCR) of larval bodywall tissue. Cartridges were watered and equilibrated according to the manufacturer's instruction. Plates were coated with poly-L-lysine. Bodywall muscles of 3rd instar larvae were dissected in HL3A buffer (115 mM sucrose, 70 mM NaCl, 20 mM MgCl2, 10 mM NaHCO3, 5 mM KCl, 5 mM HEPES, 5 mM trehalose) by inside-out preparation and attached to the bottom of the well (n = 6). Tissue was covered with 180 µl HL3A buffer. Assay was performed at 25 °C. For the assay, three measurements without injection (baseline), three with pyruvate and malate (end concentration 10 and 1 mM, respectively) and three with rotenone (end concentration 5 µM) were taken.

Western Blot

For the detection of p-AMPK, 15 µL 1X PBS were added and animals were homogenized. 1x Lämmli buffer was added and the lysate was boiled at 99°C for 3 minutes to destroy all proteases. For the detection of Drp1-HA, 1X Laemmli buffer was added to the cytoplasmic and mitochondrial fraction, and the fractions were boiled at 99°C for 3 min. Electrophoresis was performed at 150 V in 1X SDS running buffer. Semi-dry blotting was performed to transfer the proteins onto a PVDF (polyvinylidene difluoride) membrane. Blotting was done at 100 V for 1.5 hours on a prior in methanol activated membrane. The membrane was blocked in 5% milk in TBS-T buffer (1M) for 20 minutes followed by incubation with anti-p-AMPK (Cell Signaling, 1:1000), anti-HA (Roche, 1:400) or anti-Creld (Davids Biotechnologie, 1:100) antibody in 5% milk/TBS-T buffer at 4°C o/n. For immunodetection of the antibody membrane was incubated with HRP-coupled secondary antibody (Santa Cruz Biotechnology, 1:7500) in 5% milk/TBS-T buffer in the dark at RT for 2 hours. Detection of antibodies was done with SuperSignalTM West Femto Maximum Sensitivity Substrate (Thermofisher Scientific) incubated for 1 minute and exposed for 30 seconds. Signal acquisition was performed with Curix 60 (AGFA).

Histology

For semi-thin sections, heads of Creld and w- adult *D. melanogaster* were fixed in 4% formaldehyde in 1X PBS over night at 4°C. Following dehydration of tissue in a graded ethanol series (70%, 80%, 90%, 96%, and 100%) for half an hour per step, the tissue was embedded in JB-4 solution (Polysciences, Inc.). Embedded tissue was cut into 5 µm sections with an ultramicrotome by a glass knife and transferred to a coated microscope slide (superfrost® plus, thermofisher scientific). Furthermore, cut tissue was stained with Hematoxylin for 3 minutes, then washed in ddH2O for 3 minutes and stained with Eosin for 3 minutes followed by washing in ddH2O for 30 seconds. Sections were mounted in Entellan® New (Merck).

Hydrogen peroxide detection

H_2O_2 was measured in extracts of 3 adult female flies. 3 flies were homogenized in ice-cold PBS and centrifuged for 15 min at 4°C at 12000 g. 1 ml working reagent contained 970 µl PBS, 20 µl horse-reddish peroxidase (HRP) and 10 µl Amplex Red. 50 µl supernatant of each sample was measured in triplicates. Fluorescence was measured at 544/590 excitation/emission using a TECAN plate reader. A 3 µM dilution of H_2O_2 was used for the standard curve.

Imaging

Antibodies used in this study were α-GFP, α-KDEL (both Santa Cruz Biotechnology), α-DsRed (Takara), α-HA (Invitrogen), α-TOMM20 (Sigma-Aldrich). α-Creld was generated by immunization with a peptide targeting the conserved WE domain (TAWEEEKLRSYKNSE, Davids Biotechnologie). For immunohistochemistry, brains from adult female flies were dissected in PBS and fixed for 1 h in 0.5 % PBS-Tween20 and 4 % formaldehyde. Tissue was washed with 0.5 % PBS-Tween20 and blocked with donkey serum before incubation with the primary antibody (over night at 4 °C). Tissue was washed in 0.1 % PBS-Tween20 before incubation with the secondary antibody at room temperature in the dark for 1 h. Secondary antibodies coupled to Alexa or Cyanine dyes were from Molecular probes. Tissue was washed and incubated for 5 min with DAPI (4',6-diamidino-2-phenylindole). For colocalization analysis of KDEL and mitoOMM-mcherry, adult brains were stained with α-KDEL-mouse and α-DsRed-rabbit. Secondary antibodies were donkey-α-mouse-Alexa488 and donkey-α-rabbit-Cy3. Single confocal sections of dopaminergic neuron PPL1, PPL2 and PAL clusters were analyzed with the ImageJ colocalization threshold tool. For live staining with MitoSOX (ThermoFisher), adult gut tissue was used because its large cells are suitable for live imaging of subcellular structures. Guts were dissected in cold PBS and incubated with 5 µM MitoSOX for 10 min. Tissue was washed in PBS, mounted in Fluoromount (ThermoFisher) and analyzed immediately. For staining of superoxide with dihydroethidium (DHE, Sigma Aldrich), tissue was dissected as described above and incubated for 15 min in 30 µM DHE and fixed for 15 min in 4 % formaldehyde. Tissue was washed and incubated with DAPI, mounted in Fluoromount and analyzed immediately. For

imaging, we used a Zeiss LSM 710 with a 25x water lens (Plan-Neofluar, Zeiss), 40x water lens (C-Apochromat, Zeiss) and 63 x water lens (Plan-Apochromat, Zeiss) and a Zeiss LSM 880 with Airyscan detector.

Subcellular fractionation

For the analysis of cytoplasmic and mitochondrial protein, the mitochondrial fraction was enriched from extracts of 10 female flies by homogenization in 200 µl mitochondria isolation buffer (250 mM sucrose, 10 mM Tris, pH 7.4, 0.15 mM $MgCl_2$). Homogenates were filtered with cotton by centrifugation at 4000 g for 15 min, and the cleared homogenate was transferred to a fresh cup. Mitochondria and cytoplasm were fractionated by centrifugation at 16000 g for 30 min at 4 °C. The cytoplasmic fraction in the supernatant was transferred to fresh cups, and the mitochondrial pellet was dissolved in 200 µl mitochondria isolation buffer. For isolation of MAMs, we followed the protocol by Wieckowski et al. (Wieckowski *et al.*, 2009). In brief, 200 flies (100 male, 100 female) were homogenized in isolation buffer 1, 10 µl per fly, using a Precellys (peqlab) homogenizer. The homogenate was centrifuged twice at 1000 g to remove chitin and other bulk material. The cleared homogenate was centrifuged at 7000 g for 10 min and contained cytosol, ER, plasma membrane and lysosomes in the supernatant and crude mitochondria in the pellet. The pellet was resuspended in 200 µl isolation buffer 2 and pelleted again at 10000 g. The pellet was resuspended in 2 ml mitochondria resuspension buffer (MRB) and ultracentrifuged in a Beckman Optima L-60 Ultracentrifuge on Percoll medium to isolate mitochondria from MAMs. Lipidomics analysis of cytoplasmic fraction, crude mitochondria and MAM was performed. For each isolation step, we included a technical sample containing only buffer. A minimum of 5 replicates were measured for each fraction. Lipidomics analysis was performed in a Thermo Scientific Q Exactive Plus Hybrid quadrupole-orbitrap mass spectrometer as described previously (Thiele, Wunderling and Leyendecker, 2019). Reads were normalized to protein content of the fraction, and reads from the technical samples were subtracted.

Quantitative real-time PCR

Whole RNA of 5 individuals or ~ 300,000 HeLa cells were isolated using Trizol reagent (Invitrogen, Cat.# 15596026). Tissue was homogenized using a Precellys 24 homogenizer (peqlab). Transcription to cDNA was performed using the Luna® Universal One-Step RT-qPCR Kit (New England Biolabs, Cat.# E3005). Quantitative PCR was performed with a CFX Connect cycler (biorad). A minus-RT was analyzed in a PCR for each cDNA. Quantitative PCR was performed with a CFX Connect cycler (biorad) using Luna® Universal qPCR Master Mix (New England Biolabs, Cat.# E3003). Values were normalized against two house-keeping genes (actin5c and rp49), and against control (w1118, e.g. female brain to female body, ΔΔCq). Each experiment was repeated at least 4 times. Primers were actin-5C 5'-GGCCATCTCCTGCTCAAAGTC-3' and 5'-GATCTGGCTGGTCGCGATT-3', rp49 5'-TCCTACCAGCTTCAAGATGAC-3' and 5'-CACGTTGTGCACCAGGAACT-3', Creld 5'-GGCAGGACTCGAAAGGACAA-3' and 5'- CAGGTTGTGGCAGTGATCCT-3', Creld-RA 5'-GCCACCTGTGTCATCTTCCA-3' and 5'- TCTATTTCGGGTTGGTGGCC-3', Creld-RB 5'-AGTTGCCTGGAGTGTGATCG-3' and 5'- TCTTCGTGCGTGGACTCTTC-3', Sod1 5'-GGTCAACATCACCGACTCCA-3' and 5'- CGCTTAGACCTTGGCAATGC-3', Sod2 5'-

ATCACCAGAAGCACCACCAG -3' and 5'- CTTGTTGGGCGAGAGGTTCT -3', NOS 5'-TCGGAGTCGTCCCATTATTC-3' and 5'- CAGCCAAAGAAGAGCCACA -3', Catalase 5'-GATGCGGCTTCCAATCAGTTG-3' and 5'- GCAGCAGGATAGGTCCTCG -3'. Relative expression of human CRELD1 knockdown was analyzed as described above and normalized to hs-Beta-Actin using non-targeting negative control as baseline. Primers were as follows: hs-Beta-Actin 5'-GCATCCACGAAACTACCTTCAA-3' and 5'-TCAGGAGGAGCAATGATCTTGAT-3', HPRT 5'-CATTATGCTGAGGATTTGGAAAGG-3' and 5'-CTTGAGCACACAGAGGGCTACA-3', CRELD1 5'-CTATGAGTGCCGAGACTGTG-3' and 5'-ATCCACATCGAGACACTTGG-3'

Statistics

Bar charts represent mean and standard deviation. Boxes in box plots represent the interquartile range and median, whiskers represent minimum and maximum. Green squares in box plots represent single data points. We used Microsoft Excel for bar charts and Origin Pro 8G for box plots. We used the software GraphPad Instat for our statistical analyses. Two-sided Student's t-test was applied for normally distributed data in single comparisons, assuming heteroschedasticy. One-way ANOVA with Tukey-Kramer post-test was used for multiple comparisons. The Kolmogorov-Smirnow test was applied to test normality, and Bartlett's method was used to test for equal standard deviations within groups. Asterisks represent * = $p < 0.05$, ** = $p < 0.01$, *** = $p < 0.001$. A minimum of 3 biological replicates was used for each analysis.

9.2.Vectors

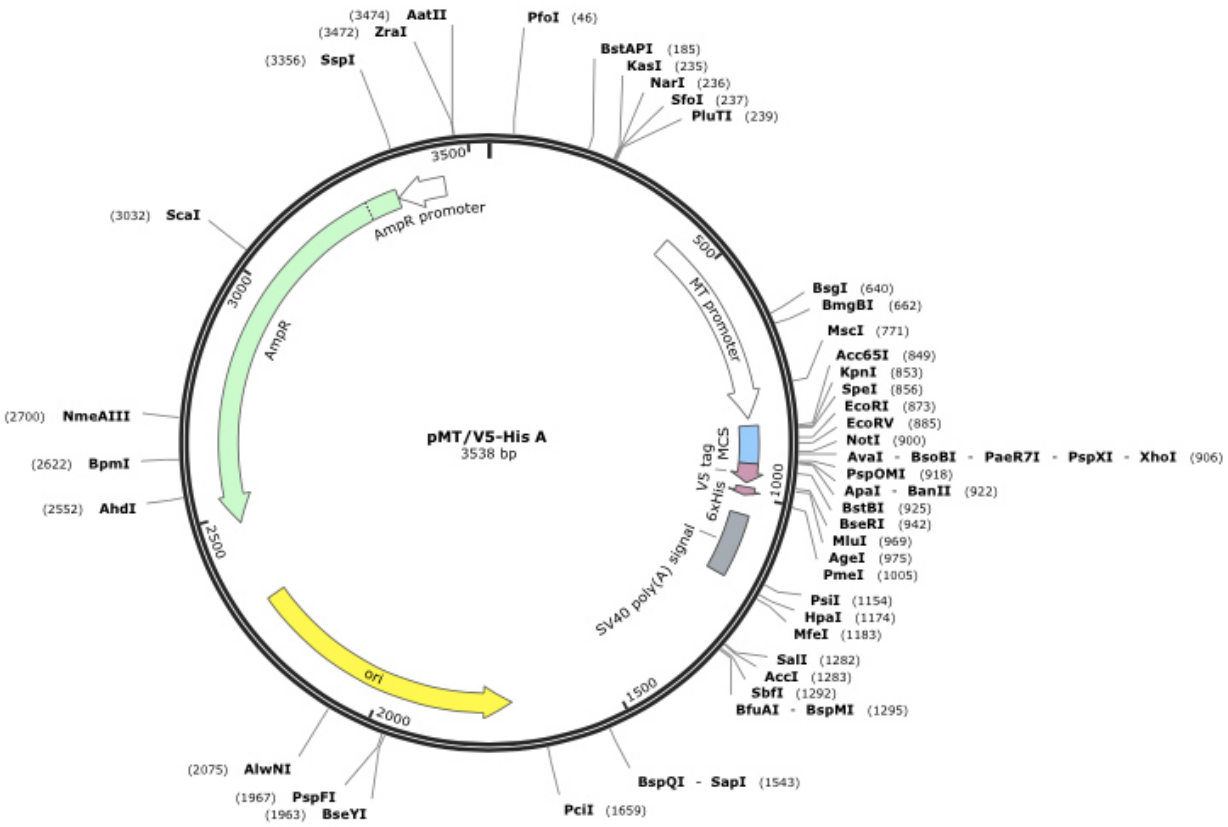

Figure S1. pMT/V5-HisA Plasmid Map

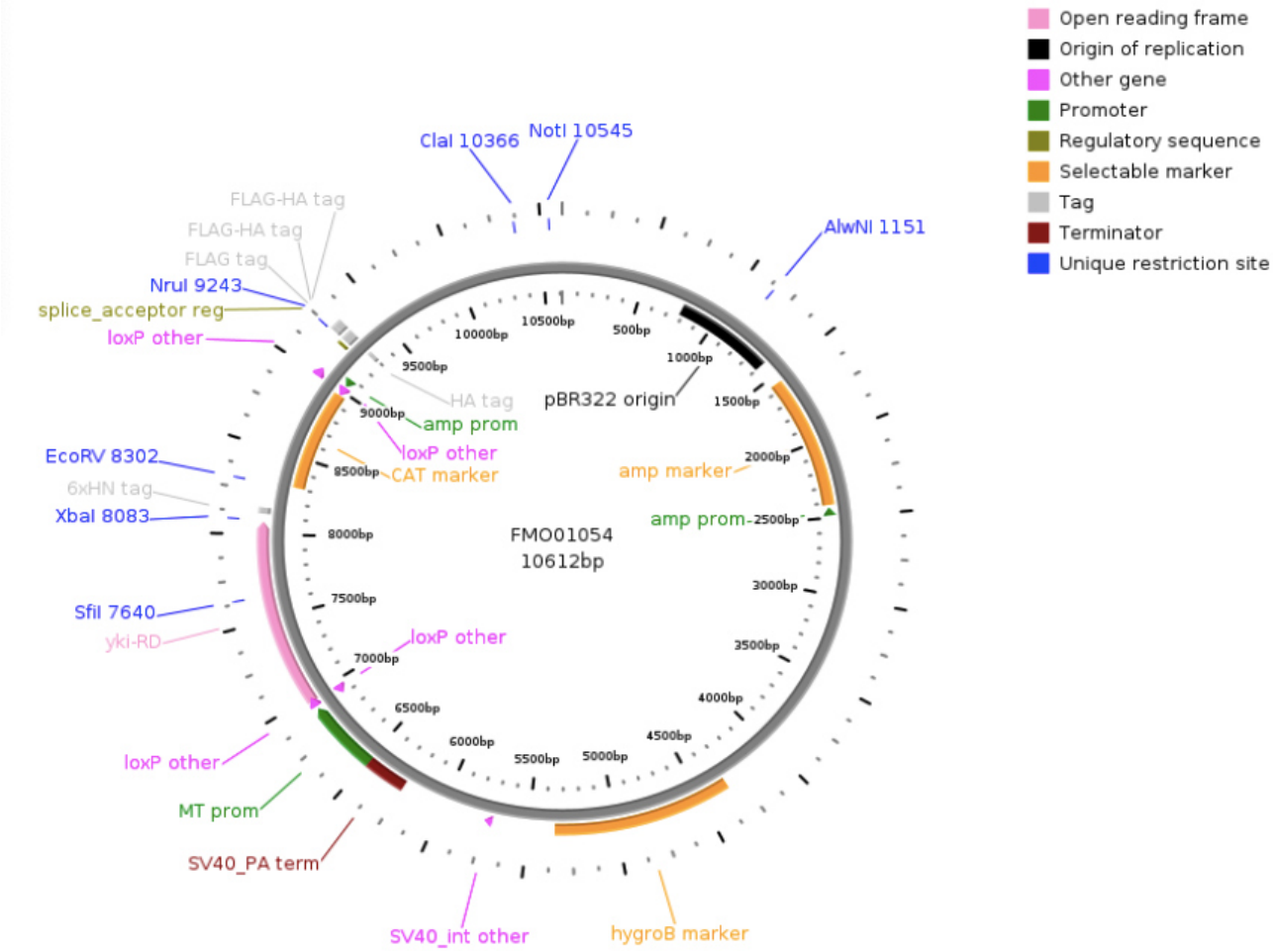

Figure S2. FMO01054/Yki-RD Plasmid Map

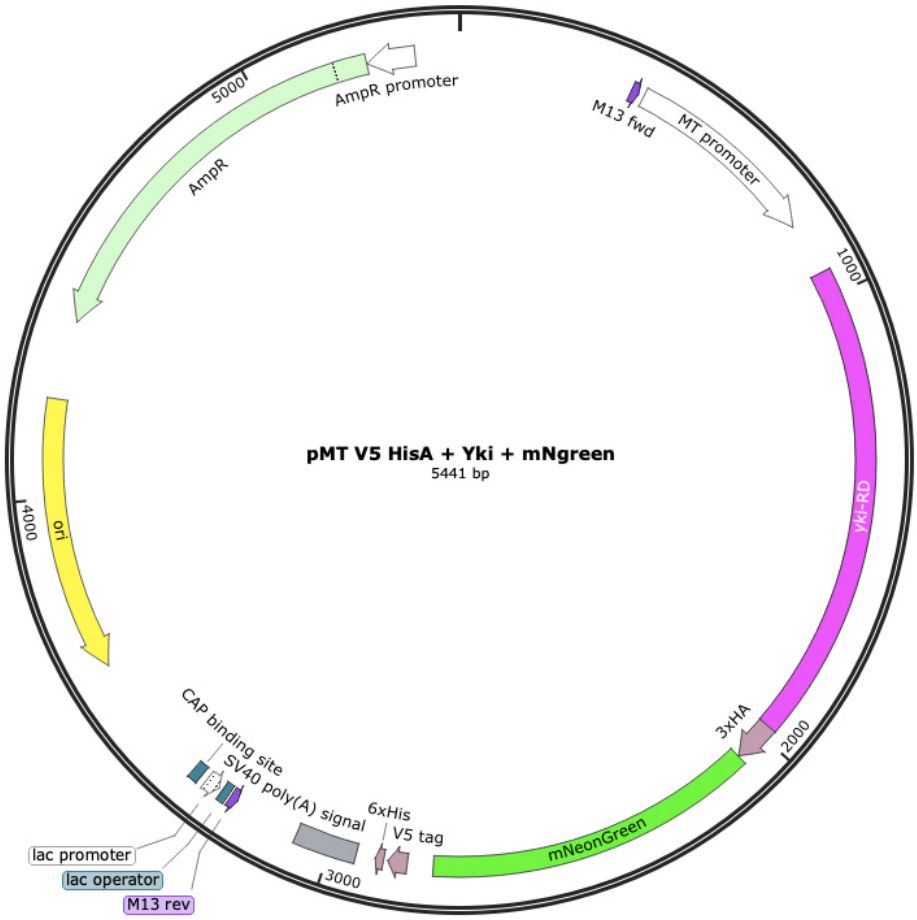

Figure S3. pMT-Yki-HA-mNeonGreen Plasmid Map

Sequence

TCGCGCGTTTCGGTGATGACGGTGAAAACCTCTGACACATGCAGCTCCCGGAGACGGTCACAGCT
TGTCTGTAAGCGGATGCCGGGAGCAGACAAGCCCGTCAGGGCGCGTCAGCGGGTGTTGGCGGG
TGTCGGGGCTGGCTTAACTATGCGGCATCAGAGCAGATTGTACTGAGAGTGCACCATATGCGGT
GTGAAATACCGCACAGATGCGTAAGGAGAAAATACCGCATCAGGCGCCATTCGCCATTCAGGCT
GCGCAACTGTTGGGAAGGGCGATCGGTGCGGGCCTCTTCGCTATTACGCCAGCTGGCGAAAGGG
GGATGTGCTGCAAGGCGATTAAGTTGGGTAACGCCAGGGTTTTCCCAGTCACGACGTTGTAAAA
CGACGGCCAGTGCCAGTGAATTAATTCGTTGCAGGACAGGATGTGGTGCCCGATGTGACTAGCT
CTTTGCTGCAGGCCGTCCTATCCTCTGGTTCCGATAAGAGACCCAGAACTCCGGCCCCCCACCGCC
CACCGCCACCCCCATACATATGTGGTACGCAAGTAAGAGTGCCTGCGCATGCCCCATGTGCCCCA
CCAAGAGTTTTGCATCCCATACAAGTCCCCAAAGTGGAGAACCGAACCAATTCTTCGCGGGCAGA
ACAAAAGCTTCTGCACACGTCTCCACTCGAATTTGGAGCCGGCCGGCGTGTGCAAAAGAGGTGA
ATCGAACGAAAGACCCGTGTGTAAAGCCGCGTTTCCAAAATGTATAAAACCGAGAGCATCTGGCC
AATGTGCATCAGTTGTGGTCAGCAGCAAAATCAAGTGAATCATCTCAGTGCAACTAAAGGGGGGG
ATCTAGATCGGGGTACCTACTAGTCCAGTGTGGTGGCAAAatgtgcgcgtgcctaatcgctaagataattcta
tgtagttttcgtttgtatacaataagtgccttttatatgttaacgacgatgtcagccagcagcaatacaaacagcctgatcgagaa
ggagatcgacgacgaggacatgctttcgccgatcaagtccaacaacctggtggtgcgggtcaaccaggacacggacgacaac
ctgcaggcgctattcgacagcgtcctgaatccgggtgacgccaagcgcccgctgcagctgcccctgcgcatgcggaagctgccc
aactccttcttcacgcccccggcgccctcgcactcgcgggccaacagcgccgactccacctacgacgcgggctcccagtcgagc
atcaacatcgggaacaaggcgtccatcgtccagcagccagatggccagtcgcccatcgccgccatcccccagctccagattcag
ccgtctccccagcacagccgcctggcgatacatcactccgagcccgcagcagccccgcctcgctgcagcagaactacaatgtg

cgcgcccggagcgacgcagcagcagccaacaatccgaatgccaatccgagcagccaacagcagcccgctgggcccactttcc
cagagaacagtgcccaagagttccccagcggcgccccggccagctcggccattgatctggacgccatgaacacctgcatgtcgc
aggacattcccatgtccatgcagacagtgcacaagaagcagcgctcctacgacgtcatcagccccattcagttgaaccgccaac
taggcgccttgccgccgggatgggagcaagccaagaccaatgatggccagatctactacttgaatcatactacaaaatctacgc
agtgggaggatcccagaatccaatatcgccagcagcagcaaatcttgatggccgagcgaataaagcagaatgaatctgggctt
agcgtgctcgactgcccagataacttagtgtcttccctccagattgaggataatctttgcagtaacttgttcaatgacgcacaggc
cattgtaaatccgccgtcttcccacaaacctGACGATTTGGAATGGTATAAAATTAATTACCCATACGATGTT
CCTGACTATGcgggctatccctatgacgtcccggactatgcaggatcctatccatatgacgttccagattacgctatggtatc
caagggagaggaagacaacatggcttcccctcccggcaactcacgagttgcacatatttggtagtataaacggagtggacttcga
catggtgggacaaggtacgggaaatccgaatgatggctacgaagaactcaatctcaagagtactaagggtgacctccagttta
gcccgtggattctggtacctcacattggctatggcttccatcaatacctgccatatccagatggaatgagtccgttccaggccgct
atggtagacggtagtggataccaagtccaccgcacgatgcagtttgaagacggcgccagtctgacagtgaactatcgttatacc
tatgagggctcgcatataaagggagaagctcaagtcaaaggaactggtttccccgccgatggacccgtaatgacgaacagcct
cacagcagccgattggtgtaggagcaagaaaacttaccctaacgataagacgataatctcgacattcaaatggagctacacta
ctggaaatggcaagcggtaccggagtacggcccggacaacatatacatttgccaaaccgatggcagcgaattatctgaaaaac
cagcccatgtacgtgttccgcaaaaccgagttgaagcattcgaagactgagctcaattttaaagaatggcagaaggcctttact
gacgtgatGGGCATGGATGAGCTCTATAAATAAAATTCTGCAGATATCCAGCACAGTGGCGGCCGC
TCGAGTCTAGAGGGCCCTTCGAAGGTAAGCCTATCCCTAACCCTCTCCTCGGTCTCGATTCTACGC
GTACCGGTCATCATCACCATCACCATTGAGTTTAAACCCGCTGATCAGCCTCGACTGTGCCTTCTA
AGATCCAGACATGATAAGATACATTGATGAGTTTGGACAAACCACAACTAGAATGCAGTGAAAA
AAATGCTTTATTTGTGAAATTTGTGATGCTATTGCTTTATTTGTAACCATTATAAGCTGCAATAAAC
AAGTTAACAACAACAATTGCATTCATTTTATGTTTCAGGTTCAGGGGGAGGTGTGGGAGGTTTTT
TAAAGCAAGTAAAACCTCTACAAATGTGGTATGGCTGATTATGATCAGTCGACCTGCAGGCATGC
AAGCTTGGCGTAATCATGGTCATAGCTGTTTCCTGTGTGAAATTGTTATCCGCTCACAATTCCACA
CAACATACGAGCCGGAAGCATAAAGTGTAAAGCCTGGGGTGCCTAATGAGTGAGCTAACTCACA
TTAATTGCGTTGCGCTCACTGCCCGCTTTCCAGTCGGGAAACCTGTCGTGCCAGCTGCATTAATGA
ATCGGCCAACGCGCGGGGAGAGGCGGTTTGCGTATTGGGCGCTCTTCCGCTTCCTCGCTCACTGA
CTCGCTGCGCTCGGTCGTTCGGCTGCGGCGAGCGGTATCAGCTCACTCAAAGGCGGTAATACGG
TTATCCACAGAATCAGGGGATAACGCAGGAAAGAACATGTGAGCAAAAGGCCAGCAAAAGGCC
AGGAACCGTAAAAAGGCCGCGTTGCTGGCGTTTTTCCATAGGCTCCGCCCCCCTGACGAGCATCA
CAAAAATCGACGCTCAAGTCAGAGGTGGCGAAACCCGACAGGACTATAAAGATACCAGGCGTTT
CCCCCTGGAAGCTCCCTCGTGCGCTCTCCTGTTCCGACCCTGCCGCTTACCGGATACCTGTCCGCC
TTTCTCCCTTCGGGAAGCGTGGCGCTTTCTCATAGCTCACGCTGTAGGTATCTCAGTTCGGTGTAG
GTCGTTCGCTCCAAGCTGGGCTGTGTGCACGAACCCCCCGTTCAGCCCGACCGCTGCGCCTTATCC
GGTAACTATCGTCTTGAGTCCAACCCGGTAAGACACGACTTATCGCCACTGGCAGCAGCCACTGG
TAACAGGATTAGCAGAGCGAGGTATGTAGGCGGTGCTACAGAGTTCTTGAAGTGGTGGCCTAAC
TACGGCTACACTAGAAGGACAGTATTTGGTATCTGCGCTCTGCTGAAGCCAGTTACCTTCGGAAA
AAGAGTTGGTAGCTCTTGATCCGGCAAACAAACCACCGCTGGTAGCGGTGGTTTTTTTGTTTGCA
AGCAGCAGATTACGCGCAGAAAAAAAGGATCTCAAGAAGATCCTTTGATCTTTTCTACGGGGTCT
GACGCTCAGTGGAACGAAAACTCACGTTAAGGGATTTTGGTCATGAGATTATCAAAAAGGATCTT
CACCTAGATCCTTTTAAATTAAAAATGAAGTTTTAAATCAATCTAAAGTATATATGAGTAAACTTG
GTCTGACAGTTACCAATGCTTAATCAGTGAGGCACCTATCTCAGCGATCTGTCTATTTCGTTCATCC
ATAGTTGCCTGACTCCCCGTCGTGTAGATAACTACGATACGGGAGGGCTTACCATCTGGCCCCAG
TGCTGCAATGATACCGCGAGACCCACGCTCACCGGCTCCAGATTTATCAGCAATAAACCAGCCAG
CCGGAAGGGCCGAGCGCAGAAGTGGTCCTGCAACTTTATCCGCCTCCATCCAGTCTATTAATTGT
TGCCGGGAAGCTAGAGTAAGTAGTTCGCCAGTTAATAGTTTGCGCAACGTTGTTGCCATTGCTAC
AGGCATCGTGGTGTCACGCTCGTCGTTTGGTATGGCTTCATTCAGCTCCGGTTCCCAACGATCAAG

GCGAGTTACATGATCCCCCATGTTGTGCAAAAAAGCGGTTAGCTCCTTCGGTCCTCCGATCGTTGT
CAGAAGTAAGTTGGCCGCAGTGTTATCACTCATGGTTATGGCAGCACTGCATAATTCTCTTACTGT
CATGCCATCCGTAAGATGCTTTTCTGTGACTGGTGAGTACTCAACCAAGTCATTCTGAGAATAGTG
TATGCGGCGACCGAGTTGCTCTTGCCCGGCGTCAATACGGGATAATACCGCGCCACATAGCAGA
ACTTTAAAAGTGCTCATCATTGGAAAACGTTCTTCGGGGCGAAAACTCTCAAGGATCTTACCGCT
GTTGAGATCCAGTTCGATGTAACCCACTCGTGCACCCAACTGATCTTCAGCATCTTTTACTTTCACC
AGCGTTTCTGGGTGAGCAAAAACAGGAAGGCAAAATGCCGCAAAAAAGGGAATAAGGGCGACA
CGGAAATGTTGAATACTCATACTCTTCCTTTTTCAATATTATTGAAGCATTTATCAGGGTTATTGTC
TCATGAGCGGATACATATTTGAATGTATTTAGAAAAATAAACAAATAGGGGTTCCGCGCACATTT
CCCCGAAAAGTGCCACCTGACGTCTAAGAAACCATTATTATCATGACATTAACCTATAAAAATAGG
CGTATCACGAGGCCCTTTCGT

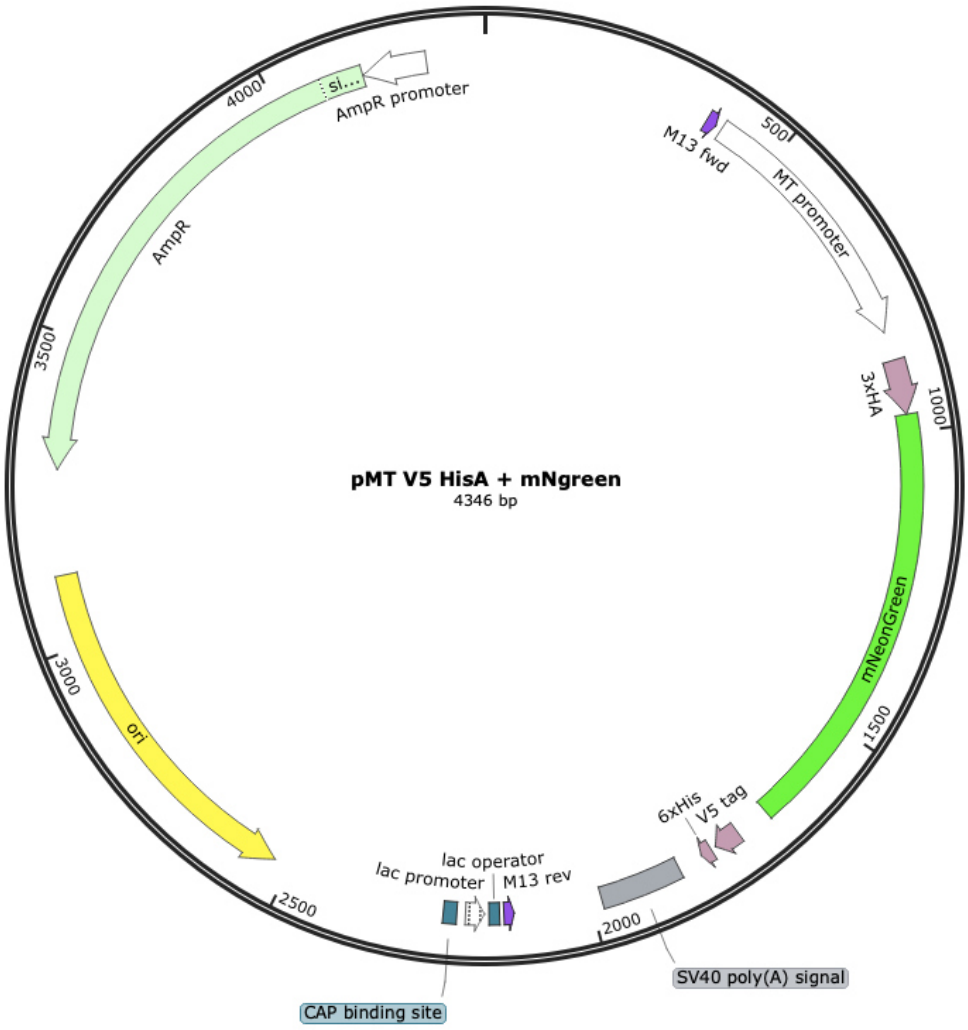

Figure S4. pMT-HA-mNeonGreen Plasmid Map

Sequence

TCGCGCGTTTCGGTGATGACGGTGAAAACCTCTGACACATGCAGCTCCCGGAGACGGTCACAGCT
TGTCTGTAAGCGGATGCCGGGAGCAGACAAGCCCGTCAGGGCGCGTCAGCGGGTGTTGGCGGG
TGTCGGGGCTGGCTTAACTATGCGGCATCAGAGCAGATTGTACTGAGAGTGCACCATATGCGGT
GTGAAATACCGCACAGATGCGTAAGGAGAAAATACCGCATCAGGCGCCATTCGCCATTCAGGCT
GCGCAACTGTTGGGAAGGGCGATCGGTGCGGGCCTCTTCGCTATTACGCCAGCTGGCGAAAGGG
GGATGTGCTGCAAGGCGATTAAGTTGGGTAACGCCAGGGTTTTCCCAGTCACGACGTTGTAAAA
CGACGGCCAGTGCCAGTGAATTAATTCGTTGCAGGACAGGATGTGGTGCCCGATGTGACTAGCT
CTTTGCTGCAGGCCGTCCTATCCTCTGGTTCCGATAAGAGACCCAGAACTCCGGCCCCCCACCGCC
CACCGCCACCCCCATACATATGTGGTACGCAAGTAAGAGTGCCTGCGCATGCCCCATGTGCCCCA
CCAAGAGTTTTGCATCCCATACAAGTCCCCAAAGTGGAGAACCGAACCAATTCTTCGCGGGCAGA
ACAAAAGCTTCTGCACACGTCTCCACTCGAATTTGGAGCCGGCCGGCGTGTGCAAAAGAGGTGA
ATCGAACGAAAGACCCGTGTGTAAAGCCGCGTTTCCAAAATGTATAAAACCGAGAGCATCTGGCC
AATGTGCATCAGTTGTGGTCAGCAGCAAAATCAAGTGAATCATCTCAGTGCAACTAAAGGGGGG
ATCTAGATCGGGGTACCTACTAGTCCAGTGTGGTGGCAAAATGtacccatacgatgttcctgactatgcggg
ctatccctatgacgtcccggactatgcaggatcctatccatatgacgttccagattacgctatggtatccaagggagaggaagac
aacatggcttccctcccggcaactcacgagttgcacatatttggtagtataaacggagtggacttcgacatggtgggacaaggta
cgggaaatccgaatgatggctacgaagaactcaatctcaagagtactaagggtgacctccagtttagcccgtggattctggtac
ctcacattggctatggcttccatcaatacctgccatatccagatggaatgagtccgttccaggccgctatggtagacggtagtgg

ataccaagtccaccgcacgatgcagtttgaagacggcgccagtctgacagtgaactatcgttatacctatgagggctcgcatata
aagggagaagctcaagtcaaaggaactggtttccccgccgatggacccgtaatgacgaacagcctcacagcagccgattggtg
taggagcaagaaaacttaccctaacgataagacgataatctcgacattcaaatggagctacactactggaaatggcaagcggt
accggagtacggcccggacaacatatacatttgccaaaccgatggcagcgaattatctgaaaaaccagcccatgtacgtgttcc
gcaaaaccgagttgaagcattcgaagactgagctcaattttaaagaatggcagaaggcctttactgacgtgatGGGCATGG
ATGAGCTCTATAAATAAAATTCTGCAGATATCCAGCACAGTGGCGGCCGCTCGAGTCTAGAGGGC
CCTTCGAAGGTAAGCCTATCCCTAACCCTCTCCTCGGTCTCGATTCTACGCGTACCGGTCATCATCA
CCATCACCATTGAGTTTAAACCCGCTGATCAGCCTCGACTGTGCCTTCTAAGATCCAGACATGATA
AGATACATTGATGAGTTTGGACAAACCACAACTAGAATGCAGTGAAAAAAATGCTTTATTTGTGA
AATTTGTGATGCTATTGCTTTATTTGTAACCATTATAAGCTGCAATAAACAAGTTAACAACAACAA
TTGCATTCATTTTATGTTTCAGGTTCAGGGGGAGGTGTGGGAGGTTTTTTAAAGCAAGTAAAACC
TCTACAAATGTGGTATGGCTGATTATGATCAGTCGACCTGCAGGCATGCAAGCTTGGCGTAATCA
TGGTCATAGCTGTTTCCTGTGTGAAATTGTTATCCGCTCACAATTCCACACAACATACGAGCCGGA
AGCATAAAGTGTAAAGCCTGGGGTGCCTAATGAGTGAGCTAACTCACATTAATTGCGTTGCGCTC
ACTGCCCGCTTTCCAGTCGGGAAACCTGTCGTGCCAGCTGCATTAATGAATCGGCCAACGCGCGG
GGAGAGGCGGTTTGCGTATTGGGCGCTCTTCCGCTTCCTCGCTCACTGACTCGCTGCGCTCGGTC
GTTCGGCTGCGGCGAGCGGTATCAGCTCACTCAAAGGCGGTAATACGGTTATCCACAGAATCAG
GGGATAACGCAGGAAAGAACATGTGAGCAAAAGGCCAGCAAAAGGCCAGGAACCGTAAAAAG
GCCGCGTTGCTGGCGTTTTTCCATAGGCTCCGCCCCCCTGACGAGCATCACAAAAATCGACGCTC
AAGTCAGAGGTGGCGAAACCCGACAGGACTATAAAGATACCAGGCGTTTCCCCCTGGAAGCTCC
CTCGTGCGCTCTCCTGTTCCGACCCTGCCGCTTACCGGATACCTGTCCGCCTTTCTCCCTTCGGGAA
GCGTGGCGCTTTCTCATAGCTCACGCTGTAGGTATCTCAGTTCGGTGTAGGTCGTTCGCTCCAAGC
TGGGCTGTGTGCACGAACCCCCCGTTCAGCCCGACCGCTGCGCCTTATCCGGTAACTATCGTCTTG
AGTCCAACCCGGTAAGACACGACTTATCGCCACTGGCAGCAGCCACTGGTAACAGGATTAGCAG
AGCGAGGTATGTAGGCGGTGCTACAGAGTTCTTGAAGTGGTGGCCTAACTACGGCTACACTAGA
AGGACAGTATTTGGTATCTGCGCTCTGCTGAAGCCAGTTACCTTCGGAAAAAGAGTTGGTAGCTC
TTGATCCGGCAAACAAACCACCGCTGGTAGCGGTGGTTTTTTTGTTTGCAAGCAGCAGATTACGC
GCAGAAAAAAAGGATCTCAAGAAGATCCTTTGATCTTTTCTACGGGGTCTGACGCTCAGTGGAAC
GAAAACTCACGTTAAGGGATTTTGGTCATGAGATTATCAAAAAGGATCTTCACCTAGATCCTTTTA
AATTAAAAATGAAGTTTTAAATCAATCTAAAGTATATATGAGTAAACTTGGTCTGACAGTTACCAA
TGCTTAATCAGTGAGGCACCTATCTCAGCGATCTGTCTATTTCGTTCATCCATAGTTGCCTGACTCC
CCGTCGTGTAGATAACTACGATACGGGAGGGCTTACCATCTGGCCCCAGTGCTGCAATGATACCG
CGAGACCCACGCTCACCGGCTCCAGATTTATCAGCAATAAACCAGCCAGCCGGAAGGGCCGAGC
GCAGAAGTGGTCCTGCAACTTTATCCGCCTCCATCCAGTCTATTAATTGTTGCCGGGAAGCTAGA
GTAAGTAGTTCGCCAGTTAATAGTTTGCGCAACGTTGTTGCCATTGCTACAGGCATCGTGGTGTC
ACGCTCGTCGTTTGGTATGGCTTCATTCAGCTCCGGTTCCCAACGATCAAGGCGAGTTACATGATC
CCCCATGTTGTGCAAAAAAGCGGTTAGCTCCTTCGGTCCTCCGATCGTTGTCAGAAGTAAGTTGG
CCGCAGTGTTATCACTCATGGTTATGGCAGCACTGCATAATTCTCTTACTGTCATGCCATCCGTAA
GATGCTTTTCTGTGACTGGTGAGTACTCAACCAAGTCATTCTGAGAATAGTGTATGCGGCGACCG
AGTTGCTCTTGCCCGGCGTCAATACGGGATAATACCGCGCCACATAGCAGAACTTTAAAAGTGCT
CATCATTGGAAAACGTTCTTCGGGGCGAAAACTCTCAAGGATCTTACCGCTGTTGAGATCCAGTT
CGATGTAACCCACTCGTGCACCCAACTGATCTTCAGCATCTTTTACTTTCACCAGCGTTTCTGGGTG
AGCAAAAACAGGAAGGCAAAATGCCGCAAAAAAGGGAATAAGGGCGACACGGAAATGTTGAAT
ACTCATACTCTTCCTTTTTCAATATTATTGAAGCATTTATCAGGGTTATTGTCTCATGAGCGGATAC
ATATTTGAATGTATTTAGAAAAATAAACAAATAGGGGTTCCGCGCACATTTCCCCGAAAAGTGCC
ACCTGACGTCTAAGAAACCATTATTATCATGACATTAACCTATAAAAATAGGCGTATCACGAGGCC
CTTTCGT

9.3.Supplementary Data

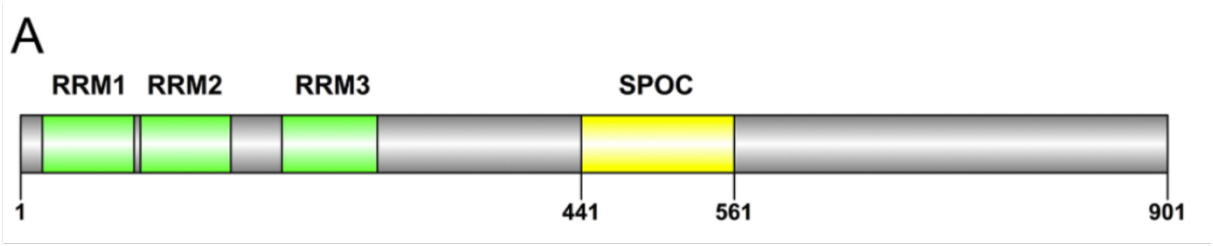

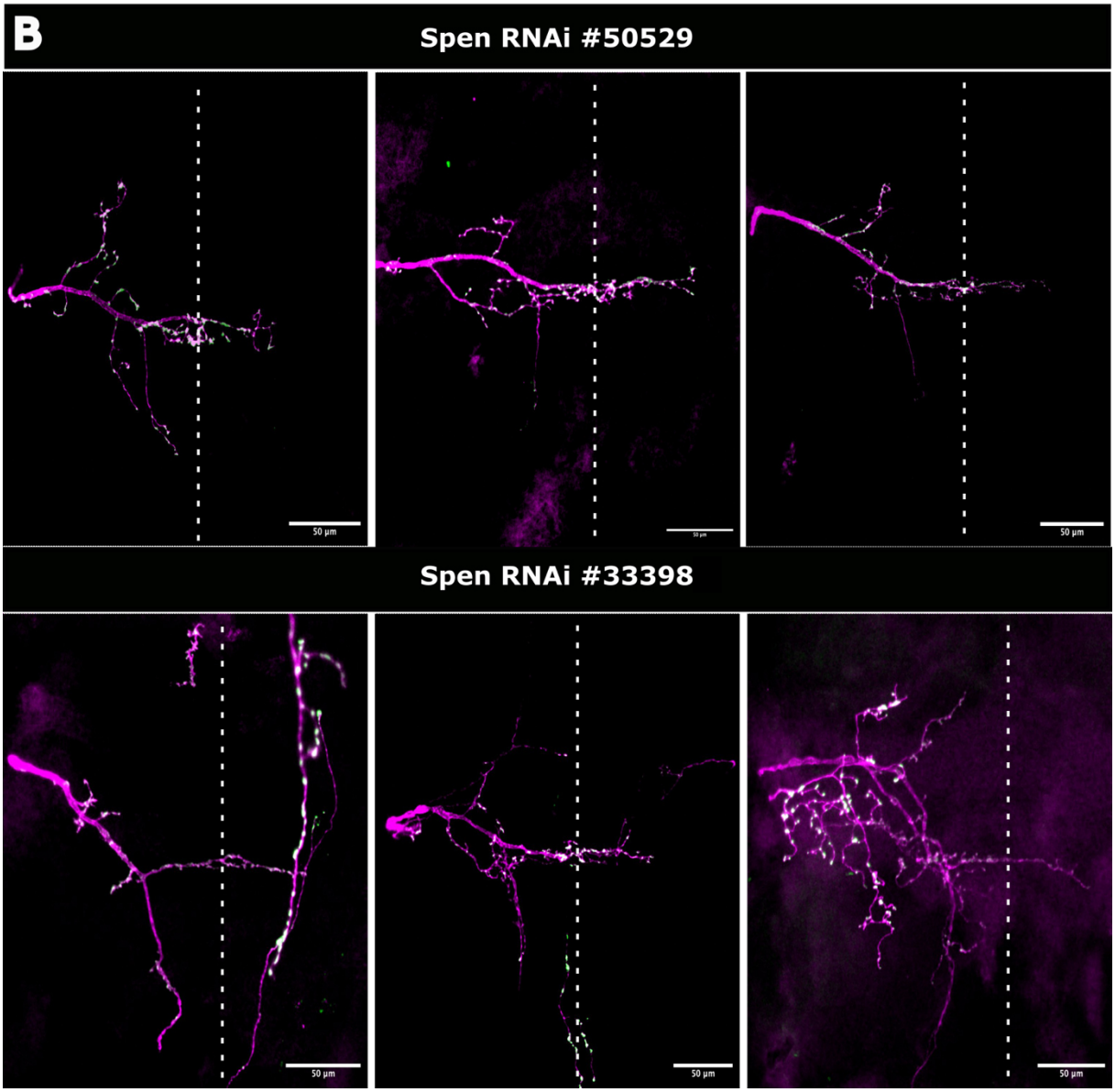

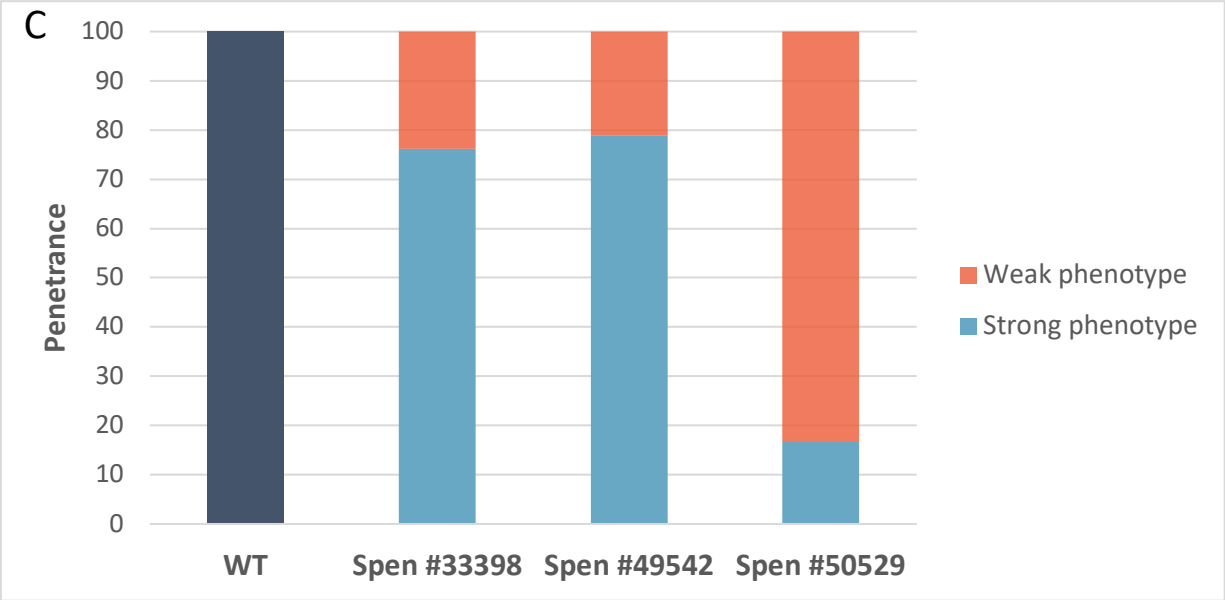

Figure S5. Impact of Spen Knock-down on Axon Length in Ms-neurons.

(A) Protein structure of Spen includes three RNP-type RNA binding motifs (RRM1-RRM3) and a SPOC domain.
(B) Confocal images depicting the consequences of Spen gene knock-down in Ms-neurons of RNAi lines #50529 and #33398.
(C) Quantitative analysis of axon length following Spen knock-down. All Spen RNAi lines demonstrate a visible phenotype, with Spen RNAi #33389 and #49542 showing a stronger phenotype and RNAi #50529 showing a weaker phenotype.
Dotted lines indicate CNS midline. Anterior is top and posterior is bottom.
Scale bar: 50 µm.

9.4. Flyfood

Standard fly food:

130 g	Yarn Agar
248 g	Baker's yeast
1223 g	Cornmeal
1.5 L	Sugar Beet Syrup
20 L	dH_2O

Fly food was prepared by adding the ingredients above. The solution was boiled and cooled down to 60°C. Subsequently, 10% Nipagin (in 70% EtOH) was added, and the food was stored at 4°C.

9.5. qPCR Primer

Table S1. Quantitative PCR Primer Sequences Used in this Dissertation.

Gene	Forward	Reverse
Actin 5c	5’-GTGCACCGCAAGTGCTTCTAA-3’	5’-TGCTGCACTCCAAACTTCCAC-3’
alrm	5’-ATGGCGGTACTCTGGTGGT-3’	5’-CCGCACTGCAATGATCCTG-3’
Brat	5’-TCAGCGGTTGCGGCAGTAC-3’	5’-GATGCCCGAGTTGCCGCC-3’
Brp	5’-AGGACGAGCTCTATGGCAGA-3’	5’-CAGGTCGGTGTTCTGATGCT-3’
CycE	5’-GTTGCCTCCTCGGTCTACAC-3’	5’-CGTCTGCTTGCTTCCACGA-3’
Diap1	5’-CCCCAGTATCCCGAATACGC-3’	5’-TCTGTTTCAGGTTCCTCGGC-3’
Dscam1	5’-TAAGGCCTTCGCCCAGGGATCC-3’	5’-TCTCCGGGGGTGTCGCCAACT-3’
E(spl)m6-BFM	5’-GAACAAGGCAAACGAGAGGA-3’	5’-AAGCAGATGACCAGGTGCTC-3’
Elav	5’-CGCAGCCCAATACGAATGG-3’	5’-CATTGTTTGCGGCAAGTAGTTG-3’
Ex	5’-TTGTACTTCCTAGTCGATGCC-3’	5’-CGCCATCTATGAGCACAGCC-3’
Gat	5’-AGCTTGCAGTCCAGCTCAC-3’	5’-GCTAGGCCCACTACTGATAGTAT-3’
Gcm	5’-ACAAGGCCAGAAGGAAGCAG-3’	5’-CAAGCCTGGATTTCCAAGCGA-3’
Hey	5’-AAAACTCTCGACTCGCTTAGC-3’	5’-CTGGAGGTGGGACATAAGGC-3’
Hpo	5’-CCATTATGCAACAATGCGACTC-3’	5’-GATCCACAGGTCATACTGCTT-3’
Insb	5’-CGCCATCGTCCTCTAACTCC-3’	5’-GGATTCGATTGGGGGCATCT-3’
Insc	5’-CCCTGGGCAATCTGTCCTG-3’	5’-CCCTGGGCAATCTGTCCTG-3’
Kibra	5’-CAGAGATTGCTACACAAAGCCG-3’	5’-TTCGAATCGTAGGATTCCTCC-3’
lncRNA:noe	5’-AAAGGCACAGGAGCACAGG-3’	5’-ACATGTCTTAGACTTTTGCGG-3’
Mira	5’-ACTCCCAGTCACACGGATAC-3’	5’-CTTGCCCTTCAGACGGCTG-3’
nSyb	5’-GACATCATGCGCACGAACG-3’	5’-TAATGCCCACGACAACCAGG-3’
Prl-1	5’-GAGACACAAGGCATTACCGT-3’	5’-CAAGGCAACAAGGACAGGAG-3’
Ptp61F	5’-AACGGCATCGATCCAATTC-3’	5’-CCGCTTCAGCTCGTTCTC-3’
Repo	5’-TCGCCCAACTATGTGACCAAG-3’	5’-CGGCGCACTAATGTACTCG-3’
RP49	5’-CCAGTCGGATCGATATGCTAA-3’	5’-ACGTTGTGCACCAGGAACTT-3’
Wts	5’-ATCAAGCAGGACCTAACCCG-3’	5’-GCCGTGTATCGCAGAGGTGT-3’
Yki	5’-CCTGGCGATACATCACTCCC -3’	5’-CACGCTAAGCCCAGATTCATT -3’

9.6. Chemicals

Table S2. Chemicals Used in this Dissertation.

Chemical	Manufacturer
2-Propanol	Carl Roth, Germany
Ampicillin	VWR, Germany
Chloroform	Carl Roth, Germany
E. coli Top10 cells	Lab Material, AG Schmucker
EDTA	Carl Roth, Germany
Ethanol absolute	VWR, Germany
Methanol	Carl Roth, Germany
Milk powder	Carl Roth, Germany
NaCl	Carl Roth, Germany
Nipagin	Carl Roth, Germany
Paraformaldehyde	Carl Roth, Germany
Primer	Integrated DNA Technologies, Leuven
RNAse A	Invitrogen, USA
TRIzol®	Peqlab, VWR, Germany
Tween-20	Carl Roth, Germany

Table S3. Devices Used in this Dissertation.

Device	Manufacturer
Balance Kern ew 4200-2NM	Kern & Sohn
Binocular Zeiss Stemi 2000	Carl Zeiss
Centrifuge Eppendorf 5415 R; 5424 R	Eppendorf
Fine scale BP211D	Satorius, Germany
Incubator	Rubarth Apparate GmbH
Light Sheet Microscope 710 Confocal microscope	Carl Zeiss
Photometer NanoDrop 2000	Peqlab
Precellys 24 homogenizer	Peqlab, VWR, Germany
QRT-PCR machine CFX96	BioRad
SZX12 fluorescence binocular	Olympus, Japan
Thermomixer	Eppendorf
Vortex Genie	Scientific Industries
Western blot equipment	Bio-Rad

Table S4. Materials Used in this Dissertation.

Materials	Manufacturer
15mL/50mL falcon tubes	Greiner Bio-One, Austria
Cover slips 24x60, 24x24 mm	Menzel
Glass beads	Carl Roth, Germany
qRT-PCR plastic plates 96 well	BioRad
qRT-PCR plate plastic cover film	BioRad
Cell culture dishes	Sarstedt, Germany
Screw cap tubes	Sarstedt, Germany
Syringe 10 mL plus sterile filter	Braun
Pipettes	Eppendorf, Germany
Cell Culture dishes	Sarstedt, Germany
PCR tubes	Sarstedt, Germany
Microscope slides	VWR, Germany
Cover glasses	Menzel, Germany
Accu-jet Pro Pipette Controller	BrandTech Scientific, USA
0.5/1.5/2 mL plastic tubes	Greiner Bio-One, Austria

10. References

Accogli, A., Addour-Boudrahem, N. and Srour, M. (2020) 'Chapter 4 - Neurogenesis, neuronal migration, and axon guidance', in A. Gallagher et al. (eds) *Handbook of Clinical Neurology*. Elsevier (Neurocognitive Development: Normative Development), pp. 25–42. Available at: https://doi.org/10.1016/B978-0-444-64150-2.00004-6.

Allen, A.M. *et al.* (2020) 'A single-cell transcriptomic atlas of the adult Drosophila ventral nerve cord', *eLife*. Edited by R.S. Mann, K. VijayRaghavan, and P.A. Sims, 9, p. e54074. Available at: https://doi.org/10.7554/eLife.54074.

Apitanyasai, K. *et al.* (2019) 'The gene structure and hypervariability of the complete Penaeus monodon Dscam gene', *Scientific Reports*, 9(1), p. 16595. Available at: https://doi.org/10.1038/s41598-019-52656-x.

Arama, E. *et al.* (2000) 'Mutations in the beta-propeller domain of the Drosophila brain tumor (brat) protein induce neoplasm in the larval brain', *Oncogene*, 19(33), pp. 3706–3716. Available at: https://doi.org/10.1038/sj.onc.1203706.

Asim, A. *et al.* (2018) 'CRELD1 gene variants and atrioventricular septal defects in Down syndrome', *Gene*, 641. Available at: https://doi.org/10.1016/j.gene.2017.10.044.

Awasaki, T. *et al.* (2011) 'Glia instruct developmental neuronal remodeling through TGF-β signaling', *Nature Neuroscience*, 14(7), pp. 821–823. Available at: https://doi.org/10.1038/nn.2833.

Awasaki, T. and Ito, K. (2004) 'Engulfing Action of Glial Cells Is Required for Programmed Axon Pruning during Drosophila Metamorphosis', *Current Biology*, 14(8), pp. 668–677. Available at: https://doi.org/10.1016/j.cub.2004.04.001.

Babot, M. *et al.* (2014) 'Characterisation of the active/de-active transition of mitochondrial complex I', *Biochimica et Biophysica Acta (BBA) - Bioenergetics*, 1837(7). Available at: https://doi.org/10.1016/j.bbabio.2014.02.018.

Bar-Peled, L. and Sabatini, D.M. (2014) 'Regulation of mTORC1 by amino acids', *Trends in Cell Biology*, 24(7), pp. 400–406. Available at: https://doi.org/10.1016/j.tcb.2014.03.003.

Barton, L.J. *et al.* (2013) 'The *Drosophila* Nuclear Lamina Protein Otefin Is Required for Germline Stem Cell Survival', *Developmental Cell*, 25(6), pp. 645–654. Available at: https://doi.org/10.1016/j.devcel.2013.05.023.

Baserga, S.J., DiMario, P.J. and Duncan, F.E. (2020) 'Emerging Roles for the Nucleolus 2019', *Journal of Biological Chemistry*, 295(16), pp. 5535–5537. Available at: https://doi.org/10.1074/jbc.MT120.013346.

Basso, V. *et al.* (2018) 'Regulation of ER-mitochondria contacts by Parkin via Mfn2', *Pharmacological Research*, 138. Available at: https://doi.org/10.1016/j.phrs.2018.09.006.

Bayarmagnai, B. *et al.* (2012) 'Drosophila GAGA factor is required for full activation of the dE2f1-Yki/Sd transcriptional program', *Cell Cycle (Georgetown, Tex.)*, 11(22), pp. 4191–4202. Available at: https://doi.org/10.4161/cc.22486.

BD FACSAria™ III | High Sensitivity Flow Cytometer (no date). Available at: https://www.bdbiosciences.com/en-eu/products/instruments/flow-cytometers/research-cell-sorters/bd-facsaria-iii (Accessed: 12 March 2024).

Beckert, V., Rassmann, S., Kayvanjoo, A.H., Klausen, C., Bonaguro, L., Botermann, D.S., Krause, M., Moreth, K., Spielmann, N., da Silva-Buttkus, P., Fuchs, H., Gailus-Durner, V., de Angelis, M.H., Händler, K., Ulas, T., Aschenbrenner, Anna C, *et al.* (2021) 'Creld1 regulates myocardial development and function', *Journal of molecular and cellular cardiology*, 156, pp. 45–56. Available at: https://doi.org/10.1016/j.yjmcc.2021.03.008.

Beckert, V., Rassmann, S., Kayvanjoo, A.H., Klausen, C., Bonaguro, L., Botermann, D.S., Krause, M., Moreth, K., Spielmann, N., da Silva-Buttkus, P., Fuchs, H., Gailus-Durner, V., de Angelis, M.H., Händler, K., Ulas, T., Aschenbrenner, Anna C., *et al.* (2021) 'Creld1 regulates myocardial development and function', *Journal of Molecular and Cellular Cardiology*, 156. Available at: https://doi.org/10.1016/j.yjmcc.2021.03.008.

Beckett, D., Kovaleva, E. and Schatz, P.J. (1999) 'A minimal peptide substrate in biotin holoenzyme synthetase-catalyzed biotinylation.', *Protein Science : A Publication of the Protein Society*, 8(4), pp. 921–929.

Beckstead, R.B., Lam, G. and Thummel, C.S. (2005) 'The genomic response to 20-hydroxyecdysone at the onset of Drosophila metamorphosis', *Genome Biology*, 6(12), p. R99. Available at: https://doi.org/10.1186/gb-2005-6-12-r99.

Bocci, F., Onuchic, J.N. and Jolly, M.K. (2020) 'Understanding the Principles of Pattern Formation Driven by Notch Signaling by Integrating Experiments and Theoretical Models', *Frontiers in Physiology*, 11. Available at: https://www.frontiersin.org/journals/physiology/articles/10.3389/fphys.2020.00929 (Accessed: 8 February 2024).

Böhme, M.A. *et al.* (2021) 'Glial Synaptobrevin mediates peripheral nerve insulation, neural metabolic supply, and is required for motor function', *Glia*, 69(8), pp. 1897–1915. Available at: https://doi.org/10.1002/glia.24000.

Boldyreva, L.V. *et al.* (2017) 'Protein and Genetic Composition of Four Chromatin Types in Drosophila melanogaster Cell Lines', *Current Genomics*, 18(2), pp. 214–226. Available at: https://doi.org/10.2174/1389202917666160512164913.

Bonaguro, L. *et al.* (2020) 'CRELD1 modulates homeostasis of the immune system in mice and humans', *Nature Immunology*, 21(12). Available at: https://doi.org/10.1038/s41590-020-00811-2.

Bonello, T.T. and Peifer, M. (2019) 'Scribble: A master scaffold in polarity, adhesion, synaptogenesis, and proliferation', *The Journal of Cell Biology*, 218(3), pp. 742–756. Available at: https://doi.org/10.1083/jcb.201810103.

Borgen, M. *et al.* (2017) 'Axon Termination, Pruning, and Synaptogenesis in the Giant Fiber System of Drosophila melanogaster Is Promoted by Highwire', *Genetics*, 205(3), pp. 1229–1245. Available at: https://doi.org/10.1534/genetics.116.197343.

Boulanger, A. and Dura, J.-M. (2015) 'Nuclear receptors and Drosophila neuronal remodeling', *Biochimica Et Biophysica Acta*, 1849(2), pp. 187–195. Available at: https://doi.org/10.1016/j.bbagrm.2014.05.024.

Bray, S.J. (2016) 'Notch signalling in context', *Nature Reviews Molecular Cell Biology*, 17(11), pp. 722–735. Available at: https://doi.org/10.1038/nrm.2016.94.

Bronshtein, I. *et al.* (2015) 'Loss of lamin A function increases chromatin dynamics in the nuclear interior', *Nature Communications*, 6, p. 8044. Available at: https://doi.org/10.1038/ncomms9044.

Campos-Ortega, J.A. (1999) 'Early Neurogenesis in Drosophila', in V.E.A. Russo et al. (eds) *Development: Genetics, Epigenetics and Environmental Regulation*. Berlin, Heidelberg: Springer, pp. 331–345. Available at: https://doi.org/10.1007/978-3-642-59828-9_20.

CFX Connect Real-Time PCR Detection System | Bio-Rad (no date). Available at: https://www.bio-rad.com/de-de/product/cfx-connect-real-time-pcr-detection-system?ID=LN5TFG15 (Accessed: 12 March 2024).

Cherbas, L. and Gong, L. (2014) 'Cell lines', *Methods*, 68(1), pp. 74–81. Available at: https://doi.org/10.1016/j.ymeth.2014.01.006.

Cho, P.F. *et al.* (2006) 'Cap-dependent translational inhibition establishes two opposing morphogen gradients in Drosophila embryos', *Current biology: CB*, 16(20), pp. 2035–2041. Available at: https://doi.org/10.1016/j.cub.2006.08.093.

Chou, V.T., Johnson, S.A. and Van Vactor, D. (2020) 'Synapse development and maturation at the drosophila neuromuscular junction', *Neural Development*, 15, p. 11. Available at: https://doi.org/10.1186/s13064-020-00147-5.

Clarke, A. *et al.* (2020) 'Dynamic morphogenesis of a pioneer axon in Drosophila and its regulation by Abl tyrosine kinase', *Molecular Biology of the Cell*, 31(6), pp. 452–465. Available at: https://doi.org/10.1091/mbc.E19-10-0563.

Collier, J.R. *et al.* (1996) 'Pattern formation by lateral inhibition with feedback: a mathematical model of delta-notch intercellular signalling', *Journal of Theoretical Biology*, 183(4), pp. 429–446. Available at: https://doi.org/10.1006/jtbi.1996.0233.

Collins, T.J. (2002) 'Mitochondria are morphologically and functionally heterogeneous within cells', *The EMBO Journal*, 21(7), pp. 1616–1627. Available at: https://doi.org/10.1093/emboj/21.7.1616.

Connacher, R.P. and Goldstrohm, A.C. (2021) 'Molecular and Biological Functions of TRIM-NHL RNA-Binding Proteins', *Wiley interdisciplinary reviews. RNA*, 12(2), p. e1620. Available at: https://doi.org/10.1002/wrna.1620.

Cosmanescu, F. *et al.* (2018) 'Neuron-Subtype-Specific Expression, Interaction Affinities, and Specificity Determinants of DIP/Dpr Cell Recognition Proteins', *Neuron*, 100(6), pp. 1385-1400.e6. Available at: https://doi.org/10.1016/j.neuron.2018.10.046.

Dahl *et al.* (1920) 'Anatomie und Histologie des vegetativen Nervensystemes', in Dahl et al. (eds) *Das Vegetative Nervensystem*. Berlin, Heidelberg: Springer, pp. 5–47. Available at: https://doi.org/10.1007/978-3-642-90954-2_3.

D'Alessandro, M. *et al.* (2018) 'CRELD1 is an evolutionarily-conserved maturational enhancer of ionotropic acetylcholine receptors', *eLife*, 7. Available at: https://doi.org/10.7554/eLife.39649.

D'Alessandro, M. *et al.* (no date) 'CRELD1 is an evolutionarily-conserved maturational enhancer of ionotropic acetylcholine receptors', *eLife*, 7, p. e39649. Available at: https://doi.org/10.7554/eLife.39649.

Dapples, C.C. and King, R.C. (1970) 'The development of the nucleolus of the ovarian nurse cell of Drosophila melanogaster', *Zeitschrift für Zellforschung und Mikroskopische Anatomie*, 103(1), pp. 34–47. Available at: https://doi.org/10.1007/BF00335399.

Dascenco, D. (2015) 'Mechanisms of Axon Branching in the Central Nervous System', *RPTP69D and Slit regulate Dscam1-mediated axon collateral formation*, Doctoral thesis, p. 138.

Daul, A.L., Komori, H. and Lee, C.-Y. (2010) 'EdU (5-ethynyl-2'-deoxyuridine) labeling of Drosophila mitotic neuroblasts', *Cold Spring Harbor Protocols*, 2010(7), p. pdb.prot5461. Available at: https://doi.org/10.1101/pdb.prot5461.

Dehnen, L. *et al.* (2020) 'A trimeric metazoan Rab7 GEF complex is crucial for endocytosis and scavenger function', *Journal of Cell Science* [Preprint]. Available at: https://doi.org/10.1242/jcs.247080.

Dent, E.W. and Gertler, F.B. (2003) 'Cytoskeletal dynamics and transport in growth cone motility and axon guidance', *Neuron*, 40(2), pp. 209–227. Available at: https://doi.org/10.1016/s0896-6273(03)00633-0.

Dickson, B.J. (2002) 'Molecular Mechanisms of Axon Guidance', *Science*, 298(5600), pp. 1959–1964. Available at: https://doi.org/10.1126/science.1072165.

Dietrich, M.O., Liu, Z.-W. and Horvath, T.L. (2013) 'Mitochondrial Dynamics Controlled by Mitofusins Regulate Agrp Neuronal Activity and Diet-Induced Obesity', *Cell*, 155(1), pp. 188–199. Available at: https://doi.org/10.1016/j.cell.2013.09.004.

Dow, L.E. *et al.* (2007) 'The tumour-suppressor Scribble dictates cell polarity during directed epithelial migration: regulation of Rho GTPase recruitment to the leading edge', *Oncogene*, 26(16), pp. 2272–2282. Available at: https://doi.org/10.1038/sj.onc.1210016.

Drosophila Cells in Culture - 2nd Edition (no date). Available at: https://shop.elsevier.com/books/drosophila-cells-in-culture/echalier/978-0-12-809473-0 (Accessed: 8 December 2023).

Dumitriu, A. *et al.* (2015a) 'Integrative analyses of proteomics and RNA transcriptomics implicate mitochondrial processes, protein folding pathways and GWAS loci in Parkinson disease', *BMC Medical Genomics*, 9(1). Available at: https://doi.org/10.1186/s12920-016-0164-y.

Dumitriu, A. *et al.* (2015b) 'Integrative analyses of proteomics and RNA transcriptomics implicate mitochondrial processes, protein folding pathways and GWAS loci in Parkinson disease', *BMC Medical Genomics*, 9(1). Available at: https://doi.org/10.1186/s12920-016-0164-y.

Dutta, S.B. *et al.* (2023) 'EGFR-dependent suppression of synaptic autophagy is required for neuronal circuit development', *Current Biology*, 33(3), pp. 517-532.e5. Available at: https://doi.org/10.1016/j.cub.2022.12.039.

Ecdysone Receptor - an overview | ScienceDirect Topics (no date). Available at: https://www.sciencedirect.com/topics/agricultural-and-biological-sciences/ecdysone-receptor# (Accessed: 4 March 2024).

Edwards, T.A. *et al.* (2003) 'Model of the Brain Tumor–Pumilio translation repressor complex', *Genes & Development*, 17(20), pp. 2508–2513. Available at: https://doi.org/10.1101/gad.1119403.

Effectene Transfection Reagent (no date a). Available at: https://www.qiagen.com/us/products/discovery-and-translational-research/functional-and-cell-analysis/transfection/effectene-transfection-reagent (Accessed: 7 September 2023).

Effectene Transfection Reagent (no date b). Available at: https://www.qiagen.com/us/products/discovery-and-translational-research/functional-and-cell-analysis/transfection/effectene-transfection-reagent (Accessed: 12 March 2024).

Egger, B., Chell, J.M. and Brand, A.H. (2008) 'Insights into neural stem cell biology from flies', *Philosophical Transactions of the Royal Society B: Biological Sciences*, 363(1489), pp. 39–56. Available at: https://doi.org/10.1098/rstb.2006.2011.

Elkahlah, N.A. *et al.* (2020) 'Presynaptic developmental plasticity allows robust sparse wiring of the Drosophila mushroom body', *eLife*, 9, p. e52278. Available at: https://doi.org/10.7554/eLife.52278.

Extracellular Matrix Proteins and Tools for Cell Culture Optimization (no date). Available at: https://www.sigmaaldrich.com/DE/de/technical-documents/technical-article/cell-culture-and-cell-culture-analysis/3d-cell-culture/attachment-factors-for-cell-culture (Accessed: 4 March 2024).

Fernández-Chacón, R. and Südhof, T.C. (1999) 'Genetics of synaptic vesicle function: toward the complete functional anatomy of an organelle', *Annual Review of Physiology*, 61, pp. 753–776. Available at: https://doi.org/10.1146/annurev.physiol.61.1.753.

Flis, V. V. and Daum, G. (2013) 'Lipid Transport between the Endoplasmic Reticulum and Mitochondria', *Cold Spring Harbor Perspectives in Biology*, 5(6), pp. a013235–a013235. Available at: https://doi.org/10.1101/cshperspect.a013235.

FlyBase Insertion Report: Dmel\P{lacW}brat[k06028] (no date). Available at: http://flybase.org/reports/FBti0007106.htm (Accessed: 12 March 2024).

Fouquet, W. *et al.* (2009) 'Maturation of active zone assembly by Drosophila Bruchpilot', *The Journal of Cell Biology*, 186(1), pp. 129–145. Available at: https://doi.org/10.1083/jcb.200812150.

Fuenzalida-Uribe, N. and Campusano, J.M. (2018) 'Unveiling the Dual Role of the Dopaminergic System on Locomotion and the Innate Value for an Aversive Olfactory Stimulus in Drosophila', *Neuroscience*, 371. Available at: https://doi.org/10.1016/j.neuroscience.2017.12.032.

García-García, M.J. *et al.* (1999) 'Different contributions of pannier and wingless to the patterning of the dorsal mesothorax of Drosophila', *Development*, 126(16), pp. 3523–3532. Available at: https://doi.org/10.1242/dev.126.16.3523.

Gargano, J.W. *et al.* (2005) 'Rapid iterative negative geotaxis (RING): A new method for assessing age-related locomotor decline in Drosophila', *Experimental Gerontology*, 40(5), pp. 386–395. Available at: https://doi.org/10.1016/j.exger.2005.02.005.

Gerhart, J. and Kirschner, M. (2020) *Normal Table of Xenopus Laevis (Daudin)*. Edited by P.D. Nieuwkoop and J. Faber. Garland Science. Available at: https://doi.org/10.1201/9781003064565.

Ghysen, A. (1978) 'Sensory neurones recognise defined pathways in Drosophila central nervous system', *Nature*, 274(5674), pp. 869–872. Available at: https://doi.org/10.1038/274869a0.

Ghysen, A. (1980) 'The projection of sensory neurons in the central nervous system of Drosophila: Choice of the appropriate pathway', *Developmental Biology*, 78(2), pp. 521–541. Available at: https://doi.org/10.1016/0012-1606(80)90351-6.

Gibson, D.G. *et al.* (2009) 'Enzymatic assembly of DNA molecules up to several hundred kilobases', *Nature Methods*, 6(5), pp. 343–345. Available at: https://doi.org/10.1038/nmeth.1318.

Gillette, C.M. *et al.* (2020) 'Gene-Diet Interactions: Dietary Rescue of Metabolic Effects in spen-Depleted Drosophila melanogaster', *Genetics*, 214(4), pp. 961–975. Available at: https://doi.org/10.1534/genetics.119.303015.

Gómez-Suaga, P. *et al.* (2018) 'ER–mitochondria signaling in Parkinson's disease', *Cell Death & Disease*, 9(3). Available at: https://doi.org/10.1038/s41419-017-0079-3.

Gordon, J., Amini, S. and White, M.K. (2013) 'General overview of neuronal cell culture', *Methods in molecular biology (Clifton, N.J.)*, 1078, pp. 1–8. Available at: https://doi.org/10.1007/978-1-62703-640-5_1.

Goulev, Y. *et al.* (2008) 'SCALLOPED Interacts with YORKIE, the Nuclear Effector of the Hippo Tumor-Suppressor Pathway in *Drosophila*', *Current Biology*, 18(6), pp. 435–441. Available at: https://doi.org/10.1016/j.cub.2008.02.034.

Greene, J.C. *et al.* (2003) 'Mitochondrial pathology and apoptotic muscle degeneration in Drosophila parkin mutants', *Proceedings of the National Academy of Sciences*, 100(7). Available at: https://doi.org/10.1073/pnas.0737556100.

Gu, T. *et al.* (2017) 'The large and small SPEN family proteins stimulate axon outgrowth during neurosecretory cell remodeling in Drosophila', *Developmental Biology*, 431(2), pp. 226–238. Available at: https://doi.org/10.1016/j.ydbio.2017.09.013.

Hacohen, N. *et al.* (1998) 'sprouty encodes a novel antagonist of FGF signaling that patterns apical branching of the Drosophila airways', *Cell*, 92(2), pp. 253–263. Available at: https://doi.org/10.1016/s0092-8674(00)80919-8.

Haelterman, N.A. *et al.* (2014) 'A Mitocentric View of Parkinson's Disease', *Annual Review of Neuroscience*, 37(1). Available at: https://doi.org/10.1146/annurev-neuro-071013-014317.

Hakim, Y., Yaniv, S.P. and Schuldiner, O. (2014) 'Astrocytes Play a Key Role in Drosophila Mushroom Body Axon Pruning', *PLOS ONE*, 9(1), p. e86178. Available at: https://doi.org/10.1371/journal.pone.0086178.

Halder, G. and Johnson, R.L. (2011) 'Hippo signaling: growth control and beyond', *Development (Cambridge, England)*, 138(1), pp. 9–22. Available at: https://doi.org/10.1242/dev.045500.

Han, H. *et al.* (2020) '<scp>PINK</scp> 1 phosphorylates Drp1 ^{S616} to regulate mitophagy-independent mitochondrial dynamics', *EMBO reports*, 21(8). Available at: https://doi.org/10.15252/embr.201948686.

Harvey, K.F., Pfleger, C.M. and Hariharan, I.K. (2003) 'The Drosophila Mst Ortholog, hippo, Restricts Growth and Cell Proliferation and Promotes Apoptosis', *Cell*, 114(4), pp. 457–467. Available at: https://doi.org/10.1016/S0092-8674(03)00557-9.

Hattori, D. *et al.* (2008) 'Dscam-mediated cell recognition regulates neural circuit formation', *Annual Review of Cell and Developmental Biology*, 24, pp. 597–620. Available at: https://doi.org/10.1146/annurev.cellbio.24.110707.175250.

He, H. *et al.* (2014) 'Cell-intrinsic requirement of Dscam1 isoform diversity for axon collateral formation', *Science (New York, N.Y.)*, 344(6188), pp. 1182–1186. Available at: https://doi.org/10.1126/science.1251852.

Heitzler, P. *et al.* (1996) 'A genetic analysis of pannier, a gene necessary for viability of dorsal tissues and bristle positioning in Drosophila', *Genetics*, 143(3), pp. 1271–1286. Available at: https://doi.org/10.1093/genetics/143.3.1271.

Henikoff, S. (1996) 'Dosage-dependent modification of position-effect variegation in Drosophla', *BioEssays*, 18(5), pp. 401–409. Available at: https://doi.org/10.1002/bies.950180510.

Hewitt, V.L. *et al.* (2020) 'Decreasing pdzd8-mediated mitochondrial-ER contacts in neurons improves fitness by increasing mitophagy', *BioRxiv* [Preprint].

Hillmer, R.E. and Link, B.A. (2019) 'The Roles of Hippo Signaling Transducers Yap and Taz in Chromatin Remodeling', *Cells*, 8(5), p. 502. Available at: https://doi.org/10.3390/cells8050502.

Homem, C.C.F. and Knoblich, J.A. (2012) 'Drosophila neuroblasts: a model for stem cell biology', *Development*, 139(23), pp. 4297–4310. Available at: https://doi.org/10.1242/dev.080515.

Hong, W. and Luo, L. (2014) 'Genetic Control of Wiring Specificity in the Fly Olfactory System', *Genetics*, 196(1), pp. 17–29. Available at: https://doi.org/10.1534/genetics.113.154336.

Huang, J. *et al.* (2005) 'The Hippo Signaling Pathway Coordinately Regulates Cell Proliferation and Apoptosis by Inactivating Yorkie, the Drosophila Homolog of YAP', *Cell*, 122(3), pp. 421–434. Available at: https://doi.org/10.1016/j.cell.2005.06.007.

Huang, J. *et al.* (2009) 'Directed, efficient, and versatile modifications of the Drosophila genome by genomic engineering', *Proceedings of the National Academy of Sciences*, 106(20). Available at: https://doi.org/10.1073/pnas.0900641106.

Humbert, P., Russell, S. and Richardson, H. (2003) 'Dlg, Scribble and Lgl in cell polarity, cell proliferation and cancer', *BioEssays*, 25(6), pp. 542–553. Available at: https://doi.org/10.1002/bies.10286.

Invitrogen, Molecular Probes (no date) 'Click-iT® EdU Imaging Kits'. Available at: https://www.thermofisher.com/document-connect/document-connect.html?url=https://assets.thermofisher.com/TFS-Assets%2FLSG%2Fmanuals%2Fmp10338.pdf.

Islam, Md.T. (2017) 'Oxidative stress and mitochondrial dysfunction-linked neurodegenerative disorders', *Neurological Research*, 39(1), pp. 73–82. Available at: https://doi.org/10.1080/01616412.2016.1251711.

Izadifar, A. *et al.* (2021) 'Axon morphogenesis and maintenance require an evolutionary conserved safeguard function of Wnk kinases antagonizing Sarm and Axed', *Neuron*, 109(18), pp. 2864-2883.e8. Available at: https://doi.org/10.1016/j.neuron.2021.07.006.

Izadifar, A. 'unpublished data'.

JBrowse 2R:24065912..24068147 (no date). Available at: http://flybase.org/jbrowse/?data=data%2Fjson%2Fdmel&loc=2R%3A24065912..24068147&tracks=Gene_span%2CGene&highlight= (Accessed: 12 June 2024).

Jin, L.H. *et al.* (2009) 'Requirement of Split ends for Epigenetic Regulation of Notch Signal-Dependent Genes during Infection-Induced Hemocyte Differentiation', *Molecular and Cellular Biology*, 29(6), pp. 1515–1525. Available at: https://doi.org/10.1128/MCB.01239-08.

Kass, D.A., Bronzwaer, J.G.F. and Paulus, W.J. (2004) 'What Mechanisms Underlie Diastolic Dysfunction in Heart Failure?', *Circulation Research*, 94(12). Available at: https://doi.org/10.1161/01.RES.0000129254.25507.d6.

Keder, A. and Carmena, A. (2013) 'Cytoplasmic protein motility and polarized sorting during asymmetric cell division', *WIREs Developmental Biology*, 2(6), pp. 797–808. Available at: https://doi.org/10.1002/wdev.116.

Keeney, P.M. (2006) 'Parkinson's Disease Brain Mitochondrial Complex I Has Oxidatively Damaged Subunits and Is Functionally Impaired and Misassembled', *Journal of Neuroscience*, 26(19). Available at: https://doi.org/10.1523/JNEUROSCI.0984-06.2006.

Kern, P., Balzer, N.R., Blank, N., Cygon, C., Wunderling, K., Bender, F., Frolov, A., Sowa, J.-P., *et al.* (2021) 'Creld2 function during unfolded protein response is essential for liver metabolism homeostasis', *The FASEB Journal*, 35(10), p. e21939. Available at: https://doi.org/10.1096/fj.202002713RR.

Kleinman, H.K. *et al.* (1987) 'Use of extracellular matrix components for cell culture', *Analytical Biochemistry*, 166(1), pp. 1–13. Available at: https://doi.org/10.1016/0003-2697(87)90538-0.

Kolodkin, A.L. and Tessier-Lavigne, M. (2011) 'Mechanisms and Molecules of Neuronal Wiring: A Primer', *Cold Spring Harbor Perspectives in Biology*, 3(6), p. a001727. Available at: https://doi.org/10.1101/cshperspect.a001727.

Kowalczyk, W. *et al.* (2022) 'Hippo signaling instructs ectopic but not normal organ growth', *Science*, 378(6621), p. eabg3679. Available at: https://doi.org/10.1126/science.abg3679.

Kraft, R., Levine, R.B. and Restifo, L.L. (1998) 'The Steroid Hormone 20-Hydroxyecdysone Enhances Neurite Growth ofDrosophila Mushroom Body Neurons Isolated during Metamorphosis', *The Journal of Neuroscience*, 18(21), pp. 8886–8899. Available at: https://doi.org/10.1523/JNEUROSCI.18-21-08886.1998.

Kraus, F. *et al.* (2021) 'Function and regulation of the divisome for mitochondrial fission', *Nature*, 590(7844). Available at: https://doi.org/10.1038/s41586-021-03214-x.

Kuang, B. *et al.* (2000) 'split ends encodes large nuclear proteins that regulate neuronal cell fate and axon extension in the Drosophila embryo', *Development (Cambridge, England)*, 127(7), pp. 1517–1529. Available at: https://doi.org/10.1242/dev.127.7.1517.

Lacin, H. *et al.* (2014) 'Transcription factor expression uniquely identifies most postembryonic neuronal lineages in the Drosophila thoracic central nervous system', *Development*, 141(5), pp. 1011–1021. Available at: https://doi.org/10.1242/dev.102178.

Landskron, L. *et al.* (2018) 'The asymmetrically segregating lncRNA cherub is required for transforming stem cells into malignant cells', *eLife*. Edited by H.J. Bellen, 7, p. e31347. Available at: https://doi.org/10.7554/eLife.31347.

Lapointe, J. and Hekimi, S. (2010) 'When a theory of aging ages badly', *Cellular and Molecular Life Sciences*, 67(1). Available at: https://doi.org/10.1007/s00018-009-0138-8.

Lehmacher, C., Abeln, B. and Paululat, A. (2012) 'The ultrastructure of Drosophila heart cells', *Arthropod Structure & Development*, 41(5). Available at: https://doi.org/10.1016/j.asd.2012.02.002.

Lexogen (2015) 'QuantSeq 3' mRNA-Seq Library Prep Kit FWD | Lexogen', 31 March. Available at: https://www.lexogen.com/quantseq-3mrna-sequencing/ (Accessed: 8 September 2023).

Lin, Y.-F. *et al.* (2009) 'Comparison of several radiation effects in human MCF10A mammary epithelial cells cultured as 2D monolayers or 3D acinar stuctures in matrigel', *Radiation Research*, 171(6), pp. 708–715. Available at: https://doi.org/10.1667/RR1554.1.

Loedige, I. *et al.* (2014) 'The NHL domain of BRAT is an RNA-binding domain that directly contacts the hunchback mRNA for regulation', *Genes & Development*, 28(7), pp. 749–764. Available at: https://doi.org/10.1101/gad.236513.113.

Luhur, A. *et al.* (2019) 'Thawing, Culturing, and Cryopreserving Drosophila Cell Lines', *Journal of Visualized Experiments*, (146), p. 59459. Available at: https://doi.org/10.3791/59459.

Luhur, A., Klueg, K.M. and Zelhof, A.C. (2019) 'Generating and working with Drosophila cell cultures: Current challenges and opportunities.', *Wiley interdisciplinary reviews. Developmental biology*, 8(3), p. e339. Available at: https://doi.org/10.1002/wdev.339.

Luna® Universal qPCR Master Mix | NEB (no date). Available at: https://www.neb.com/en/products/m3003-luna-universal-qpcr-master-mix (Accessed: 12 March 2024).

LunaScript® RT SuperMix Kit | NEB (no date). Available at: https://www.neb.com/en/products/e3010-luna-script-rt-supermix-kit (Accessed: 12 March 2024).

Luo, J. *et al.* (2012) 'Insulin-producing cells in the brain of adult Drosophila are regulated by the serotonin 5-HT1A receptor', *Cellular and Molecular Life Sciences*, 69(3). Available at: https://doi.org/10.1007/s00018-011-0789-0.

Luo, L. and O'Leary, D.D.M. (2005) 'Axon retraction and degeneration in development and disease', *Annual Review of Neuroscience*, 28, pp. 127–156. Available at: https://doi.org/10.1146/annurev.neuro.28.061604.135632.

Mace, K. and Tugores, A. (2004) 'The product of the split ends gene is required for the maintenance of positional information during Drosophiladevelopment', *BMC Developmental Biology*, 4(1), p. 15. Available at: https://doi.org/10.1186/1471-213X-4-15.

Mahul-Mellier, A.-L. *et al.* (2020) 'The process of Lewy body formation, rather than simply α-synuclein fibrillization, is one of the major drivers of neurodegeneration', *Proceedings of the National Academy of Sciences*, 117(9). Available at: https://doi.org/10.1073/pnas.1913904117.

Manning, S.A. *et al.* (2018) 'Dynamic Fluctuations in Subcellular Localization of the Hippo Pathway Effector Yorkie In Vivo', *Current biology: CB*, 28(10), pp. 1651-1660.e4. Available at: https://doi.org/10.1016/j.cub.2018.04.018.

Mass, E. *et al.* (2014) 'Murine Creld1 Controls Cardiac Development through Activation of Calcineurin/NFATc1 Signaling', *Developmental Cell*, 28(6). Available at: https://doi.org/10.1016/j.devcel.2014.02.012.

Menon, K.P., Carrillo, R.A. and Zinn, K. (2013) 'Development and plasticity of the Drosophila larval neuromuscular junction', *WIREs Developmental Biology*, 2(5), pp. 647–670. Available at: https://doi.org/10.1002/wdev.108.

Michki, N.S. *et al.* (2021) 'The molecular landscape of neural differentiation in the developing Drosophila brain revealed by targeted scRNA-seq and multi-informatic analysis', *Cell Reports*, 35(4), p. 109039. Available at: https://doi.org/10.1016/j.celrep.2021.109039.

De Miranda, B.R. *et al.* (2020) 'Protection from α-Synuclein induced dopaminergic neurodegeneration by overexpression of the mitochondrial import receptor TOM20', *npj Parkinson's Disease*, 6(1). Available at: https://doi.org/10.1038/s41531-020-00139-6.

Moeyaert, B. *et al.* (2018) 'Improved methods for marking active neuron populations', *Nature Communications*, 9(1). Available at: https://doi.org/10.1038/s41467-018-06935-2.

Morais, V.A. *et al.* (2014) 'PINK1 Loss-of-Function Mutations Affect Mitochondrial Complex I Activity via NdufA10 Ubiquinone Uncoupling', *Science*, 344(6180). Available at: https://doi.org/10.1126/science.1249161.

Morán, M. *et al.* (2012) 'Mitochondrial respiratory chain dysfunction: Implications in neurodegeneration', *Free Radical Biology and Medicine*, 53(3). Available at: https://doi.org/10.1016/j.freeradbiomed.2012.05.009.

Morey, M. (2017) 'Dpr-DIP matching expression in Drosophila synaptic pairs', *Fly*, 11(1), pp. 19–26. Available at: https://doi.org/10.1080/19336934.2016.1214784.

Mosca, T.J. and Luo, L. (2014) 'Synaptic organization of the Drosophila antennal lobe and its regulation by the Teneurins', *eLife*, 3, p. e03726. Available at: https://doi.org/10.7554/eLife.03726.

Muraro, N.I. *et al.* (2008) 'Pumilio Binds para mRNA and Requires Nanos and Brat to Regulate Sodium Current in Drosophila Motoneurons', *The Journal of Neuroscience*, 28(9), pp. 2099–2109. Available at: https://doi.org/10.1523/JNEUROSCI.5092-07.2008.

Nagaraj, R. *et al.* (2012) 'Control of mitochondrial structure and function by the Yorkie/YAP oncogenic pathway', *Genes & Development*, 26(18), pp. 2027–2037. Available at: https://doi.org/10.1101/gad.183061.111.

Nakajima, Y. (2021) 'Scrib module proteins: Control of epithelial architecture and planar spindle orientation', *The International Journal of Biochemistry & Cell Biology*, 136, p. 106001. Available at: https://doi.org/10.1016/j.biocel.2021.106001.

'Next Generation Sequencing' (no date). Available at: https://btc.uni-bonn.de/ngs/ (Accessed: 10 September 2023).

Niens, J. *et al.* (2017) 'Dopamine Modulates Serotonin Innervation in the Drosophila Brain', *Frontiers in Systems Neuroscience*, 11. Available at: https://doi.org/10.3389/fnsys.2017.00076.

Nieto-Estévez, V. *et al.* (2016) 'Brain Insulin-Like Growth Factor-I Directs the Transition from Stem Cells to Mature Neurons During Postnatal/Adult Hippocampal Neurogenesis', *Stem Cells*, 34(8), pp. 2194–2209. Available at: https://doi.org/10.1002/stem.2397.

Nikolakaki, E., Mylonis, I. and Giannakouros, T. (2017) 'Lamin B Receptor: Interplay between Structure, Function and Localization', *Cells*, 6(3), p. 28. Available at: https://doi.org/10.3390/cells6030028.

Oh, H. *et al.* (2013) 'Genome-wide association of Yorkie with chromatin and chromatin remodeling complexes', *Cell reports*, 3(2), pp. 309–318. Available at: https://doi.org/10.1016/j.celrep.2013.01.008.

Oh, H. and Irvine, K.D. (2008) 'In vivo regulation of Yorkie phosphorylation and localization', *Development (Cambridge, England)*, 135(6), pp. 1081–1088. Available at: https://doi.org/10.1242/dev.015255.

Oh, H. and Irvine, K.D. (2010) 'Yorkie: the final destination of Hippo signaling', *Trends in cell biology*, 20(7), pp. 410–417. Available at: https://doi.org/10.1016/j.tcb.2010.04.005.

Ohashi, M. *et al.* (2016) 'Hydrogen peroxide modulates neuronal excitability and membrane properties in ventral horn neurons of the rat spinal cord', *Neuroscience*, 331. Available at: https://doi.org/10.1016/j.neuroscience.2016.06.033.

Oh-hashi, K. *et al.* (2009) 'CRELD2 is a novel endoplasmic reticulum stress-inducible gene', *Biochemical and Biophysical Research Communications*, 387(3), pp. 504–510. Available at: https://doi.org/10.1016/j.bbrc.2009.07.047.

Oldham, S. *et al.* (2000) 'Genetic and biochemical characterization of dTOR, the Drosophila homolog of the target of rapamycin', *Genes & Development*, 14(21), pp. 2689–2694.

Oswald, M.C. *et al.* (2018) 'Reactive oxygen species regulate activity-dependent neuronal plasticity in Drosophila', *eLife*, 7. Available at: https://doi.org/10.7554/eLife.39393.

Paradis, M. *et al.* (2022) 'The ER protein Creld regulates ER-mitochondria contact dynamics and respiratory complex 1 activity', *Science Advances*, 8(29). Available at: https://doi.org/10.1126/sciadv.abo0155.

Parker, J. and Struhl, G. (2015) 'Scaling the Drosophila Wing: TOR-Dependent Target Gene Access by the Hippo Pathway Transducer Yorkie', *PLoS Biology*, 13(10), p. e1002274. Available at: https://doi.org/10.1371/journal.pbio.1002274.

Perez-Gomez, R. *et al.* (2020) 'Downregulation of respiratory complex I mediates major signalling changes triggered by TOR activation', *Scientific Reports*, 10(1). Available at: https://doi.org/10.1038/s41598-020-61244-3.

Pickersgill, H. *et al.* (2006) 'Characterization of the Drosophila melanogaster genome at the nuclear lamina', *Nature Genetics*, 38(9), pp. 1005–1014. Available at: https://doi.org/10.1038/ng1852.

Pogson, J.H. *et al.* (2014) 'The Complex I Subunit NDUFA10 Selectively Rescues Drosophila pink1 Mutants through a Mechanism Independent of Mitophagy', *PLoS Genetics*, 10(11). Available at: https://doi.org/10.1371/journal.pgen.1004815.

Poon, C.L.C. *et al.* (2016) 'The Hippo Pathway Regulates Neuroblasts and Brain Size in Drosophila melanogaster', *Current biology: CB*, 26(8), pp. 1034–1042. Available at: https://doi.org/10.1016/j.cub.2016.02.009.

Pouchieu, C. *et al.* (2018) 'Pesticide use in agriculture and Parkinson's disease in the AGRICAN cohort study', *International Journal of Epidemiology*, 47(1). Available at: https://doi.org/10.1093/ije/dyx225.

Qing, Y. *et al.* (2014) 'The Hippo effector Yorkie activates transcription by interacting with a histone methyltransferase complex through Ncoa6', *eLife*, 3, p. e02564. Available at: https://doi.org/10.7554/eLife.02564.

Rabanal-Ruiz, Y., Otten, E.G. and Korolchuk, V.I. (2017) 'mTORC1 as the main gateway to autophagy', *Essays in Biochemistry*. Edited by J.D. Lane, V.I. Korolchuk, and J.T. Murray, 61(6), pp. 565–584. Available at: https://doi.org/10.1042/EBC20170027.

Ramalingam, M., Huh, Y.-J. and Lee, Y.-I. (2019) 'The Impairments of α-Synuclein and Mechanistic Target of Rapamycin in Rotenone-Induced SH-SY5Y Cells and Mice Model of Parkinson's Disease', *Frontiers in Neuroscience*, 13. Available at: https://doi.org/10.3389/fnins.2019.01028.

Reichardt, I. *et al.* (2018) 'The tumor suppressor Brat controls neuronal stem cell lineages by inhibiting Deadpan and Zelda', *EMBO reports*, 19(1), pp. 102–117. Available at: https://doi.org/10.15252/embr.201744188.

Ren, F., Zhang, L. and Jiang, J. (2010) 'Hippo signaling regulates Yorkie nuclear localization and activity through 14-3-3 dependent and independent mechanisms', *Developmental biology*, 337(2), pp. 303–312. Available at: https://doi.org/10.1016/j.ydbio.2009.10.046.

Rodríguez-Arribas, M. *et al.* (2017) 'Mitochondria-Associated Membranes (MAMs): Overview and Its Role in Parkinson's Disease', *Molecular Neurobiology*, 54(8), pp. 6287–6303. Available at: https://doi.org/10.1007/s12035-016-0140-8.

Roegiers, F. *et al.* (2001) 'Two types of asymmetric divisions in the Drosophila sensory organ precursor cell lineage', *Nature Cell Biology*, 3(1), pp. 58–67. Available at: https://doi.org/10.1038/35050568.

Rotstein, B. and Paululat, A. (2016) 'On the Morphology of the Drosophila Heart', *Journal of Cardiovascular Development and Disease*, 3(2). Available at: https://doi.org/10.3390/jcdd3020015.

Rupp, P.A. *et al.* (2002) 'Identification, genomic organization and mRNA expression of CRELD1 , the founding member of a unique family of matricellular proteins', *Gene*, 293(1–2). Available at: https://doi.org/10.1016/S0378-1119(02)00696-0.

Ryczko, D. and Dubuc, R. (2017) 'Dopamine and the Brainstem Locomotor Networks: From Lamprey to Human', *Frontiers in Neuroscience*, 11. Available at: https://doi.org/10.3389/fnins.2017.00295.

Salic, A. and Mitchison, T.J. (2008) 'A chemical method for fast and sensitive detection of DNA synthesis in vivo', *Proceedings of the National Academy of Sciences of the United*

States of America, 105(7), pp. 2415–2420. Available at: https://doi.org/10.1073/pnas.0712168105.

Sanyal, S. (2009) 'Genomic mapping and expression patterns of C380, OK6 and D42 enhancer trap lines in the larval nervous system of Drosophila', *Gene Expression Patterns*, 9(5). Available at: https://doi.org/10.1016/j.gep.2009.01.002.

Saxton, R.A. and Sabatini, D.M. (2017) 'mTOR Signaling in Growth, Metabolism, and Disease', *Cell*, 168(6), pp. 960–976. Available at: https://doi.org/10.1016/j.cell.2017.02.004.

Schmeisser, K. and Parker, J.A. (2019) 'Pleiotropic Effects of mTOR and Autophagy During Development and Aging', *Frontiers in Cell and Developmental Biology*, 7. Available at: https://doi.org/10.3389/fcell.2019.00192.

Schmucker, D. *et al.* (2000) 'Drosophila Dscam Is an Axon Guidance Receptor Exhibiting Extraordinary Molecular Diversity', *Cell*, 101(6), pp. 671–684. Available at: https://doi.org/10.1016/S0092-8674(00)80878-8.

Schneider, I. (1972) 'Cell lines derived from late embryonic stages of *Drosophila melanogaster*', *Development*, 27(2), pp. 353–365. Available at: https://doi.org/10.1242/dev.27.2.353.

Schweisguth, F. (2004) 'Regulation of Notch Signaling Activity', *Current Biology*, 14(3), pp. R129–R138. Available at: https://doi.org/10.1016/j.cub.2004.01.023.

Schweisguth, F. (2015) 'Asymmetric cell division in the Drosophila bristle lineage: from the polarization of sensory organ precursor cells to Notch-mediated binary fate decision', *Wiley Interdisciplinary Reviews. Developmental Biology*, 4(3), pp. 299–309. Available at: https://doi.org/10.1002/wdev.175.

Scialò, F. *et al.* (2016) 'Mitochondrial ROS Produced via Reverse Electron Transport Extend Animal Lifespan', *Cell Metabolism*, 23(4). Available at: https://doi.org/10.1016/j.cmet.2016.03.009.

Sellin, J. *et al.* (2006) 'Dynamics of heart differentiation, visualized utilizing heart enhancer elements of the Drosophila melanogaster bHLH transcription factor Hand', *Gene Expression Patterns*, 6(4). Available at: https://doi.org/10.1016/j.modgep.2005.09.012.

Sergeeva, A.P. *et al.* (2020) 'DIP/Dpr interactions and the evolutionary design of specificity in protein families', *Nature Communications*, 11(1), p. 2125. Available at: https://doi.org/10.1038/s41467-020-15981-8.

Shahmoradian, S.H. *et al.* (2019) 'Lewy pathology in Parkinson's disease consists of crowded organelles and lipid membranes', *Nature Neuroscience*, 22(7). Available at: https://doi.org/10.1038/s41593-019-0423-2.

Shaner, N.C. *et al.* (2013) 'A bright monomeric green fluorescent protein derived from Branchiostoma lanceolatum', *Nature Methods*, 10(5), pp. 407–409. Available at: https://doi.org/10.1038/nmeth.2413.

Sharpley, M.S. *et al.* (2006) 'Interactions between Phospholipids and NADH:Ubiquinone Oxidoreductase (Complex I) from Bovine Mitochondria †', *Biochemistry*, 45(1). Available at: https://doi.org/10.1021/bi051809x.

Shen, W. and Ganetzky, B. (2009) 'Autophagy promotes synapse development in Drosophila', *The Journal of Cell Biology*, 187(1), pp. 71–79. Available at: https://doi.org/10.1083/jcb.200907109.

Shi, W. *et al.* (2013) 'Brain Tumor Regulates Neuromuscular Synapse Growth and Endocytosis in Drosophila by Suppressing Mad Expression', *The Journal of Neuroscience*, 33(30), pp. 12352–12363. Available at: https://doi.org/10.1523/JNEUROSCI.0386-13.2013.

Sieglitz, F. *et al.* (2013) 'Antagonistic feedback loops involving Rau and Sprouty in the Drosophila eye control neuronal and glial differentiation', *Science Signaling*, 6(300), p. ra96. Available at: https://doi.org/10.1126/scisignal.2004651.

Snigdha, K. *et al.* (2019) 'Hippo Signaling in Cancer: Lessons From Drosophila Models', *Frontiers in Cell and Developmental Biology*, 7. Available at: https://www.frontiersin.org/articles/10.3389/fcell.2019.00085 (Accessed: 20 February 2024).

Sonoda, J. and Wharton, R.P. (2001) 'Drosophila Brain Tumor is a translational repressor', *Genes & Development*, 15(6), pp. 762–773. Available at: https://doi.org/10.1101/gad.870801.

Srivastava, D. *et al.* (2021) 'Modulation of Yorkie activity by alternative splicing is required for developmental stability', *The EMBO journal*, 40(3), p. e104895. Available at: https://doi.org/10.15252/embj.2020104895.

Staley, B.K. and Irvine, K.D. (2012) 'Hippo signaling in Drosophila: recent advances and insights', *Developmental dynamics : an official publication of the American Association of Anatomists*, 241(1), pp. 3–15. Available at: https://doi.org/10.1002/dvdy.22723.

Stil, A. *et al.* (2023) 'A simple method for poly-D-lysine coating to enhance adhesion and maturation of primary cortical neuron cultures in vitro', *Frontiers in Cellular Neuroscience*, 17, p. 1212097. Available at: https://doi.org/10.3389/fncel.2023.1212097.

Stoiber, M. *et al.* (2016) 'Diverse Hormone Response Networks in 41 Independent *Drosophila* Cell Lines', *G3 Genes|Genomes|Genetics*, 6(3), pp. 683–694. Available at: https://doi.org/10.1534/g3.115.023366.

Strutt, H. and Strutt, D. (2003) 'EGF Signaling and Ommatidial Rotation in the Drosophila Eye', *Current Biology*, 13(16), pp. 1451–1457. Available at: https://doi.org/10.1016/S0960-9822(03)00545-1.

Su, W.-H. *et al.* (2012) 'Polarity protein complex Scribble/Lgl/Dlg and epithelial cell barriers', *Advances in Experimental Medicine and Biology*, 763, pp. 149–170. Available at: https://doi.org/10.1007/978-1-4614-4711-5_7.

Sudhof, T.C. (2004) 'The synaptic vesicle cycle', *Annual Review of Neuroscience*, 27, pp. 509–547. Available at: https://doi.org/10.1146/annurev.neuro.26.041002.131412.

Südhof, T.C. (2018) 'Towards an Understanding of Synapse Formation', *Neuron*, 100(2), pp. 276–293. Available at: https://doi.org/10.1016/j.neuron.2018.09.040.

Sun, J. *et al.* (2018) 'Neural Control of Startle-Induced Locomotion by the Mushroom Bodies and Associated Neurons in Drosophila', *Frontiers in Systems Neuroscience*, 12. Available at: https://doi.org/10.3389/fnsys.2018.00006.

Szymczak, A.L. *et al.* (2004) 'Correction of multi-gene deficiency in vivo using a single "self-cleaving" 2A peptide–based retroviral vector', *Nature Biotechnology*, 22(5), pp. 589–594. Available at: https://doi.org/10.1038/nbt957.

Talbot, D.E. *et al.* (2023) 'Prostaglandins limit nuclear actin to control nucleolar function during oogenesis', *Frontiers in Cell and Developmental Biology*, 11. Available at: https://doi.org/10.3389/fcell.2023.1072456.

Talbot, W.S., Swyryd, E.A. and Hogness, D.S. (1993) 'Drosophila tissues with different metamorphic responses to ecdysone express different ecdysone receptor isoforms', *Cell*, 73(7), pp. 1323–1337. Available at: https://doi.org/10.1016/0092-8674(93)90359-X.

TANG, J. and SAITO, T. (2017) 'Human plasma fibronectin promotes proliferation and differentiation of odontoblast', *Journal of Applied Oral Science*, 25(3), pp. 299–309. Available at: https://doi.org/10.1590/1678-7757-2016-0442.

Tessier-Lavigne, M. and Goodman, C.S. (1996) 'The molecular biology of axon guidance', *Science (New York, N.Y.)*, 274(5290), pp. 1123–1133. Available at: https://doi.org/10.1126/science.274.5290.1123.

Thiele, C., Wunderling, K. and Leyendecker, P. (2019) 'Multiplexed and single cell tracing of lipid metabolism', *Nature Methods*, 16(11). Available at: https://doi.org/10.1038/s41592-019-0593-6.

Tominaga, M. *et al.* (2010) 'Neurite elongation from Drosophila neural BG2-c6 cells stimulated by 20-hydroxyecdysone', *Neuroscience Letters*, 482(3), pp. 250–254. Available at: https://doi.org/10.1016/j.neulet.2010.07.049.

Trist, B.G., Hare, D.J. and Double, K.L. (2019) 'Oxidative stress in the aging substantia nigra and the etiology of Parkinson's disease', *Aging Cell*, 18(6). Available at: https://doi.org/10.1111/acel.13031.

TRIzol™ Reagenz (no date). Available at: https://www.thermofisher.com/order/catalog/product/de/de/15596026 (Accessed: 12 March 2024).

Truman, J.W. (1990) 'Metamorphosis of the central nervous system of Drosophila', *Journal of Neurobiology*, 21(7), pp. 1072–1084. Available at: https://doi.org/10.1002/neu.480210711.

Tudureanu, R. *et al.* (2022) 'Insight and Recent Advances into the Role of Topography on the Cell Differentiation and Proliferation on Biopolymeric Surfaces', *International Journal of Molecular Sciences*, 23(14), p. 7731. Available at: https://doi.org/10.3390/ijms23147731.

Ui, K. *et al.* (1994) 'Newly established cell lines fromDrosophila larval CNS express neural specific characteristics', *In Vitro Cellular & Developmental Biology - Animal*, 30(4), pp. 209–216. Available at: https://doi.org/10.1007/BF02632042.

Ulianov, S.V. *et al.* (2021) 'Order and stochasticity in the folding of individual Drosophila genomes', *Nature Communications*, 12(1), p. 41. Available at: https://doi.org/10.1038/s41467-020-20292-z.

Urwyler, O. *et al.* (2015) 'Investigating CNS synaptogenesis at single-synapse resolution by combining reverse genetics with correlative light and electron microscopy', *Development (Cambridge, England)*, 142(2), pp. 394–405. Available at: https://doi.org/10.1242/dev.115071.

Urwyler, O. *et al.* (2019) 'Branch-restricted localization of phosphatase Prl-1 specifies axonal synaptogenesis domains', *Science (New York, N.Y.)*, 364(6439), p. eaau9952. Available at: https://doi.org/10.1126/science.aau9952.

Valadas, J.S. *et al.* (2018) 'ER Lipid Defects in Neuropeptidergic Neurons Impair Sleep Patterns in Parkinson's Disease', *Neuron*, 98(6), pp. 1155-1169.e6. Available at: https://doi.org/10.1016/J.NEURON.2018.05.022.

Verghese, S. *et al.* (2012) 'Scribble Acts in the Drosophila Fat-Hippo Pathway to Regulate Warts Activity', *PLOS ONE*, 7(11), p. e47173. Available at: https://doi.org/10.1371/journal.pone.0047173.

Wagh, D.A. *et al.* (2006) 'Bruchpilot, a Protein with Homology to ELKS/CAST, Is Required for Structural Integrity and Function of Synaptic Active Zones in Drosophila', *Neuron*, 49(6), pp. 833–844. Available at: https://doi.org/10.1016/j.neuron.2006.02.008.

Watts, R.J., Hoopfer, E.D. and Luo, L. (2003) 'Axon pruning during Drosophila metamorphosis: evidence for local degeneration and requirement of the ubiquitin-proteasome system', *Neuron*, 38(6), pp. 871–885. Available at: https://doi.org/10.1016/s0896-6273(03)00295-2.

Wei, Z. *et al.* (2018) 'Oxidative Stress in Parkinson's Disease: A Systematic Review and Meta-Analysis', *Frontiers in Molecular Neuroscience*, 11. Available at: https://doi.org/10.3389/fnmol.2018.00236.

Wichmann, C. and Sigrist, S.J. (2010) 'The Active Zone T-Bar—A Plasticity Module?', *Journal of Neurogenetics*, 24(3), pp. 133–145. Available at: https://doi.org/10.3109/01677063.2010.489626.

Wieckowski, M.R. *et al.* (2009) 'Isolation of mitochondria-associated membranes and mitochondria from animal tissues and cells', *Nature Protocols*, 4(11), pp. 1582–1590. Available at: https://doi.org/10.1038/nprot.2009.151.

Willoughby, L.F. *et al.* (2017) 'Differential regulation of protein tyrosine kinase signalling by Dock and the PTP61F variants', *The FEBS journal*, 284(14), pp. 2231–2250. Available at: https://doi.org/10.1111/febs.14118.

Wilson, E.L. and Metzakopian, E. (2021) 'ER-mitochondria contact sites in neurodegeneration: genetic screening approaches to investigate novel disease mechanisms', *Cell Death & Differentiation*, 28(6). Available at: https://doi.org/10.1038/s41418-020-00705-8.

Wu, J.S. and Luo, L. (2006) 'A protocol for mosaic analysis with a repressible cell marker (MARCM) in Drosophila', *Nature Protocols*, 1(6), pp. 2583–2589. Available at: https://doi.org/10.1038/nprot.2006.320.

Wu, S. *et al.* (2008) 'The TEAD/TEF family protein Scalloped mediates transcriptional output of the Hippo growth-regulatory pathway', *Developmental Cell*, 14(3), pp. 388–398. Available at: https://doi.org/10.1016/j.devcel.2008.01.007.

Xu, J. *et al.* (2018) 'Yorkie functions at the cell cortex to promote myosin activation in a non-transcriptional manner', *Developmental cell*, 46(3), pp. 271-284.e5. Available at: https://doi.org/10.1016/j.devcel.2018.06.017.

Xu, S. *et al.* (2018) 'Interactions between the Ig-Superfamily Proteins DIP-α and Dpr6/10 Regulate Assembly of Neural Circuits', *Neuron*, 100(6), pp. 1369-1384.e6. Available at: https://doi.org/10.1016/j.neuron.2018.11.001.

Yang, Y. *et al.* (2008) 'Pink1 regulates mitochondrial dynamics through interaction with the fission/fusion machinery', *Proceedings of the National Academy of Sciences*, 105(19). Available at: https://doi.org/10.1073/pnas.0711845105.

Yao, B. *et al.* (2018) 'Active N6-Methyladenine Demethylation by DMAD Regulates Gene Expression by Coordinating with Polycomb Protein in Neurons', *Molecular Cell*, 71(5), pp. 848-857.e6. Available at: https://doi.org/10.1016/j.molcel.2018.07.005.

Yogev, S. and Shen, K. (2014) 'Cellular and molecular mechanisms of synaptic specificity', *Annual Review of Cell and Developmental Biology*, 30, pp. 417–437. Available at: https://doi.org/10.1146/annurev-cellbio-100913-012953.

Yu, F. and Schuldiner, O. (2014) 'Axon and dendrite pruning in Drosophila', *Current Opinion in Neurobiology*, 27, pp. 192–198. Available at: https://doi.org/10.1016/j.conb.2014.04.005.

Yu, J. *et al.* (2010) 'Kibra Functions as a Tumor Suppressor Protein that Regulates Hippo Signaling in Conjunction with Merlin and Expanded', *Developmental Cell*, 18(2), pp. 288–299. Available at: https://doi.org/10.1016/j.devcel.2009.12.012.

Yu, R. *et al.* (2019) 'The phosphorylation status of Ser-637 in dynamin-related protein 1 (Drp1) does not determine Drp1 recruitment to mitochondria', *Journal of Biological Chemistry*, 294(46). Available at: https://doi.org/10.1074/jbc.RA119.008202.

Zhao, H., Moberg, K.H. and Veraksa, A. (2023) 'Hippo pathway and Bonus control developmental cell fate decisions in the Drosophila eye', *Developmental Cell*, 58(5), pp. 416-434.e12. Available at: https://doi.org/10.1016/j.devcel.2023.02.005.

Zhu, Y. *et al.* (2015) 'Brahma regulates the Hippo pathway activity through forming complex with Yki–Sd and regulating the transcription of Crumbs', *Cellular Signalling*, 27(3), pp. 606–613. Available at: https://doi.org/10.1016/j.cellsig.2014.12.002.

Zschätzsch, M. *et al.* (2014) 'Regulation of branching dynamics by axon-intrinsic asymmetries in Tyrosine Kinase Receptor signaling', *eLife*. Edited by F. Polleux, 3, p. e01699. Available at: https://doi.org/10.7554/eLife.01699.

11. Eidesstaatliche Erklärung

Name	**Kucharowski**
Vorname	**Nicole Barbara**
Titel der Dissertation	**Dissecting Synaptogenesis and Axonal Branching Mechanisms in *Drosophila Melanogaster***

Hiermit erkläre ich durch meine Unterschrift an Eides statt:

1. Die von mir eingereichte Dissertation habe ich selbstständig und ohne unzulässige fremde Hilfe verfasst. Hierbei habe ich weder Textstellen von Dritten oder aus eigenen Prüfungsarbeiten noch Grafiken oder sonstige Materialien ohne Kennzeichnung übernommen.
2. Es sind ausschließlich die von mir angegebenen Quellen und Hilfsmittel verwendet worden.
3. Sämtliche wörtliche und nicht wörtliche Zitate aus anderen Werken sind gemäß den wissenschaftlichen Zitierregeln kenntlich gemacht.
4. Die von mir vorgelegte Arbeit ist bisher noch nicht oder an der nachstehend aufgeführten Stelle vollständig/auszugsweise veröffentlicht.
5. Die von mir vorgelegte Arbeit ist bisher noch in keiner Form als Bestandteil einer Prüfungs-/Qualifikationsleistung vorgelegt worden.
6. Ich bin nicht zweimal in einem Promotionsverfahren an einer deutschen Hochschule aufgrund einer Ablehnung der Dissertation oder nicht bestandener Prüfungsleistungen gescheitert.
7. Die von mir eingereichte Dissertation habe ich unter Beachtung der Grundsätze zur Sicherung guter wissenschaftlicher Praxis erstellt.
8. Über die Bedeutung und die strafrechtlichen Folgen einer falschen eidesstattlichen Erklärung gemäß § 156 StGB bin ich mir bewusst.
9. Meine Angaben entsprechen der Wahrheit und ich habe diese nach bestem Wissen und Gewissen gemacht.

_____ _____

Ort, Datum Unterschrift der **Doktorandin**